Dynamic Analysis of Semi-Active Control Techniques for Vehicle Applications

by

Fernando D. Goncalves

Thesis submitted to the Faculty of the

Virginia Polytechnic Institute and State University

in partial fulfillment of the requirements for the degree of

Master of Science

in

Mechanical Engineering

Approved:

_____
Mehdi Ahmadian, Chairman

_____ _____
Harry Robertshaw Daniel Inman

August 2001
Blacksburg, Virginia

Keywords: Semi-active, Magneto-Rheological, Skyhook, Groundhook, Suspensions, Experimental, Vehicle Dynamics

Dynamic Analysis of Semi-Active Control Techniques for Vehicle Applications

by

Fernando D. Goncalves

Mehdi Ahmadian, Chairman

Mechanical Engineering

This experimental study evaluates the dynamic response of five semi-active control policies as tested on a single suspension quarter-car system. Incorporating a magneto-rheological damper, the full-scale 2DOF quarter-car system was used to evaluate skyhook, groundhook, and hybrid control. Two alternative skyhook policies were also considered, namely displacement skyhook and relative displacement skyhook. As well as exploring the relative benefits of each of these controllers, the performance of each semi-active controller was compared to the performance of conventional passive damping.

Each control policy is evaluated for its control performance under three different base excitations: chirp, step, and pure tone. Corresponding to the chirp input, transmissibilities and auto spectrums are considered for each control policy. Specifically, transmissibilities between the sprung mass displacement and the unsprung mass displacement are generated relative to the input displacement. Further, the ratio between the relative displacement across the damper and the input displacement is evaluated for each control technique. The chirp input also reveals the results of the auto spectrums of the sprung and unsprung mass accelerations. Both the step input and the pure tone input were used to generate time domain values of RMS and peak-to-peak displacements and accelerations.

This study shows that semi-active control offers benefits beyond those of conventional passive damping. Further, traditional skyhook control is shown to outperform the less conventional alternative skyhook policies.

ACKNOWLEDGEMENTS

I would like to thank my advisor Dr. Mehdi Ahmadian (aka The General) for his guidance and support throughout my time as a Master's student in the Mechanical Engineering Department. His enthusiasm and interest in the work of all his students is encouraging. I would also like to thank Drs. Daniel Inman and Harry Robertshaw for serving on my graduate committee. I would also like to thank Dr. Xubin Song, at Visteon Corp., for his help and patience in the betterment of the quarter-car rig at Virginia Tech. The generous contributions by UniMeasure to the Advanced Vehicle Dynamics Laboratory are greatly appreciated. I would also like to thank Mr. Peter Trogos at The MathWorks, Inc. for his generous, and timely, contributions to the Advanced Vehicle Dynamics Laboratory.

I would also like to thank my lab mates, Jeong-Hoi Koo, James C. Poynor, David Simon, and Wei Huang for their contributions to my work. Each of them offered a valuable bit of assistance for which I am truly grateful.

I would also like to thank my mom and dad, Manuel and Joana Goncalves, for their love and support during my time as a student. The gift they've given and continue to give surpasses all that I could have expected. I promise I will get a job someday. I would also like to thank my brother Manny, for thoughts of him always bring a smile to my face. I would also like to thank my girlfriend Courtney for her encouragement and patience during my time at Virginia Tech. Her enthusiasm in my education is a truly selfless act and does not go unnoticed.

I would also like to thank the friends I've made here at Virginia Tech for their companionship and memories. In particular, I would like to thank Casey Carter and Karl Sheldon for their unique and unmatched friendship.

Finally, I would like to thank the Lord for guiding me to where I am today. My faith in God and his faith in me is a powerful and wonderful tool.

CONTENTS

Abstract ii

Acknowledgements iii

List of Nomenclature viii

List of Figures ix

List of Tables xv

1 INTRODUCTION 1

1.1 MOTIVATION 1

1.2 OBJECTIVES 3

1.3 APPROACH 3

1.4 OUTLINE 4

2 BACKGROUND 5

2.1 2DOF PASSIVE SUSPENSION SYSTEM 5

2.2 CONTROL SCHEMES FOR A 2DOF SYSTEM 8

2.2.1 Skyhook Control 8

2.2.2 Groundhook Control 13

2.2.3 Hybrid Control 15

2.2.4 Alternative Skyhook Control Policies 16

2.2.5 Passive vs. Semi-Active Dampers 17

2.3 MAGNETO-RHEOLOGICAL DAMPERS 18

2.3.1 Magneto-Rheological Fluids 18

2.3.2 Construction of an MR Damper 19

2.3.3 MR Damper Dynamics 23

2.4 LITERATURE REVIEW 26

2.4.1 Keyword: Semi-Active 26

2.4.2 Keyword: Magneto-Rheological Damper 27

2.4.3 Keyword: Skyhook 28

2.4.4 Literature Review Summary 29

3 EXPERIMENTAL SETUP 30

3.1 MECHANICS OF THE QUARTER-CAR RIG 30
3.2 COMPONENTS OF ACTUATION SYSTEM 37
3.3 DATA ACQUISITION SYSTEM 40
3.4 CONTROLLER DEVELOPMENT 43
3.4.1 Skyhook Control Development 43
3.4.2 Groundhook Control Development 45
3.4.3 Hybrid Control Development 46
3.4.4 Displacement Skyhook Control Development 47
3.4.5 Relative Displacement Skyhook Control Development 48
3.4.6 Current Driver Circuit 49

4 FREQUENCY RESPONSE ANALYSIS 51

4.1 EXCITATION FOR FREQUENCY RESPONSE ANALYSIS 51
4.2 SIGNAL PROCESSING METHODS 54
4.3 PASSIVE CONTROL FREQUENCY ANALYSIS 56
4.4 SKYHOOK CONTROL FREQUENCY ANALYSIS 59
4.5 GROUNDHOOK CONTROL FREQUENCY ANALYSIS 64
4.6 HYBRID CONTROL FREQUENCY ANALYSIS 69
4.7 DISPLACEMENT SKYHOOK FREQUENCY ANALYSIS 76
4.8 RELATIVE DISPLACEMENT SKYHOOK CONTROL FREQUENCY ANALYSIS 80
4.9 FREQUENCY ANALYSIS COMPARISON 84

5 TRANSIENT RESPONSE ANALYSIS 89

5.1 EXCITATION FOR TRANSIENT RESPONSE ANALYSIS 89
5.2 TRANSIENT ANALYSIS PERFORMANCE CRITERION 90
5.3 PASSIVE CONTROL TRANSIENT ANALYSIS 91
5.4 SKYHOOK CONTROL TRANSIENT ANALYSIS 95
5.5 GROUNDHOOK CONTROL TRANSIENT ANALYSIS 99
5.6 HYBRID CONTROL TRANSIENT ANALYSIS 103
5.7 DISPLACEMENT SKYHOOK CONTROL TRANSIENT ANALYSIS 107
5.8 RELATIVE DISPLACEMENT SKYHOOK CONTROL TRANSIENT ANALYSIS 111

6 STEADY STATE RESPONSE ANALYSIS 116

6.1 EXCITATION FOR STEADY STATE RESPONSE ANALYSIS 116

6.2 STEADY STATE PERFORMANCE CRITERION 117

6.3 PASSIVE CONTROL STEADY STATE EVALUATION 118

6.3.1 Pure Tone 1.5 Hz 118

6.3.2 Pure Tone 10.5 Hz 121

6.3.3 Damper Work 125

6.4 SKYHOOK CONTROL STEADY STATE EVALUATION 127

6.4.1 Pure Tone 1.5 Hz 127

6.4.2 Pure Tone 10.5 Hz 130

6.4.3 Damper Work 133

6.5 GROUNDHOOK STEADY STATE EVALUATION 136

6.5.1 Pure Tone 1.5 Hz 136

6.5.2 Pure Tone 10.5 Hz 140

6.5.3 Damper Work 143

6.6 HYBRID CONTROL STEADY STATE EVALUATION 145

6.6.1 Pure Tone 1.5 Hz 145

6.6.2 Pure Tone 10.5 Hz 149

6.6.3 Damper Work 152

6.7 DISPLACEMENT SKYHOOK STEADY STATE EVALUATION 154

6.7.1 Pure Tone 1.5 Hz 154

6.7.2 Pure Tone 10.5 Hz 157

6.7.3 Damper Work 160

6.8 RELATIVE DISPLACEMENT SKYHOOK STEADY STATE EVALUATION 163

6.8.1 Pure Tone 1.5 Hz 163

6.8.2 Pure Tone 10.5 Hz 166

6.8.3 Damper Work 169

7 CONCLUSION AND RECOMMENDATIONS 173

7.1 SUMMARY 173

7.2 RECOMMENDATIONS FOR FUTURE RESEARCH 175

References 176
Vita 180

LIST OF NOMENCLATURE

m_1	sprung mass
m_2	unsprung mass
x_1	sprung mass displacement
x_2	unsprung mass displacement
k_s	suspension stiffness
k_t	tire stiffness
x_{in}	input displacement
ζ_1	sprung mass damping ratio
ζ_2	unsprung mass damping ratio
ω	natural frequency
ω_{n1}	sprung mass natural frequency
ω_{n2}	unsprung mass natural frequency
$\ddot{x}_1$	sprung mass acceleration
$\ddot{x}_2$	unsprung mass acceleration
c	damping coefficient
k_1	stiffness
$\dot{x}_1$	sprung mass velocity
$\dot{x}_2$	unsprung mass velocity
c_{sky}	skyhook damping coefficient
v_1	sprung mass velocity
v_2	unsprung mass velocity
c_{gnd}	groundhook damping coefficient
F_{sa}	semi-active damping force
F_{sky}	skyhook damping force
v_{12}	relative velocity
c_{sa}	semi-active damping coefficient
σ_{sky}	skyhook component of damping force for hybrid control
σ_{gnd}	groundhook component of damping force for hybrid control
α	relative ratio between skyhook and groundhook for hybrid control
G	controller gain
x_{12}	relative velocity
i	electric current

LIST OF FIGURES

Figure 1-1. Suspension Compromise, (adapted from Reference [2]) 2
Figure 2-1. 2DOF Quarter-Car Model 5
Figure 2-2. Passive Suspension Transmissibility: 7
Figure 2-3. Skyhook Damper Configuration 9
Figure 2-4. Skyhook Configuration Transmissibility: 10
Figure 2-5. Semi-Active Equivalent Model 11
Figure 2-6. Groundhook Damper Configuration 13
Figure 2-7. Groundhook Configuration Transmissibility: 14
Figure 2-8. Hybrid Configuration 15
Figure 2-9. Hybrid Configuration Transmissibility: 16
Figure 2-10. Transmissibility Comparison of Passive and Semiactive Dampers: 18
Figure 2-11. Functional Representation of an MR Damper 20
Figure 2-12. Sectional view of MR damper built by James Poynor 21
Figure 2-13. Close-up sectional identifying "choking regions" and fluid gap 22
Figure 2-14. Test MR damper and internal components 22
Figure 2-15. Linear Damper Characteristics 23
Figure 2-16. Bilinear, Asymmetric Damping Characteristics 24
Figure 2-17. Ideal MR Damper Performance 25
Figure 2-18. MR Damper Damping Force Envelope 26
Figure 3-1. 2DOF "Quarter-Car Model": (a) 2DOF System; (b) Quarter-Car Rig 31
Figure 3-2. Structural Support Members: (a) Eliminates side-to-side and torsional modes; (b) Eliminates fore/aft mode 32
Figure 3-3. Close-up of Teflon Bushings 33
Figure 3-4. Arrangement Used for Emulating Tire Vertical Stiffness 34
Figure 3-5. Close-up of Roller Wheels 35
Figure 3-6. Quarter-Car Representation of Primary Suspension 36
Figure 3-7. Quarter-Car Rig and Primary Components 37
Figure 3-8. MTS 242 Series Hydraulic Actuator 38

Figure 3-9. MTS 407 Controller 38
Figure 3-10. MTS SilentFlo Hydraulic Power Unit 39
Figure 3-11. MTS Hydraulic Service Manifold 40
Figure 3-12. dSPACE AutoBox 41
Figure 3-13. Data Acquisition and Control Block Diagram 42
Figure 3-14. UniMeasure VP510-10 Velocity-Position Transducer 44
Figure 3-15. Block Diagram for Skyhook Control Logic 45
Figure 3-16. Block Diagram for Groundhook Control Logic 46
Figure 3-17. Block Diagram for Hybrid Control Logic 47
Figure 3-18. Block Diagram for Displacement Skyhook Logic 48
Figure 3-19. Block Diagram for Relative Displacement Skyhook Control Logic 49
Figure 3-20. Current Driver Circuit for MR Damper 50
Figure 4-1. Bode Plot of the Filter for Chirp Signal Input 53
Figure 4-2. Chirp Input Signal 54
Figure 4-3. Passive Transmissibility for Different Damper Currents: 57
Figure 4-4. Passive Control Relative Displacement Transmissibility 58
Figure 4-5. Passive Control Acceleration Auto Spectrums: 59
Figure 4-6. Sample Time History of Skyhook Execution 60
Figure 4-7. Block Diagram for Skyhook Control Logic 61
Figure 4-8. Skyhook Control Transmissibility: 62
Figure 4-9. Skyhook Control Relative Displacement Transmissibility 63
Figure 4-10. Skyhook Control Acceleration Auto Spectrums: 64
Figure 4-11. Sample Time History for Groundhook Execution 65
Figure 4-12. Block Diagram for Groundhook Control Logic 66
Figure 4-13. Groundhook Control Transmissibility: 67
Figure 4-14. Groundhook Control Relative Displacement Transmissibility 68
Figure 4-15. Groundhook Control Acceleration Auto Spectrums: 69
Figure 4-16. Block Diagram for Hybrid Control Logic 70
Figure 4-17. Hybrid Control Transmissibility G = 0.5: 71
Figure 4-18. Hybrid Control Transmissibility $\alpha = 0.5$: 72
Figure 4-19: Hybrid Control 3-D Mesh for Sprung Mass Transmissibility Amplitude 73

Figure 4-20: Hybrid Control 3-D Mesh for Unsprung Mass Transmissibility Amplitude 74
Figure 4-21. Hybrid Control Relative Displacement Transmissibility G = 0.5 75
Figure 4-22. Hybrid Control Acceleration Auto Spectrums G = 0.5: 76
Figure 4-23. Block Diagram for Displacement Skyhook Control Logic 77
Figure 4-24. Sample Time History of Displacement Skyhook Execution 77
Figure 4-25. Displacement Skyhook Control Transmissibility: 78
Figure 4-26. Displacement Skyhook Control Relative Displacement Transmissibility 79
Figure 4-27. Displacement Skyhook Control Acceleration Auto Spectrums: 80
Figure 4-28. Sample Time History of Relative Displacement Skyhook Execution 81
Figure 4-29. Block Diagram for Relative Displacement Control Logic 82
Figure 4-30. Relative Displacement Skyhook Control Transmissibilities: 82
Figure 4-31. Relative Displacement Transmissibility for Relative Displacement Skyhook Control 83
Figure 4-32. Relative Displacement Skyhook Control Acceleration Auto Spectrums: 84
Figure 4-33. Sprung Mass Transmissibility for Different Control Techniques 85
Figure 4-34. Unsprung Mass Transmissibility for Different Control Techniques 86
Figure 4-35. Sprung Mass Acceleration Auto Spectrum for Different Control Techniques 87
Figure 4-36. Unsprung Mass Acceleration Auto Spectrum for Different Control Techniques 88
Figure 5-1. Step Input Signal 90
Figure 5-2. Step Response 91
Figure 5-3. Passive Control Displacement Response: 92
Figure 5-4. Passive Control Peak-to-Peak Displacement for Step Input 93
Figure 5-5. Passive Control Acceleration Response: 94
Figure 5-6. Passive Control Peak-to-Peak Acceleration for Step Input 95
Figure 5-7. Skyhook Control Displacement Response: 96
Figure 5-8. Skyhook Control Peak-to-Peak Displacement for Step Input 97
Figure 5-9. Skyhook Control Acceleration Response: 98
Figure 5-10. Skyhook Control Peak-to-Peak Acceleration for Step Input 99

Figure 5-11. Groundhook Control Displacement Response: 100
Figure 5-12. Groundhook Control Peak-to-Peak Displacement for Step Input 101
Figure 5-13. Groundhook Control Acceleration Response: 102
Figure 5-14. Groundhook Control Peak-to-Peak Acceleration for Step Input 103
Figure 5-15. Hybrid Control Displacement Response: 104
Figure 5-16. Hybrid Control Peak-to-Peak Displacement for Step Input 105
Figure 5-17. Hybrid Control Acceleration Response: 106
Figure 5-18. Hybrid Control Peak-to-Peak Acceleration for Step Input 107
Figure 5-19. Displacement Skyhook Control Displacement Response: 108
Figure 5-20. Displacement Skyhook Control Peak-to-Peak Displacement for Step Input 109
Figure 5-21. Displacement Skyhook Control Acceleration Response: 110
Figure 5-22. Displacement Skyhook Control Peak-to-Peak Acceleration for Step Input 111
Figure 5-23. Relative Displacement Skyhook Control Displacement Response: 112
Figure 5-24. Relative Displacement Skyhook Control Peak-to-Peak Displacement for Step Input 113
Figure 5-25. Relative Displacement Skyhook Control Acceleration Response: 114
Figure 5-26. Relative Displacement Skyhook Control Peak-to-Peak Acceleration for Step Input 115
Figure 6-1. Passive Control Peak-to-Peak Displacement at 1.5 Hz 118
Figure 6-2. Passive Control RMS Displacement at 1.5 Hz 119
Figure 6-3. Passive Control Peak-to-Peak Acceleration at 1.5 Hz 120
Figure 6-4. Passive Control RMS Acceleration at 1.5 Hz 121
Figure 6-5. Passive Control Peak-to-Peak Displacement at 10.5 Hz 122
Figure 6-6. Passive Control RMS Displacement at 10.5 Hz 123
Figure 6-7. Passive Control Peak-to-Peak Acceleration at 10.5 Hz 124
Figure 6-8. Passive Control RMS Acceleration at 10.5 Hz 124
Figure 6-9. Passive Control Damper Work 125
Figure 6-10. Passive Control Force Displacement Relationship 126
Figure 6-11. Passive Control Force Velocity Relationship 127

Figure 6-12. Skyhook Control Peak-to-Peak Displacement at 1.5 Hz 128
Figure 6-13. Skyhook Control RMS Displacement at 1.5 Hz 128
Figure 6-14. Skyhook Control Peak-to-Peak Acceleration at 1.5 Hz 129
Figure 6-15. Skyhook Control RMS Acceleration at 1.5 Hz 130
Figure 6-16. Skyhook Control Peak-to-Peak Displacement at 10.5 Hz 131
Figure 6-17. Skyhook Control RMS Displacement at 10.5 Hz 131
Figure 6-18. Skyhook Control Peak-to-Peak Acceleration at 10.5 Hz 132
Figure 6-19. Skyhook Control RMS Acceleration at 10.5 Hz 133
Figure 6-20. Skyhook Control Damper Work 134
Figure 6-21. Skyhook Control Force Displacement Relationship 135
Figure 6-22. Skyhook Control Force Velocity Relationship 136
Figure 6-23. Groundhook Control Peak-to-Peak Displacement at 1.5 Hz 137
Figure 6-24. Groundhook Control RMS Displacement at 1.5 Hz 138
Figure 6-25. Groundhook Control Peak-to-Peak Acceleration at 1.5 Hz 139
Figure 6-26. Groundhook Control RMS Acceleration at 1.5 Hz 139
Figure 6-27. Groundhook Control Peak-to-Peak Displacement at 10.5 Hz 140
Figure 6-28. Groundhook Control RMS Displacement at 10.5 Hz 141
Figure 6-29. Groundhook Control Peak-to-Peak Accelerations at 10.5 Hz 142
Figure 6-30. Groundhook Control RMS Acceleration at 10.5 Hz 142
Figure 6-31. Groundhook Control Damper Work 143
Figure 6-32. Groundhook Control Force Displacement Relationship 144
Figure 6-33. Groundhook Control Force Velocity Relationship 145
Figure 6-34. Hybrid Control Peak-to-Peak Displacement at 1.5 Hz 146
Figure 6-35. Hybrid Control RMS Displacement at 1.5 Hz 147
Figure 6-36. Hybrid Control Peak-to-Peak Accelerations at 1.5 Hz 148
Figure 6-37. Hybrid Control RMS Acceleration at 1.5 Hz 148
Figure 6-38. Hybrid Control Peak-to-Peak Displacement at 10.5 Hz 149
Figure 6-39. Hybrid Control RMS Displacement at 10.5 Hz 150
Figure 6-40. Hybrid Control Peak-to-Peak Acceleration at 10.5 Hz 151
Figure 6-41. Hybrid Control RMS Acceleration at 10.5 Hz 151
Figure 6-42. Hybrid Control Damper Work 152

Figure 6-43. Hybrid Control Force Displacement Relationship 153
Figure 6-44. Hybrid Control Force Velocity Relationship 154
Figure 6-45. Displacement Skyhook Control Peak-to-Peak Displacement at 1.5 Hz 155
Figure 6-46. Displacement Skyhook Control RMS Displacement at 1.5 Hz 155
Figure 6-47. Displacement Skyhook Control Peak-to-Peak Acceleration at 1.5 Hz 156
Figure 6-48. Displacement Skyhook Control RMS Acceleration at 1.5 Hz 157
Figure 6-49. Displacement Skyhook Control Peak-to-Peak Displacement at 10.5 Hz 158
Figure 6-50. Displacement Skyhook Control RMS Displacement at 10.5 Hz 158
Figure 6-51. Displacement Skyhook Control Peak-to-Peak Acceleration at 10.5 Hz 159
Figure 6-52. Displacement Skyhook Control RMS Acceleration at 10.5 Hz 160
Figure 6-53. Displacement Skyhook Control Damper Work 161
Figure 6-54. Displacement Skyhook Control Force Velocity Relationship 162
Figure 6-55. Displacement Skyhook Control Force Velocity Relationship 163
Figure 6-56. Relative Displacement Skyhook Control Peak-to-Peak Displacement at 1.5 Hz 164
Figure 6-57. Relative Displacement Skyhook Control RMS Displacement at 1.5 Hz 164
Figure 6-58. Relative Displacement Skyhook Control Peak-to-Peak Acceleration at 1.5 Hz 165
Figure 6-59. Relative Displacement Skyhook Control RMS Acceleration at 1.5 Hz 166
Figure 6-60. Relative Displacement Skyhook Control Peak-to-Peak Displacement at 10.5 Hz 167
Figure 6-61. Relative Displacement Skyhook Control RMS Displacement at 10.5 Hz 167
Figure 6-62. Relative Displacement Skyhook Peak-to-Peak Acceleration at 10.5 Hz 168
Figure 6-63. Relative Displacement Skyhook Control RMS Accelerations at 10.5 Hz 169
Figure 6-64. Relative Displacement Skyhook Control Damper Work 170
Figure 6-65. Relative Displacement Skyhook Control Force Displacement Relationship 171
Figure 6-66. Relative Displacement Skyhook Control Force Velocity Relationship 172

LIST OF TABLES

Table 2-1. System Parameters ____ *6*

Table 1-1. Chirp Signal Parameters ____ *52*

1 Introduction

This chapter presents the motivation for the work in this thesis by giving a general comparison of passive versus semi-active and active suspensions. The objectives and approach to this research are then discussed. The chapter ends with an outline of the thesis.

1.1 Motivation

So often in engineering a compromise affects the design process of a particular component. The design of automotive suspensions falls into this category. The familiar trade off between ride comfort and vehicle stability has been the driving force for advancements in automotive suspensions. Though subjective, ride comfort can be quantified by the amount of energy transmitted through the suspension into the passenger compartment (sprung mass). Ride quality is closely tied to the acceleration of the sprung mass [1]. A Cadillac is a good example of a vehicle whose passengers feel few road disturbances. Conversely, a Corvette's suspension will transmit many of the road disturbances into the passenger compartment in return for higher vehicle stability. Vehicle stability can also be thought of as road holding ability. Compared to a Cadillac, a Corvette is a much more maneuverable vehicle and holds the road significantly better. Ideally, a vehicle suspension would respond just as well to aggressive driving as it does to highway cruising. The intent of this work is to try to approach this ideal. Figure 1-1 illustrates the classic suspension compromise.

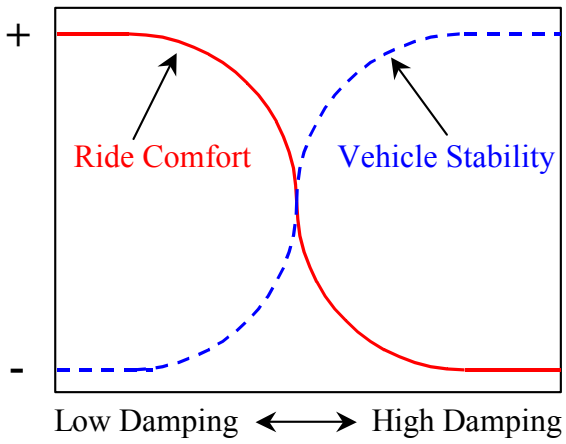

Figure 1-1. Suspension Compromise, (adapted from Reference [2])

A typical vehicle suspension is made up of two components: a spring and a damper. The spring is chosen based solely on the weight of the vehicle, while the damper is the component that defines the suspension's placement on the compromise curve. Depending on the type of vehicle, a damper is chosen to make the vehicle perform best in its application. Ideally, the damper should isolate passengers from low-frequency road disturbances and absorb high-frequency road disturbances. Passengers are best isolated from low-frequency disturbances when the damping is high. However, high damping provides poor high frequency absorption. Conversely, when the damping is low, the damper offers sufficient high-frequency absorption, at the expense of low-frequency isolation.

The need to reduce the effects of this compromise has given rise to several new advancements in automotive suspensions. Three types of suspensions that will be reviewed here are passive, fully active, and semi-active suspensions. A conventional passive suspension is composed of a spring and a damper. The suspension stores energy in the spring and dissipates energy through the damper. Both components are fixed at the design stage. For this reason, this type of suspension falls victim to the classic suspension compromise.

If the damper is replaced with a force actuator, the suspension becomes a fully active suspension. Hindered by its complexity and its power consumption, fully active

suspensions have yet to be accepted for conventional use. The idea behind fully active suspensions is that the force actuator is able to apply a force to the suspension in either jounce or rebound. This force is actively governed by the control scheme employed in the suspension. Several different control schemes will be discussed later.

The third and final type of suspension that will be mentioned here is a semi-active suspension. In a semi-active suspension, the passive damper is replaced with a semi-active damper. A semi-active damper is capable of changing its damping characteristics. Whether through mechanically changing orifices or fluid with adjustable viscosity, a semi-active damper offers greater variation in damping. Again, the control algorithm used in the design governs the amount of damping.

1.2 Objectives

This study focuses on three primary objectives. The first is to reevaluate and improve the design and functioning of a quarter-car rig that will be used for testing. The function of the quarter-car rig is to identify the dynamics of various suspensions and to evaluate the use of this suspension in vehicle applications. Second, the quarter-car rig will be used to perform a series of tests that will help to evaluate the benefits of various semi-active control policies that are commonly considered for vehicle applications. This evaluation will be done through a comparative analysis of semi-active control techniques and existing passive suspensions. The evaluation is a three step evaluation which includes a frequency response analysis, a transient response analysis, and a steady state response analysis. The third objective is to suggest alternative semi-active control policies that will provide dynamic benefits beyond those currently used for vehicle applications.

1.3 Approach

The approach adopted for this research included using a quarter-car rig available at the Advanced Vehicle Dynamics Laboratory (AVDL) of Virginia Tech. The quarter-car rig was tuned such that it can effectively represent the sprung and unsprung mass dynamics

that are observed in a typical passenger vehicle. Then the rig was used to evaluate the effect of different semi-active control policies on various dynamic aspects of the sprung and unsprung masses. The test results were used to determine the dynamic effect of semi-active suspensions on vehicle dynamics as they are controlled in real time using commonly considered control policies, such as skyhook, groundhook, and hybrid control. Finally, the results of the study are used to provide recommendations for future studies.

1.4 Outline

The reader will find that this work follows in an experimental fashion. The next chapter provides the necessary background information to understand semi-active suspensions. Comparisons are drawn between passive, fully active, and semi-active suspensions. It also contains a literature search on semi-active suspensions and policies, along with magneto-rheological (MR) dampers. Chapter 3 describes the test setup. This includes a detailed description of the quarter-car rig and its mechanics. Furthermore, the actuation system used to excite the system is discussed, along with the data acquisition system used to record the dynamic response of the suspension. This chapter also describes the sensory equipment used along with the manner in which the MR damper was controlled. In Chapter 4, the test results for the frequency response analysis are revealed along with observations drawn from these results. Chapter 5 discusses the results of the transient response analysis. The steady state analysis results then follow in Chapter 6. Chapter 7 provides concluding remarks and a summary of the work. Significant results are highlighted and recommendations for future research are also discussed.

2 Background

The purpose of this chapter is to provide the background for the research conducted in this study. Along with this background, the results of a literature search are presented. First, five different theoretical control schemes for a two-degree-of-freedom (2DOF) system will be presented. In addition to the individual algorithms, the aim of each control scheme will be shown with the intended performance benefits. The discussion will then turn to the physical implementation of these control schemes on a 2DOF system. Following this is a discussion of the practical design considerations and performance of a semi-active MR damper. The chapter concludes with a literature search on past research done in areas relating to this work.

2.1 2DOF Passive Suspension System

A typical vehicle primary suspension can be modeled as shown in Figure 2-1. Since the model represents a single suspension from one of the four corners of the vehicle, this 2DOF system is often referred to as the "quarter-car" model.

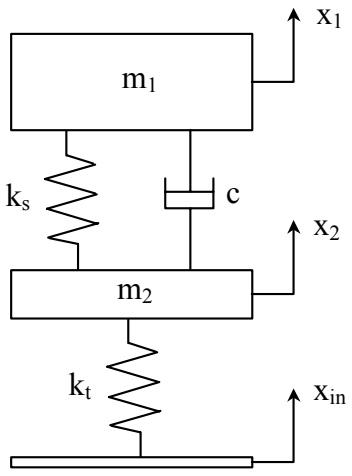

Figure 2-1. 2DOF Quarter-Car Model

The parameters used in the simulation of this model are the actual system parameters of the physical quarter-car apparatus described in Chapter 3. These system parameters, which closely model actual vehicle parameters, are shown in Table 2-1.

Table 2-1. System Parameters

Parameter	Value
Sprung Body Weight (m_1)	950 lbs
Unsprung Body Weight (m_2)	100 lbs
Suspension Stiffness (k_1)	200 lb/in
Tire Stiffness (k_2)	1085 lb/in

The input to this model is a displacement input which is representative of a typical road profile. The input excites the first degree of freedom (the unsprung mass of a quarter of the vehicle, representing the wheel, tire, and some suspension components) through a spring element which represents the tire stiffness. The unsprung mass is connected to the second degree of freedom (the sprung mass, representing the body of the vehicle) through the primary suspension spring and damper. The transmissibility of the 2DOF system, if all the elements of the quarter-car are passive, is shown in Figure 2-2 for various damping coefficients. The first plot shows the displacement of the sprung mass (x_1) with respect to the input (x_{in}), while the second plot shows the displacement of the unsprung mass (x_2) with respect to the input (x_{in}).

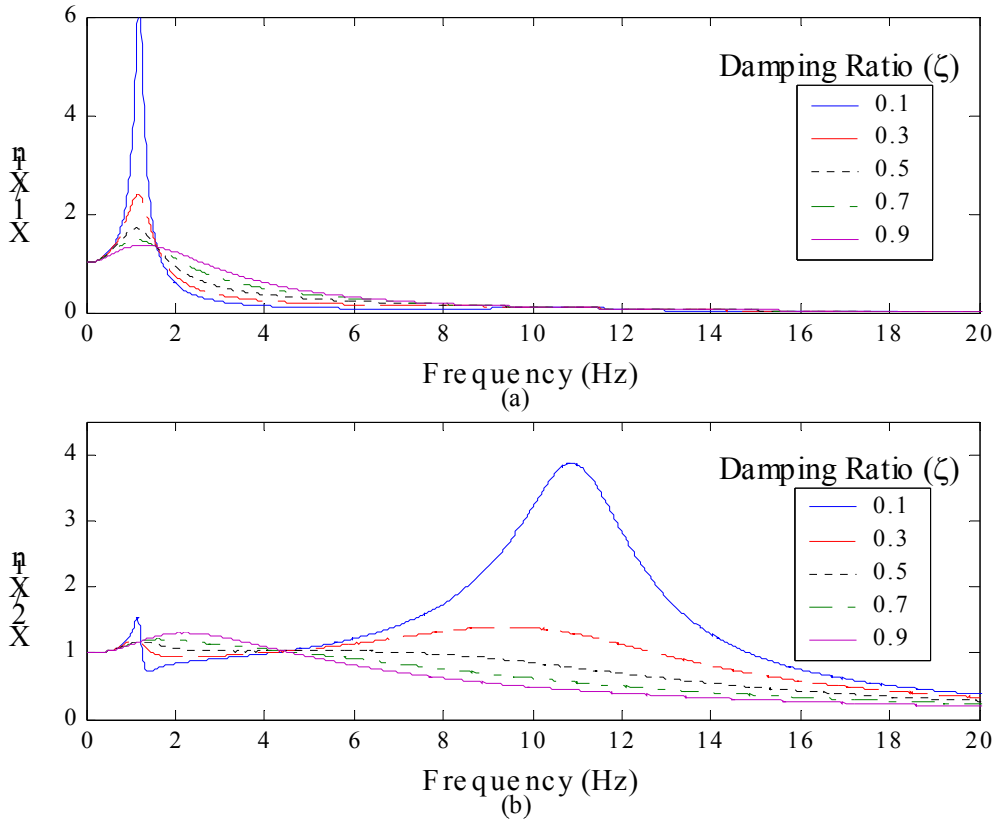

Figure 2-2. Passive Suspension Transmissibility:
(a) Sprung Mass Transmissibility; (b) Unsprung Mass Transmissibility

Notice that at low passive damping, the resonant transmissibility (around $\omega = \omega_{n1}$ or 1.5 Hz and $\omega = \omega_{n2}$ or 10.5Hz) is relatively large, while the transmissibility at higher frequencies is quite low. As the damping is increased, the resonant peaks are attenuated, but isolation is lost both at high frequency and at frequencies between the two natural frequencies of the system. The lack of isolation between the two natural frequencies is caused by the increased coupling of the two degrees of freedom with a stiffer damper. The lack of isolation at higher frequencies will result in a harsher vehicle ride. These transmissibility plots graphically illustrate the inherent tradeoff between resonance control and high frequency isolation that is associated with the design of passive vehicle suspension systems.

The equations of motion for the 2DOF system can be written in matrix form as

$$\begin{bmatrix} m_1 & 0 \\ 0 & m_2 \end{bmatrix}\begin{Bmatrix} \ddot{x}_1 \\ \ddot{x}_2 \end{Bmatrix}+\begin{bmatrix} c & -c \\ -c & c \end{bmatrix}\begin{Bmatrix} \dot{x}_1 \\ \dot{x}_2 \end{Bmatrix}+\begin{bmatrix} k_1 & -k_1 \\ -k_1 & k_1+k_2 \end{bmatrix}\begin{Bmatrix} x_1 \\ x_2 \end{Bmatrix}=\begin{bmatrix} 0 \\ k_2 \end{bmatrix}x_{in} \tag{2.1}$$

Knowing the physical parameters of the 2DOF system, we can calculate the damping ratio for each DOF. To facilitate this calculation, we will treat the system as two SDOF systems. In order to present the transmissibility plots as a function of damping ratio rather than damping coefficient, we can decouple the equations of motion by neglecting the off-diagonal terms, and then estimate the damping ratio for each mass as

$$\varsigma_1 = \frac{c}{2\sqrt{k_1 m_1}} \tag{2.2}$$

$$\varsigma_2 = \frac{c}{2\sqrt{(k_1+k_2)m_2}} \tag{2.3}$$

While this method of calculating the damping ratio is only valid at low damping, the intent is not to precisely define the damping ratio, but rather to show the effects of increased damping on transmissibility.

2.2 Control Schemes for a 2DOF System

This section will introduce the five 2DOF control schemes of interest in this study. Skyhook, groundhook, and hybrid semi-active control will be presented and compared with a typical 2DOF passive suspension. Two alternative skyhook policies will be discusses as well.

2.2.1 Skyhook Control

As the name implies, the skyhook configuration shown in Figure 2-3 has a damper connected to some inertial reference in the sky. With the skyhook configuration, the tradeoff between resonance control and high-frequency isolation, common in passive suspensions, is eliminated [3]. Notice that skyhook control focuses on the sprung mass; as c_{sky} increases, the sprung mass motion decreases. This, of course, comes at a cost. The skyhook configuration excels at isolating the sprung mass from base excitations, at the expense of increased unsprung mass motion.

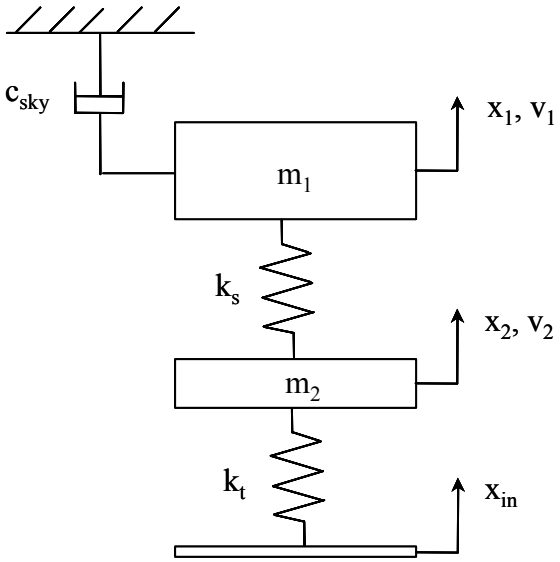

Figure 2-3. Skyhook Damper Configuration

The transmissibility for this system is shown in Figure 2-4 for different values of the skyhook-damping coefficient, c_{sky}. Notice that as the skyhook damping ratio increases, the resonant transmissibility near ω_{n1} decreases, even to the point of isolation, but the transmissibility near ω_{n2} increases. In essence, this skyhook configuration is adding more damping to the sprung mass and taking away damping from the unsprung mass. The skyhook configuration is ideal if the primary goal is isolating the sprung mass from base excitations [4], even at the expense of excessive unsprung mass motion. An additional benefit is apparent in the frequency range between the two natural frequencies. With the skyhook configuration, isolation in this region actually increases with increasing c_{sky}.

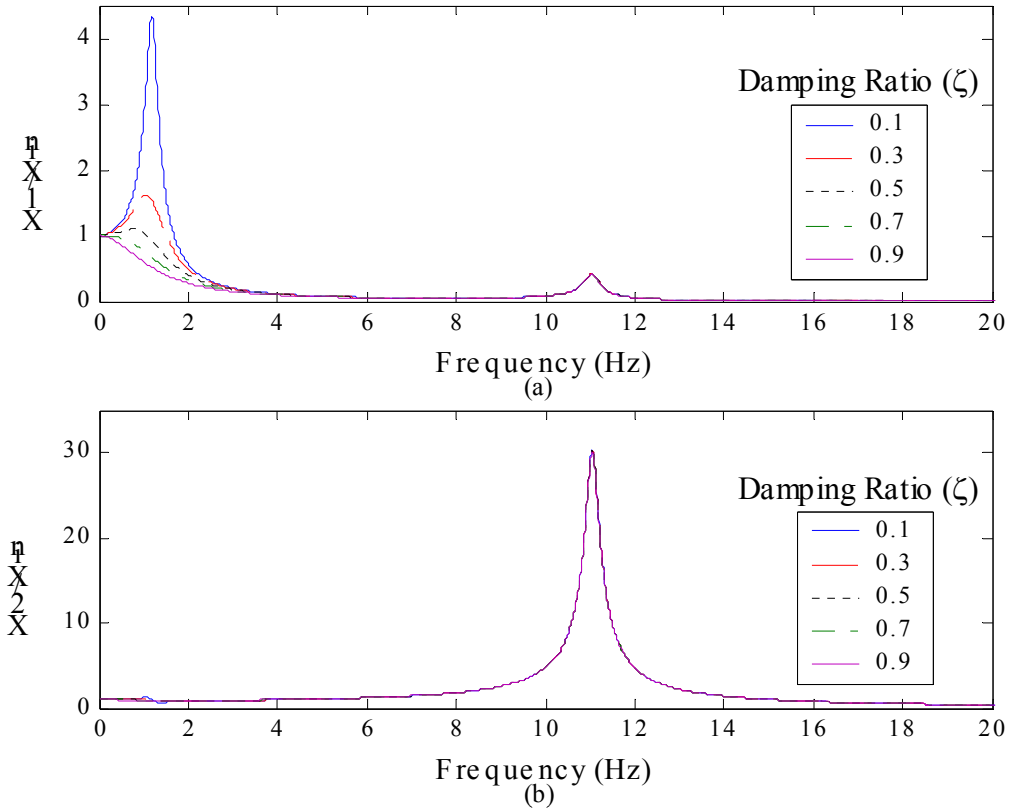

Figure 2-4. Skyhook Configuration Transmissibility:
(a) Sprung Mass Transmissibility; (b) Unsprung Mass Transmissibility

Because this damper configuration is not possible in realistic automotive applications, a controllable damper is often used to achieve a similar response to the system modeled in Figure 2-3. The semi-active damper is commanded such that it acts like a damper connected to an inertial reference in the sky. Figure 2-5 shows the semi-active equivalent model with the use of a semi-active damper.

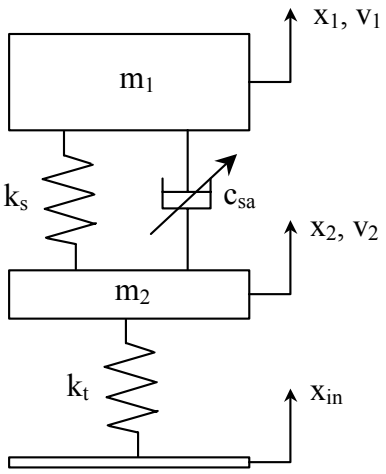

Figure 2-5. Semi-Active Equivalent Model

Several methods exist for representing the equivalent skyhook damping force with the configuration shown in Figure 2-5. Perhaps the most comprehensive way to arrive at the equivalent skyhook damping force is to examine the forces on the sprung mass under several conditions. First, let us define certain parameters and conventions that will be used throughout controller development. Referring to Figure 2-5, the relative velocity, v_{12}, is defined as the velocity of the sprung mass (m_1) relative to the unsprung mass (m_2). When the two masses are separating, v_{12} is positive. For all other cases, up is positive and down is negative.

Now, with these definitions, let us consider the case when the sprung mass is moving upwards and the two masses are separating. Under the ideal skyhook configuration we find that the force due to the skyhook damper is

$$F_{sky} = -c_{sky} v_1 \tag{2.4}$$

where F_{sky} is the skyhook damping force. Next we examine the semi-active equivalent model and find that the damper is in tension and the damping force due to the semi-active damper is

$$F_{sa} = -c_{sa} v_{12} \tag{2.5}$$

where F_{sa} is the semi-active damping force. Now, in order for the semi-active equivalent model to perform like the skyhook model, the damping forces must be equal, or

$$F_{sky} = -c_{sky} v_1 = -c_{sa} v_{12} = F_{sa} \tag{2.6}$$

We can solve for the semi-active damping in terms of the skyhook damping (2.7) and use this to find the semi-active damping force needed to represent skyhook damping when both v_1 and v_{12} are positive (2.8).

$$c_{sa} = \frac{c_{sky} v_1}{v_{12}} \tag{2.7}$$

$$F_{sa} = c_{sky} v_1 \tag{2.8}$$

Next, let us consider the case when both v_1 and v_{12} are negative. Now the sprung mass is moving down and the two masses are coming together. In this scenario, the skyhook damping force would be in the positive direction, or

$$F_{sky} = c_{sky} v_1 \tag{2.9}$$

Likewise, because the semi-active damper is in compression, the force due to the semi-active damper is also positive, or

$$F_{sa} = c_{sa} v_{12} \tag{2.10}$$

Following the same procedure as the first case, equating the damping forces reveals the same semi-active damping force as the first case. Thus, we can conclude that when the product of the two velocities is positive, the semi-active force is defined by equation (2.8).

Now consider the case when the sprung mass is moving upwards and the two masses are coming together. The skyhook damper would again apply a force on the sprung mass in the negative direction. In this case, the semi-active damper is in compression and cannot apply a force in the same direction as the skyhook damper. For this reason, we would want to minimize the damping, thus minimizing the force on the sprung mass.

The final case to consider is the case when the sprung mass is moving downwards and the two masses are separating. Again, under this condition the skyhook damping force and the semi-active damping force are not in the same direction. The skyhook

damping force would be in the positive direction, while the semi-active damping force would be in the negative direction. The best that can be achieved is to minimize the damping in the semi-active damper.

Summarizing these four conditions, we arrive at the well-known semi-active skyhook control policy:

$$\begin{Bmatrix} v_1 v_{12} \geq 0 & F_{sa} = c_{sky} v_1 \\ v_1 v_{12} < 0 & F_{sa} = 0 \end{Bmatrix} \tag{2.11}$$

It is worth emphasizing that when the product of the two velocities is positive that the semi-active damping force is proportional to the velocity of the sprung mass. Otherwise, the semi-active damping force is at a minimum.

2.2.2 Groundhook Control

The groundhook model differs from the skyhook model in that the damper is now connected to the unsprung mass rather than the sprung mass. This modified configuration is shown in Figure 2-6.

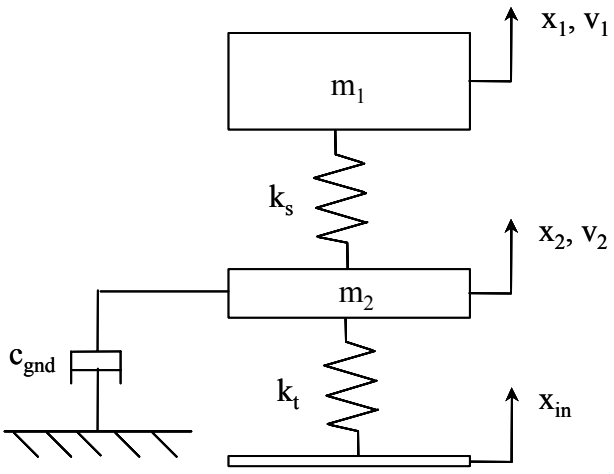

Figure 2-6. Groundhook Damper Configuration

Under the groundhook configuration, the focus shifts from the sprung mass to the unsprung mass. As skyhook control excelled at isolating the sprung mass from base

excitations, groundhook control performs just as well at isolating the unsprung mass from base excitations. Again, this performance comes at the cost of excessive sprung mass motion. The groundhook configuration effectively adds damping to the unsprung mass and removes it from the sprung mass as shown in the transmissibility plots in Figure 2-7.

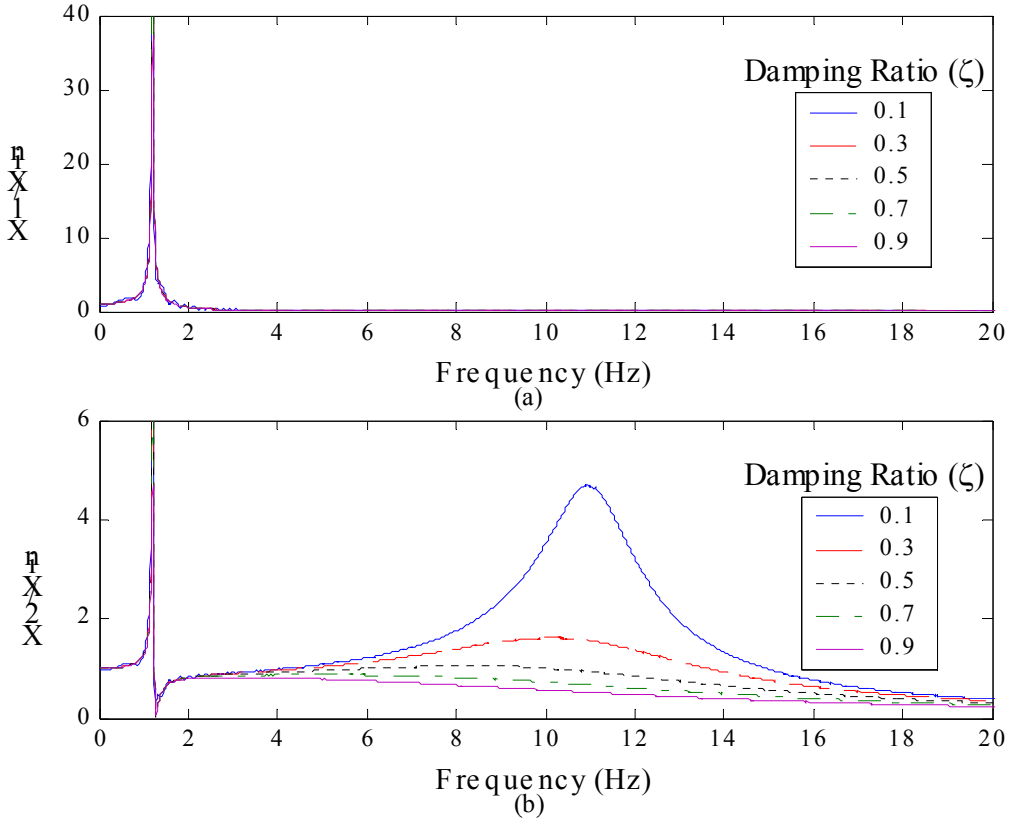

Figure 2-7. Groundhook Configuration Transmissibility:
(a) Sprung Mass Transmissibility; (b) Unsprung Mass Transmissibility

Through the same reasoning used for skyhook control, it can easily be shown that the groundhook semi-active control policy reduces to:

$$\begin{Bmatrix} -v_2 v_{12} \geq 0 & F_{sa} = c_{gnd} v_2 \\ -v_2 v_{12} < 0 & F_{sa} = 0 \end{Bmatrix} \quad \textbf{(2.12)}$$

2.2.3 Hybrid Control

An alternative semi-active control policy known as hybrid control has been shown to take advantage of the benefits of both skyhook and groundhook control [5]. With hybrid control, the user has the ability to specify how closely the controller emulates skyhook or groundhook. In other words, hybrid control can divert the damping energy to the bodies in a manner that eliminates the compromise that is inherent in passive dampers. The hybrid configuration is shown in Figure 2-8.

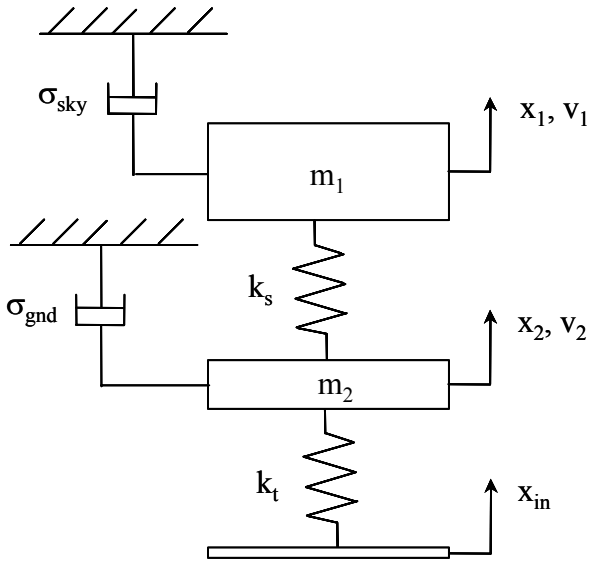

Figure 2-8. Hybrid Configuration

Using hybrid control, the user can specify how closely the controller resembles skyhook or groundhook. Combining the equations (2.11) and (2.12) we arrive at the semi-active hybrid control policy:

$$\begin{Bmatrix} v_1 v_{12} \geq 0 & \sigma_{sky} = v_1 \\ v_1 v_{12} < 0 & \sigma_{sky} = 0 \end{Bmatrix}$$

$$\left\{F_{sa} = G\left[\alpha\sigma_{sky} + (1-\alpha)\sigma_{gnd}\right]\right\} \qquad \textbf{(2.13)}$$

$$\begin{Bmatrix} -v_2 v_{12} \geq 0 & \sigma_{gnd} = v_2 \\ -v_2 v_{12} < 0 & \sigma_{gnd} = 0 \end{Bmatrix}$$

where σ_{sky} and σ_{gnd} are the skyhook and groundhook components of the damping force. The variable α is the relative ratio between the skyhook and groundhook control, and G is a constant gain. As the transmissibility plots in Figure 2-9 show, when α is 1, the control policy reduces to pure skyhook, whereas when α is 0, the control is purely groundhook. These transmissibilities were generated with a damping ratio of 0.3.

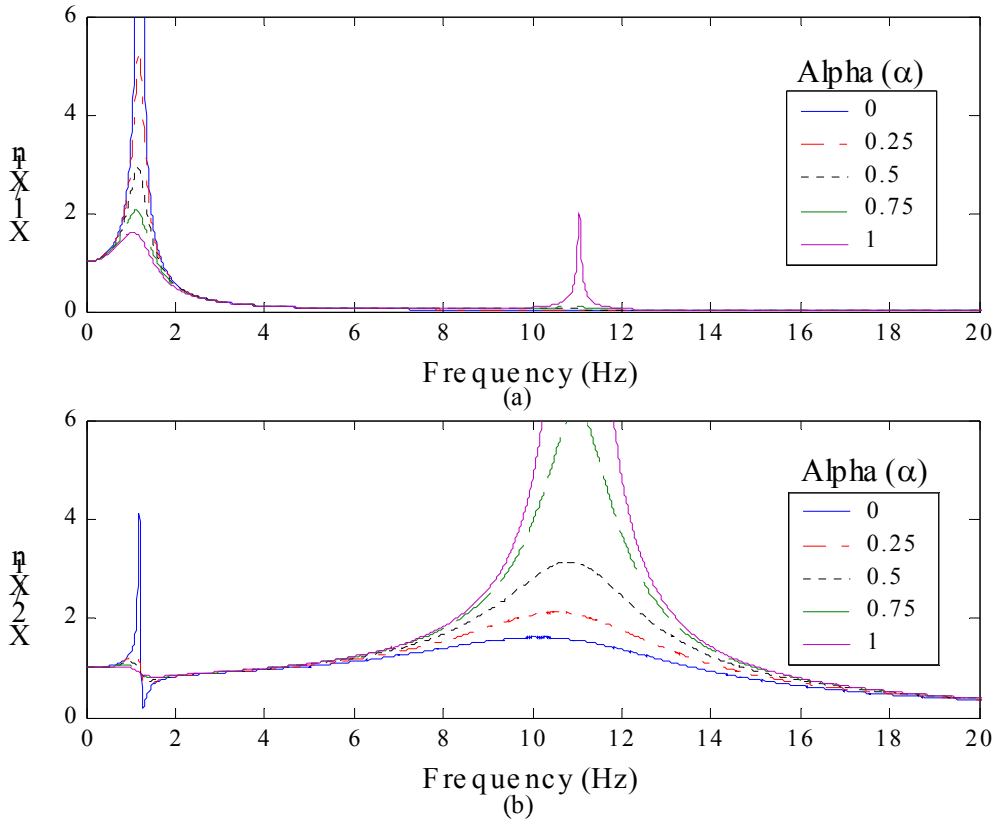

Figure 2-9. Hybrid Configuration Transmissibility:
(a) Sprung Mass Transmissibility; (b) Unsprung Mass Transmissibility

2.2.4 Alternative Skyhook Control Policies

This research also explored the benefits of two alternative skyhook based control strategies. The physical representation of these two policies remains unchanged from conventional skyhook. Distinguishing these two controllers from skyhook is the

condition by which the damper force is applied. The first alternative skyhook policy is a displacement based skyhook algorithm and can be described by:

$$\begin{Bmatrix} x_1 v_{12} \geq 0 & F_{sa} = c_{sky} v_1 \\ x_1 v_{12} < 0 & F_{sa} = 0 \end{Bmatrix} \quad \textbf{(2.14)}$$

In the case of displacement skyhook, the semi-active force, F_{sa}, remains the same. However, now the governing condition is the product of x_1 and v_{12} rather than v_1 and v_{12}.

The second alternative skyhook control policy is relative displacement skyhook. Relative displacement skyhook can be expressed as:

$$\begin{Bmatrix} v_1 x_{12} \geq 0 & F_{sa} = c_{sky} v_1 \\ v_1 x_{12} < 0 & F_{sa} = 0 \end{Bmatrix} \quad \textbf{(2.15)}$$

where now the governing condition is the product of v_1 and x_{12}. The semi-active force remains the same. The two alternative skyhook policies were evaluated for their benefits relative to traditional skyhook control.

2.2.5 Passive vs. Semi-Active Dampers

The previously mentioned benefits of semi-active dampers over passive dampers are clearly evident if we compare the transmissibilities for passive, skyhook, groundhook, and hybrid damping. Figure 2-10 shows the transmissibility of each at a damping ratio of 0.3. The hybrid control transmissibility is shown with an alpha of 0.5.

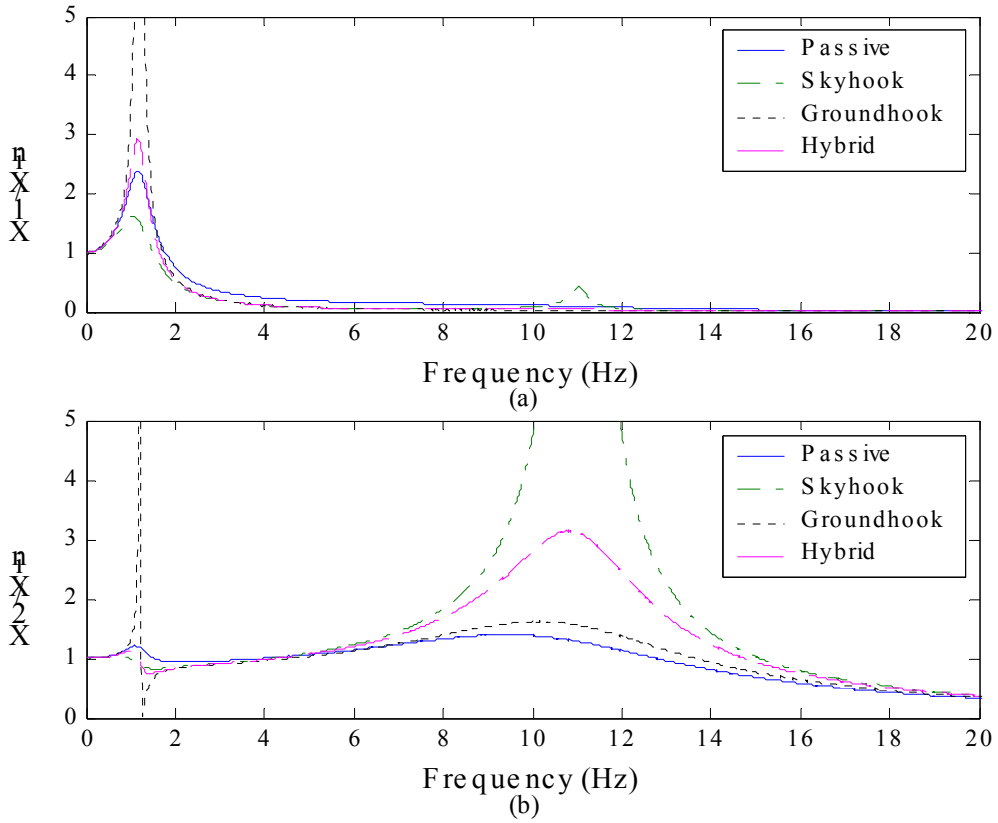

Figure 2-10. Transmissibility Comparison of Passive and Semiactive Dampers: (a) Sprung Mass Transmissibility; (b) Unsprung Mass Transmissibility

2.3 Magneto-Rheological Dampers

The purpose of this section is to introduce the theoretical and practical applications of magneto-rheological (MR) fluid for a controllable MR damper. First, the concept of MR fluid will be introduced. Next, the practical realization of an MR damper will be discussed. Finally, the performance of the MR damper used for this research will be investigated.

2.3.1 Magneto-Rheological Fluids

Magneto-rheological fluids are materials that exhibit a change in rheological properties (elasticity, plasticity, or viscosity) with the application of a magnetic field. The MR effects are often greatest when the applied magnetic field is normal to the flow of the MR

fluid. Another class of fluids that exhibit a rheological change is electro-rheological (ER) fluids. As the name suggests, ER fluids exhibit rheological changes when an electric field is applied to the fluid. However, there are many drawbacks to ER fluids, including relatively small rheological changes and extreme property changes with temperature. Although power requirements are approximately the same [6], MR fluids require only small voltages and currents, while ER fluids require very large voltages and very small currents. For these reasons, MR fluids have recently become a widely studied 'smart' fluid.

Besides the rheological changes that MR fluids experience while under the influence of a magnetic field, there are often other effects such as thermal, electrical, and acoustic property changes. However, in the area of vibration control, the MR effect is most interesting since it is possible to apply the effect to a hydraulic damper. The MR fluid essentially allows one to control the damping force of the damper by replacing mechanical valves commonly used in adjustable dampers. This offers the potential for a superior damper with little concern about reliability; if the MR damper ceases to be controllable, it simply reverts to a passive damper.

2.3.2 Construction of an MR Damper

Magneto-rheological fluids are manufactured by suspending ferromagnetic particles in a carrier fluid. The ferromagnetic particles are often carbonyl particles, since they are relatively inexpensive. Other particles, such as iron-cobalt or iron-nickel alloys, have been used to achieve higher yield stresses from the fluid [7]. Fluids containing these alloys are impractical for most applications due to the high cost of the cobalt or nickel alloys.

A wide range of carrier fluids such as silicone oil, kerosene, and synthetic oil can be used for MR fluids. The carrier fluid must be chosen carefully to accommodate the high temperatures to which the fluid can be subjected. The carrier fluid must be compatible with the specific application without suffering irreversible and unwanted property changes. The MR fluid must also contain additives to prevent the sedimentation of, and promote the dispersion of, the ferromagnetic particles.

A functional representation of an MR damper, with schematics of the components necessary for operation, is shown in Figure 2-11. The fluid that is transferred from above the piston to below (and vice versa) must pass through the MR valve. The MR valve is a fixed-size orifice with the ability to apply a magnetic field, using an electromagnet, to the orifice volume. This magnetic field results in a change in viscosity of the MR fluid, causing a pressure differential for the flow of fluid in the orifice volume. The pressure differential is directly proportional to the force required to move the damper rod. As such, the damping characteristic of the MR damper is a function of the electrical current flowing into the electromagnet. This relationship allows the damping of an MR damper to be easily controlled in real time.

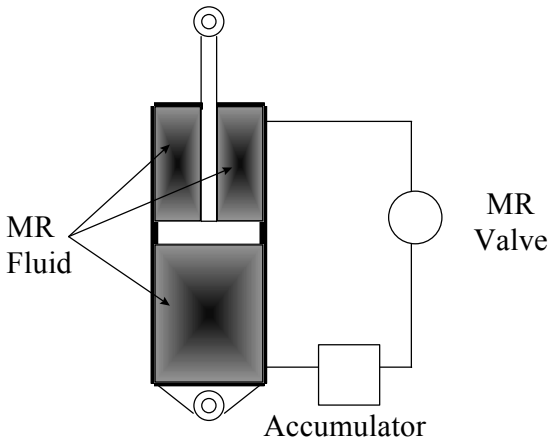

Figure 2-11. Functional Representation of an MR Damper

The accumulator is a pressurized volume of gas that is physically separated from the MR fluid by a floating piston or bladder. The accumulator serves two purposes. The first is to provide a volume for the MR fluid to occupy when the shaft is inserted into the damper cylinder. The second is to provide a pressure offset so that the pressure in the low-pressure side of the MR valve does not induce cavitation in the MR fluid by reducing the pressure below the vapor pressure of the MR fluid.

A sectional view of the MR damper designed and built by James Poynor, through the Advanced Vehicle Dynamics Laboratory at Virginia Tech is shown in Figure 2-12.

This particular damper is a mono-tube damper with a two-stage piston. A two-stage piston was chosen in order to reduce the compromise between low off-state and high on-state damping. In order to reduce the off-state damping, the fluid gap would have to be increased. An increased fluid gap, however, decreases the on-state damping. A two-stage piston compensates for the increased fluid gap by adding more "choking regions," which increases the on-state damping [8]. Figure 2-13 shows a close-up sectional which identifies the fluid gap and "choking regions."

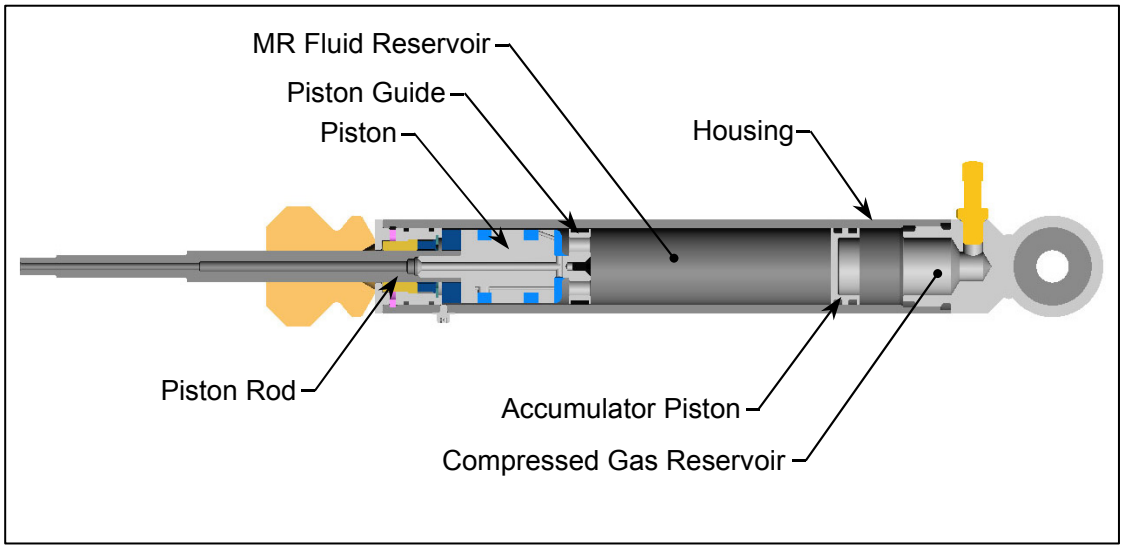

Figure 2-12. Sectional view of MR damper built by James Poynor

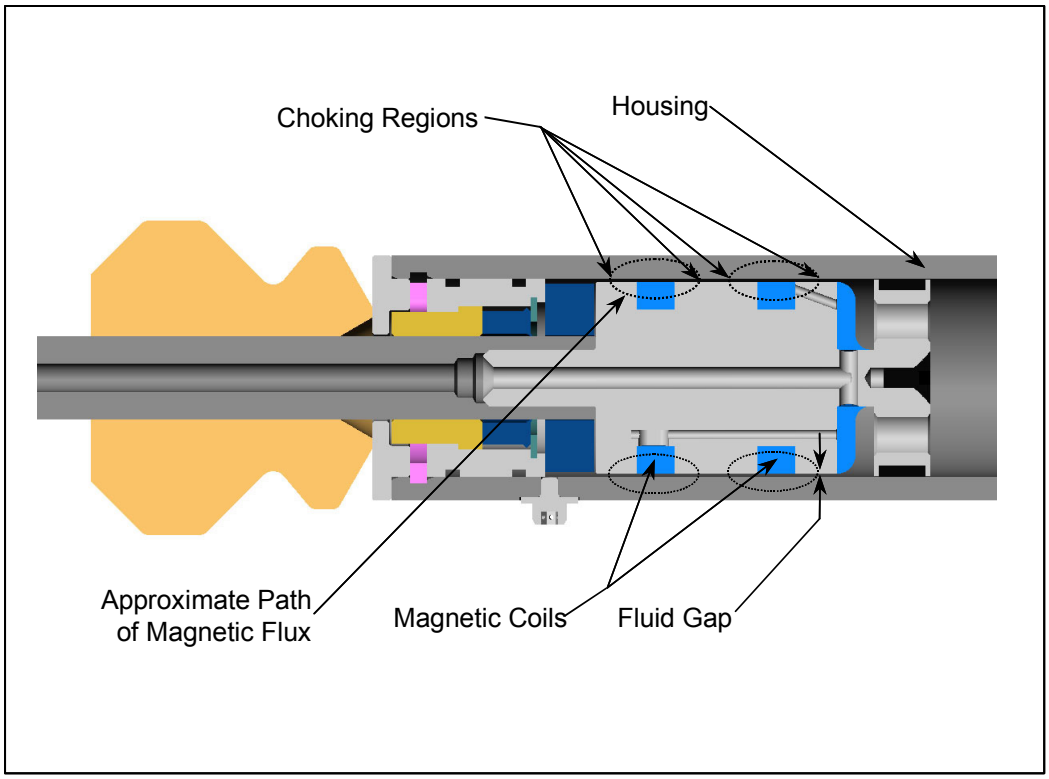

Figure 2-13. Close-up sectional identifying "choking regions" and fluid gap

The actual hardware shown in Figure 2-14 is the damper that was used throughout this work. All of the components have been incorporated internally, providing a compact design that is very similar in size and shape to existing passive vehicle dampers. The only external parts are the two electrical leads for the electromagnet, which are connected to the current source.

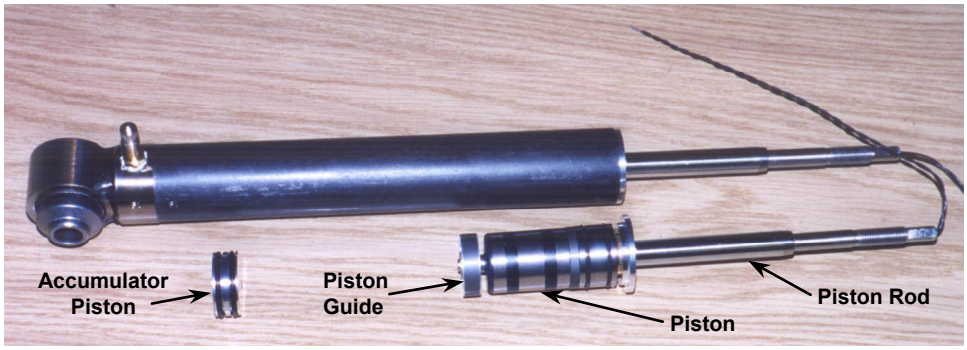

Figure 2-14. Test MR damper and internal components

2.3.3 MR Damper Dynamics

For typical passive dampers, the damper performance is often evaluated based on the force vs. velocity characteristics. For a linear viscous damper, the force vs. velocity performance is shown in Figure 2-15. The slope of the force vs. velocity line is known as the damper coefficient, *c*. In practice, however, the force vs. velocity line is frequently bilinear and asymmetric, with a different value of *c* for jounce (compression) and rebound (extension), as shown in Figure 2-16. The reason for having asymmetric damping characteristics stems from the final application of the damper in a vehicle suspension. When working in series with the primary spring of the vehicle suspension, the damper is working against the spring force in compression and is greatly aided by the spring force in rebound. If the vehicle encounters a pothole or momentary loss of contact with the road, the only mechanism preventing the suspension from rebounding to the physical stops is the rebound damping [9].

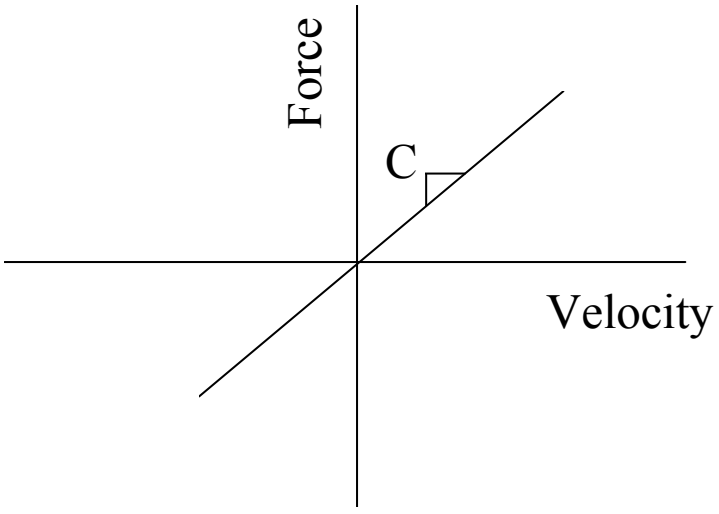

Figure 2-15. Linear Damper Characteristics

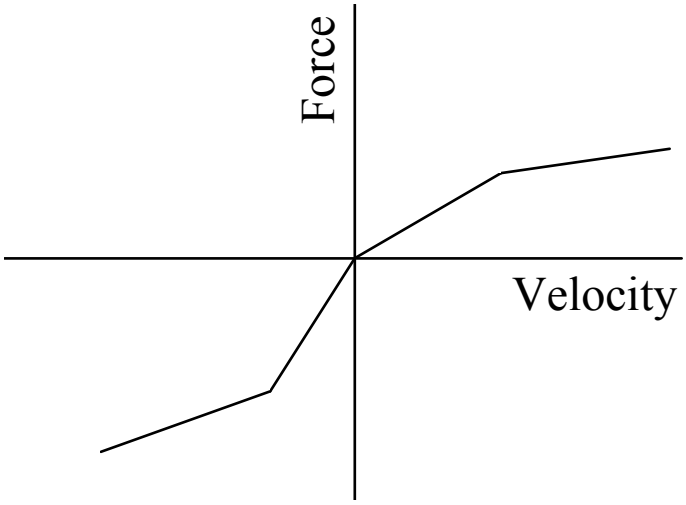

Figure 2-16. Bilinear, Asymmetric Damping Characteristics

Because the characteristics of a passive damper are fixed, the damping curve is tuned by a ride engineer for each particular application. Therefore, the operational envelope of a passive damper is confined to one pre-designed force-velocity characteristic.

In the case of MR dampers, the force-velocity characteristics are not limited to one curve. The ideal force-velocity characteristics of an MR damper are shown in Figure 2-17. The result of the MR technology is a force vs. velocity envelope that is spanned by an area rather than a line in the force-velocity plane. In this ideal case, the damper force is independent of the shaft velocity, and is only a function of the current going into the coil. Effectively, the controller can be programmed to emulate any damper force-velocity characteristic or control policy within the envelope.

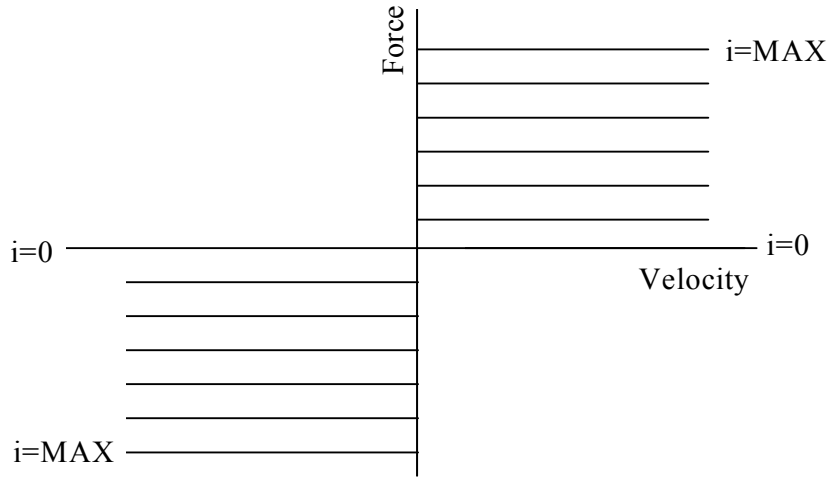

Figure 2-17. Ideal MR Damper Performance

We can model the ideal MR damper according to

$$F_{MRDamper} = \alpha i \tag{2.16}$$

where α is a constant and i is the damper current. Figure 2-18 shows the actual nonlinear force-velocity characteristics for the MR damper used for this research. The model in equation (2.14) and Figure 2-17 do not capture the fine details of the actual MR damper. Some of the effects missing from the model include the magnetic field saturation, hysteresis, and the force due to the pressurized accumulator. As will be shown in later chapters, this approximation is sufficient for designing MR dampers for most applications, including vehicle suspensions.

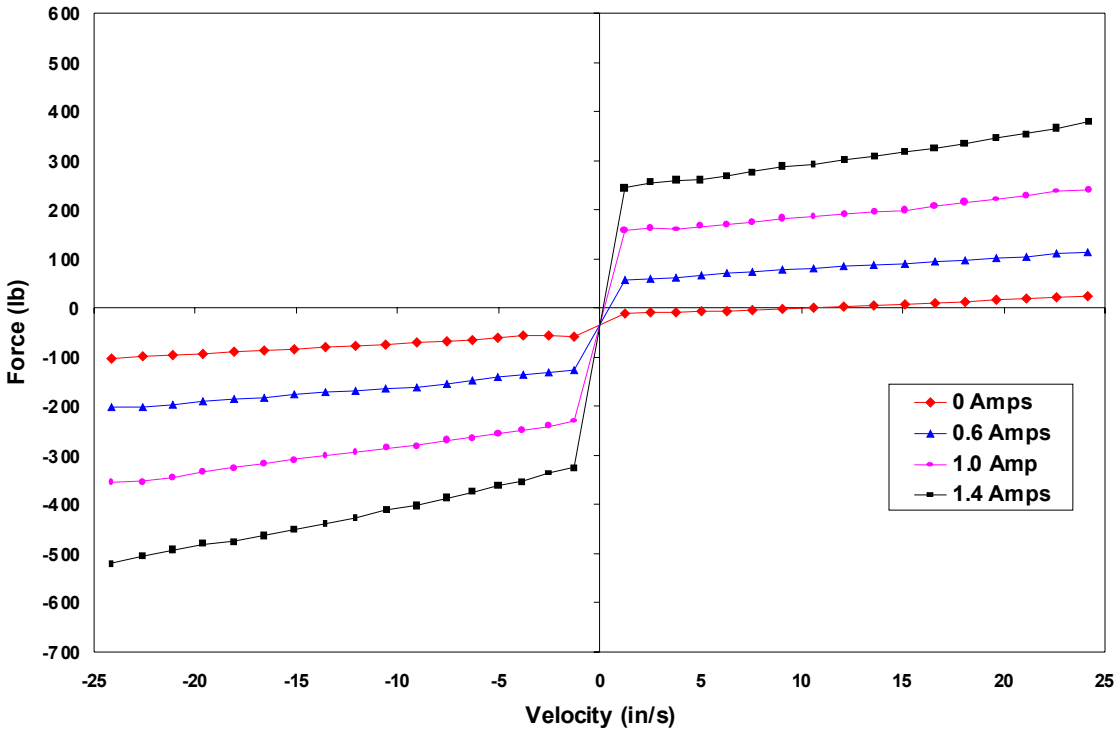

Figure 2-18. MR Damper Damping Force Envelope

2.4 Literature Review

A literature search was performed to investigate what others have done in areas relating to this work. The search included the areas of semi-active dampers, magneto-rheological fluid devices, and semi-active control. Aiding with the literature search, the Comprehensive Engineering Index or Compendex database was used to search for specific key words.

2.4.1 Keyword: Semi-Active

Searching under semi-active resulted in many papers that discussed the performance benefits of semi-active control on semi-active dampers. Lieh and Li [10] discuss the benefits of an adaptive fuzzy control compared to simple on-off and variable semi-active suspensions. The intent of their work is to apply a fuzzy logic concept to control semi-active damping that is normally nonlinear with stochastic disturbances. A quarter-car model was used to implement the fuzzy control rule.

A paper by Hennecke *et al.* [11] discussed the development of a semi-active suspension for BMW's top models. Their work showcases BMW's latest advancement in their adaptive, frequency-dependent damper control. The system has three discrete, digressive damping characteristics, and varies the damping forces at the front and rear axles independently. In their work, the authors describe the frequency-selective and amplitude-dependent control strategy. The system shows potential for improving comfort and road safety.

The study by Ahmadian [12] examines the effects of semi-active damping on a class 8 truck. The truck was tested on both city streets and highway roads under different damper configurations. Placing semi-active dampers on the front axle and passive dampers on the rear axles proved to be a better configuration than semi-active dampers on the rear axles and passive dampers on the front axle. The ride quality of the first configuration was shown to be nearly equal to that of semi-active dampers on all axles.

A preview estimation technique is used in studies performed by Hac and Youn [13], and Huisman *et al.* [14]. The semi-active controller uses knowledge of approaching road disturbances from preview sensors to minimize the response to these disturbances. Giua *et al.* [15], Lieh [16], and Giua *et al.* [17] use optimal control techniques for use in semi-active suspensions.

2.4.2 Keyword: Magneto-Rheological Damper

The papers reviewed under this search category revealed several different applications of MR dampers. The first by Lee and Choi [18] presented the control characteristics of a full-car suspension with a MR damper. This study progressed into a full-car model where vertical, pitch, and roll motions were included. The control characteristics are evaluated through hardware-in-the-loop simulations.

Sims *et al.* [19] presented a less conventional use for MR fluid. Their work used a MR damper in the squeeze-flow mode. In squeeze-flow mode large, controllable forces can be generated over small displacement ranges. The authors describe a MR squeeze-flow device incorporated as the damping element in a vibration isolator.

MR dampers have reached into several other less conventional realms. Ahmadian [20] discusses the development of MR dampers for use in bicycle suspensions. Results show that properly designed MR dampers can provide significant performance benefits over traditional passive bicycle dampers. Peel *et al.* [21] present the benefits of using MR dampers to control the lateral vibrations of a modern rail vehicle. It is shown that a controllable MR damper can be designed to improve upon the specification for a conventional lateral railcar damper. Furthermore, Ahmadian *et al.* [22] studied the advantages of using MR dampers for controlling shock loading. Their work shows that using a system that includes a 50-caliber rifle and a MR damper, the MR damper can be quiet effective in controlling the compromise that exists between shock forces and strokes across the shock absorber. This experimental study further shows that MR dampers can be used to adjust the shock loading characteristics in a manner that fits the dynamic system constraints and requirements. Choi *et al.* [23] explore the use of MR fluid dampers in semi-active seat suspensions. A skyhook control scheme is employed to reduce the vibration level at the driver's seat.

2.4.3 Keyword: Skyhook

The skyhook search resulted in several papers dealing directly with the implementation of skyhook control in vehicle applications. Shon *et al.* [24] explore skyhook control for the semi-active Macpherson suspension system. The absolute velocity of the sprung mass and the relative velocity across the damper are estimated. The semi-active damper is included in the loop of computer simulations so as to incorporate the non-linearity, time-delay, and unmodeled dynamics of the continuously variable damper. Ikenaga *et al.* [25] include skyhook damping in their study of suspension control of ground vehicles based on a full-vehicle model. Another study by Ikenaga *et al.* [26] shows that motions of the sprung mass above and below the wheel hop mode can be diminished using skyhook damping plus active filtering of spring and damping coefficients.

Several other papers demonstrate the benefits of using skyhook damping for vehicle applications. Akatsu *et al.* [27] developed an active suspension employing an electrohydraulic servo system. Their system features a skyhook damper which can reduce body vibration to less than one-half that of conventional suspensions at low

frequencies. Hrovat and Hubbard [28] explore using a skyhook spring as well as a skyhook damper in a simple single-degree-of-freedom vehicle model. Their performance index includes RMS jerk along with the more conventional RMS acceleration.

Finally, Ahmadian [29] discusses the advantages of using skyhook dampers for secondary suspensions. It is shown that semi-active skyhook dampers provide a more favorable control of the dynamic resonance without decreasing the isolation effectiveness of the suspension. Furthermore, the study shows that the skyhook damper offer more control at one body at the expense of less control on the other body. In his study, Ahmadian also introduces an alternative semi-active control policy called hybrid control which can provide better control of both bodies.

2.4.4 Literature Review Summary

Of the previous studies mentioned in this literature review, the majority have been analytical studies. Model simulations and analytical studies have dominated the studies in this area. To date, few works have thoroughly investigated the commonly considered semi-active control policies, such as skyhook control. The research presented in the following chapters intends to contribute to the investigation of semi-active control. The extensive experimental analysis presented in this research aims to complement the analytical studies of the past.

3 Experimental Setup

Included in this chapter is a detailed description of the test setup used throughout this work. Each aspect of the laboratory testing is discussed, beginning with the hardware components and ending with the software components. The chapter begins with a description of the quarter-car rig and its mechanics. This is followed by a description of both the actuation system used to excite the quarter-car rig, and the transducers used to measure the sensory information. The software components include the dSPACE package and the Simulink toolbox in MATLAB, which were used together as the data acquisition system and as the controller during all testing.

3.1 Mechanics of the Quarter-Car Rig

The quarter-car rig at the AVDL was designed as a physical representation of a classic 2-degree of freedom (2DOF) system. In the physical implementation of the 2DOF model, each component of the quarter-car was chosen to closely resemble the characteristics of one quarter of a passenger vehicle. Figure 3-1 shows a 2-DOF system along with the quarter-car rig.

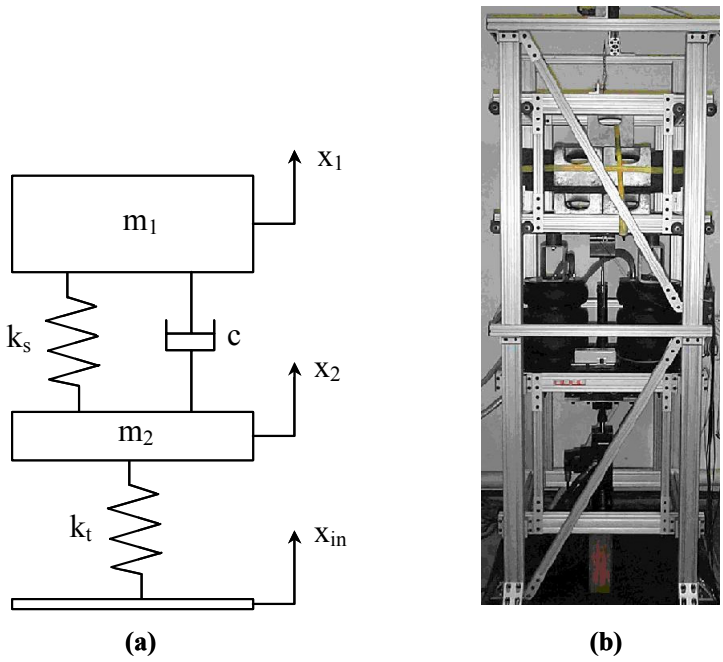

Figure 3-1. 2DOF "Quarter-Car Model": (a) 2DOF System; (b) Quarter-Car Rig

With the use of extruded aluminum manufactured by 80/20 Inc., assembly and adjustments to the quarter-car rig are simplified. The main structure is composed of four 3x3 inch support posts that stand approximately 84 inches tall. Within these four posts, the sprung and unsprung masses are restricted to vertical motion by linear bearings.

The structural integrity of the quarter-car rig is highly influenced by its stiffness. Although the base of the structure is anchored to the ground by lag bolts, three structural modes still need to be considered: side-to-side towering, fore/aft towering, and torsional rotation. In order to avoid poor coherence between input and output, the structural modes of the quarter-car rig had to be raised to well above the frequency range of interest. In the case of this testing, any structural mode below 25 Hz would corrupt the data. For this reason, the quarter-car rig was designed with diagonal members that raise the side-to-side towering mode to well above 25 Hz. These diagonal members also eliminate the torsional mode of the quarter-car rig [30]. Unfortunately, these diagonal members could not be installed in the fore/aft direction due to conflicts with the sprung and unsprung mass vertical motion. To solve this problem, the top of the quarter-car rig was anchored to a nearby wall. With this addition, the three structural modes considered were raised to

well above the frequency range of interest. The structural members used to brace the quarter-car rig are shown in Figure 3-2.

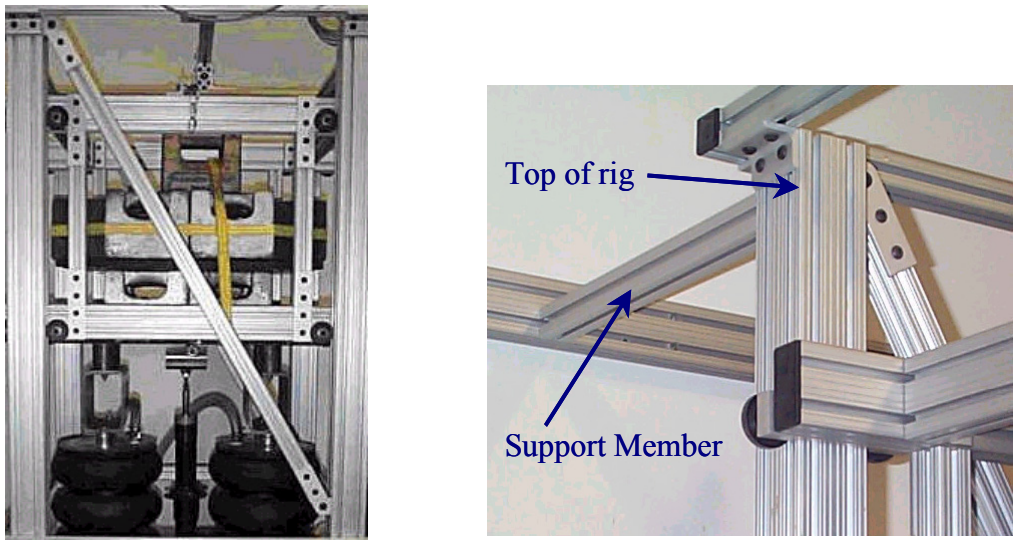

Figure 3-2. Structural Support Members: (a) Eliminates side-to-side and torsional modes; (b) Eliminates fore/aft mode

As stated earlier, the sprung and unsprung masses are mounted to the main structure via linear bearings. The unsprung mass is restricted to vertical motion by eight Teflon-padded bushings that slide along the four main posts. A close-up of one of these Teflon bushings is shown in Figure 3-3. Weighing approximately 100 lb (45 kg), the unsprung mass can represent the weight of a variety of passenger vehicles.

Figure 3-3. Close-up of Teflon Bushings

Connecting the unsprung mass to the hydraulic actuator are eight elastomeric mounts, manufactured by the Lord Corporation. When mounted in parallel, the stiffness of the elastomeric mounts closely resembles the sidewall stiffness of a tire at appropriate air pressure. The arrangement of these mounts is such that they are flexed in their shear axis. This arrangement is shown in Figure 3-4. Because the mounts are about five times stiffer in compression than in shear, the excitations transmitted by the actuator are limited to vertical excitations only [30].

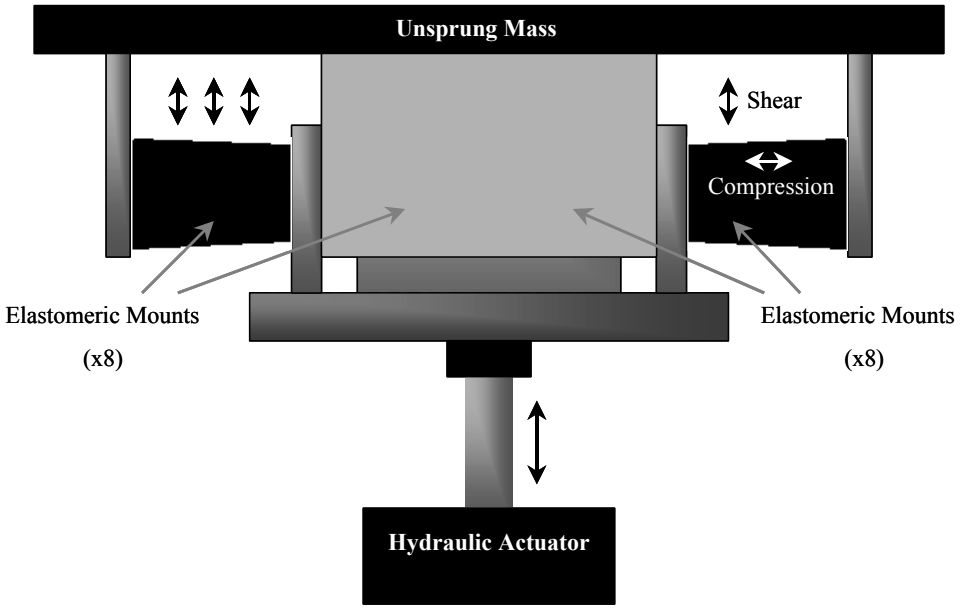

Figure 3-4. Arrangement Used for Emulating Tire Vertical Stiffness

The construction of the sprung mass is very similar to that of the unsprung mass. However, unlike the unsprung mass, the sprung mass uses Roller Wheels manufactured by 80/20 Inc. in place of the Teflon bushings. The Roller Wheels were chosen to reduce the friction, and therefore the damping, in the sprung mass natural frequency. Figure 3-5 shows a close-up of one of these bearings. The weight of the sprung mass can be adjusted with the addition or removal of 50 lb blocks that are fastened to the sprung mass using tie-down straps. For the purpose of this testing, the sprung mass weight was set to approximately 1000 lb (450 kg) to simulate one quarter of the sprung mass of a passenger vehicle.

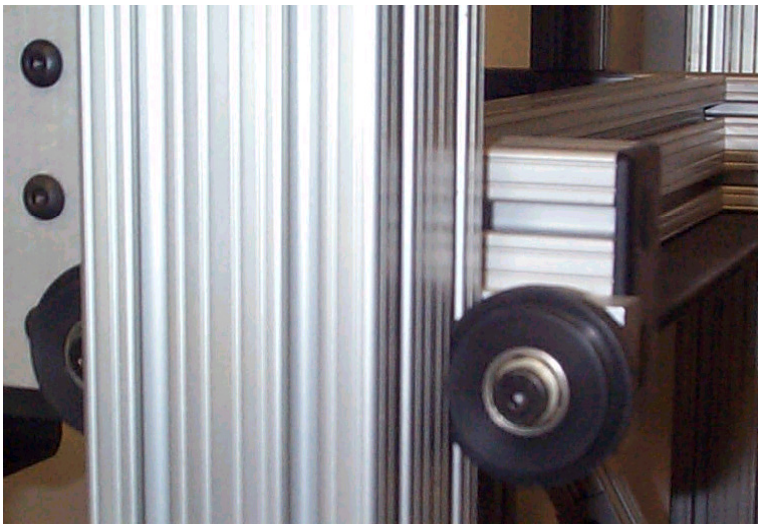

Figure 3-5. Close-up of Roller Wheels

Between the sprung and unsprung masses, two airsprings and a damper represent the primary suspension of a vehicle. The primary suspension is shown in Figure 3-6. Airsprings were chosen because of their stiffness variability, and thus, their ability to model several different vehicle stiffnesses. One problem associated with using airsprings is that they are highly non-linear, with the pressure and thus the stiffness rising as the airspring is compressed. This problem is averted by connecting the airsprings to a 30-gallon air tank that acts as a reservoir, increasing the total volume of the system. With a larger total volume, the change in volume due to the compression of the airspring becomes insignificant. The testing for this work was done with an air pressure of 10 psi which corresponds to a combined stiffness of approximately 200 lb/in. More important, this stiffness along with the arrangement of the sprung and unsprung mass corresponds to sprung and unsprung mass natural frequencies of 1.5 Hz and 10.5 Hz, respectively. These values closely resemble the natural frequencies of a passenger vehicle.

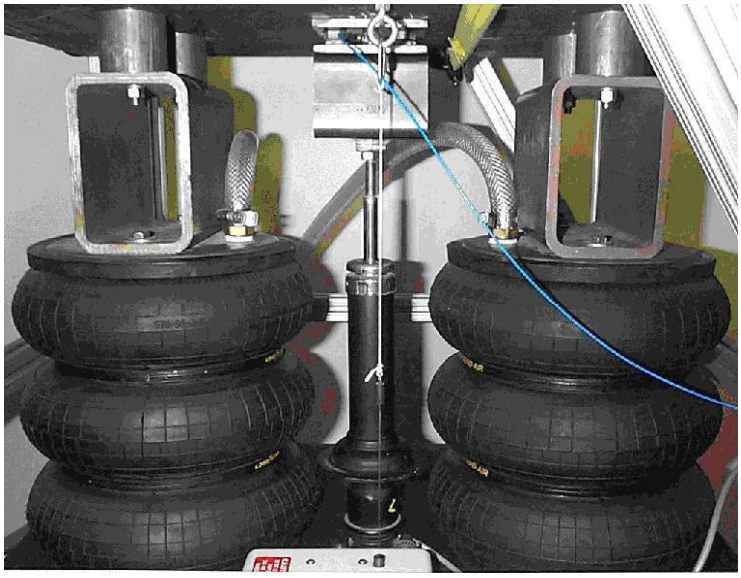

Figure 3-6. Quarter-Car Representation of Primary Suspension

Figure 3-7 identifies the primary components of the quarter car rig: the sprung mass, the unsprung mass, the air springs, the damper, the actuator, and the elastomeric mounts. Together, these six components are used to test the dynamics of a wide variety of passenger vehicles.

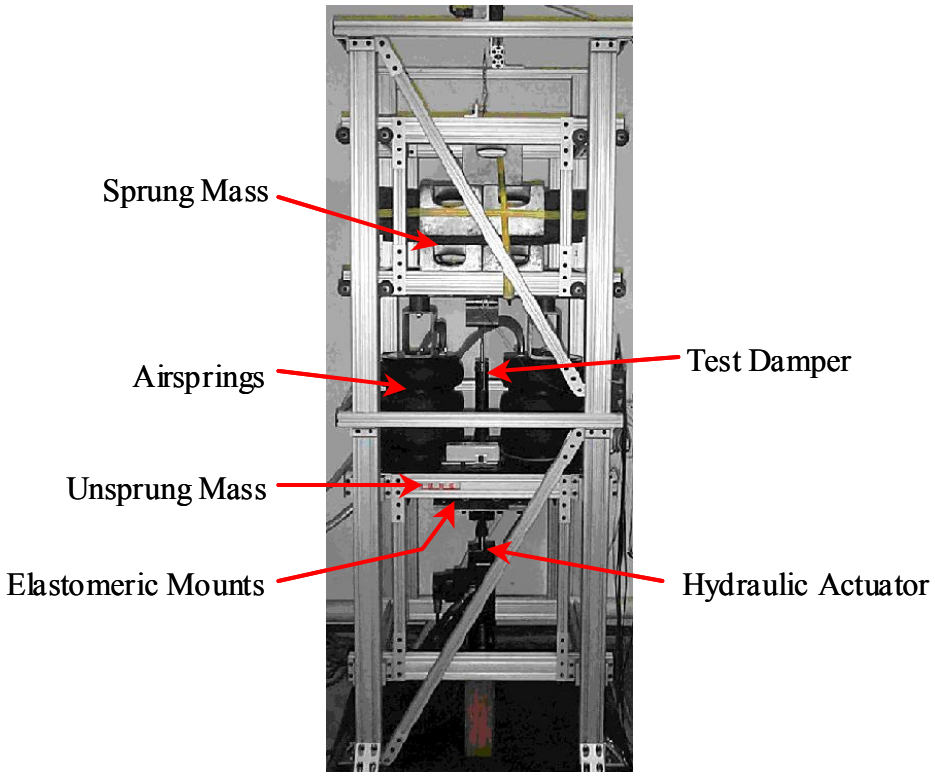

Figure 3-7. Quarter-Car Rig and Primary Components

3.2 Components of Actuation System

Road disturbances were modeled with a hydraulic actuator manufactured by Material Testing Systems (MTS). The hydraulic actuator shown in Figure 3-8 was of four components included in the actuation system. This particular model, MTS model 242.09, has a dynamic stroke of ±2 inches (±5 cm) and a force capacity of ±2200 lb (±10 kN). An internal load cell and position sensor allow for force and position measurements. To avoid any lateral loading on the actuator, MTS swivel ends were incorporated into installation on both ends of the actuator.

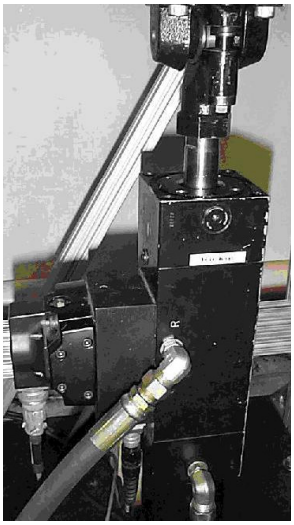

Figure 3-8. MTS 242 Series Hydraulic Actuator

The actuator is controlled by an MTS 407 Controller shown in Figure 3-9. Offering two modes of control, displacement or force, the 407 Controller is a single-channel, digitally supervised, servo controller. All input signals to the actuator, whether external or internal, must go through or be generated by the 407 Controller.

Figure 3-9. MTS 407 Controller

A SilentFlo Hydraulic Power Unit, MTS Model 505.20, is used to provide fluid to the actuation system. This hydraulic pump, shown in Figure 3-10, has a flow rate of 20 gal/min (75 L/min) and an operating pressure of 3000 psi (210 bar).

Figure 3-10. MTS SilentFlo Hydraulic Power Unit

Linking the hydraulic pump and the actuator, a MTS Model 263 Hydraulic Service Manifold is used to regulate the hydraulic pressure and flow to the actuator. The manifold is shown in Figure 3-11. The regulated flow is necessary to ensure proper dynamic response of the actuator.

Figure 3-11. MTS Hydraulic Service Manifold

3.3 Data Acquisition System

Three components made up the data acquisition system: dSPACE, MATLAB, and Simulink. MATLAB was the foundation for Simulink, which, through the Real Time Workshop toolbox, the three components were linked. All models for data acquisition and controller implementation were built within Simulink, complete with inputs and outputs. dSPACE was used to compile these models and load them to the dSPACE DSP chip. The dSPACE system consists of two components, Control Desk and the AutoBox.

Control Desk is the user interface software. Within Control Desk data can be viewed and model parameters can be tuned in real-time. The ability to adjust controller parameters real-time simplifies controller development and makes dSPACE a powerful tool for rapid prototyping.

The hardware component of dSPACE is the dSPACE AutoBox, which contains the DS 1003 processor board. The AutoBox also contains an I/O card with 20 inputs and 8 outputs that were used to collect data and output control signals. Information flows to and from the AutoBox via a dedicated Ethernet connection. The AutoBox is shown in Figure 3-12.

Figure 3-12. dSPACE AutoBox

The signals we are measuring on the quarter-car rig are coming into the AutoBox through the DS2201ADC (analog to digital converter). Within Simulink, the 20 input channels of the AutoBox are multiplexed into 5 ports with 4 input channels per port. For this reason, the signals must pass through a demultiplexer that separates the incoming signals. Real-time control occurs through the use of the DS2201DAC (digital to analog converter). In this case, the 8 ports correspond directly to the 8 output channels on the AutoBox. Figure 3-13 shows the block diagram used for all data acquisition, complete with real-time control outputs for each control policy.

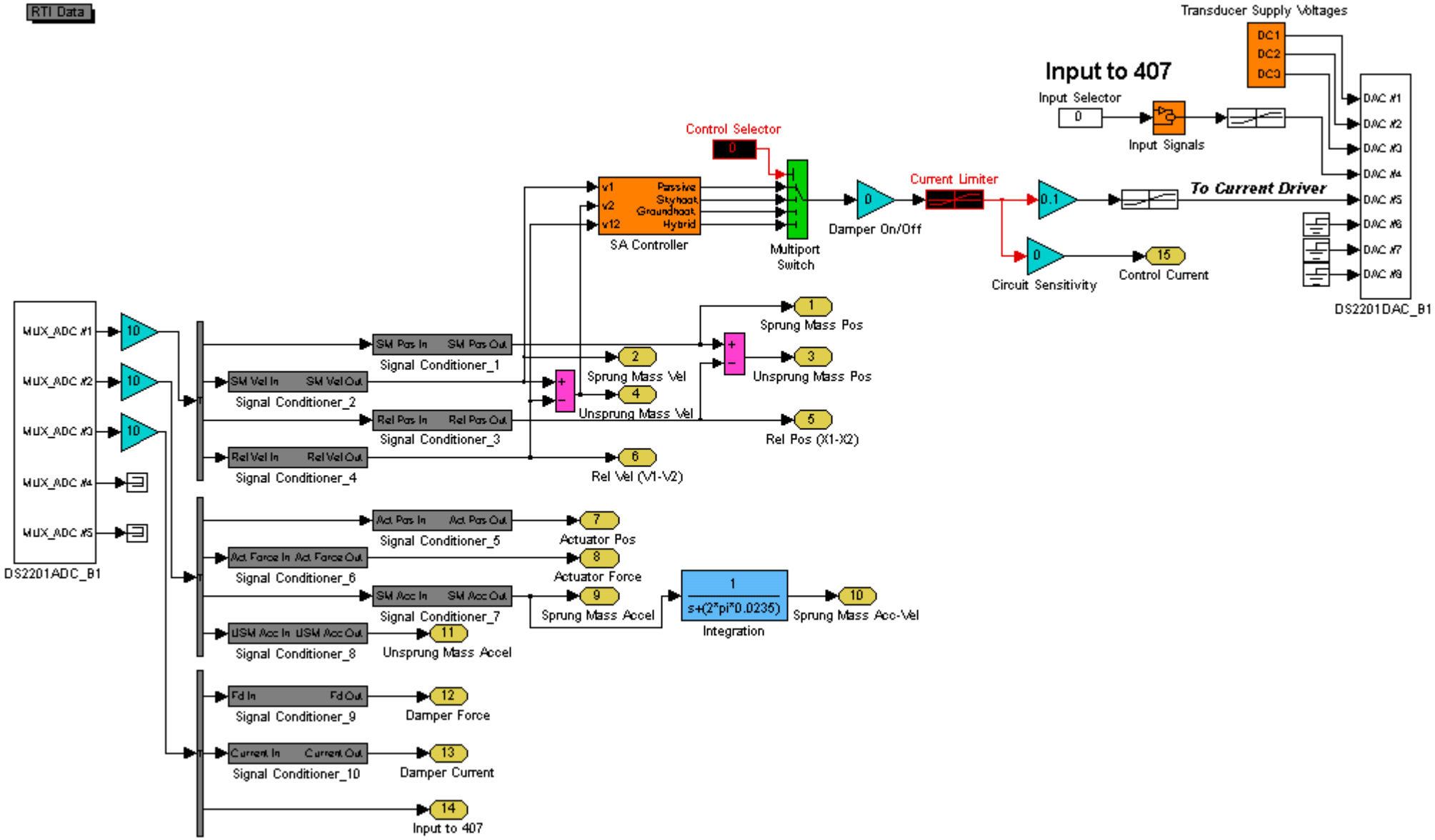

Figure 3-13. Data Acquisition and Control Block Diagram

3.4 Controller Development

Controller development begins by identifying the sensory information necessary to implement each control strategy. In this study, skyhook, groundhook, hybrid, and two alternative skyhook control strategies were employed. Each policy is then built within Simulink and physically implemented through the use of the dSPACE AutoBox.

3.4.1 Skyhook Control Development

In order to identify the sensory information needed for skyhook control, let us recall from Chapter 2 the semi-active skyhook control policy:

$$\begin{Bmatrix} v_1 v_{12} \geq 0 & F_{sa} = c_{sky} v_1 \\ v_1 v_{12} < 0 & F_{sa} = 0 \end{Bmatrix} \quad \textbf{(3.1)}$$

where:

v_1 = absolute velocity of the sprung mass relative to ground

v_{12} = relative velocity between sprung and unsprung masses

F_{sa} = semi-active damping force

c_{sky} = skyhook damping coefficient

At this point, the convenience of laboratory testing becomes clear as it allows us to measure all of these signals directly. Whereas in-vehicle testing many of these signals would have to be measured indirectly through integration or other forms of manipulation, laboratory testing offers the liberty of using many transducers to directly capture the signals needed for control.

Both the absolute velocity (v_1) and the relative velocity (v_{12}) where measured using UniMeasure Velocity-Position Transducers. UniMeasure Model VP510-10, shown in Figure 3-14, was mounted to a stationary reference above the sprung mass. In this configuration, the velocity-position transducer measured both the absolute velocity and the absolute position of the sprung mass with reference to ground. A second UniMeasure Velocity-Position Transducer, Model VPA-10, was mounted between the sprung and unsprung mass to measure both relative velocity and relative displacement. The difference between these two transducers was the power supply requirements. Model

VPA-10 required a well-regulated power supply, not exceeding 25 V, while Model VP510-10 used an unregulated power supply. The power supplies were only necessary for position measurements, as the velocity component of the transducer was self-energizing. With a sensitivity of 197 mV/in/sec and 999 mV/in for velocity and position respectively, these transducers were well suited to our applications and provided a clean signal for real-time control.

Figure 3-14. UniMeasure VP510-10 Velocity-Position Transducer

Building the actual controller used to employ skyhook control occurs within Simulink. The use of Simulink and dSPACE eliminates the need to build a hardware version of the controller. Figure 3-15 shows the control algorithm block diagram for skyhook control. Examining Figure 3-15, it is clear that this block diagram does indeed represent skyhook control; if the product of v_1 and v_{12} is greater than or equal to zero, the damping force is proportional to v_1; otherwise, the damping force is a minimum.

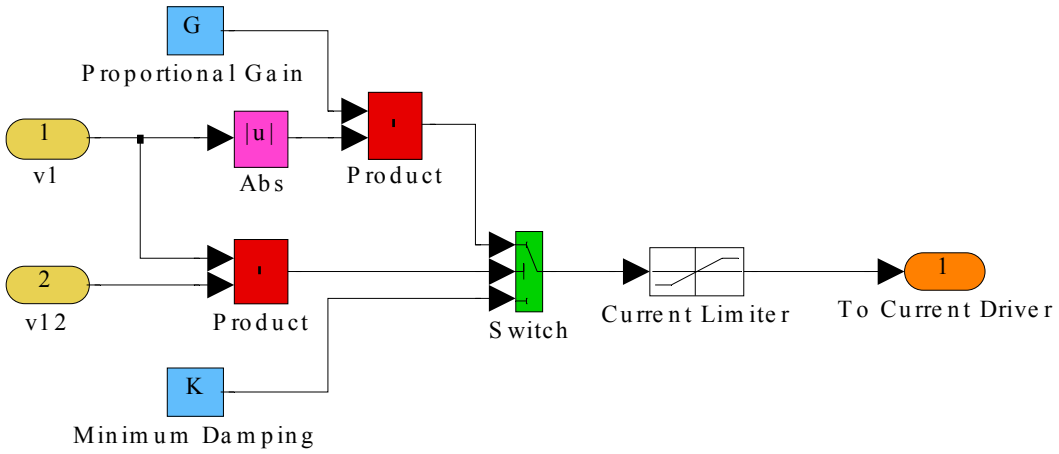

Figure 3-15. Block Diagram for Skyhook Control Logic

3.4.2 Groundhook Control Development

In order to begin with the development of the groundhook control strategy, let us review the semi-active groundhook control policy from Chapter 2.

$$\begin{Bmatrix} -v_2 v_{12} \geq 0 & F_{sa} = c_{gnd} v_2 \\ -v_2 v_{12} < 0 & F_{sa} = 0 \end{Bmatrix} \tag{3.2}$$

where,

v_2 = absolute velocity of unsprung mass with reference to ground

c_{gnd} = groundhook damping coefficient

Our method for measuring v_{12} remains unchanged from the skyhook policy, however, a means for measuring v_2 had to be determined. Since we were measuring the absolute velocity of the sprung mass and the relative velocity between the two masses, through a simple mathematical operation we arrived at v_2. Recall that the relative velocity is defined as the velocity of the sprung mass relative to the unsprung mass (v_1-v_2). Therefore, v_2 is extracted by subtracting v_{12} from v_1. The control strategy block diagram for groundhook control is shown in Figure 3-16.

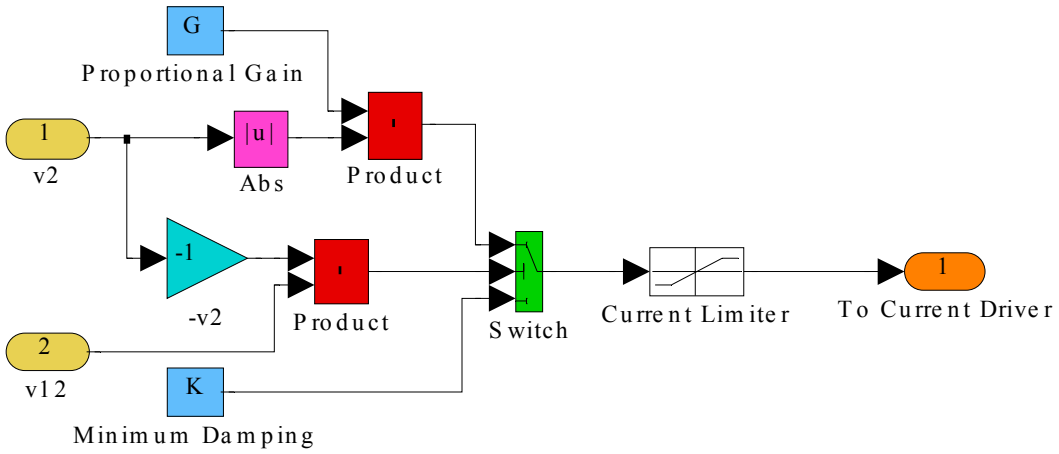

Figure 3-16. Block Diagram for Groundhook Control Logic

3.4.3 Hybrid Control Development

From Chapter 2, recall the semi-active hybrid control policy:

$$\begin{Bmatrix} v_1 v_{12} \geq 0 & \sigma_{sky} = v_1 \\ v_1 v_{12} < 0 & \sigma_{sky} = 0 \end{Bmatrix}$$

$$\left\{ F_{sa} = G\left[\alpha \sigma_{sky} + (1-\alpha)\sigma_{gnd} \right] \right\} \tag{3.3}$$

$$\begin{Bmatrix} -v_2 v_{12} \geq 0 & \sigma_{gnd} = v_2 \\ -v_2 v_{12} < 0 & \sigma_{gnd} = 0 \end{Bmatrix}$$

where,

σ_{sky} = skyhook component of damping force

σ_{gnd} = groundhook component of damping force

α = relative ratio between skyhook and groundhook

G = constant gain

Because the hybrid control policy is a linear combination of skyhook and groundhook, the block diagram for hybrid control, shown in Figure 3-17, is a simple combination of skyhook and groundhook through the use of the variable α.

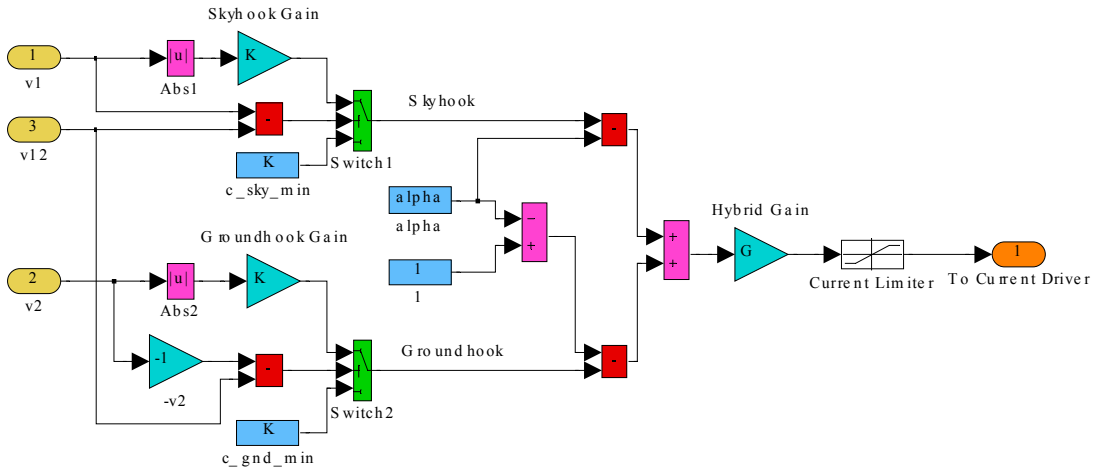

Figure 3-17. Block Diagram for Hybrid Control Logic

3.4.4 Displacement Skyhook Control Development

Recalling the algorithm that defines displacement skyhook,

$$\begin{Bmatrix} x_1 v_{12} \geq 0 & F_{sa} = c_{sky} v_1 \\ x_1 v_{12} < 0 & F_{sa} = 0 \end{Bmatrix} \tag{3.4}$$

where x_1 is the sprung mass displacement, we find that it differs from conventional skyhook by only one parameter. Rather than using v_1, this controller uses x_1 to command the damper. The sprung mass displacement is measured using the same UniMeasure Velocity-Position Transducer shown in Figure 3-14. The only changes occur within Simulink. Because the condition that governs the damper now relies on the sprung mass position, we must add that signal to the controller. The resulting controller is shown in Figure 3-18.

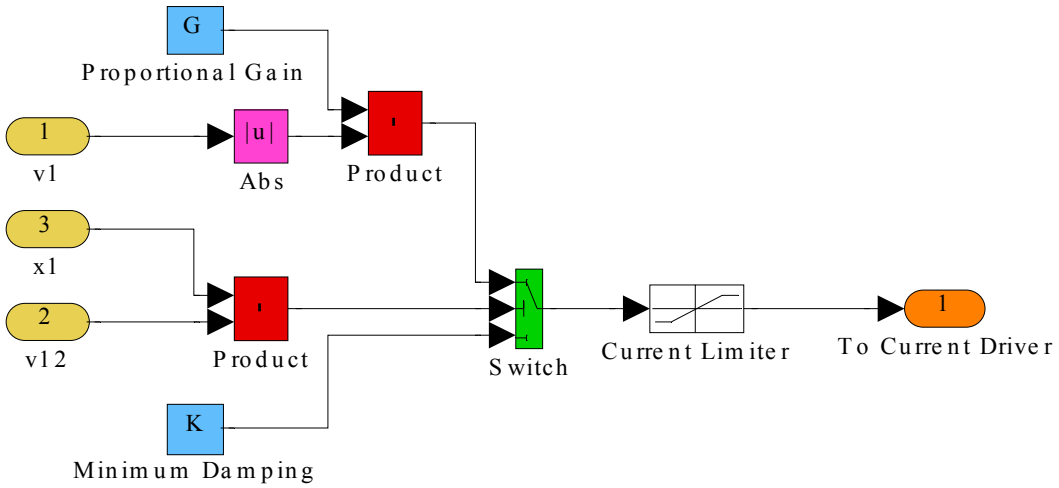

Figure 3-18. Block Diagram for Displacement Skyhook Logic

3.4.5 Relative Displacement Skyhook Control Development

Much like displacement skyhook, the relative displacement skyhook policy does not require added hardware. Recall the definition for relative displacement skyhook:

$$\begin{Bmatrix} v_1 x_{12} \geq 0 & F_{sa} = c_{sky} v_1 \\ v_1 x_{12} < 0 & F_{sa} = 0 \end{Bmatrix} \tag{3.5}$$

where x_{12} is the relative displacement across the damper. Again, we can use the same device used to measure v_{12} for conventional skyhook to measure x_{12} for relative displacement skyhook. The Simulink implementation of this policy is shown in Figure 3-19.

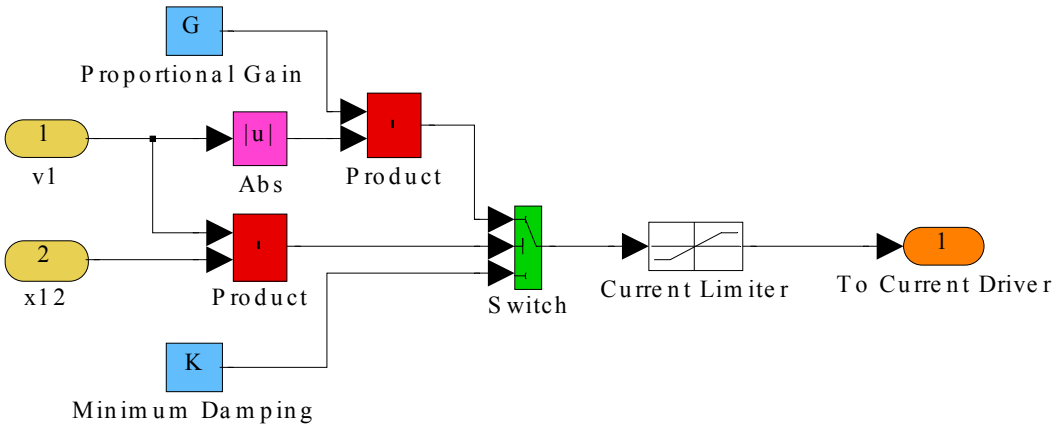

Figure 3-19. Block Diagram for Relative Displacement Skyhook Control Logic

3.4.6 Current Driver Circuit

The output of each of these control algorithms is what was used to control the damper. Because the MR damper dynamics are driven by current, the circuit shown in Figure 3-20 had to be used to essentially amplify the current in the signal coming from Control Desk. The circuit was designed such that the current to the damper was proportional to the control voltage coming from dSPACE. The first stage of the circuit converts the control voltage from dSPACE to a voltage referenced to the ground of the current driver circuit. The second stage of the circuit then uses the output from the first stage and uses a power transistor to drive a proportional current through the MR damper [31].

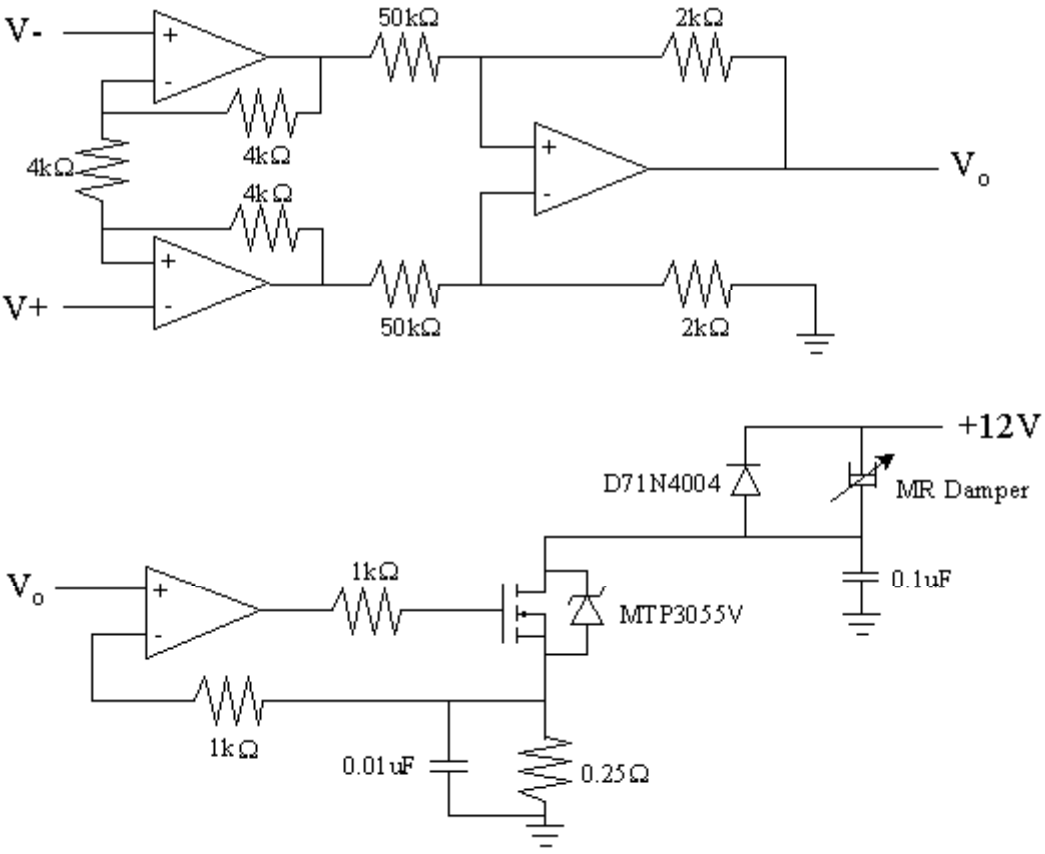

Figure 3-20. Current Driver Circuit for MR Damper

4 Frequency Response Analysis

This chapter presents an evaluation of each of the control policies through a frequency domain approach. The chapter begins with a definition of the input excitation used for this evaluation. Each of the control policies are assessed using the same signal processing techniques. The chapter ends with concluding remarks regarding the benefits of each control strategy.

4.1 Excitation for Frequency Response Analysis

A frequency response analysis is valuable for identifying the dynamics of the system. In the case of this study, the goal of the frequency response analysis was to identify the frequency dynamics of the quarter-car rig and to quantify the benefits of the control strategies in the frequency domain. From the parameters shown in Table 2-1, we can approximate the natural frequencies of the quarter-car rig as:

$$\varpi_1 = \sqrt{\frac{k_1}{m_1}} \tag{4.1}$$

$$\varpi_2 = \sqrt{\frac{k_1 + k_2}{m_2}} \tag{4.2}$$

Through this approximation we find that ω_1 = 1.5 Hz and ω_2 = 10.5 Hz. In choosing an input signal, these two frequencies must be included in the range of excitation. There are several methods available for exciting a range of frequencies. An impact or a random signal could be considered, however, the input that was chosen for this study was a chirp signal.

The chirp signal that was used in this study was a modified version of the chirp signal available in Simulink. This chirp signal allowed the user to define the frequency range of the chirp as well as the length of the chirp in time. Continuously repeating, the user also had the option of adding a period of zeros between each chirp to separate the

chirps. This function proved to be useful during testing. The parameters of the chirp signal for all testing are defined in Table 4-1.

Table 4-1. Chirp Signal Parameters

Initial Frequency	0.5 Hz
Final Frequency	16.5 Hz
Target Time	64 sec
Zero Time	4 sec

The frequencies were chosen based on the natural frequency approximations from equations (4.1) and (4.2). With a target time of 64 seconds, the time spent sweeping through each of the 16 frequencies was 4 seconds. A slow sweeping chirp signal was desired so as to be sure that the low frequency dynamics were not lost. The slow chirp also helped to minimize transient lag between the input and output. The 4 seconds of zero time aided in the data capturing process as well as the data reduction process. Each of the chirp signals were clearly separated by a period of zeros. This made the starting and ending points of the chirp easy to identify.

The reader will notice Table 4-1 does not include the amplitude of the chirp signal. Due to the physical limitations of the hydraulic actuation system, the chirp signal could not have constant amplitude. In order to excite the sprung mass natural frequency an amplitude of 0.45 inches was used. At 1.5 Hz, this amplitude leads to a velocity of approximately 4.25 in/s for the hydraulic actuator. At the unsprung mass natural frequency (ω_2 = 10.5 Hz), this same amplitude would translate to a velocity of 30 in/s which exceeds the limitations of the servo valve. For this reason, the chirp signal was passed through a first order low pass filter of the form

$$\frac{1}{\frac{1}{2\cdot 2\cdot \pi}\cdot s+1} \tag{4.3}$$

The frequency response of this filter is shown in Figure 4-1.

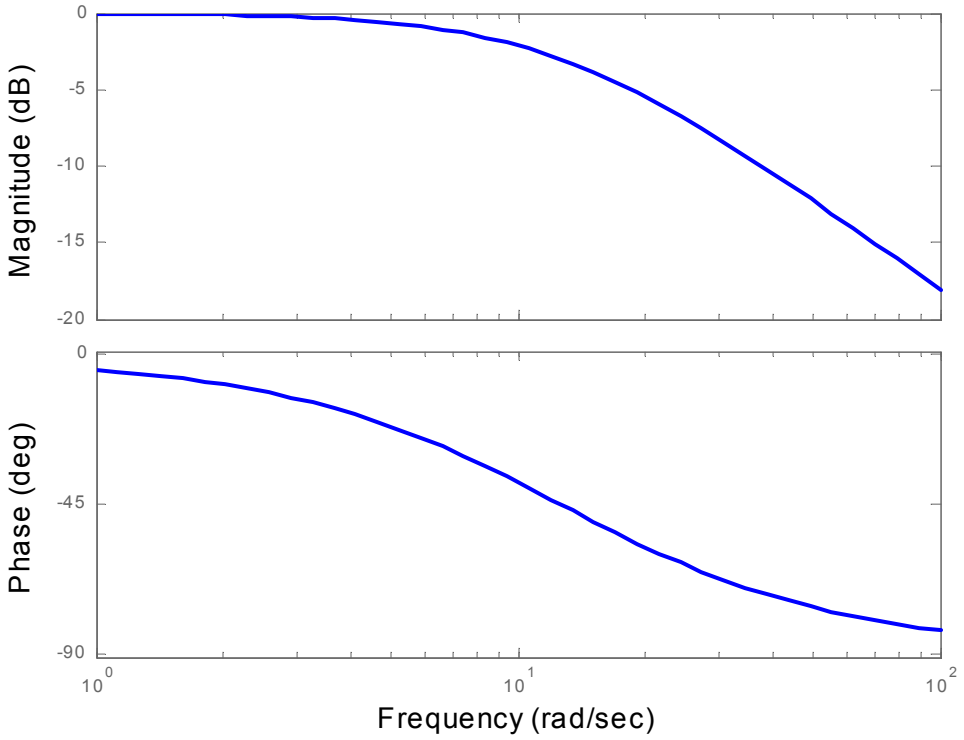

Figure 4-1. Bode Plot of the Filter for Chirp Signal Input

Using a break frequency of 2 Hz results in an 8:1 ratio between the amplitudes of the lowest frequency and the highest frequency in the chirp. This ratio corresponds to amplitudes of 0.45 inches at 1.5 Hz and 0.1 inches at 10.5 Hz. Because these amplitudes approach the limits of the hydraulic actuator as well as the quarter-car rig, we are confident that we are exciting the dynamics of the quarter-car rig sufficiently. The input chirp signal is shown in Figure 4-2.

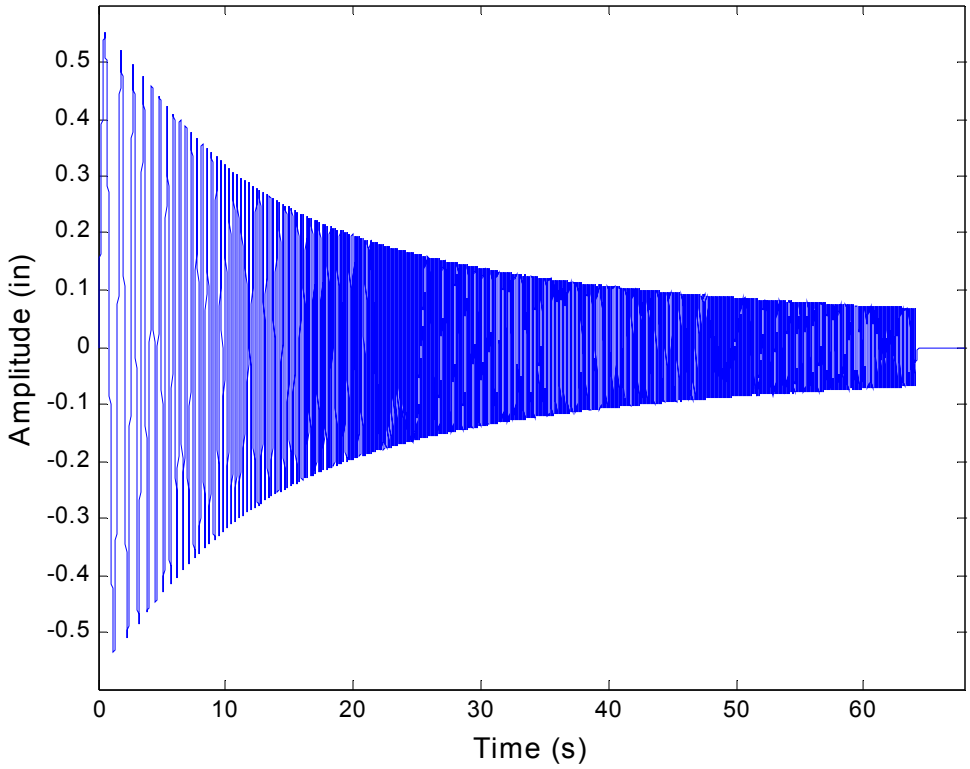

Figure 4-2. Chirp Input Signal

4.2 Signal Processing Methods

Because the frequency content of the system dynamics are below 20 Hz, it was deemed acceptable to sample the time data at 200 Hz. A sample rate of 200 Hz is 10 times faster than the fastest dynamics entering the system. This ensures that aliasing frequency content higher than the Nyquist frequency will not be an issue. Once the data is collected, it is loaded into Matlab. It is within Matlab that all the data reduction takes place. The time traces collected using Control Desk are transformed into the frequency domain in order to generate transmissibilities and auto spectrums. Of particular interest are the acceleration auto spectrums of the sprung and unsprung masses. These auto spectrums along with the transmissibilities of the sprung and unsprung mass were used to identify the frequency dynamics of the quarter-car rig.

The auto spectrums were used to evaluate the accelerations of the sprung and unsprung masses. The auto spectrum can be expressed as

$$G_{YY}(\varpi) = Y(\varpi) \cdot Y^*(\varpi) \tag{4.4}$$

where $Y^*(\omega)$ indicates the complex conjugate of the collection of frequency spectra $Y(\omega)$. The frequency spectra was obtained by using an "nfft" point Fast Fourier Transform algorithm, where nfft is the length of the conditioned acceleration time signal. Prior to entering the A/D converter, the acceleration signals are externally filtered with a Frequency Devices 8th order elliptical filter with a cutoff frequency of 25 Hz. Following this, the time signals are manipulated in order to remove the zero-time offset. Sampled at 200 Hz, what remains is a conditioned acceleration signal with 12,800 points. The final step in the process is a post-FFT Chebyshev filter. The auto spectrum results are presented in a single-sided format.

Transmissibilities between the input and output displacements of both masses were also used to quantify the benefits of each control strategy. In addition to the sprung and unsprung mass transmissibilities, the transmissibility between the relative displacement and the input displacement was also considered. Conveniently, all of these displacement signals were available from the data acquisition within Control Desk.

The frequency response function (FRF) was generated using the FRF estimator shown below,

$$H(\varpi) = \frac{G_{XY}(\varpi)}{G_{XX}(\varpi)} = \frac{X^*(\varpi) \cdot Y(\varpi)}{X^*(\varpi) \cdot X(\varpi)} \tag{4.5}$$

where $G_{XY}(\omega)$ is the cross spectrum from input to output, and $G_{XX}(\omega)$ is the auto spectrum of the input as described in equation (4.4). The displacement signals, conditioned to remove the zero-time offset, were transformed into the frequency domain using the same nfft point FFT algorithm. Once they were in the frequency domain, the cross spectrums and auto spectrums were generated and the transmissibilities were plotted for three different input/output relationships. The first two relationships considered were the ratios between the sprung and unsprung mass displacements and the input displacement. The third, less conventional relationship was the ratio between the relative displacement

(x_1-x_2) and the input displacement. The relative displacement, or rattle-space displacement, is the displacement across the damper. It is important to note that the transmissibility at low frequencies for this relationship should not be equal to one as expected. Rather, at low frequencies, the transmissibility for this relationship should be zero; at low frequencies there is no relative displacement between the two masses.

4.3 Passive Control Frequency Analysis

Before the results for the passive case are revealed, it is important to understand the manner in which passive control is being identified. Five different currents were chosen to represent the passive cases. During testing, the damper was energized to each one of these currents. The current to the damper throughout each of the tests was constant, making the damper behave like a passive damper.

The five currents that were chosen represent the range from off-state (0.0 Amps) to lockout (1.5 Amps). Lockout is defined as the current necessary to couple the sprung mass with the unsprung mass. In essence, the MR damper effectively becomes a rigid link between the two masses. The passive case transmissibilities for each of the five currents are shown in Figure 4-3. As expected, as damping increases the transmissibility at resonance decreases at the cost of increased transmissibility between the two resonant frequencies. This compromise is common in passive suspensions. This experimental data further identifies with the simulated data in the fixed point that occurs at $\sqrt{2}\varpi_1$.

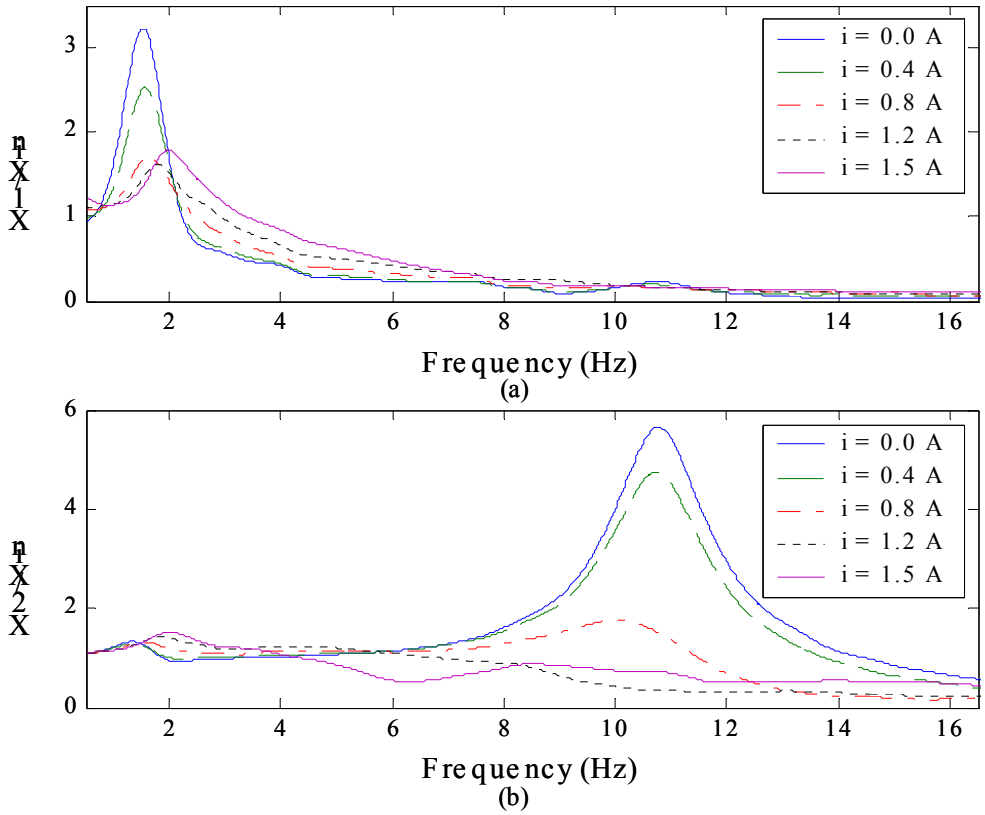

Figure 4-3. Passive Transmissibility for Different Damper Currents: (a) Sprung Mass Transmissibility; (b) Unsprung Mass Transmissibility

The resonant frequency shift due to increased coupling of the two masses is apparent at higher currents. At high currents the 2DOF system becomes coupled and behaves more like a SDOF system. The relative displacement transmissibility in Figure 4-4 supports this theory, showing only one resonant peak at high currents.

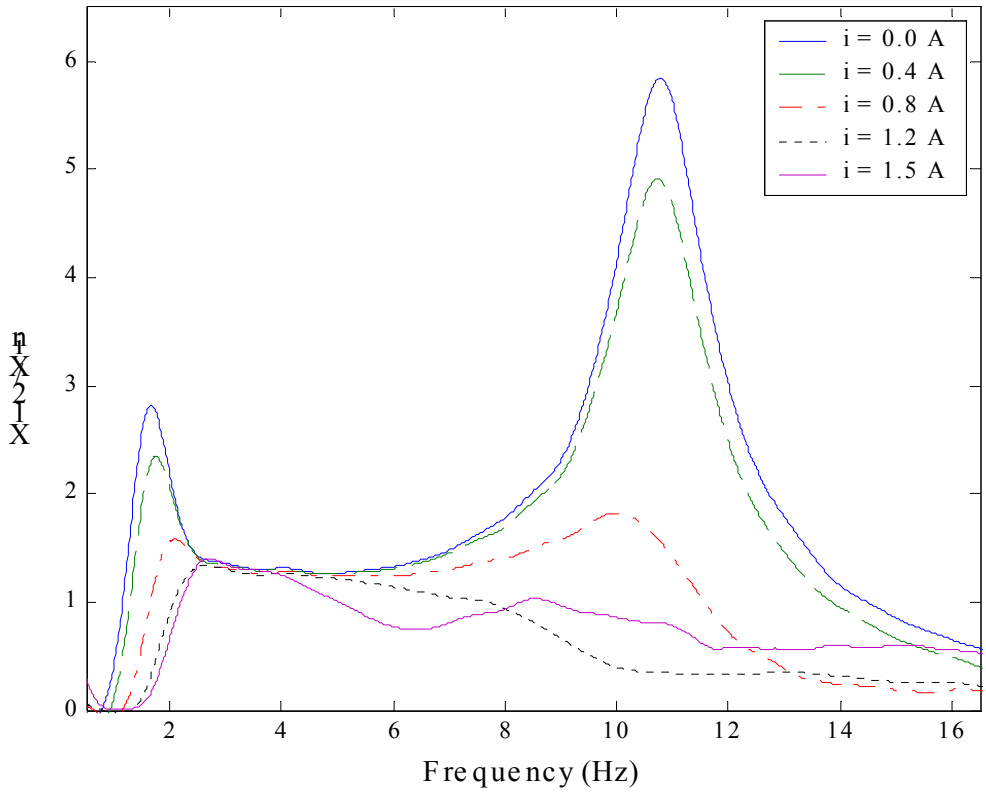

Figure 4-4. Passive Control Relative Displacement Transmissibility

Further evaluating the passive control results, the auto spectrums of the sprung and unsprung mass hold value. Recall from Chapter 1 that ride comfort is often associated with sprung mass acceleration. Ideally, the suspension would minimize the acceleration transmitted to the vehicle body. Figure 4-5 illustrates the fundamental problem with passive suspensions, specifically the lack of isolation that comes with increased passive damping. At currents above 0.8 Amps, the isolation that this passive damper offers becomes questionable. At 1.5 Amps, the damper behaves much like a band-pass filter, attenuating frequencies below 2 Hz and above 6 Hz. The region between these frequencies offers poor isolation.

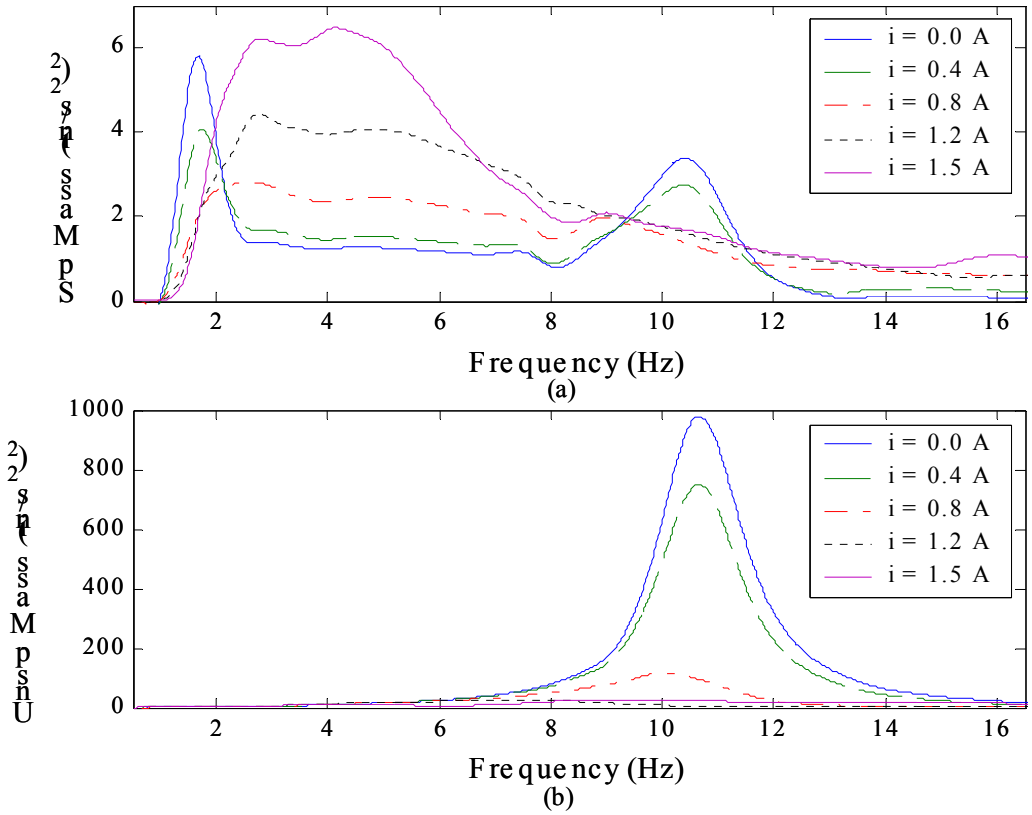

Figure 4-5. Passive Control Acceleration Auto Spectrums:
(a) Sprung Mass Auto Spectrum; (b) Unsprung Mass Auto Spectrum

4.4 Skyhook Control Frequency Analysis

The skyhook control results will be presented in the same fashion as the passive cases. With focus on the sprung mass, skyhook attempts to reduce sprung mass motion at the expense of unsprung mass motion. Recall from Chapter 2 the semi-active skyhook control law:

$$\begin{Bmatrix} v_1 v_{12} \geq 0 & F_{sa} = c_{sky} v_1 \\ v_1 v_{12} < 0 & F_{sa} = 0 \end{Bmatrix} \tag{4.6}$$

Figure 4-6 illustrates the execution of skyhook control as the damper follows the control law described in equation (4.6). The time trace for the absolute velocity of the sprung mass (v_1) is plotted along with the relative velocity (v_{12}) and damper current. Where the

product of v_1 and v_{12} is positive, the damper current is proportional to v_1. Otherwise, the damper current is zero which corresponds to minimum damping.

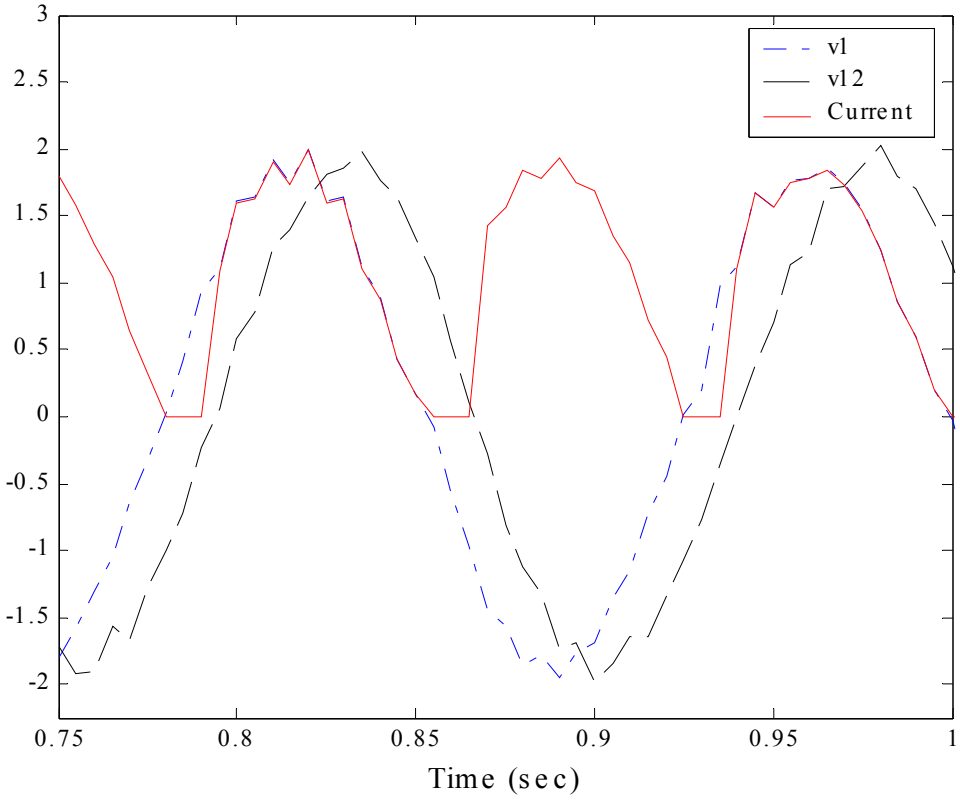

Figure 4-6. Sample Time History of Skyhook Execution

From equation (4.6), when the product of v_1 and v_{12} is positive, the semi-active force is proportional to v_1. The factor by which the force is proportional to v_1 is controlled within Control Desk. Revisiting the skyhook control block diagram from Chapter 2, in Figure 4-7, the variable G (proportional gain) is the variable that defines the constant by which F_{sa} is proportional to v_1.

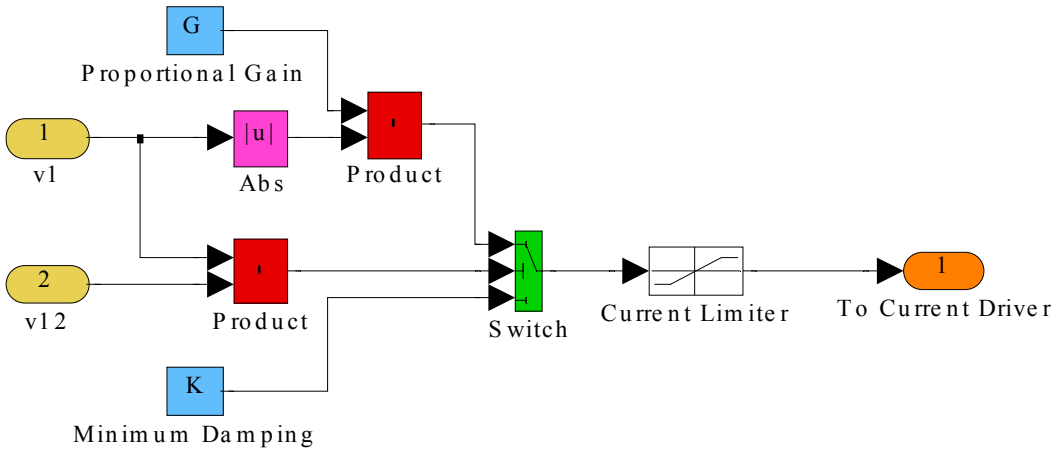

Figure 4-7. Block Diagram for Skyhook Control Logic

Assessing the dynamics of the quarter-car rig under semi-active skyhook control begins with an evaluation of the transmissibilities of the sprung and unsprung masses with respect to the input. Figure 4-8 shows the transmissibility plots for several values of the skyhook gain, G (c_{sky}). The experimental results follow closely with the simulated results of Chapter 2, with sprung mass transmissibility decreasing as skyhook damping increases. Further correspondence with the simulated results, the benefits of controlling the sprung mass come at the expense of poor control of the unsprung mass. At low frequencies, the unsprung mass transmissibility increases as the skyhook gain increases. Also notice the isolation between the two natural frequencies of the sprung mass transmissibility. Unlike passive control, increasing the skyhook gain does not affect the frequency range between the two natural frequencies. This characteristic alone eliminates the compromise common in passive suspensions.

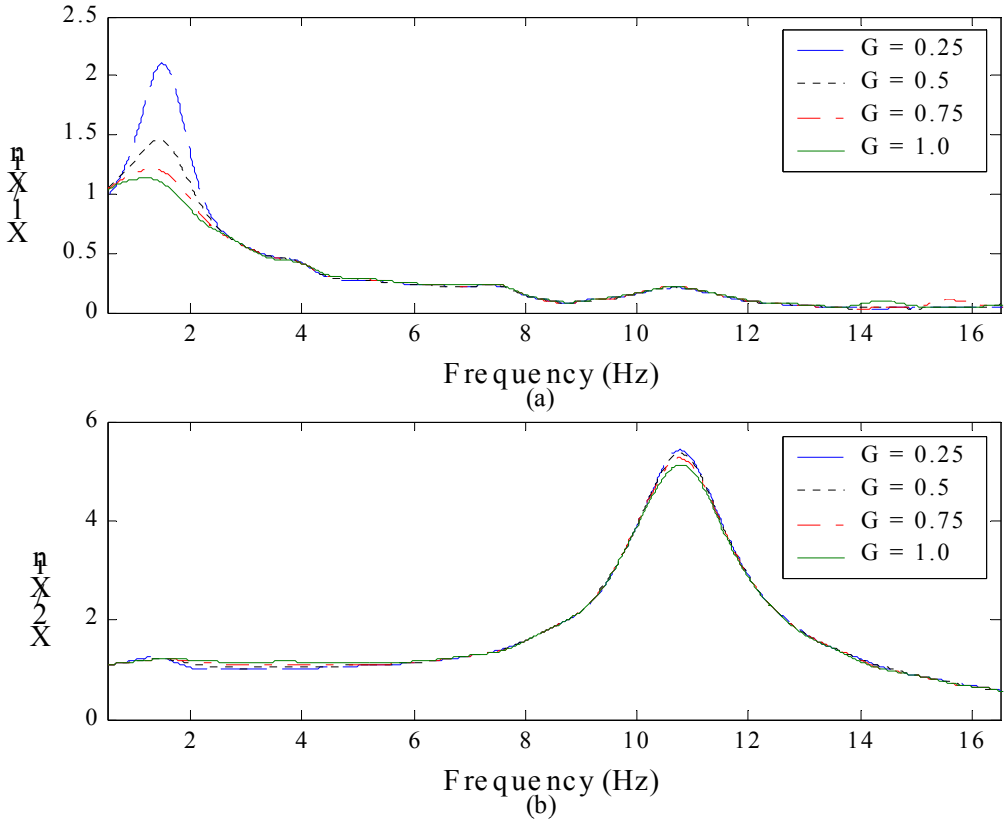

Figure 4-8. Skyhook Control Transmissibility:
(a) Sprung Mass Transmissibility; (b) Unsprung Mass Transmissibility

Proceeding with the skyhook control evaluation, Figure 4-9 shows the transmissibility between the relative displacement and the input. Once again, the benefits and compromises of skyhook control are illustrated through the attenuation at low frequencies and the lack of attenuation at high frequencies.

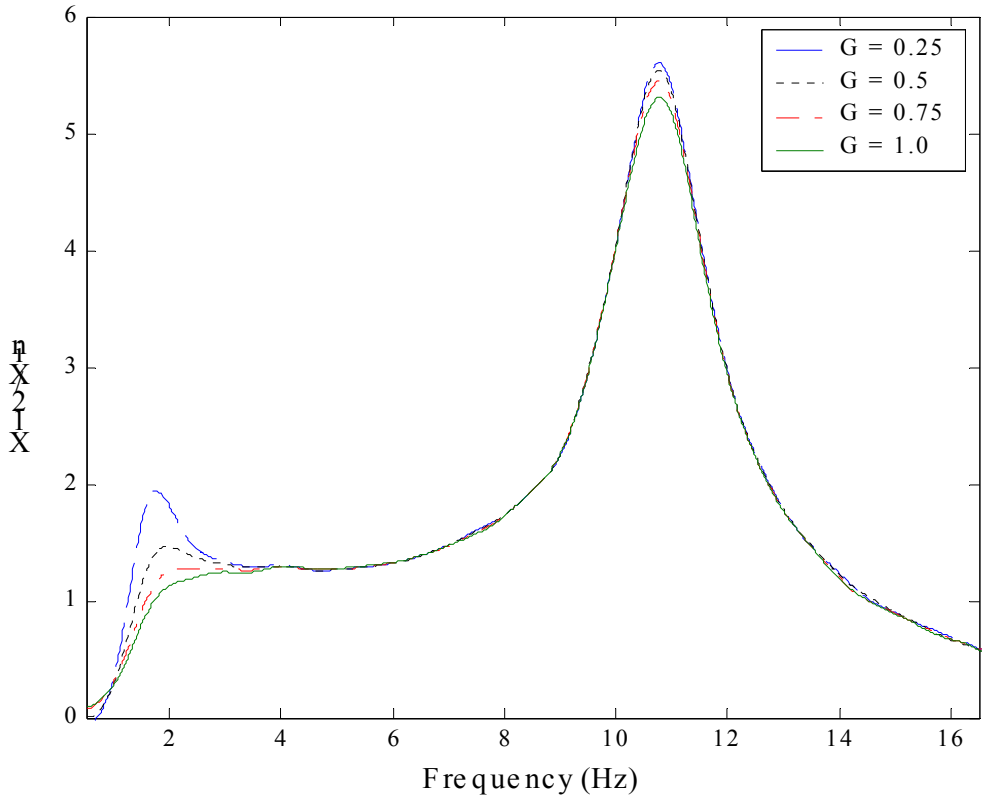

Figure 4-9. Skyhook Control Relative Displacement Transmissibility

Finalizing the evaluation of skyhook control, the auto spectrums of the sprung and unsprung mass accelerations reveal parallel results. Continuing with the focus on the sprung mass, Figure 4-10 shows that as the skyhook gain increases, the acceleration at the sprung mass natural frequency decreases. Again, the acceleration at the unsprung mass natural frequency remains virtually unchanged for different values of the skyhook gain. Another valuable observation is the increased acceleration in the frequency range between the two natural frequencies. As the skyhook gain increases, the acceleration of the sprung mass increases in the region between the natural frequencies.

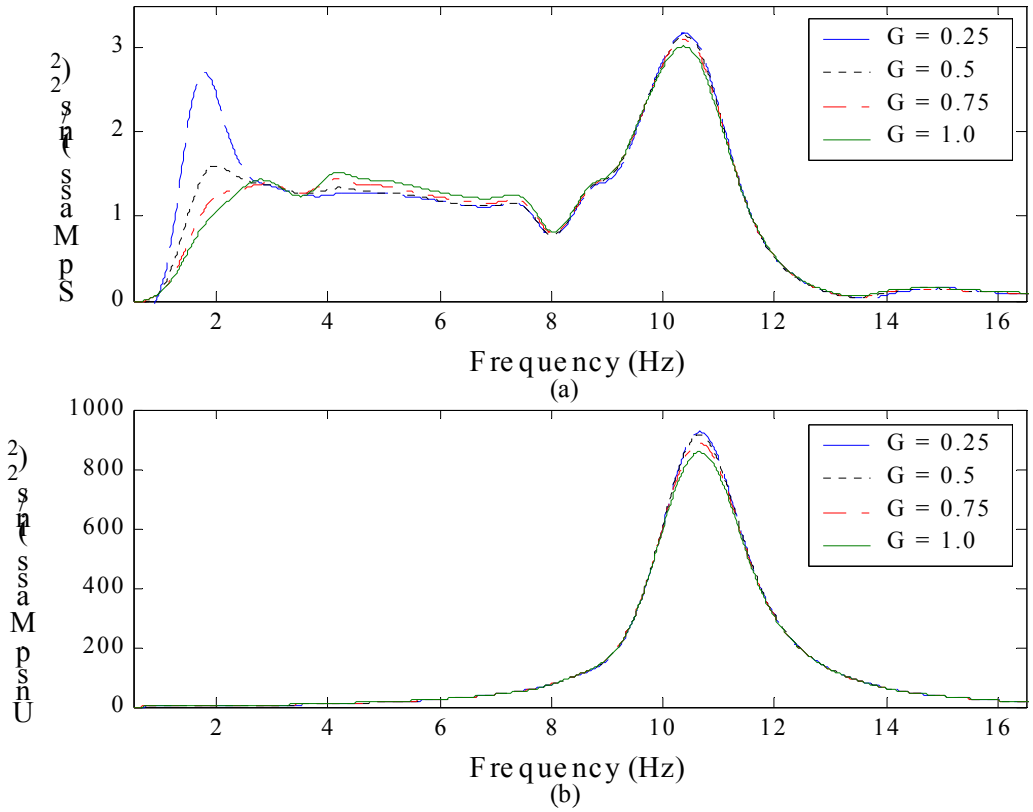

Figure 4-10. Skyhook Control Acceleration Auto Spectrums:
(a) Sprung Mass Auto Spectrum; (b) Unsprung Mass Auto Spectrum

4.5 Groundhook Control Frequency Analysis

By the same means that skyhook control excels at controlling the sprung mass, groundhook control excels at controlling the unsprung mass. Consider the semi-active groundhook control policy from Chapter 2:

$$\begin{Bmatrix} -v_2 v_{12} \geq 0 & F_{sa} = c_{gnd} v_2 \\ -v_2 v_{12} < 0 & F_{sa} = 0 \end{Bmatrix} \tag{4.7}$$

When the product of v_2 and v_{12} is negative, the semi-active damping force is proportional to the absolute velocity of the unsprung mass, v_2. Figure 4-11 illustrates the execution of the control law expressed by equation (4.7).

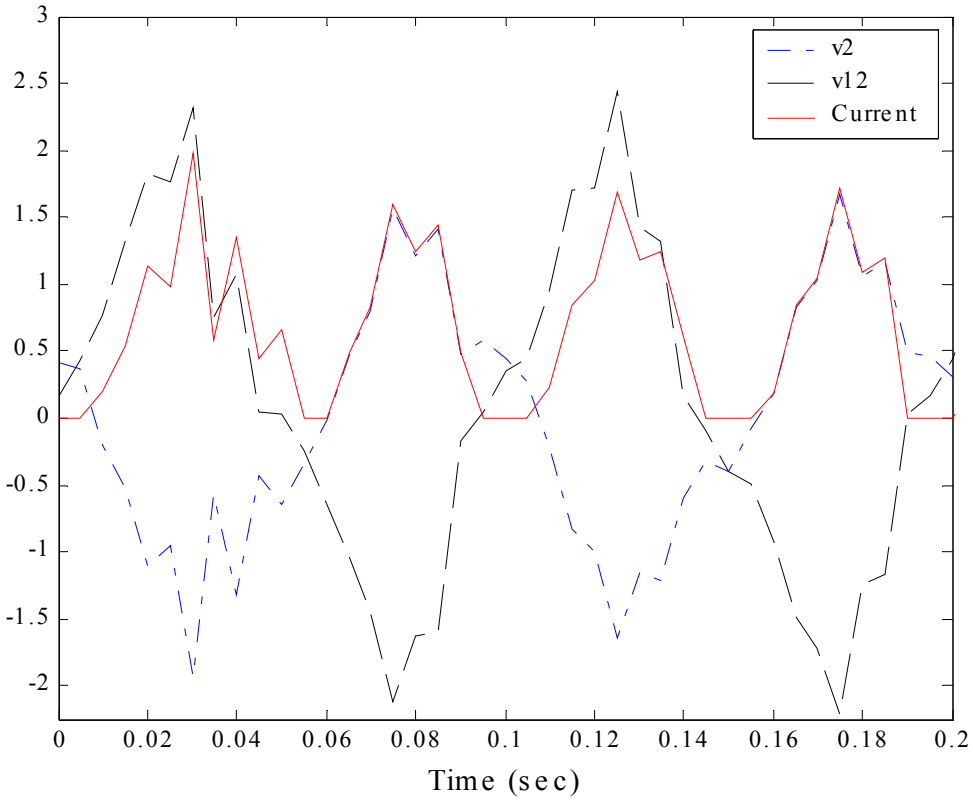

Figure 4-11. Sample Time History for Groundhook Execution

Under groundhook control the semi-active damping force is proportional to v_2. Figure 4-12 recalls the groundhook control block diagram from Chapter 2, identifying the gain by which F_{sa} is proportional to v_2. The variable G represents the groundhook gain (c_{gnd}) and was controlled from within Control Desk.

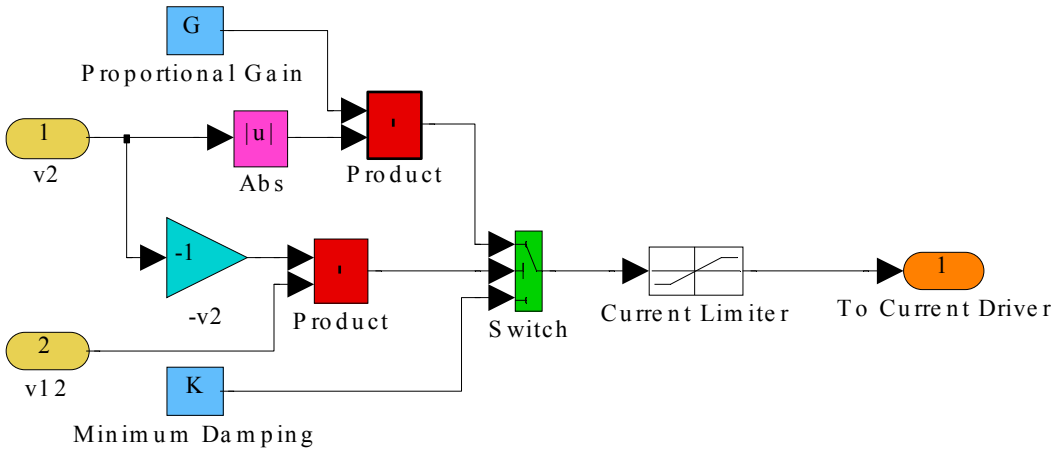

Figure 4-12. Block Diagram for Groundhook Control Logic

The transmissibilities of the sprung and unsprung masses under groundhook control are shown in Figure 4-13 for different values of groundhook gain, *G*. The neglect of sprung mass attenuation, common with groundhook control, is illustrated in the sprung mass transmissibility plot. As the groundhook gain increases, the amplitude of the sprung mass transmissibility increases. This increase in amplitude occurs not only at the sprung mass natural frequency, but rather, it is evident throughout the entire frequency range. Expectedly, as the groundhook gain increases, the amplitude of the transmissibility at the unsprung mass natural frequency decreases, even to the point of isolation. Further investigation of the unsprung mass transmissibility reveals the fixed point that occurs at approximately 3.5 Hz. Above this frequency the benefits of groundhook control are clear, while below 3.5 Hz the drawbacks of groundhook control are demonstrated.

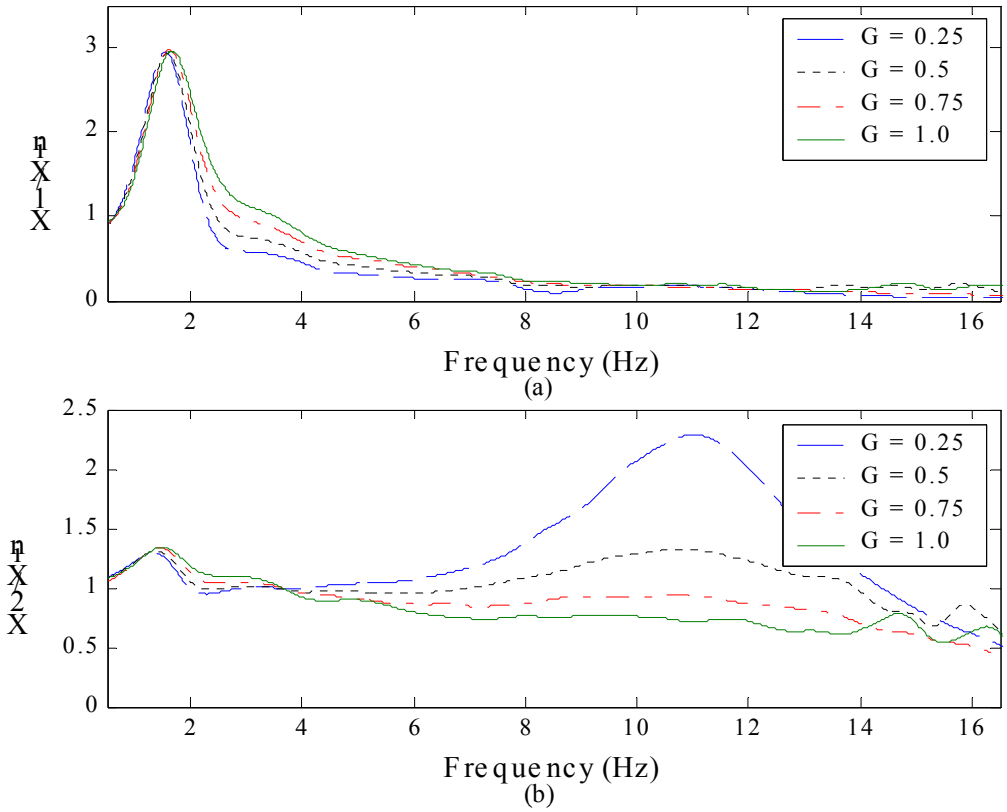

Figure 4-13. Groundhook Control Transmissibility:
(a) Sprung Mass Transmissibility; (b) Unsprung Mass Transmissibility

The same dynamics illustrated in Figure 4-13 also appear in the relative displacement transmissibility in Figure 4-14. The fixed point at 3.5 Hz and the behavior above and below this fixed point remain unchanged.

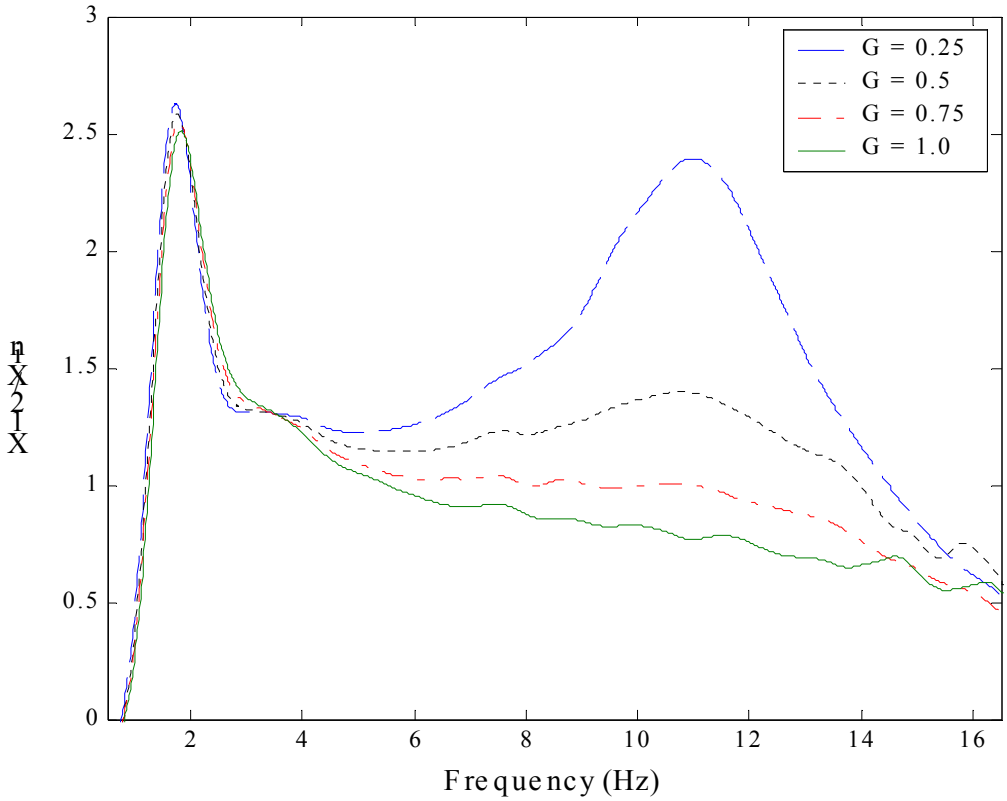

Figure 4-14. Groundhook Control Relative Displacement Transmissibility

The auto spectrums of the sprung and unsprung mass accelerations for groundhook control, shown in Figure 4-15, are especially convincing. Here, the gains and losses of groundhook control are acutely illustrated. While the sprung mass suffers through a wide frequency range as the groundhook gain increase, the unsprung mass continues to improve as the groundhook gain increases.

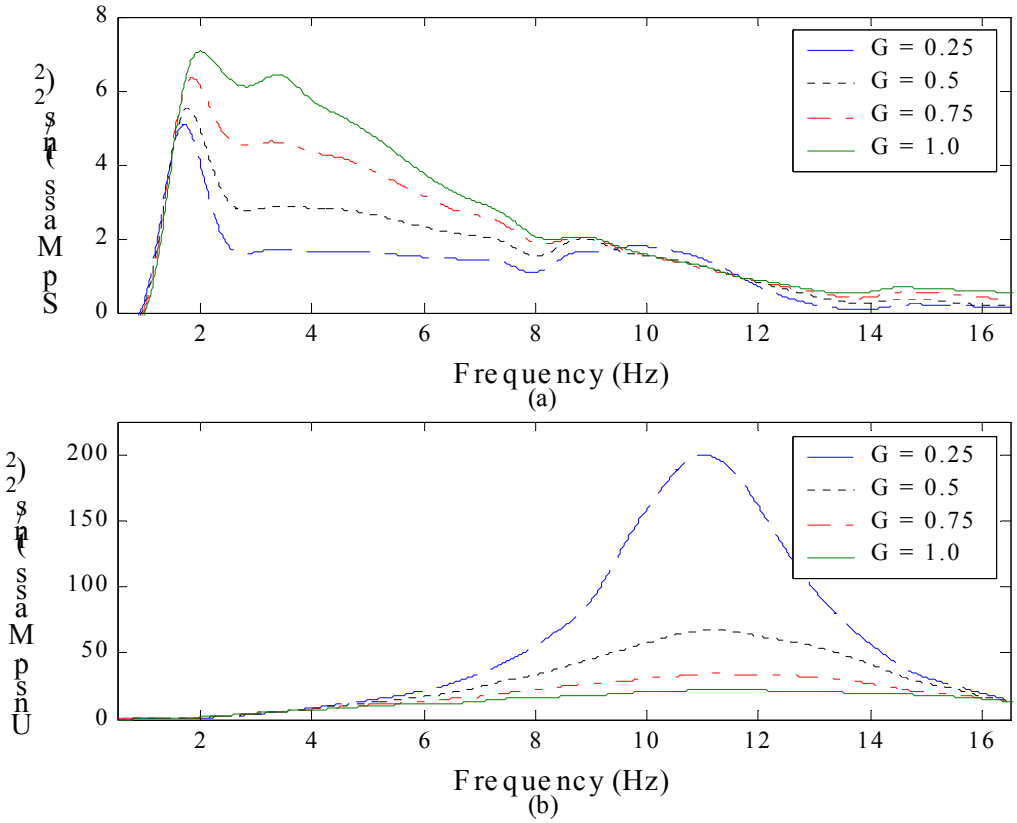

Figure 4-15. Groundhook Control Acceleration Auto Spectrums:
(a) Sprung Mass Auto Spectrum; (b) Unsprung Mass Auto Spectrum

4.6 Hybrid Control Frequency Analysis

Because hybrid control is a linear combination of skyhook and groundhook, as expressed by equation (4.8), the dynamics of skyhook and groundhook will appear in the hybrid control results.

$$\begin{Bmatrix} v_1 v_{12} \geq 0 & \sigma_{sky} = v_1 \\ v_1 v_{12} < 0 & \sigma_{sky} = 0 \end{Bmatrix}$$

$$\left\{ F_{sa} = G\left[\alpha \sigma_{sky} + (1-\alpha)\sigma_{gnd} \right] \right\} \tag{4.8}$$

$$\begin{Bmatrix} -v_2 v_{12} \geq 0 & \sigma_{gnd} = v_2 \\ -v_2 v_{12} < 0 & \sigma_{gnd} = 0 \end{Bmatrix}$$

Specifically, when $\alpha = 0$, the control law reduces to pure groundhook, and when $\alpha = 1$, the control law reduces to pure skyhook. Much like skyhook and groundhook control are proportional to v_1 and v_2 respectively, hybrid control is proportional to the linear combination of v_1 and v_2 as defined by α. Recalling the hybrid control block diagram from Chapter 2, Figure 4-16 illustrates the execution of the control law described by equation (4.8).

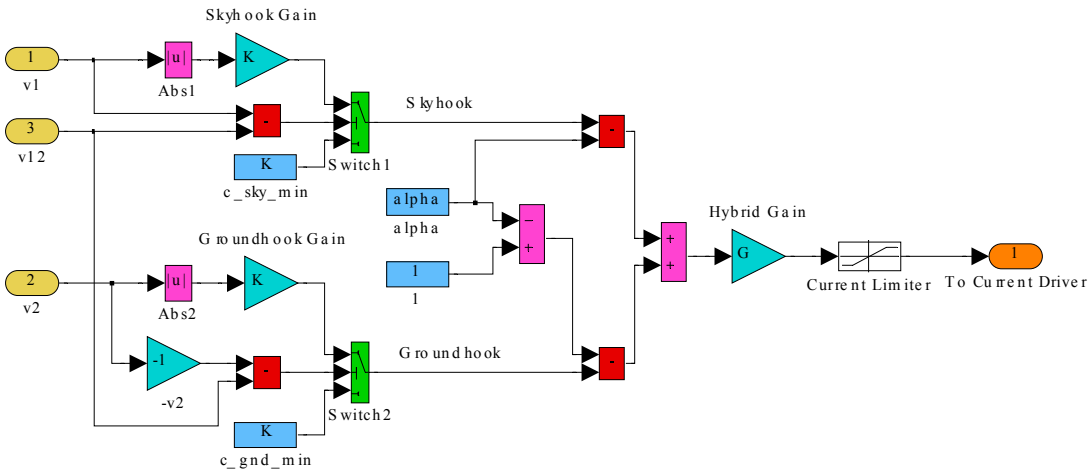

Figure 4-16. Block Diagram for Hybrid Control Logic

As the transmissibility plots in Figure 4-17 show, hybrid control, at either extreme, resembles skyhook and groundhook control. In Figure 4-17, the hybrid gain, G, is held constant for several values of α. When $\alpha = 1$, the response reduces to the familiar skyhook response, while $\alpha = 0$ returns the groundhook control response. The hybrid gain, G, at the extremes of α, correspond to the skyhook gain and groundhook gain discussed earlier. The dynamic response of the system for different values of α is clearly a weighted combination of the skyhook and groundhook components of the semi-active hybrid control law [30].

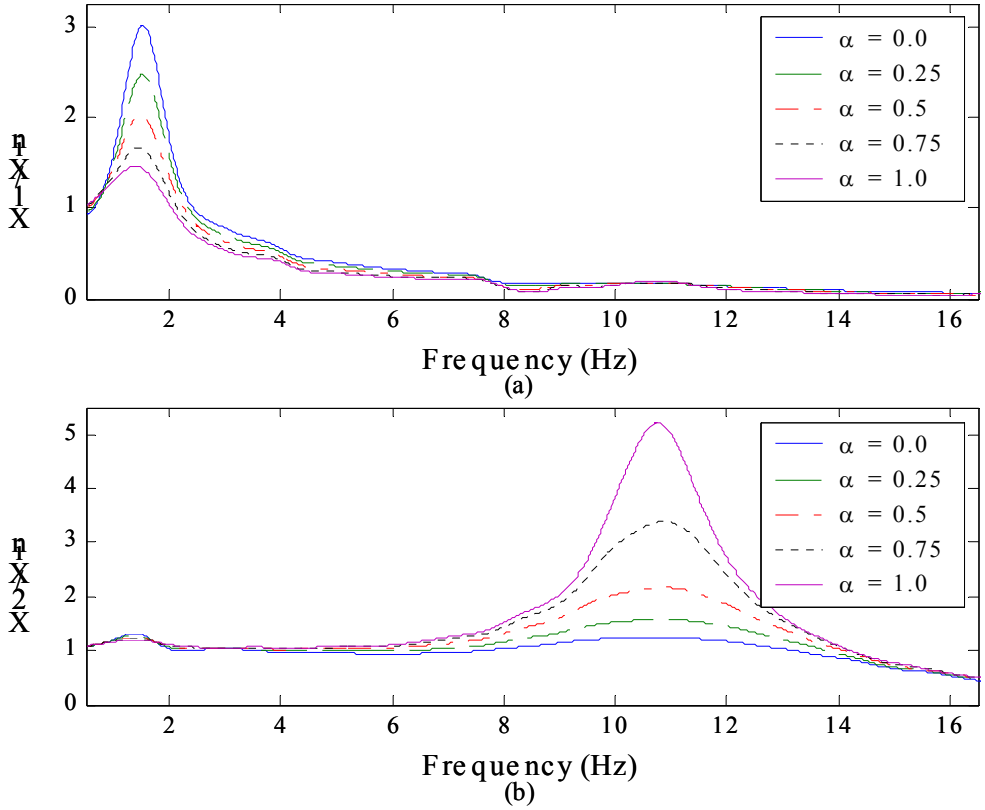

Figure 4-17. Hybrid Control Transmissibility $G = 0.5$:
(a) Sprung Mass Transmissibility; (b) Unsprung Mass Transmissibility

Another means of evaluating hybrid control is to hold α constant while changing the hybrid gain, G. Figure 4-18 shows the transmissibilities for $\alpha = 0.5$. This particular hybrid configuration represents equal contributions from skyhook and groundhook control. The common tradeoff exhibited in skyhook and groundhook control as controller gain increases is avoided in this configuration. As the hybrid gain increases, both the transmissibility of the sprung mass and the unsprung mass are attenuated.

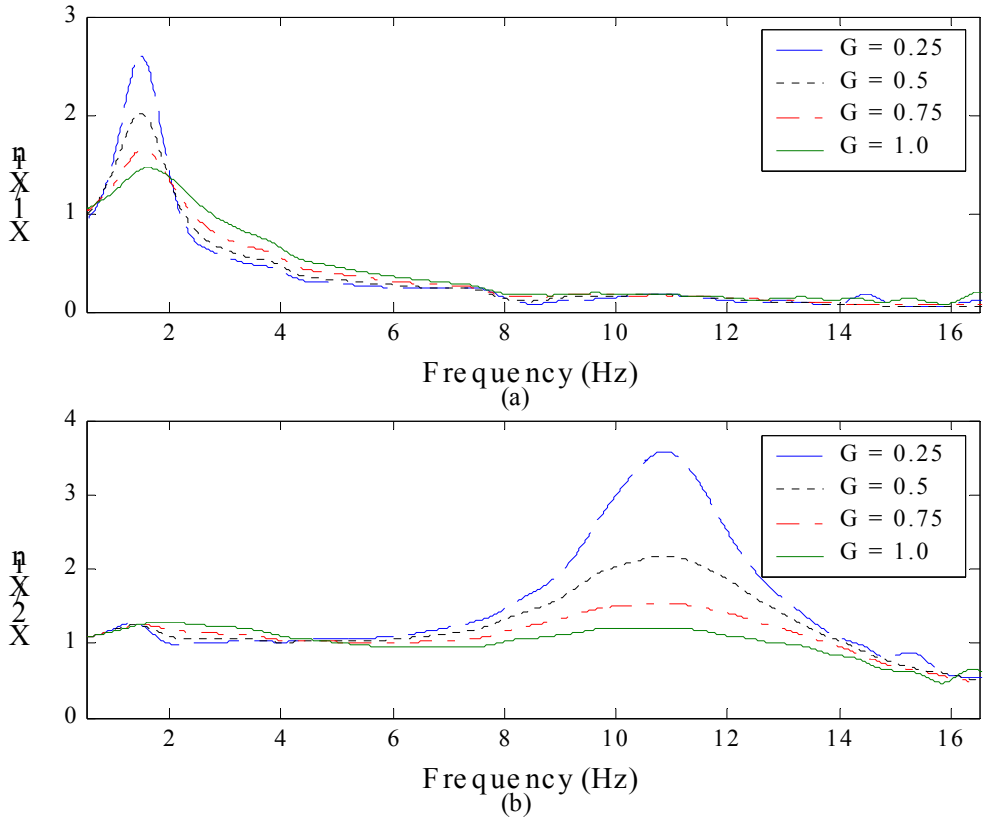

Figure 4-18. Hybrid Control Transmissibility $\alpha = 0.5$:
(a) Sprung Mass Transmissibility; (b) Unsprung Mass Transmissibility

In an attempt to view the effects of α and controller gain simultaneously, the amplitudes of the sprung and unsprung mass transmissibilities at the respective natural frequencies were compiled and plotted in a 3-D mesh. Figure 4-19 shows the amplitude of the sprung mass transmissibility versus α and gain. As expected, the best combination for the sprung mass would be α = 1 and high controller gain. This combination corresponds to pure skyhook control with a high gain.

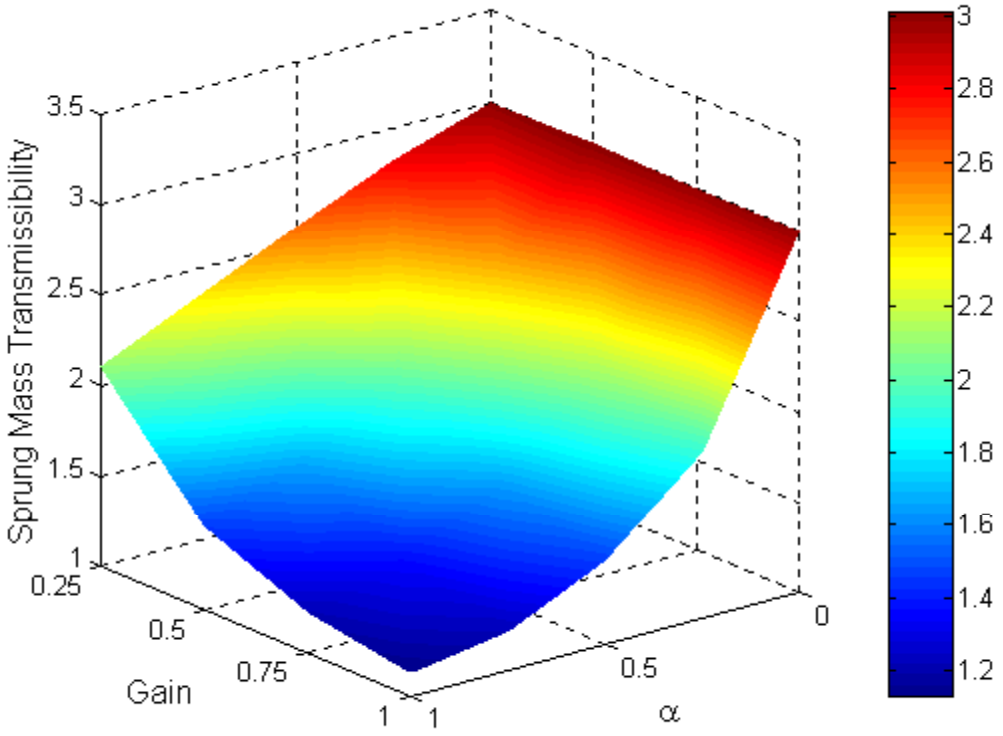

Figure 4-19: Hybrid Control 3-D Mesh for Sprung Mass Transmissibility Amplitude

Similar results are revealed for the unsprung mass in Figure 4-20. Here, the best combination of α and gain would be pure groundhook control, $\alpha = 0$, and high controller gain.

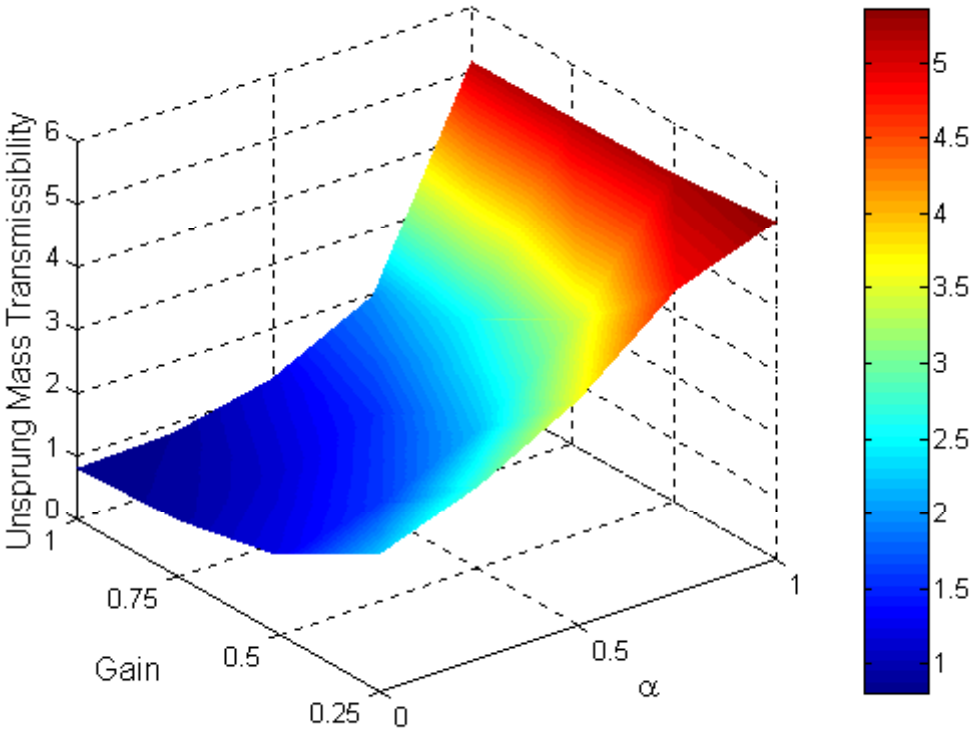

Figure 4-20: Hybrid Control 3-D Mesh for Unsprung Mass Transmissibility Amplitude

The relative displacement transmissibility emphasizes the same dynamics as Figure 4-17 and Figure 4-18. In Figure 4-21, the transition from groundhook control to skyhook control, as α increases from zero to one, is highlighted. Again, when $\alpha = 0.5$, the contributions form skyhook and groundhook control are equal, thus the tradeoff between the two is eliminated. The inflection point at 3.5 Hz is where the benefits meet the costs. At $\alpha = 0.5$ however, the response passes through the inflection point at no expense.

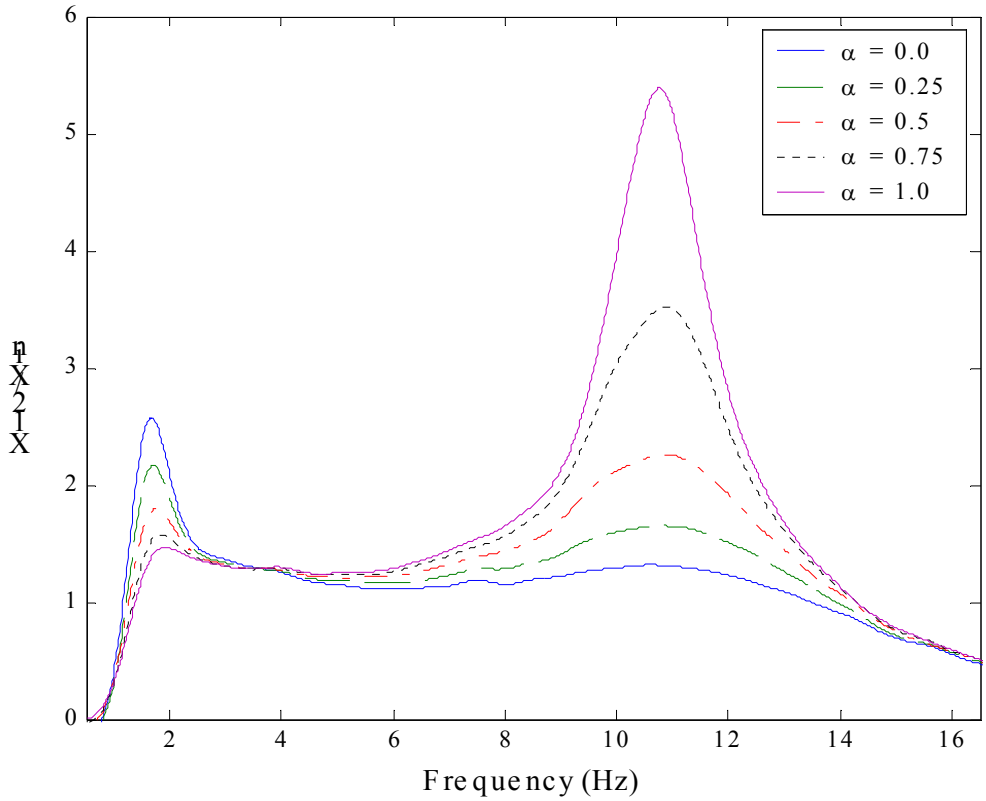

Figure 4-21. Hybrid Control Relative Displacement Transmissibility $G = 0.5$

The acceleration auto spectrums are also valuable at evaluating hybrid control and the affects of increasing α. As α approaches one, the contribution from skyhook control begins to dominate, and thus, the acceleration of the sprung mass decreases, as supported by the auto spectrums in Figure 4-22.

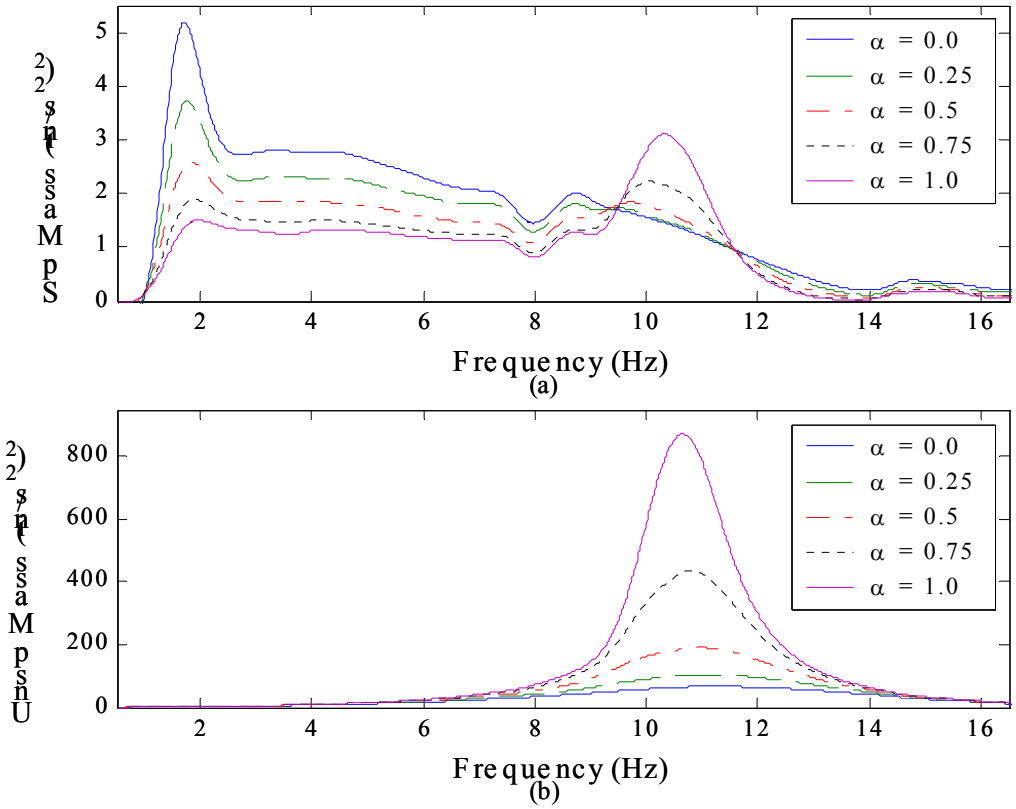

Figure 4-22. Hybrid Control Acceleration Auto Spectrums $G = 0.5$:
(a) Sprung Mass Auto Spectrum; (b) Unsprung Mass Auto Spectrum

4.7 Displacement Skyhook Frequency Analysis

The control law for displacement skyhook control can be expressed as,

$$\begin{Bmatrix} x_1 v_{12} \geq 0 & F_{sa} = c_{sky} v_1 \\ x_1 v_{12} < 0 & F_{sa} = 0 \end{Bmatrix} \tag{4.9}$$

where the semi-active force, F_{sa}, is now governed by the product of x_1 and v_{12} rather than v_1 and v_{12}. The execution of the policy described in equation (4.9) is revisited in Figure 4-23. The control signal going to the damper remains unchanged but the condition by which the force is controlled is now dependent on the absolute displacement of the sprung mass, as shown in Figure 4-24.

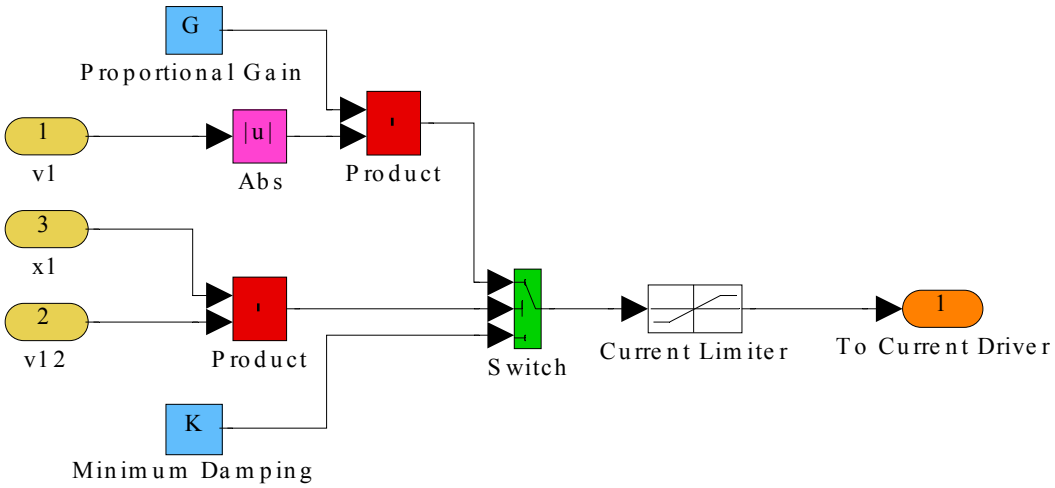

Figure 4-23. Block Diagram for Displacement Skyhook Control Logic

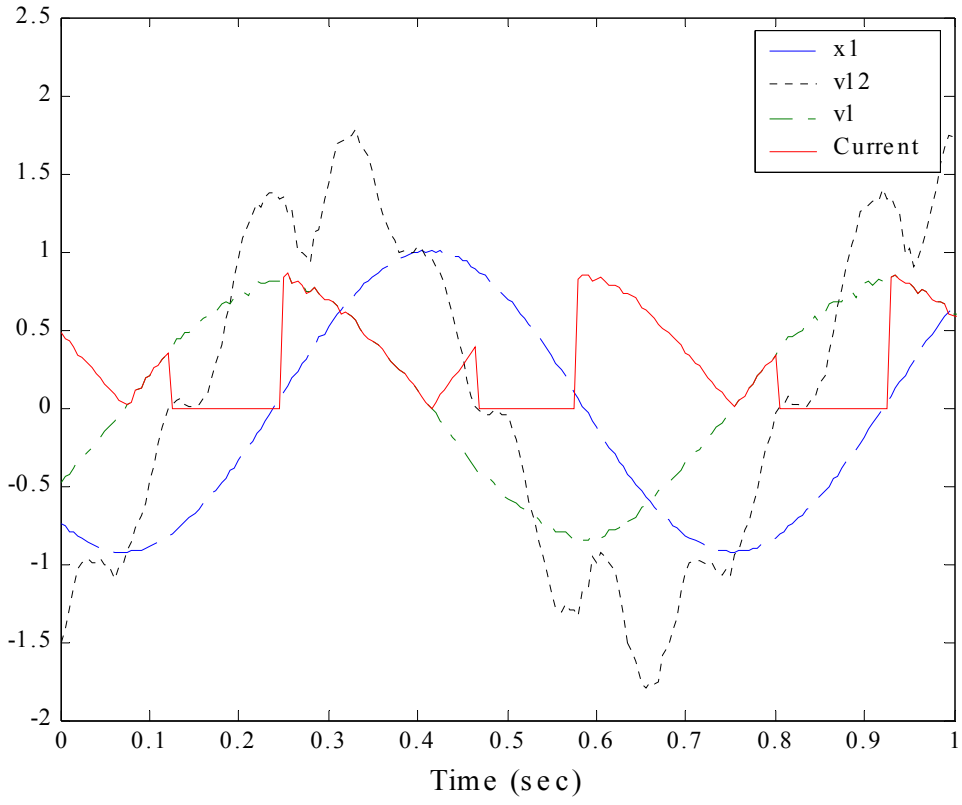

Figure 4-24. Sample Time History of Displacement Skyhook Execution

The transmissibility plots for displacement skyhook control are shown in Figure 4-25. Though not as prominent, the benefits of displacement skyhook are similar to those of skyhook control as *G* increases. One distinguishing characteristic is the behavior of displacement skyhook as *G* increases. The sprung mass transmissibility decreases substantially as *G* increases from 0.25 to 0.5. However, as *G* increases beyond 0.5, the transmissibility effectively remains the same. Another observation that should not be overlooked is the inflection point at approximately 2 Hz. In terms of the unsprung mass, displacement skyhook behaves in the same fashion as traditional skyhook control. As *G* increases, the transmissibility of the unsprung mass increases.

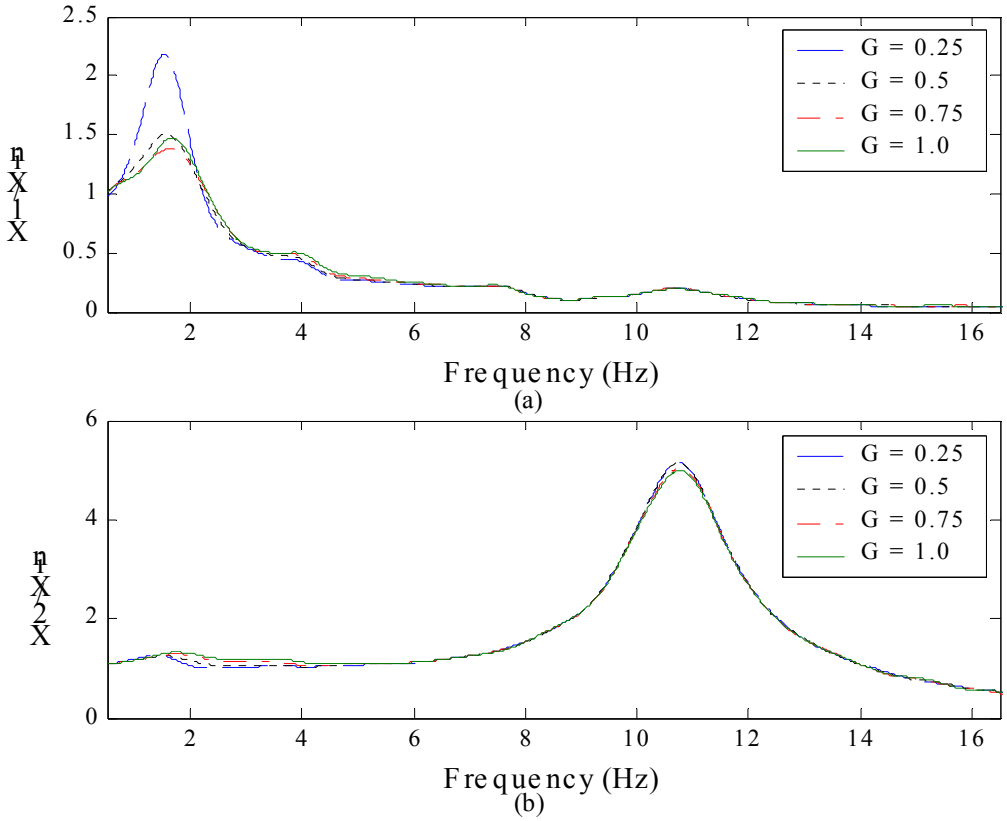

Figure 4-25. Displacement Skyhook Control Transmissibility:
(a) Sprung Mass Transmissibility; (b) Unsprung Mass Transmissibility

The relative displacement transmissibility in Figure 4-26 supports the same dynamics shown in the sprung and unsprung mass transmissibilities. Much like conventional skyhook, as *G* increases the transmissibility at the sprung mass natural frequency decreases at the expense of the increased transmissibility at the unsprung mass natural frequency.

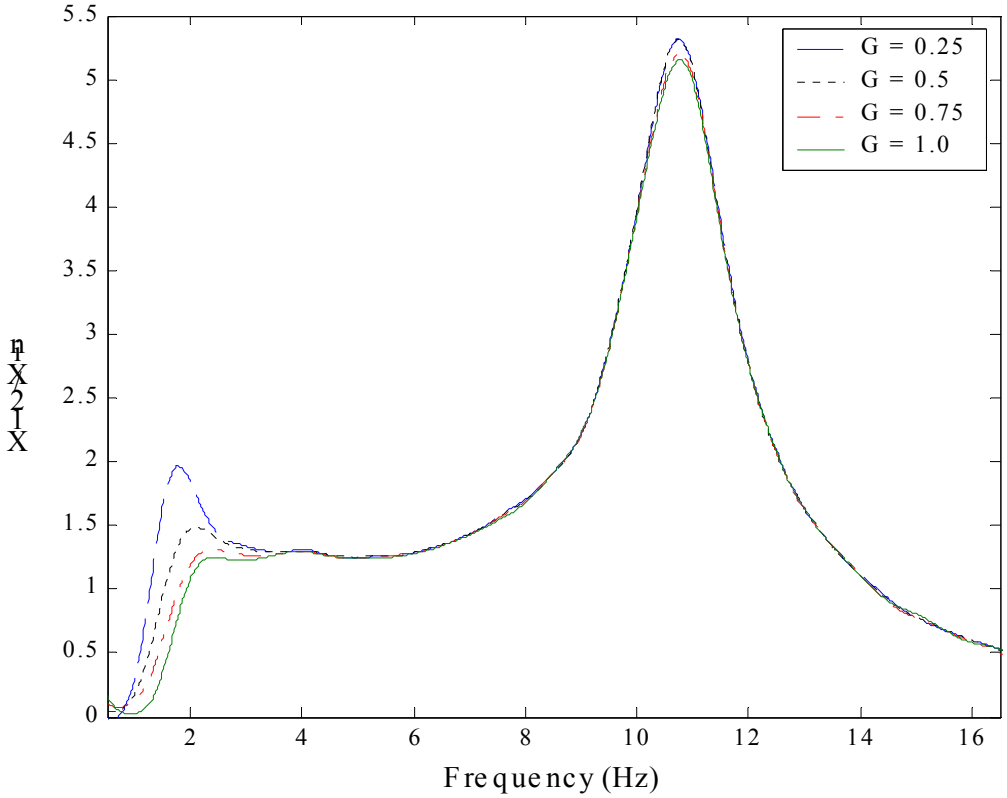

Figure 4-26. Displacement Skyhook Control Relative Displacement Transmissibility

The auto spectrums of the acceleration signals shown in Figure 4-27 reveal the same dynamics portrayed in conventional skyhook. That is, as *G* increases the acceleration at the sprung mass natural frequency decreases at the expense of increased acceleration in the frequency range between the two natural frequencies. Again, the unsprung mass acceleration is neglected even as *G* is increased.

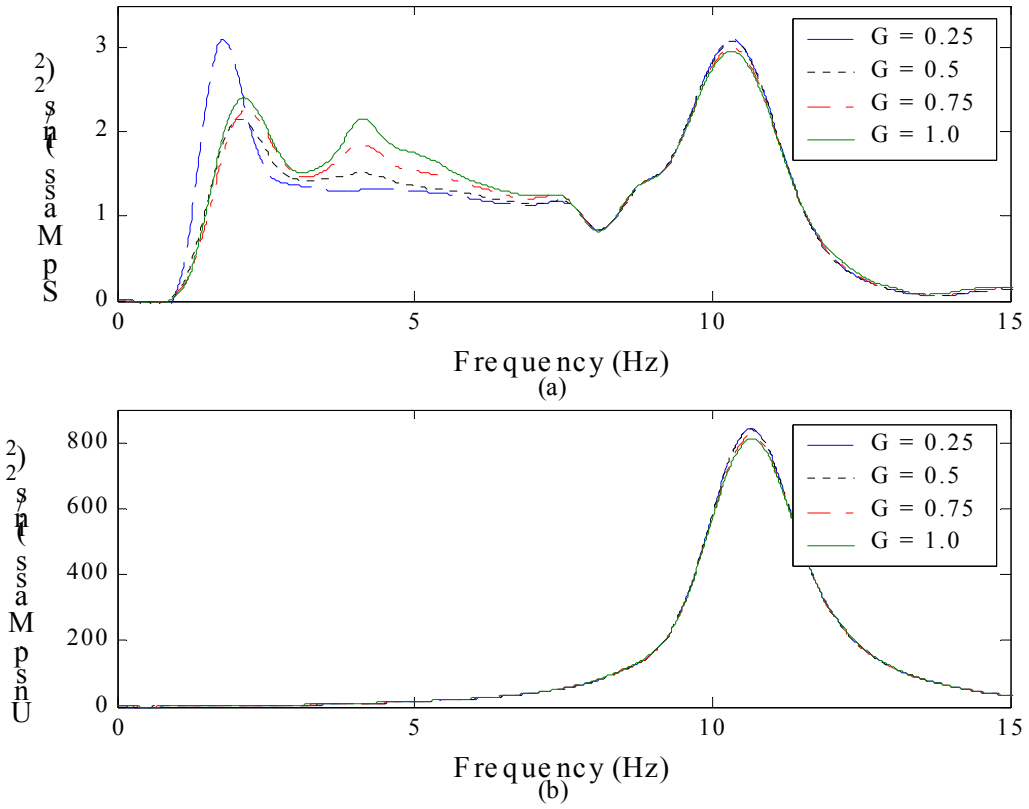

Figure 4-27. Displacement Skyhook Control Acceleration Auto Spectrums: (a) Sprung Mass Auto Spectrum; (b) Unsprung Mass Auto Spectrum

4.8 Relative Displacement Skyhook Control Frequency Analysis

The execution of relative displacement skyhook control shown in Figure 4-28 can be written as:

$$\begin{Bmatrix} v_1 x_{12} \geq 0 & F_{sa} = c_{sky} v_1 \\ v_1 x_{12} < 0 & F_{sa} = 0 \end{Bmatrix} \tag{4.10}$$

The semi-active damping force remains unchanged from skyhook and displacement skyhook control. Again, the distinguishing characteristic of relative displacement skyhook is the order by which the damper force changes. The semi-active damping force is now managed by the product of v_1 and x_{12}.

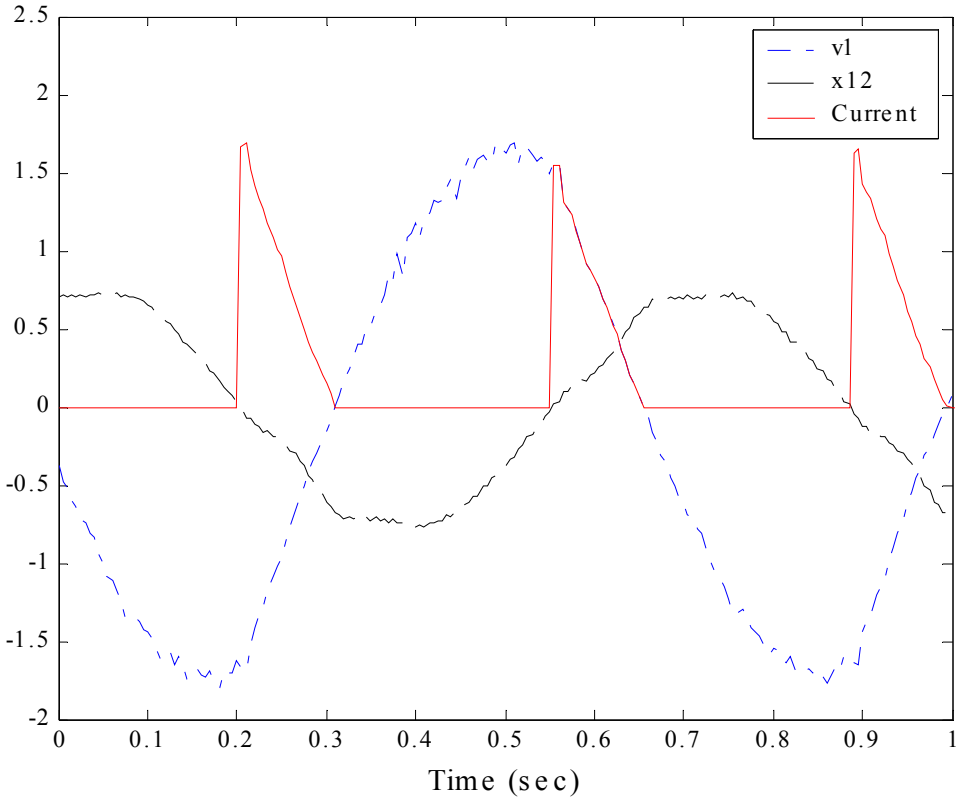

Figure 4-28. Sample Time History of Relative Displacement Skyhook Execution

The block diagram used to implement this control strategy is revisited in Figure 4-29. Again, the variable *G* represents the controller gain that was tuned within Control Desk. The transmissibilities of the sprung and unsprung masses are shown in Figure 4-30. As *G* is increased, the same dynamics observed in skyhook control appear in relative displacement skyhook control as well. However, the decrease in the sprung mass transmissibility is not nearly as dramatic as with traditional skyhook control. The disregard for control of the unsprung mass is also still evident. Both alternative skyhook control policies share a characteristic that is not observed in conventional skyhook. That is, at approximately 2 Hz there is an inflection point where the benefits of the controllers meet the apparent costs. Above 2 Hz the isolation decreases as *G* increases.

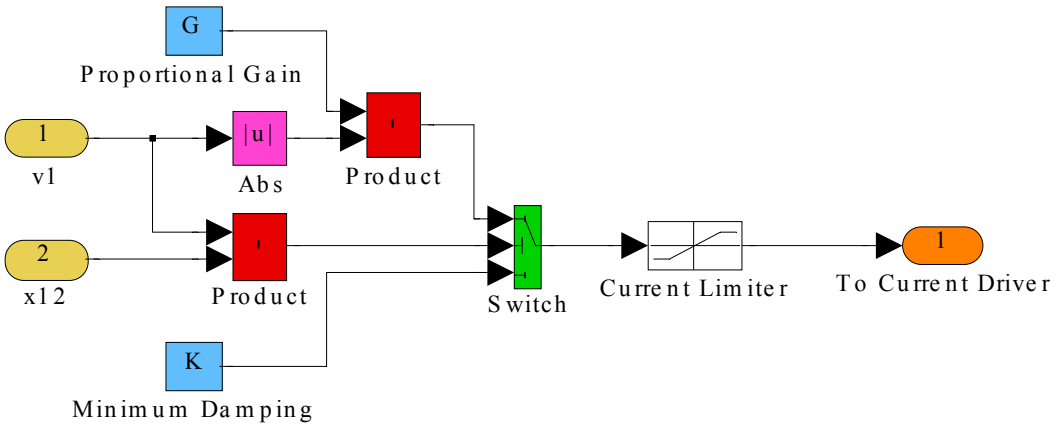

Figure 4-29. Block Diagram for Relative Displacement Control Logic

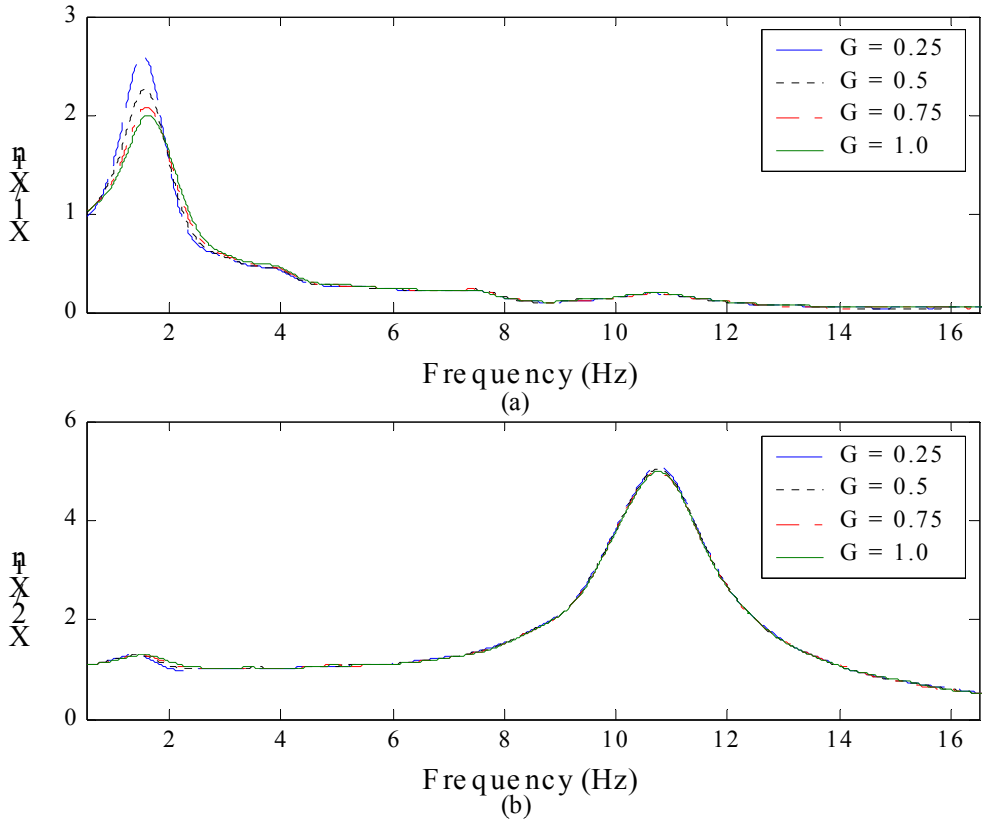

Figure 4-30. Relative Displacement Skyhook Control Transmissibilities: (a) Sprung Mass Transmissibility; (b) Unsprung Mass Transmissibility

The relative displacement transmissibility in Figure 4-31 further demonstrates the small gains achieved as *G* is increased. This observation was also demonstrated with displacement skyhook control.

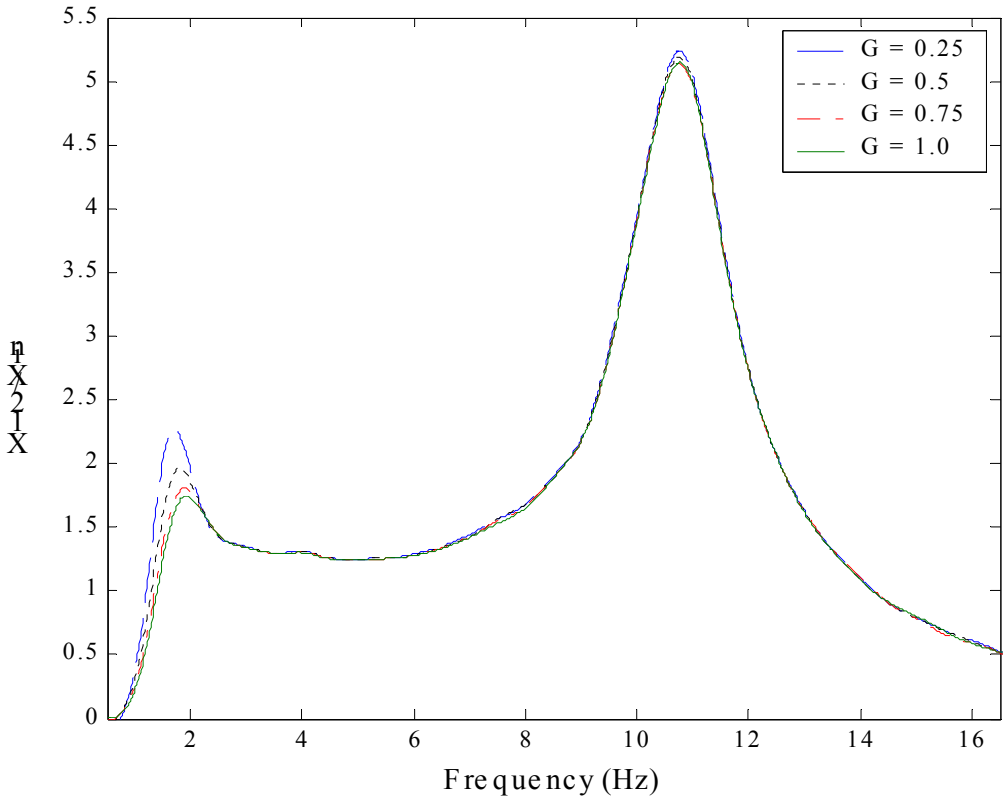

Figure 4-31. Relative Displacement Transmissibility for Relative Displacement Skyhook Control

Proceeding with the evaluation of relative displacement skyhook control, Figure 4-32 shows the acceleration auto spectrums of the sprung and unsprung masses. The same trend observed in the transmissibility plots appears here as well. The benefits of increasing *G* are minimal and they come at the cost of increased acceleration in the frequency range between the two natural frequencies.

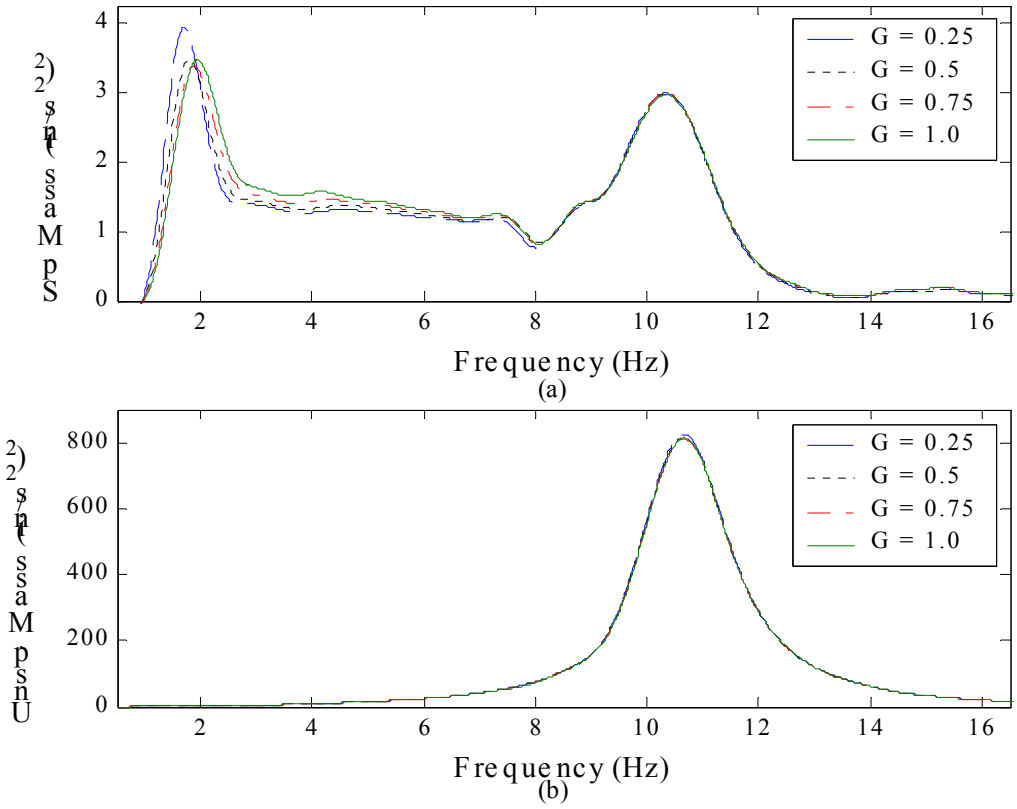

Figure 4-32. Relative Displacement Skyhook Control Acceleration Auto Spectrums: (a) Sprung Mass Auto Spectrum; (b) Unsprung Mass Auto Spectrum

4.9 Frequency Analysis Comparison

Plotting the results of each of the control policies together reveals the relative benefits of each of the control strategies. In the same manner that each controller was evaluated independently, the comparison will investigate the transmissibilities and the power spectrums of the controllers collectively. Figure 4-33 shows the sprung mass transmissibility, truncated for clarity, for each of the control techniques with G = 0.5, along with passive control with the current fixed at 0.8 Amps.

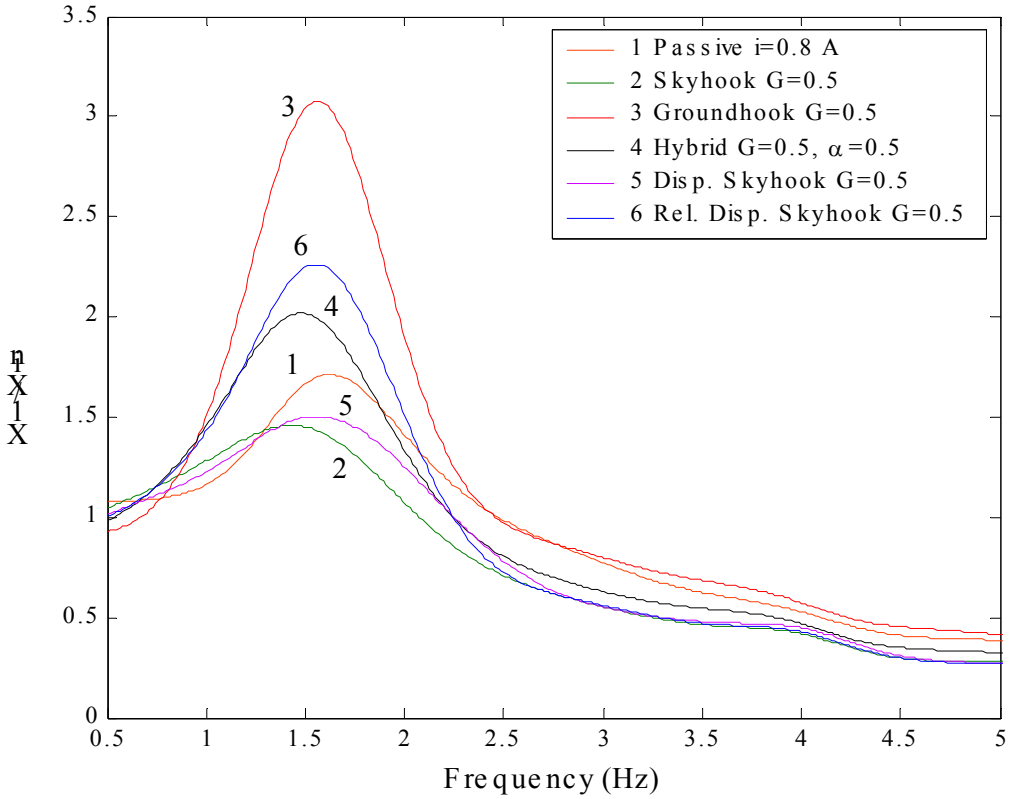

Figure 4-33. Sprung Mass Transmissibility for Different Control Techniques

As expected for the sprung mass, groundhook control sets the upper limit while skyhook control sets the lower limit. A relative comparison of the three skyhook techniques reveals that displacement skyhook can compete with conventional skyhook based on the results in Figure 4-33, while relative displacement skyhook requires more effort to achieve the response benefits of skyhook control. This idea is further emphasized when hybrid control with α = 0.5 is compared with relative displacement skyhook. Though the hybrid controller only has 50% contribution from skyhook control, the response is better than relative displacement skyhook. In other words, 50% skyhook is better than 100% relative displacement skyhook.

Figure 4-34 shows the transmissibility of the unsprung mass for the same controllers, again truncated for clarity. The semi-active controllers are displayed with

controller gain, G = 0.5, while the passive case is shown with the current fixed at 0.8 Amps. Hybrid control is shown with equal parts skyhook and groundhook, $\alpha = 0.5$.

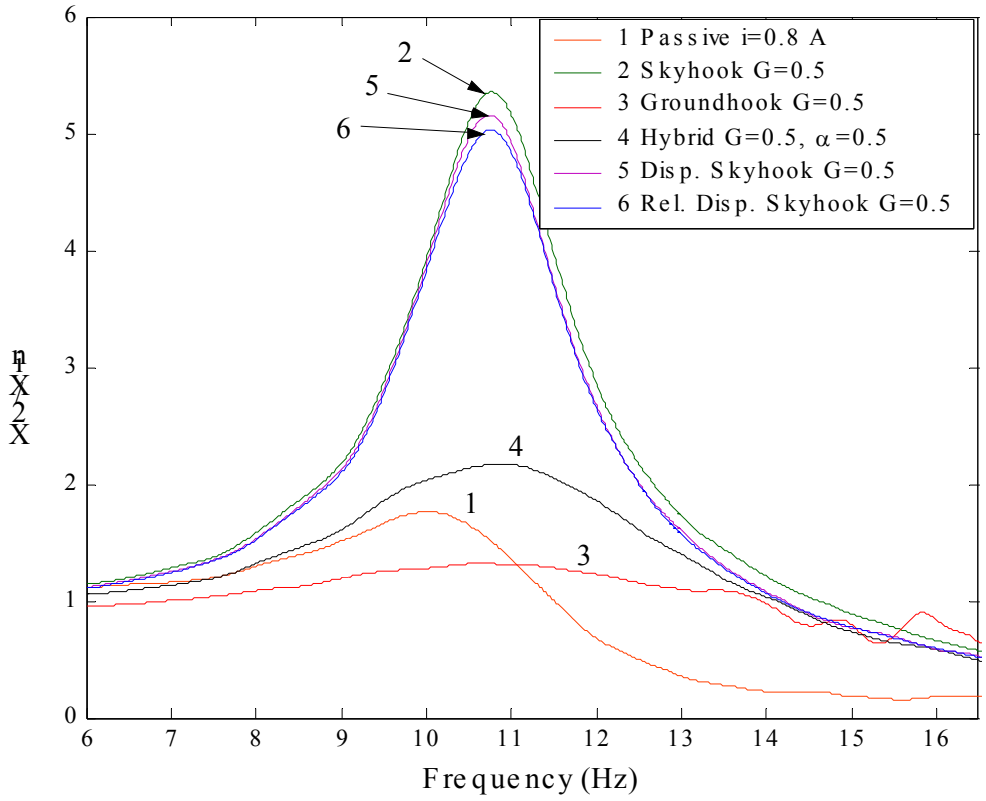

Figure 4-34. Unsprung Mass Transmissibility for Different Control Techniques

Once again, as expected, the response of each control strategy falls inside the boundaries defined by skyhook as the upper limit and groundhook as the lower limit. Figure 4-34 is valuable in that it reveals the relative performance of the three skyhook techniques at controlling the unsprung mass. Though the margin is small, displacement skyhook appears to offer better control of the unsprung mass than skyhook control. Moreover, relative displacement skyhook achieves the best unsprung mass control amongst the three skyhook techniques.

The sprung mass acceleration auto spectrum in Figure 4-35 reveals the dynamic response of the sprung mass for each control strategy. The dominance of skyhook

control in its ability to reduce the levels of sprung mass acceleration is emphasized when compared to the 5 other control techniques. With respect to the other control techniques, relative displacement skyhook fails to demonstrate its ability to reduce accelerations at the sprung mass natural frequency. However, because it is a skyhook-based technique, relative displacement skyhook surpasses all other non-skyhook policies at reducing the acceleration in the region between the two natural frequencies.

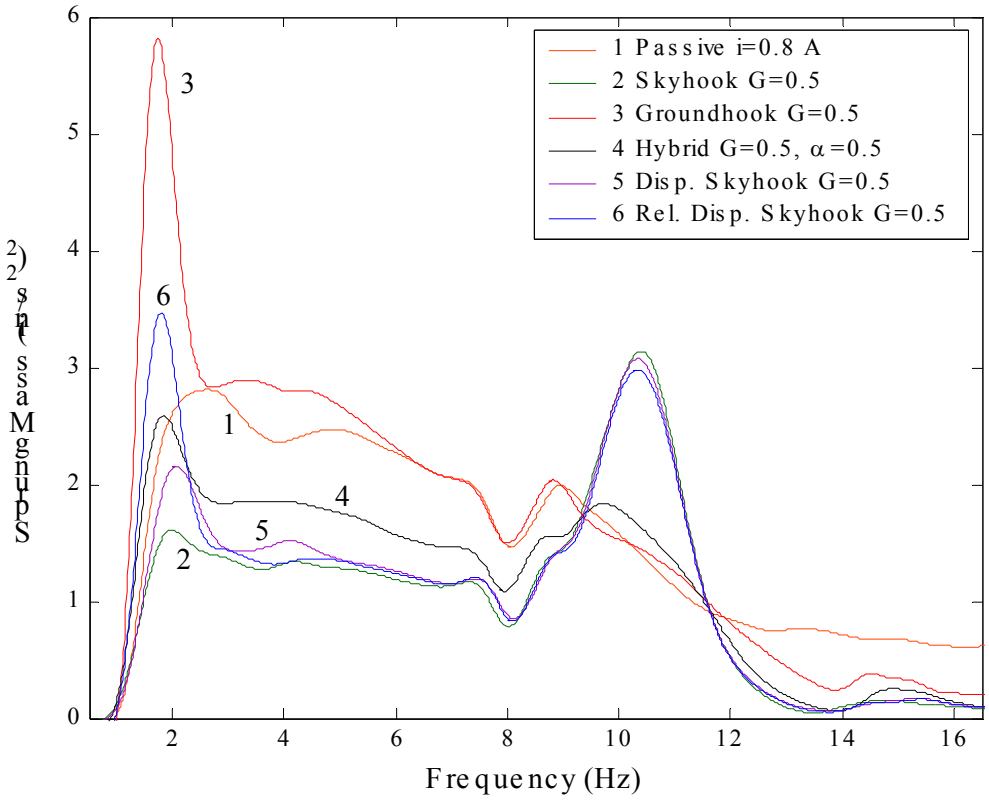

Figure 4-35. Sprung Mass Acceleration Auto Spectrum for Different Control Techniques

Figure 4-36 shows the acceleration auto spectrum for the unsprung mass. Groundhook clearly excels at minimizing the levels of acceleration at the unsprung mass. Of the three skyhook techniques, relative displacement skyhook permits the lowest level of acceleration.

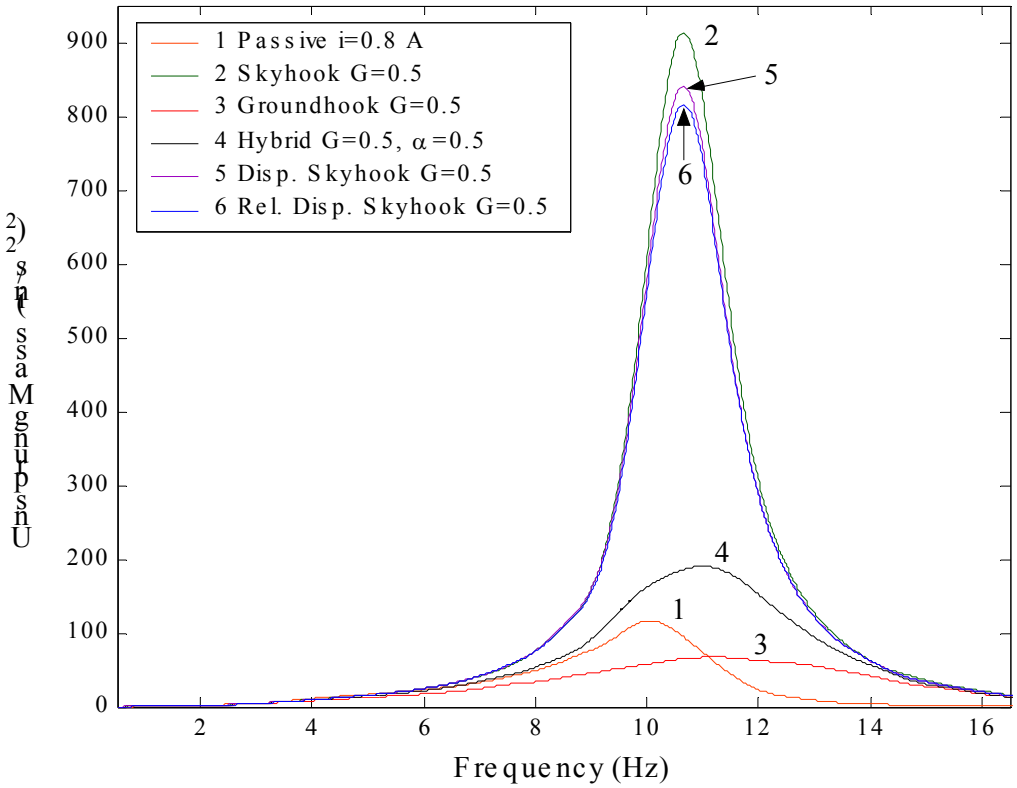

Figure 4-36. Unsprung Mass Acceleration Auto Spectrum for Different Control Techniques

5 Transient Response Analysis

In this chapter, the response dynamics for a transient input are evaluated for each type of control. Beginning with the definition of the input excitation used for this evaluation, the chapter proceeds with a discussion of the performance criteria used to measure the benefits of each control. This is followed by an assessment of the performance of each of the control policies.

5.1 Excitation for Transient Response Analysis

The transient input chosen for this study was a step input. More accurately, it was a square wave with a frequency of 0.1 Hz. The low frequency of the square wave ensured that the responses of the sprung and unsprung masses to the input had died out before the next input sequence. With a total period of 10 seconds, there was a 5 second delay between the steps in the square wave. This delay ensured that all dynamics had died out before the next input. The amplitude of the step input was limited by the physical stroke of the MR damper. We wanted to maximize the input amplitude of the step function without hitting the end stops of the damper. A peak-to-peak amplitude of 0.9 inches was found to be sufficient. The resulting input is shown in Figure 5-1.

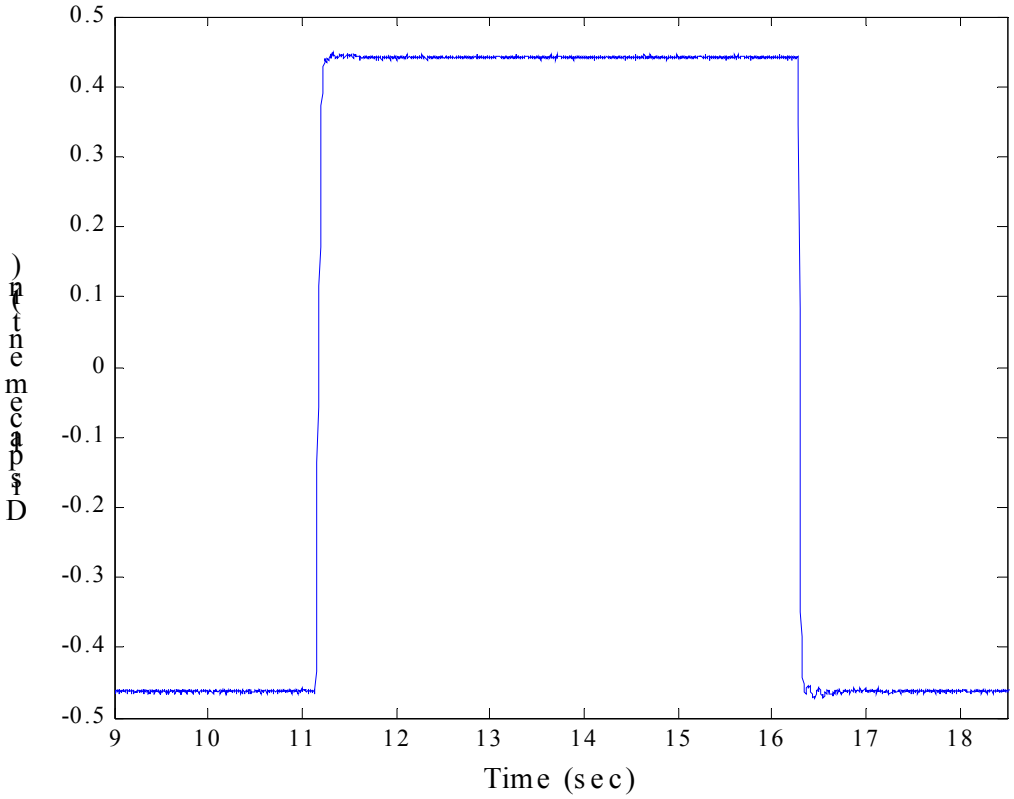

Figure 5-1. Step Input Signal

5.2 Transient Analysis Performance Criterion

Each control technique was evaluated for its performance at controlling the sprung and unsprung mass according to the following criteria:

- Peak-to-peak displacement
- Peak-to-peak acceleration

The peak-to-peak values are calculated as:

$$PTP = \max(x(t)) - \min(x(t)) \tag{5.1}$$

where *x(t)* is either the displacement or the acceleration of the sprung or unsprung masses. The minimums and maximums are defined as the minimums and maximums of

the response. Specifically, the maximums and minimums of the response refer to the maximums and minimums of the overshoot as shown in Figure 5-2.

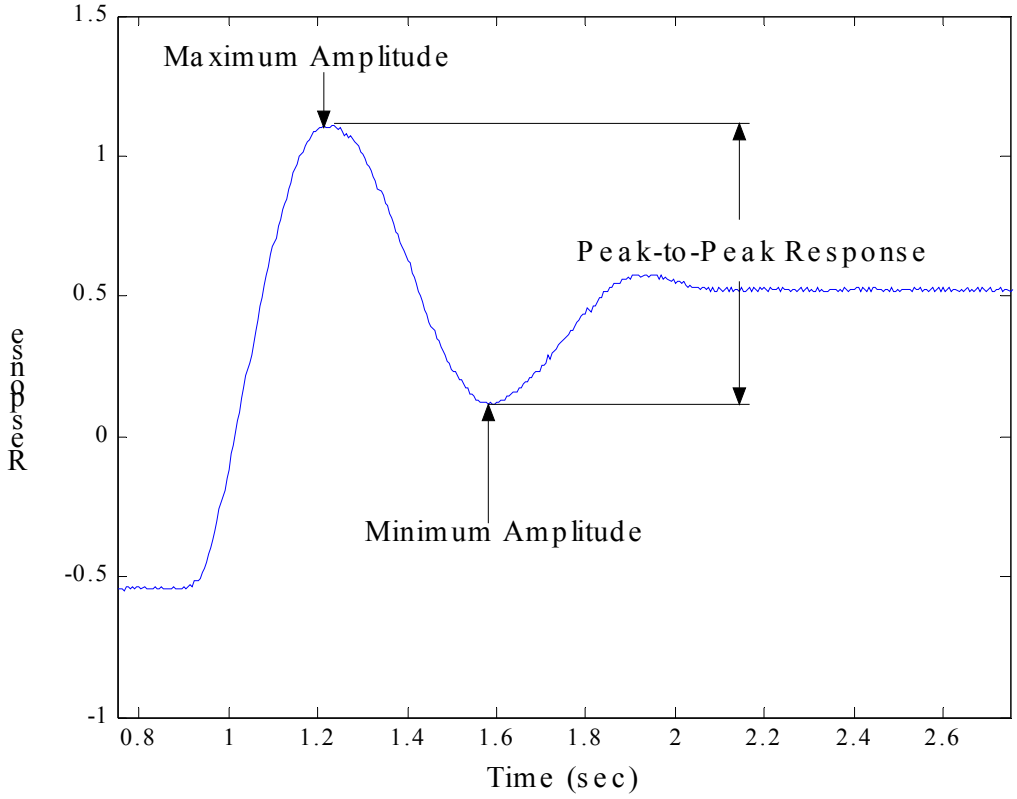

Figure 5-2. Step Response

Though the responses of the sprung and unsprung masses were measured for both the up and the down stroke of the step input, the results presented here focus on the up stroke of the input. The dynamics of the responses are different for the up and down stroke, however, we feel that the trend observed in the analysis of each of the control policies remains consistent for the up stroke and the down stroke.

5.3 Passive Control Transient Analysis

The MR damper was tested passively at five different currents. Time traces of the sprung and unsprung mass displacements are shown in Figure 5-3 for two current values, 0.0

Amps and 1.5 Amps. These currents were chosen because they define the limits of the passive damper. As the current, and therefore the damping, increases, the sprung mass overshoot decreases. The unsprung mass response displays very little overshoot for both levels of damping. This is due to the stiffness of the elastomeric mounts used to simulate the tire. We do, however, observe high frequency oscillations, particularly at low damping. Again, these oscillations are due to the unsprung mass effectively bouncing up and down on the elastomeric mounts.

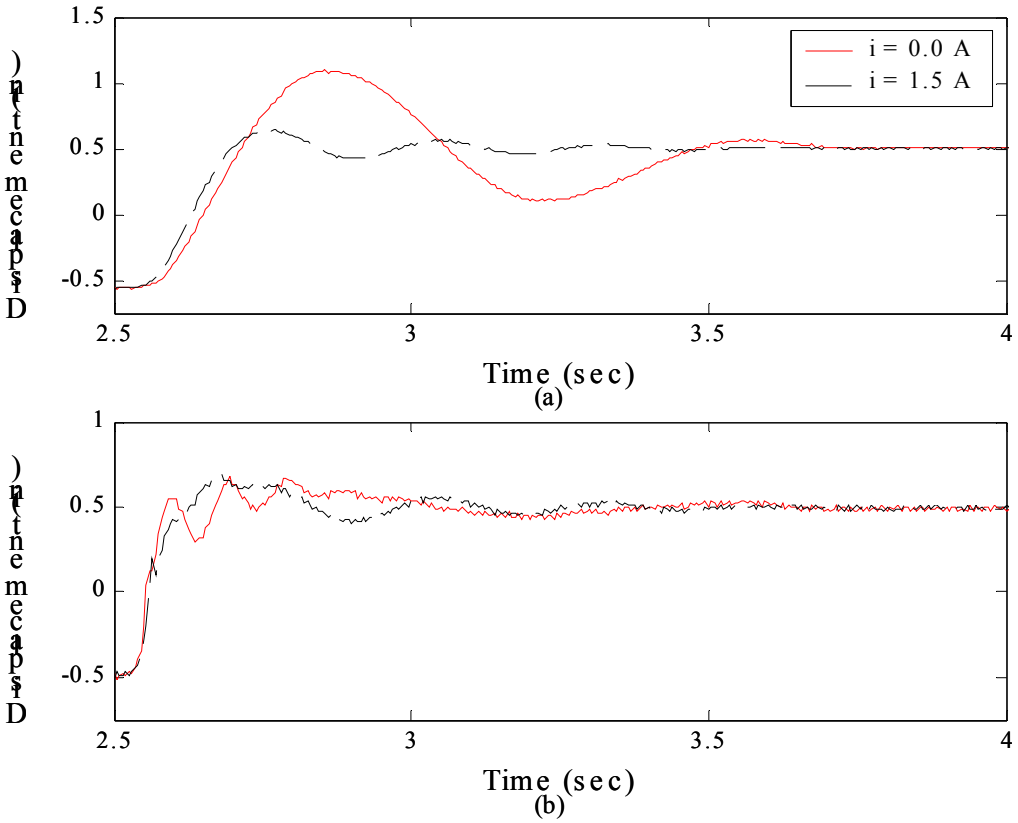

Figure 5-3. Passive Control Displacement Response:
(a) Sprung Mass Response; (b) Unsprung Mass Response

In order to quantify the results shown in Figure 5-3, the peak-to-peak values of displacement and acceleration were calculated. The results of the peak-to-peak displacement calculations are shown in Figure 5-4. As the current increases, both the

sprung and unsprung masses show a decrease in peak-to-peak displacement. However, once the damper exceeds 1.2 Amps, the displacement of the sprung mass begins to increase. The same affect appears in the unsprung mass once the current exceeds 0.8 Amps. At 1.5 Amps, the unsprung mass peak-to-peak displacement is greater than that of the damper in the off-state.

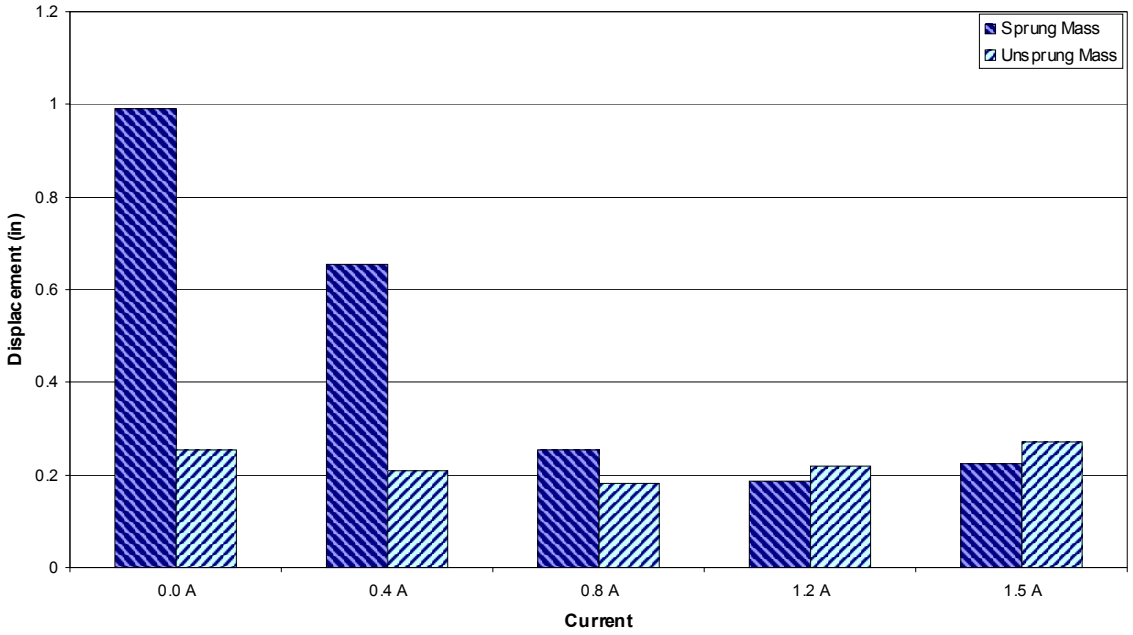

Figure 5-4. Passive Control Peak-to-Peak Displacement for Step Input

Figure 5-5 shows a sample time trace of the sprung and unsprung mass accelerations at the upper and lower limits of the MR damper. In Figure 5-5 we observe that he acceleration of the sprung mass is greater at high damping than at low damping. This is expected, as more of the energy is being transmitted rather than absorbed by the suspension. The opposite is true for the unsprung mass. At high damping, the unsprung mass acceleration decreases. Once again, the fundamental tradeoff between high and low damping is demonstrated.

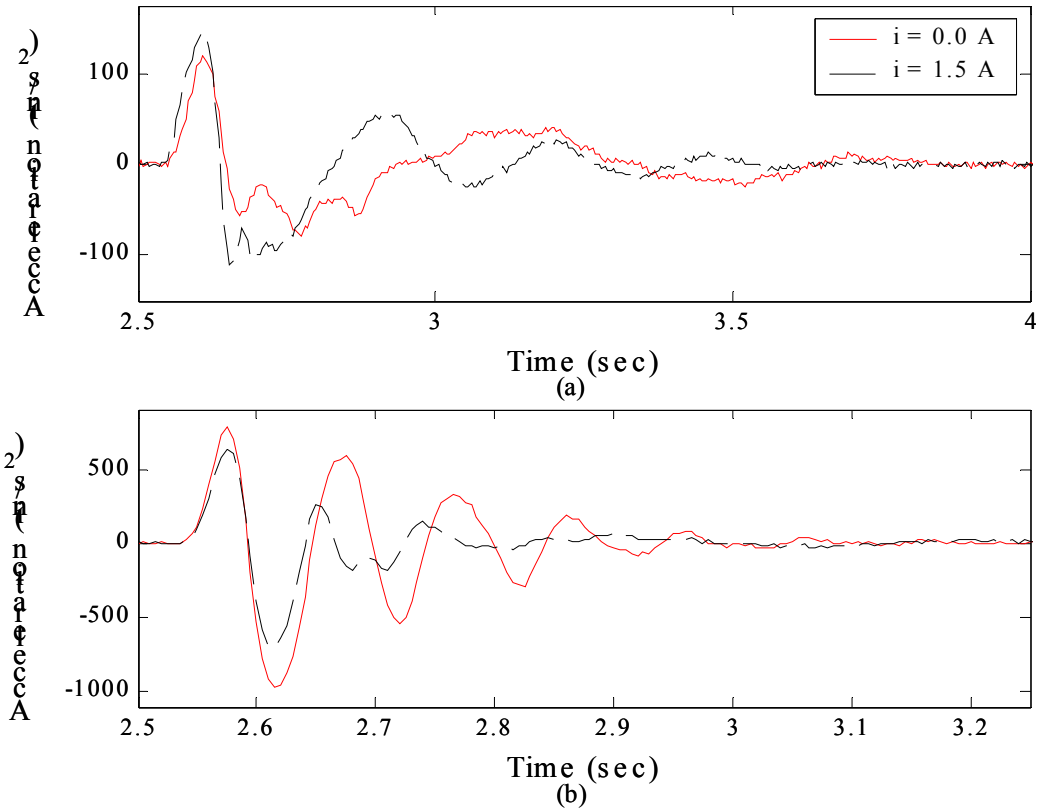

Figure 5-5. Passive Control Acceleration Response:
(a) Sprung Mass Response; (b) Unsprung Mass Response

The peak-to-peak acceleration results shown in Figure 5-6 confirm the observations made in Figure 5-5 (for scaling purposes, the sprung mass acceleration has been gained by 10). With the exception of the current increase from off-state to 0.4 Amps, the sprung mass acceleration levels increase as damper current increases. The unsprung mass, however, shows a decrease in acceleration levels as the damper current increases. Figure 5-6 visually illustrates the tradeoff common in passive suspensions.

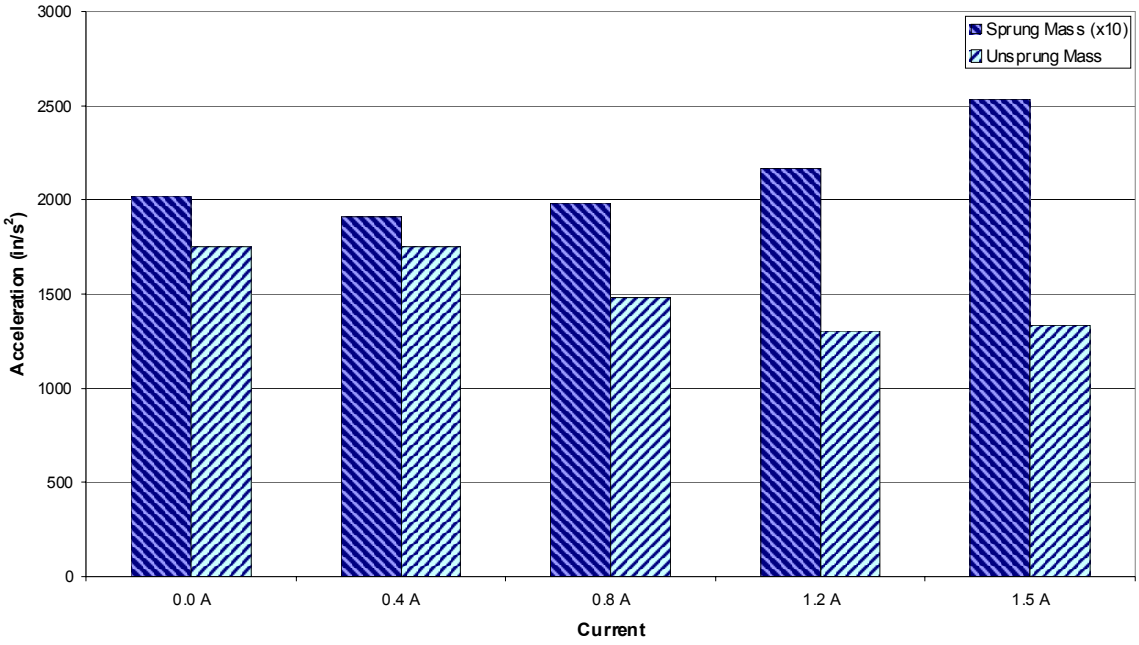

Figure 5-6. Passive Control Peak-to-Peak Acceleration for Step Input

5.4 Skyhook Control Transient Analysis

The transient analysis of skyhook control begins with the displacement time traces in Figure 5-7. Here the displacements of the sprung and unsprung mass are shown for a high and low value of the skyhook gain, *G*. At a low skyhook gain, we observe that the sprung mass overshoots its mark, while for a high skyhook gain, there is virtually no overshoot. The unsprung mass demonstrates the same dynamics observed for passive control. At low skyhook damping, the unsprung mass bounces up and down on the elastomeric mounts.

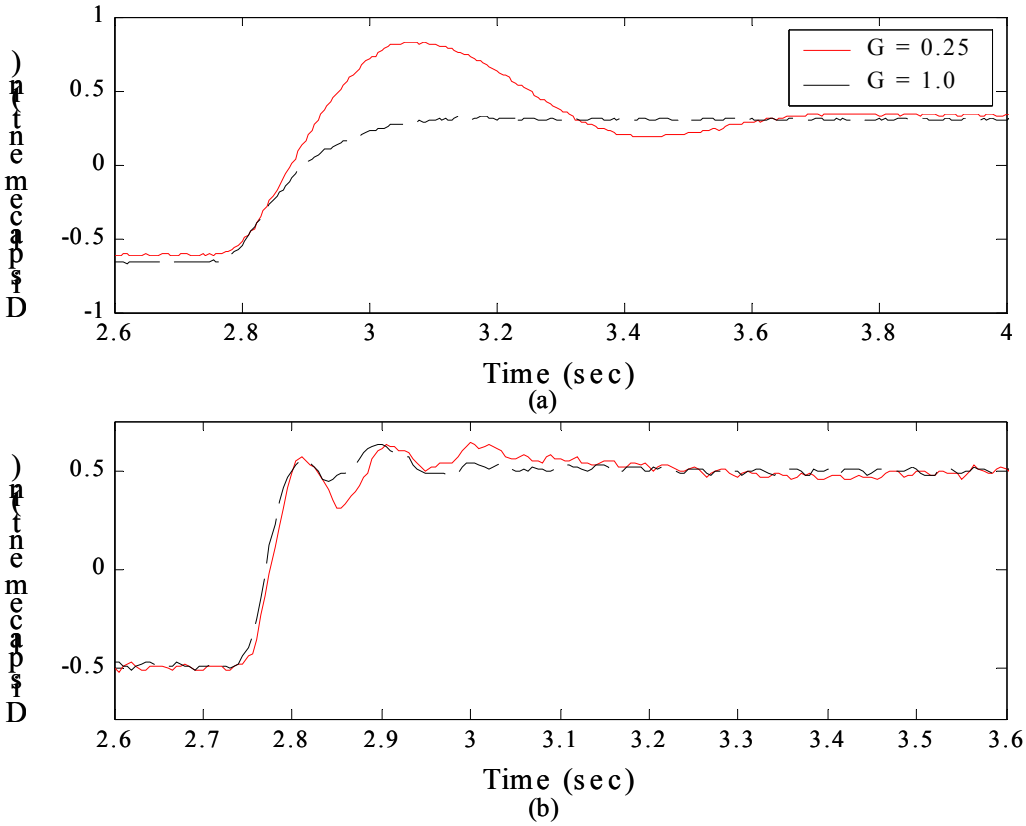

Figure 5-7. Skyhook Control Displacement Response:
(a) Sprung Mass Response; (b) Unsprung Mass Response

The peak-to-peak displacement values for several skyhook gains are shown in Figure 5-8. As observed in Figure 5-7, as the skyhook gain increases, the peak-to-peak displacement of the sprung mass decreases. The results in Figure 5-8 are powerful in their demonstration of skyhook's ability to reduce the sprung mass response to a step input. Considering the unsprung mass, we observe that the peak-to-peak displacement decreases slightly as the skyhook gain approaches 0.75. Once the controller gain exceeds 0.75, the peak-to-peak displacement increases.

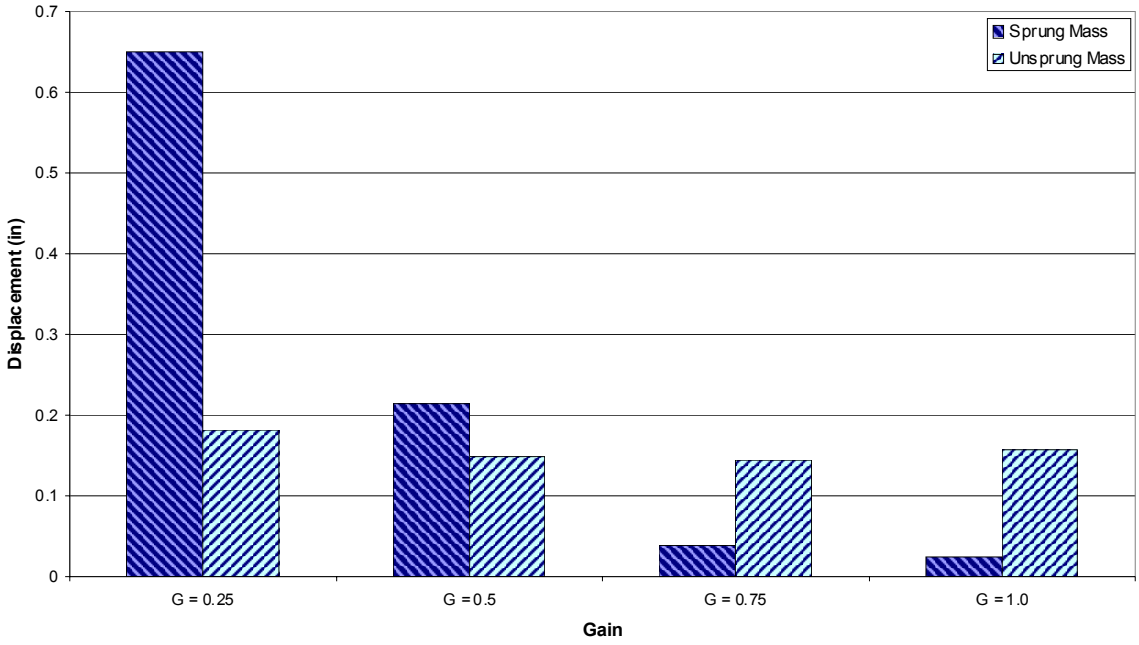

Figure 5-8. Skyhook Control Peak-to-Peak Displacement for Step Input

Figure 5-9 reveals that the benefits observed in displacement control come at the cost of acceleration. At low skyhook gain, the acceleration of the sprung mass is less than that of high skyhook damping. However, it appears that the response of the sprung mass dies out faster at a high skyhook gain. The unsprung mass acceleration remains unchanged between high and low levels of skyhook gain.

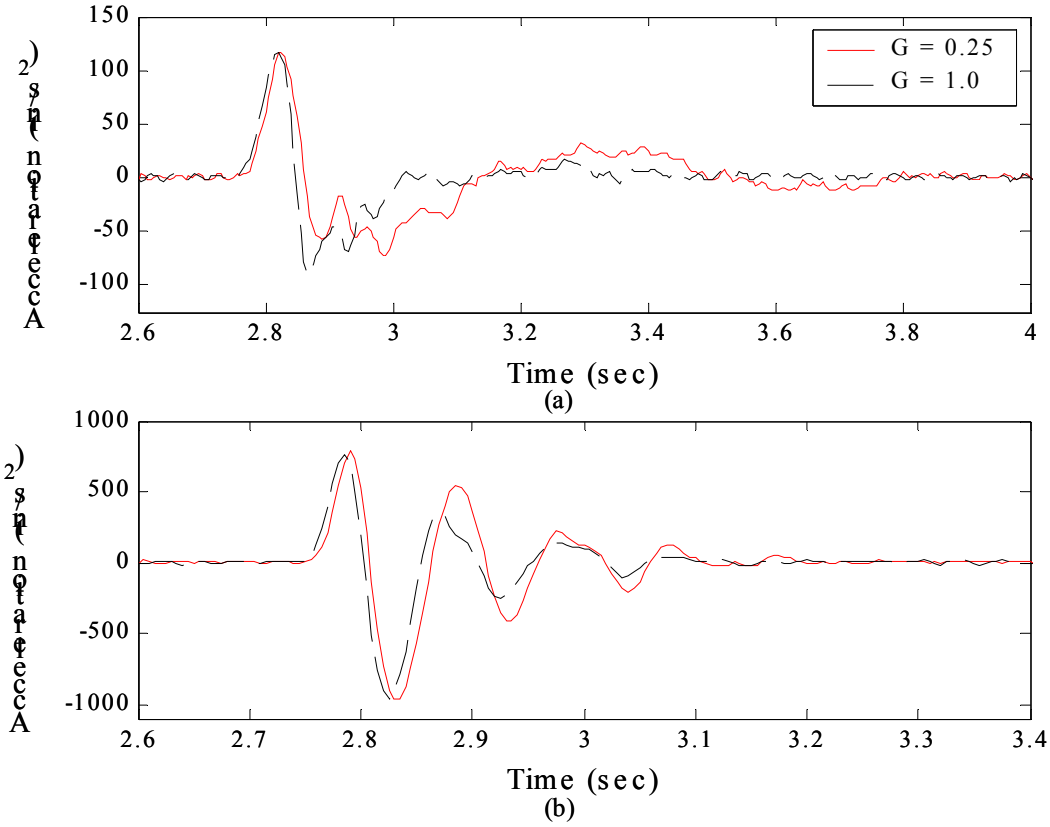

Figure 5-9. Skyhook Control Acceleration Response:
(a) Sprung Mass Response; (b) Unsprung Mass Response

The results drawn from Figure 5-9 are confirmed in Figure 5-10. Again, the sprung mass has been gained by 10 in order to match scales with the unsprung mass. As the skyhook gain increases from 0.25 to 0.5, the sprung mass acceleration decreases. Beyond 0.5, however, the peak-to-peak acceleration of the sprung mass increases. The apparent tradeoff with skyhook control is between displacement and acceleration. The reduction of peak-to-peak displacements comes at the cost of increased peak-to-peak accelerations. However, relative to the benefits achieved in reducing peak-to-peak displacements, the increases observed in the peak-to-peak accelerations are rather low. Clearly, the gains realized in control of displacement as the skyhook gain is increased outweigh the costs of increased acceleration.

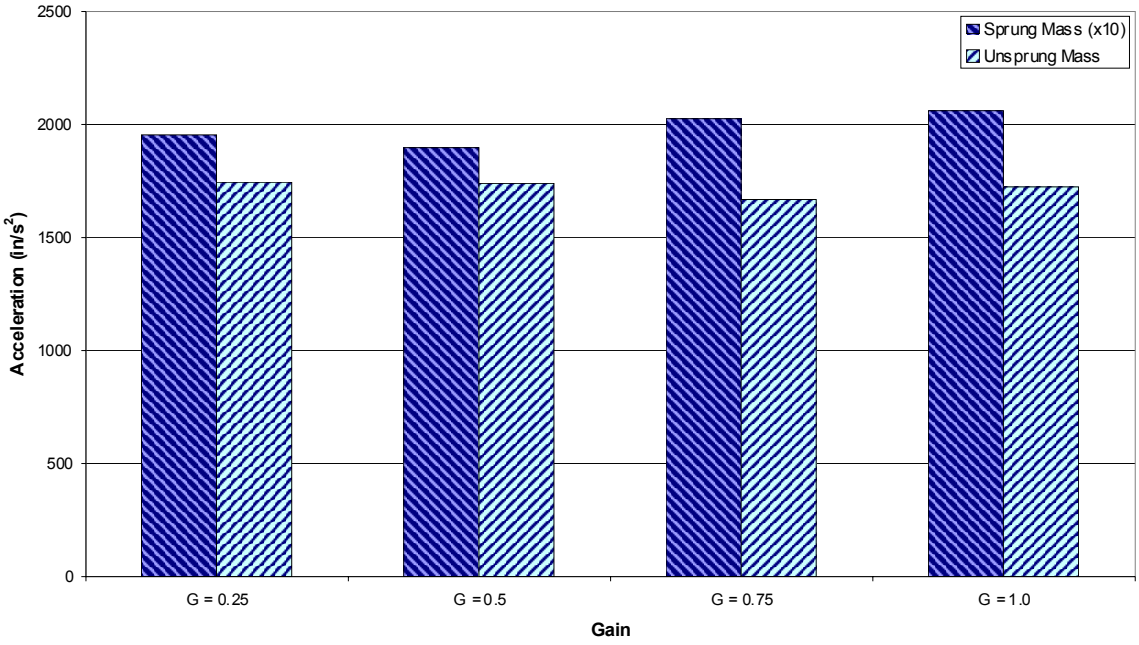

Figure 5-10. Skyhook Control Peak-to-Peak Acceleration for Step Input

5.5 Groundhook Control Transient Analysis

A sample time trace of the sprung and unsprung mass displacements under groundhook control is shown in Figure 5-11. The sprung mass displacement remains unchanged between high and low groundhook gain. In considering the unsprung mass, we must evaluate the high frequency dynamics. Though the response is dominated by the low frequency dynamics of the sprung mass, in evaluating the performance of groundhook control, the focus must be on the high frequency dynamics. From Figure 5-11, we see that the high frequency oscillations are eliminated at high groundhook gains.

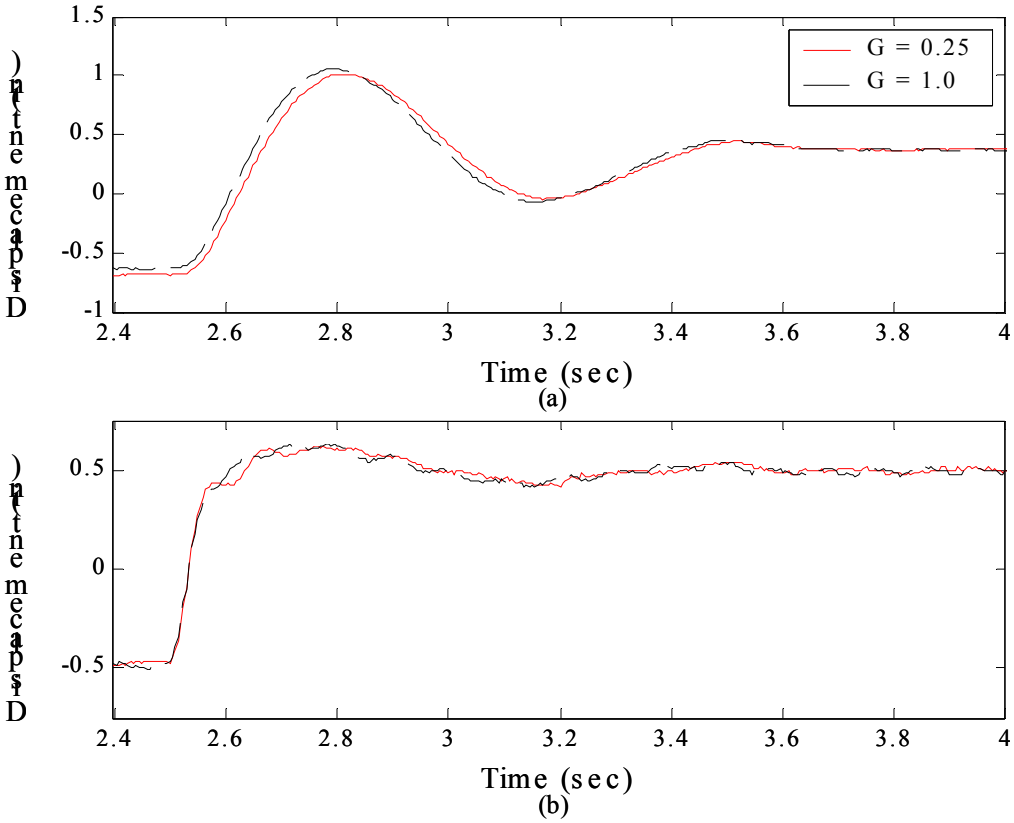

Figure 5-11. Groundhook Control Displacement Response:
(a) Sprung Mass Response; (b) Unsprung Mass Response

The impressive results shown in Figure 5-12 vividly demonstrate the benefits of groundhook control. Here, the unsprung mass displacement was gained by 10 for scaling purposes. The peak-to-peak displacements of the high frequency dynamics in the unsprung mass are effectively eliminated for high values of the groundhook gain. Figure 5-12 also shows that the sprung mass peak-to-peak displacements increase marginally as the groundhook gain increases. In regard to the sprung mass, these increases in peak-to-peak displacements are common and expected for groundhook control.

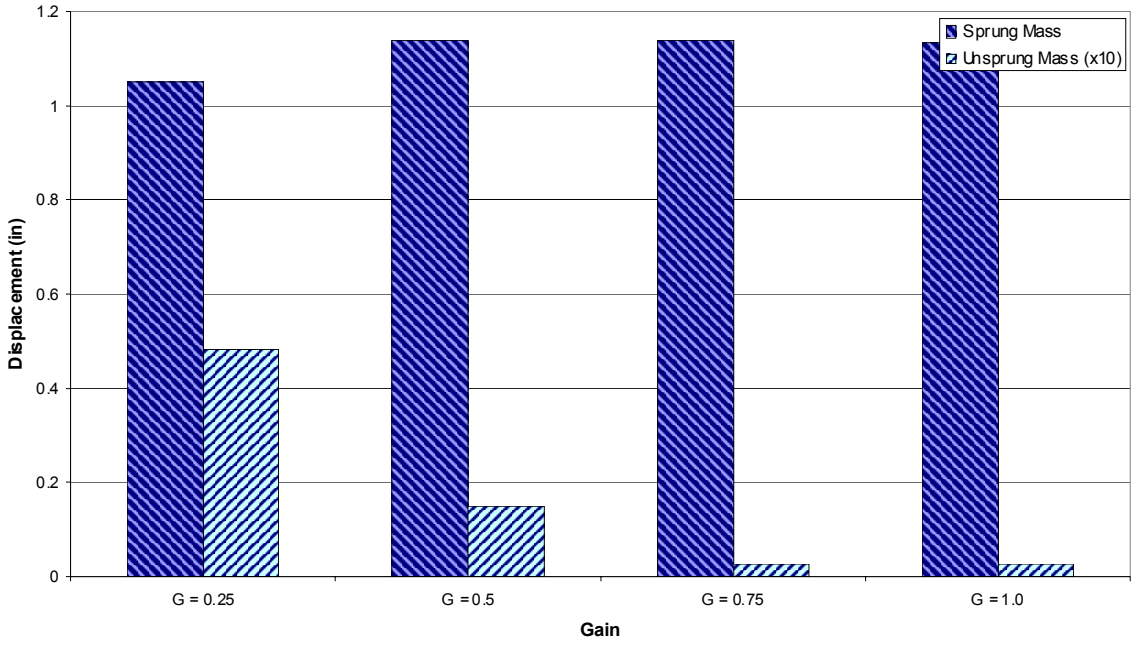

Figure 5-12. Groundhook Control Peak-to-Peak Displacement for Step Input

Next, we consider the acceleration response for groundhook control, shown in Figure 5-13. The time response of the acceleration indicates that the benefits of groundhook do not extend greatly into control of acceleration. Shown here at high and low groundhook gains, the peak-to-peak acceleration of the unsprung mass appears to remain the same. As for the sprung mass, the changes are insignificant.

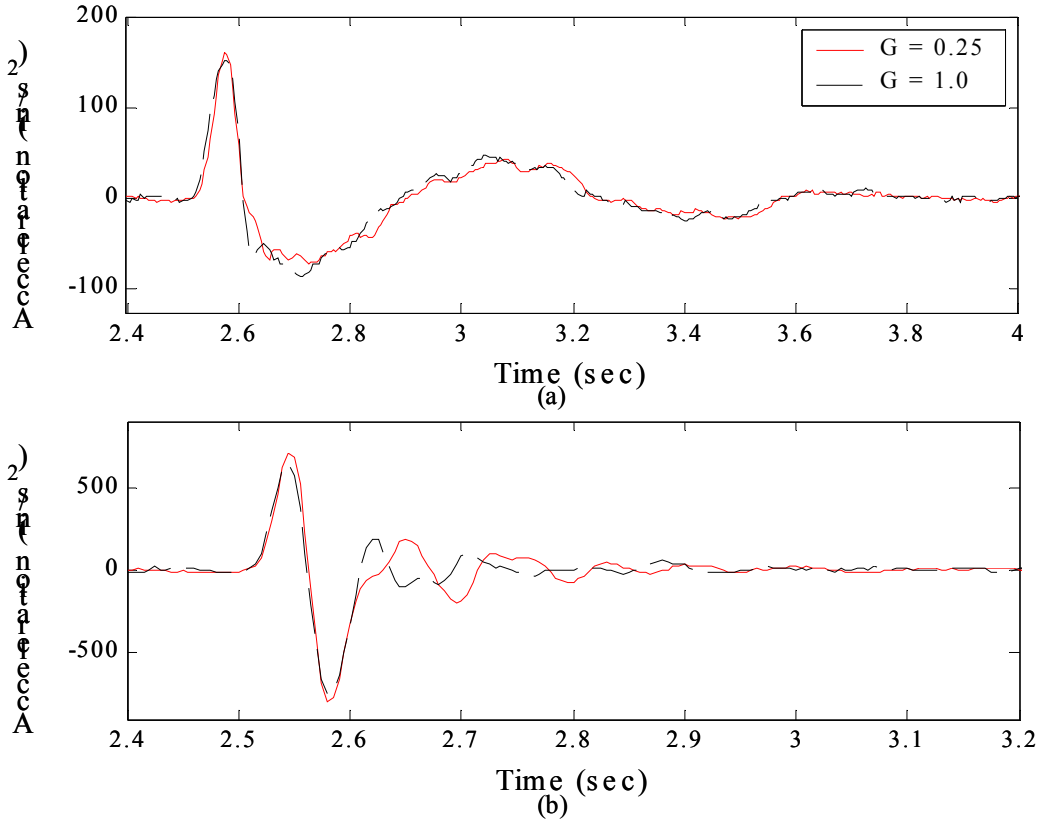

Figure 5-13. Groundhook Control Acceleration Response:
(a) Sprung Mass Response; (b) Unsprung Mass Response

Quantification of the peak-to-peak acceleration results is shown in Figure 5-14. Here we observe a small decrease in the peak-to-peak acceleration of the unsprung mass for increasing groundhook gain. Unlike the tradeoff between displacement control and acceleration control seen in skyhook, groundhook appears to offer benefits in reducing both the displacement and the acceleration of the unsprung mass. In regards to the unsprung mass solely, groundhook control is apparently cost free. When we consider the sprung mass, we see small increases in peak-to-peak accelerations as the groundhook gain increases.

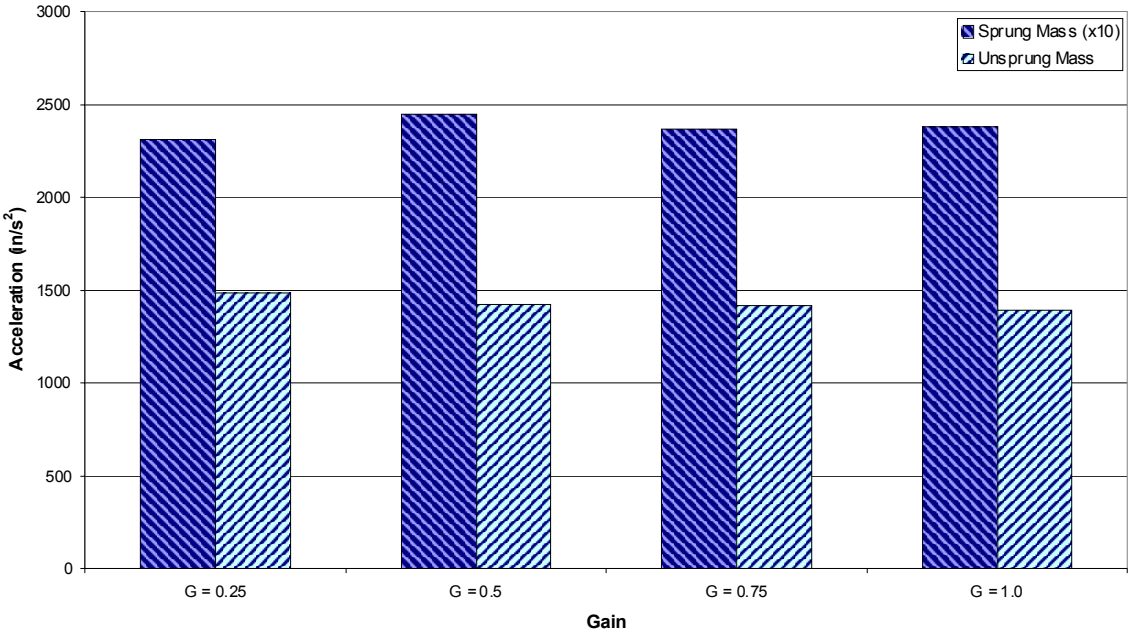

Figure 5-14. Groundhook Control Peak-to-Peak Acceleration for Step Input

5.6 Hybrid Control Transient Analysis

Figure 5-15 shows a sample time trace of the displacement response for hybrid control. This particular response is with α = 0.5. The 50/50 contribution from skyhook and groundhook is evident in the response of both masses. From low hybrid gain to high hybrid gain, we observe attenuation in the displacement of both masses. This time trace demonstrates how hybrid control can eliminate the tradeoff between skyhook and groundhook controls.

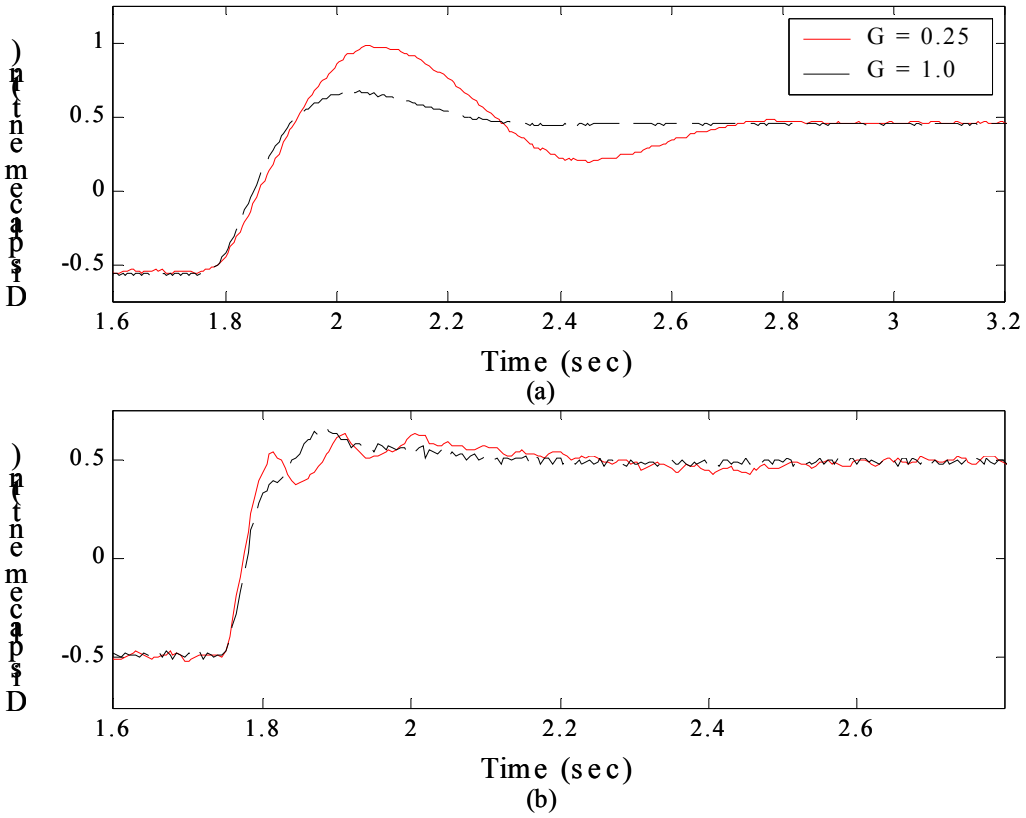

Figure 5-15. Hybrid Control Displacement Response:
(a) Sprung Mass Response; (b) Unsprung Mass Response

The peak-to-peak displacement values for hybrid control were evaluated at four combinations of α and hybrid gain. The results are shown in Figure 5-16. What we observe from Figure 5-16 is that best possible combination of α and hybrid gain for both masses is $\alpha = 0.75$ and $G = 1$. Even though the contribution from groundhook control is only 25%, the peak-to-peak displacement response at $G = 1$, equals that of a 75% contribution from groundhook with $G = 1$. The results shown here indicate that hybrid control can be weighted more towards skyhook control and still achieve dramatic benefits in regards to the unsprung mass for a step input.

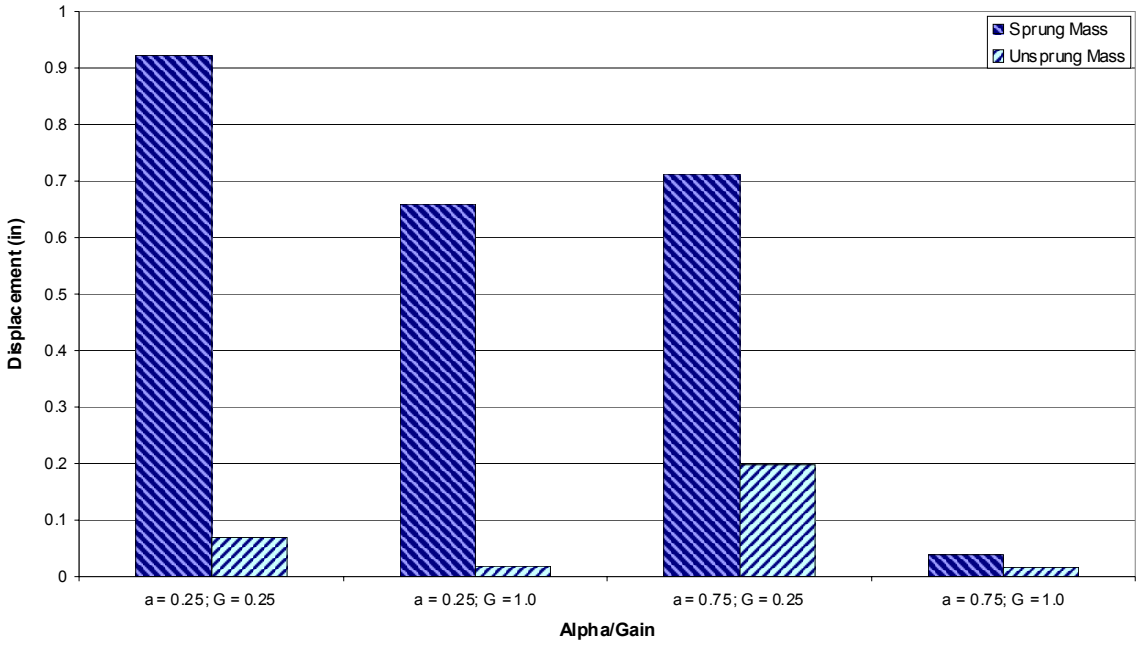

Figure 5-16. Hybrid Control Peak-to-Peak Displacement for Step Input

The acceleration time trace shown in Figure 5-17 indicates that with an α of 0.5 the sprung mass acceleration increases between low hybrid gain and high hybrid gain. The opposite is true for the unsprung mass acceleration. For both masses, the settling time is greatly reduced. In the case of the sprung mass, this comes at the cost of increased acceleration levels.

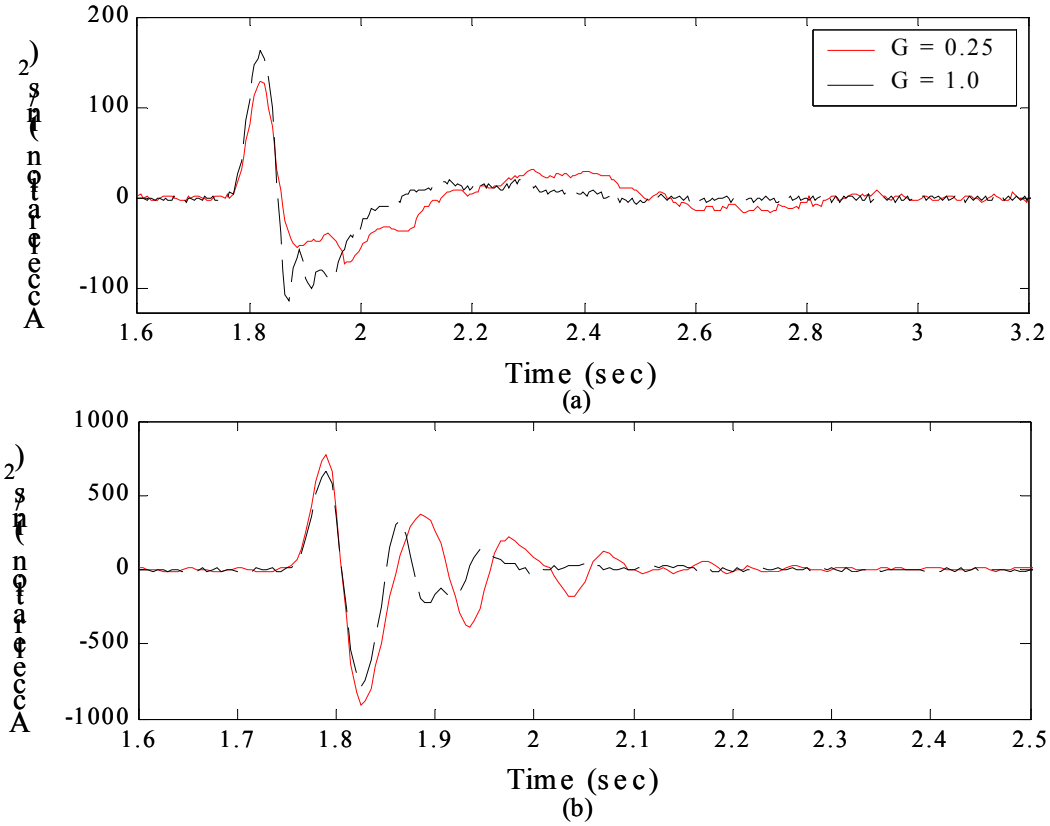

Figure 5-17. Hybrid Control Acceleration Response:
(a) Sprung Mass Response; (b) Unsprung Mass Response

Figure 5-18 shows the results of the peak-to-peak acceleration calculations. We observe that for low α, the sprung mass acceleration increases as hybrid gain increases, while the unsprung mass acceleration decreases. This result is expected. What we do not expect is the observation made at high α. Here, with 75% contribution from skyhook control, the sprung mass acceleration increases as hybrid gain increases, while the unsprung mass acceleration decreases. This result supports the statement made earlier about small contributions from groundhook control having a large impact on the control of the unsprung mass. The increase of the sprung mass acceleration at high α is greater than the increase in acceleration at low α. This implies that as the contribution from skyhook control increases, the acceleration of the sprung mass increases as well.

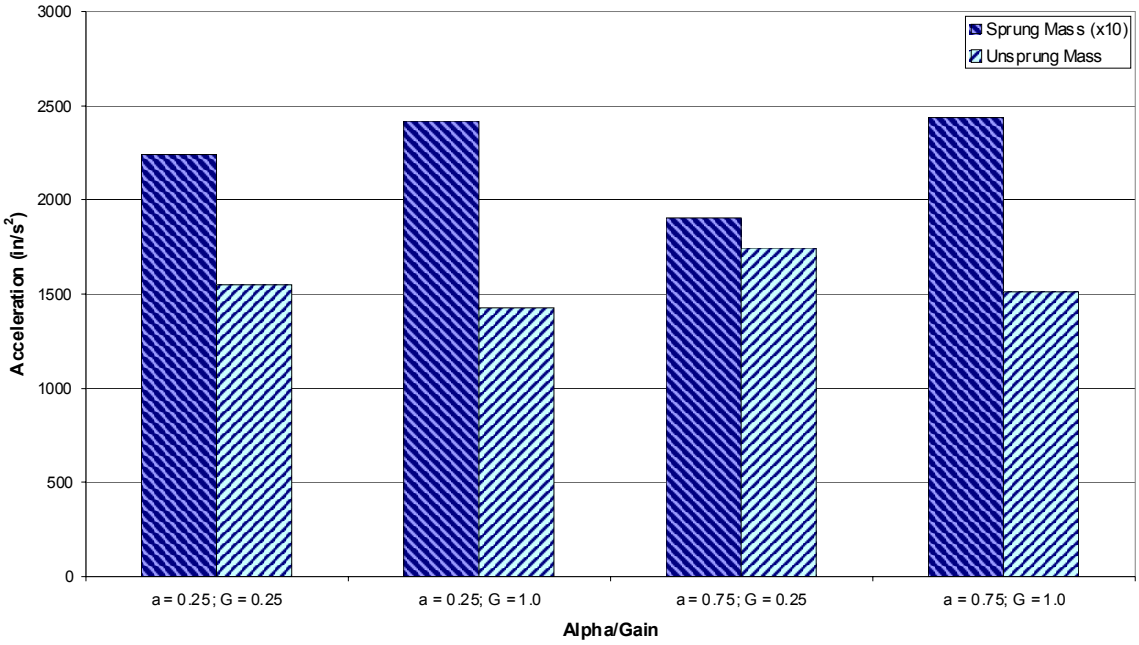

Figure 5-18. Hybrid Control Peak-to-Peak Acceleration for Step Input

5.7 Displacement Skyhook Control Transient Analysis

The step response of the sprung and unsprung masses is shown in Figure 5-19. A skyhook based controller, displacement skyhook demonstrates benefits for controlling the sprung mass. In Figure 5-19, we notice that with a controller gain of one, the sprung mass displacement overshoot is effectively eliminated. This same result was observed with conventional skyhook. The unsprung mass response appears to remain unchanged between controller gains.

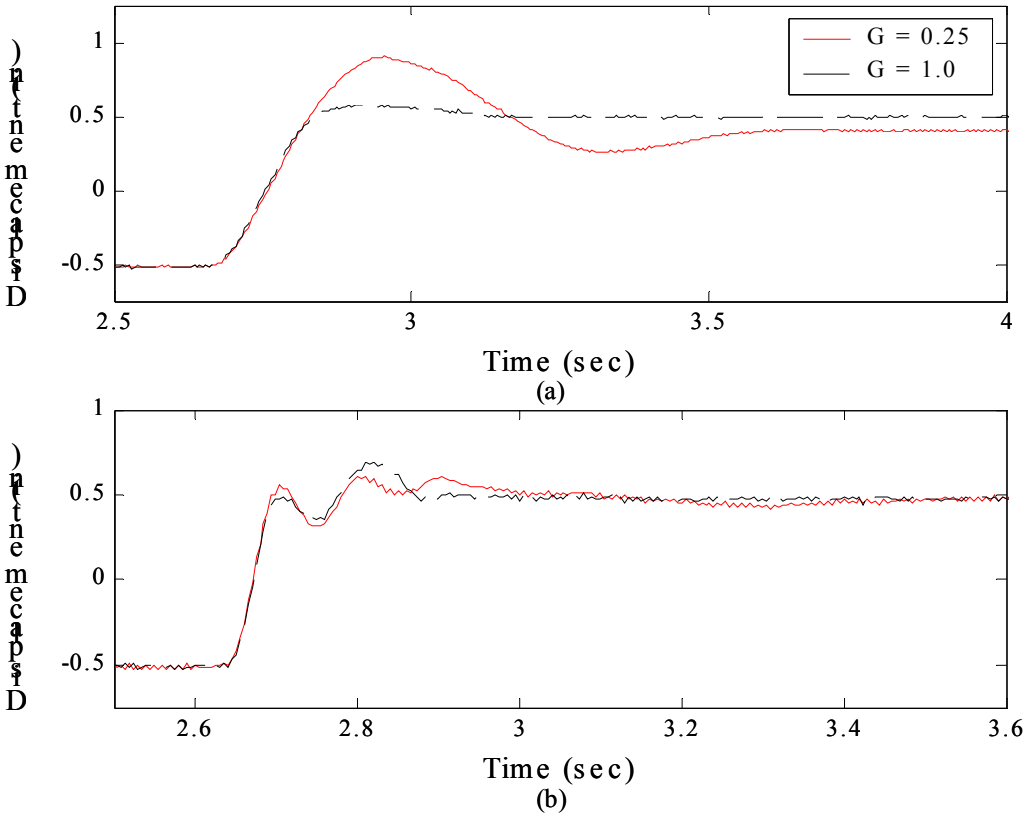

Figure 5-19. Displacement Skyhook Control Displacement Response: (a) Sprung Mass Response; (b) Unsprung Mass Response

In Figure 5-20, we quantify the benefits of displacement control. The reductions in the sprung mass peak-to-peak displacement are encouraging. We also notice a marginal decrease in the unsprung mass peak-to-peak response displacements. These marginal gains may be artifacts of the controller attempting to control the sprung mass. In any event, we observe improved response dynamics at the unsprung mass.

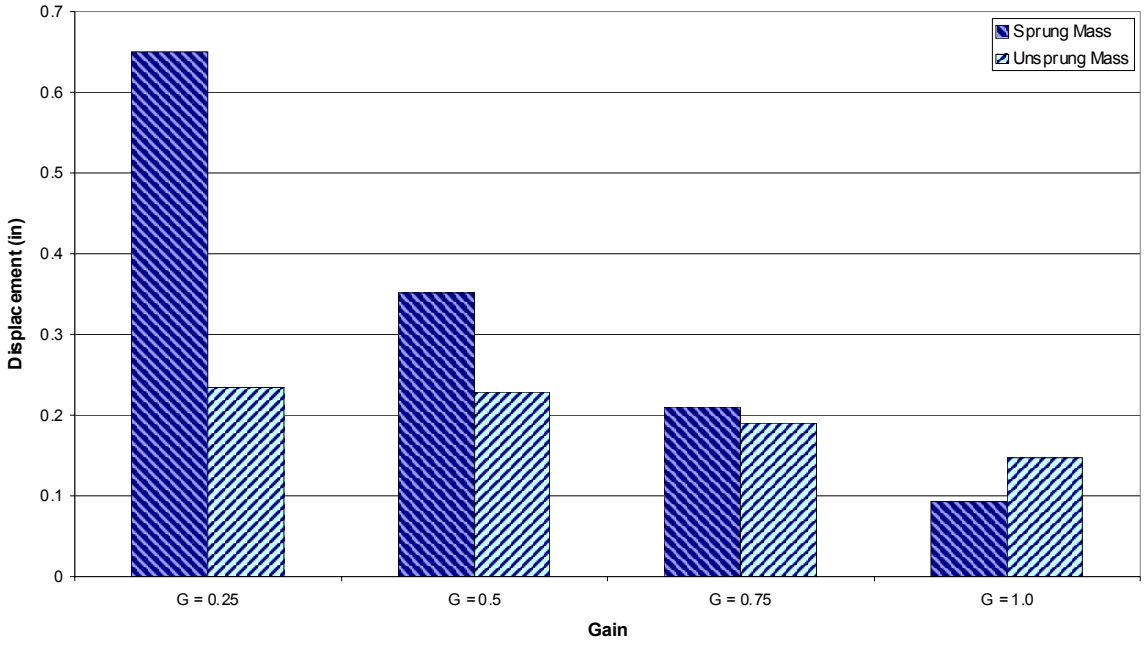

Figure 5-20. Displacement Skyhook Control Peak-to-Peak Displacement for Step Input

In considering the acceleration responses of the sprung and unsprung masses, fallbacks of displacement skyhook become evident. In the sample acceleration time response shown in Figure 5-21, we see that the peak-to-peak acceleration of the sprung mass is greater at high controller gains than at low controller gains. Once again, the unsprung mass response appears to remain unchanged between controller gains.

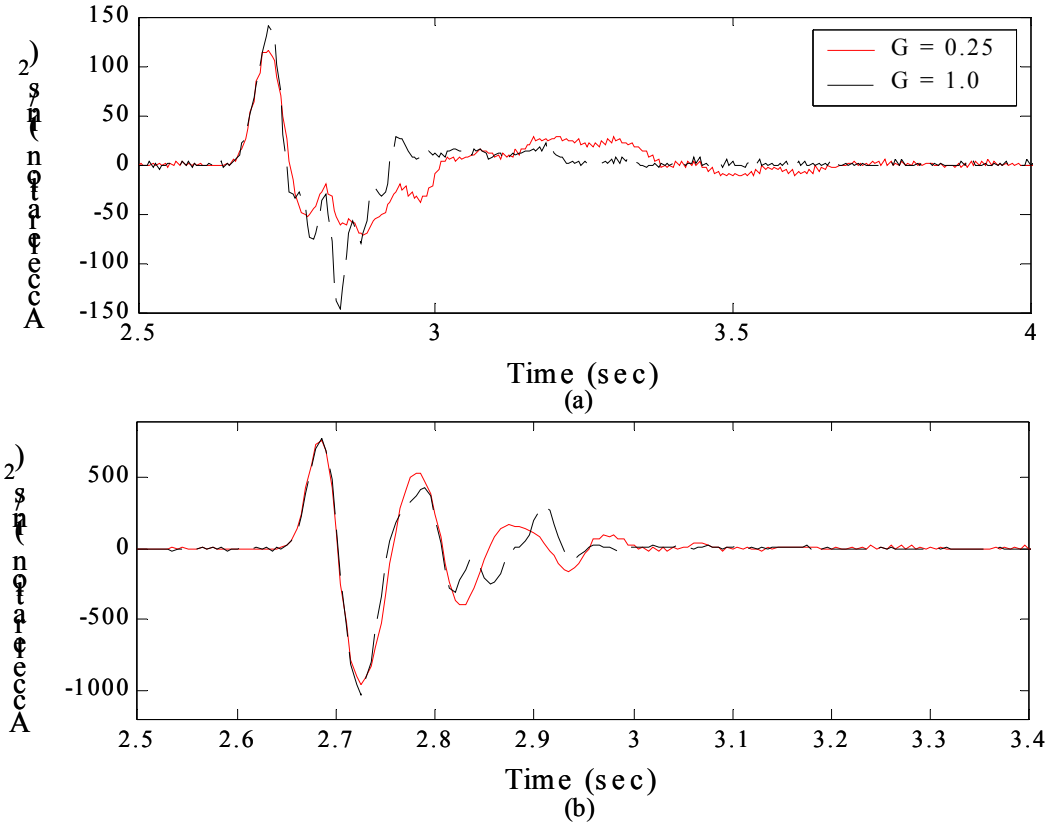

Figure 5-21. Displacement Skyhook Control Acceleration Response: (a) Sprung Mass Response; (b) Unsprung Mass Response

The observations made based on the sample time responses are confirmed in the peak-to-peak acceleration calculations shown in Figure 5-22. Here we observe a substantial increase in the acceleration of the sprung mass. This same trend was noticed in conventional skyhook control, though not to the extent shown in Figure 5-22. These results indicate that the benefits of displacement skyhook come at a greater cost than those of conventional skyhook. In Figure 5-22, the unsprung mass peak-to-peak acceleration levels remain constant for increasing controller gain.

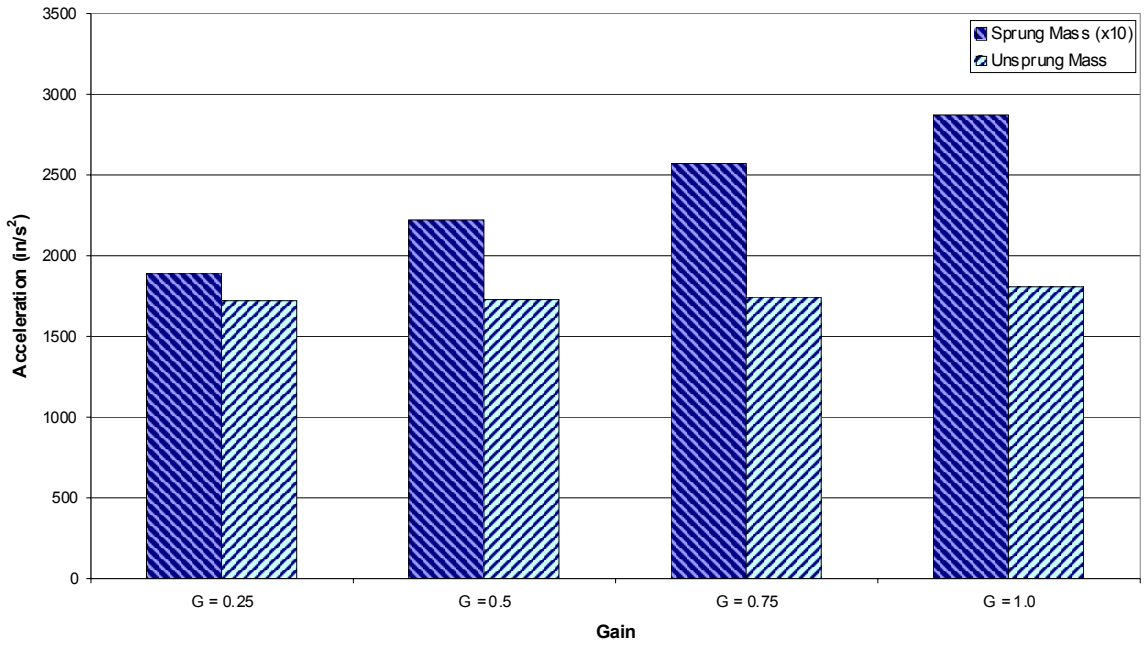

Figure 5-22. Displacement Skyhook Control Peak-to-Peak Acceleration for Step Input

5.8 Relative Displacement Skyhook Control Transient Analysis

The final control policy tested was relative displacement skyhook control. Again, a skyhook based policy, we expect to see benefits in controlling the sprung mass. This idea is supported by the time response in Figure 5-23. Though not to the extent of the other skyhook based controllers, relative displacement skyhook does show improvements in reducing the response of the sprung mass. However, for the same controller gain, the relative benefits are rather low. The response of the unsprung mass is not changed at all. At high controller gain, the response follows with the response of low controller gain.

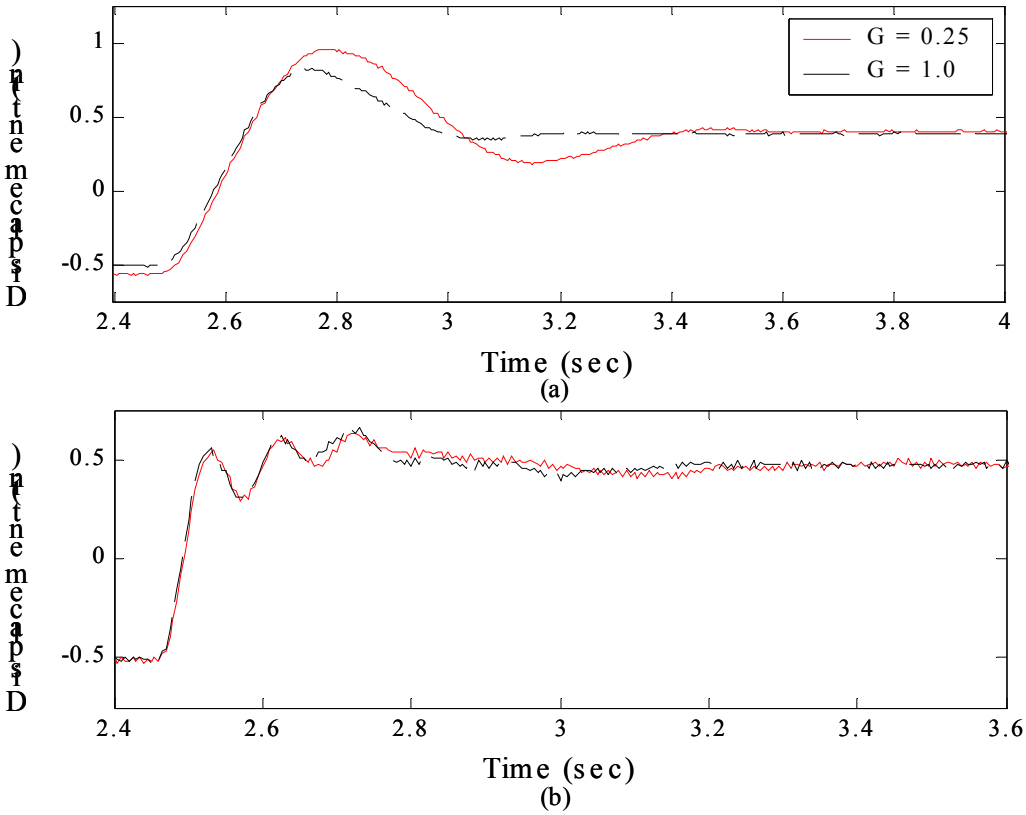

Figure 5-23. Relative Displacement Skyhook Control Displacement Response: (a) Sprung Mass Response; (b) Unsprung Mass Response

The results in Figure 5-24 reveal the modest benefits of relative displacement skyhook control. As controller gain increases, the sprung mass peak-to-peak displacement decreases. This reduction in peak-to-peak amplitude is relatively small to the reductions achieved with the other two skyhook based controllers. Figure 5-24 also shows a marginal increase in the peak-to-peak displacement of the unsprung mass as controller gain increases.

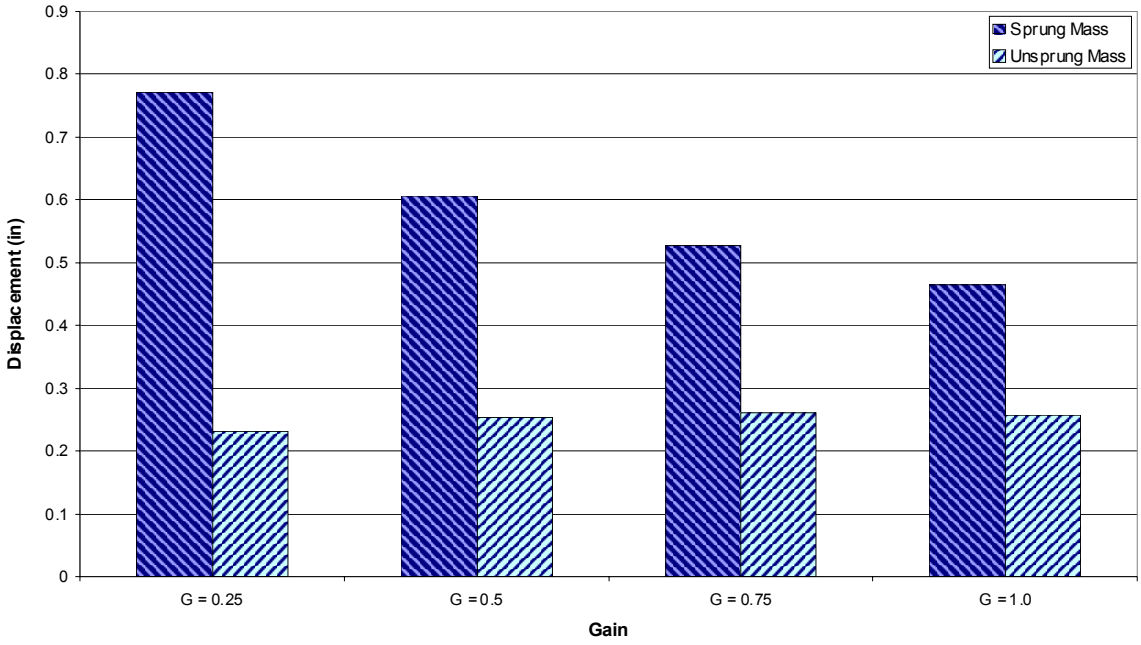

Figure 5-24. Relative Displacement Skyhook Control Peak-to-Peak Displacement for Step Input

The acceleration time response shown in Figure 5-25 reveals some interesting dynamics occurring in the sprung mass. At high controller gain, we observe a high frequency oscillation. These oscillations can be credited to the dynamics of the elastomeric mounts. We also notice larger peak-to-peak amplitude at high controller gains. The unsprung mass dynamics remain unchanged for high and low controller gains.

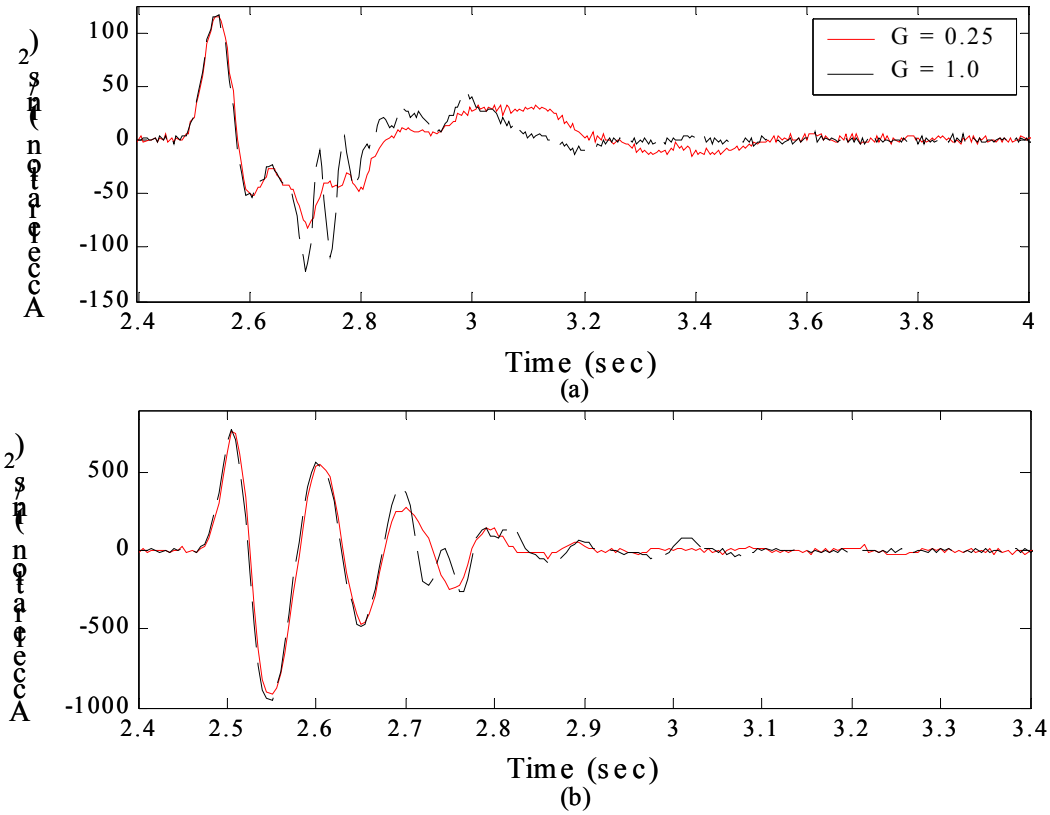

Figure 5-25. Relative Displacement Skyhook Control Acceleration Response: (a) Sprung Mass Response; (b) Unsprung Mass Response

The peak-to-peak acceleration results are shown in Figure 5-26. The sprung mass acceleration has been gained by 10 for scaling purposes. We observe the same trend that was implied in the time response. As the controller gain increases, the sprung mass peak-to-peak acceleration increases. Relative to displacement based skyhook, the increases in acceleration amplitudes are small. Figure 5-26 also shows that the unsprung mass acceleration does not change for increasing values of controller gain.

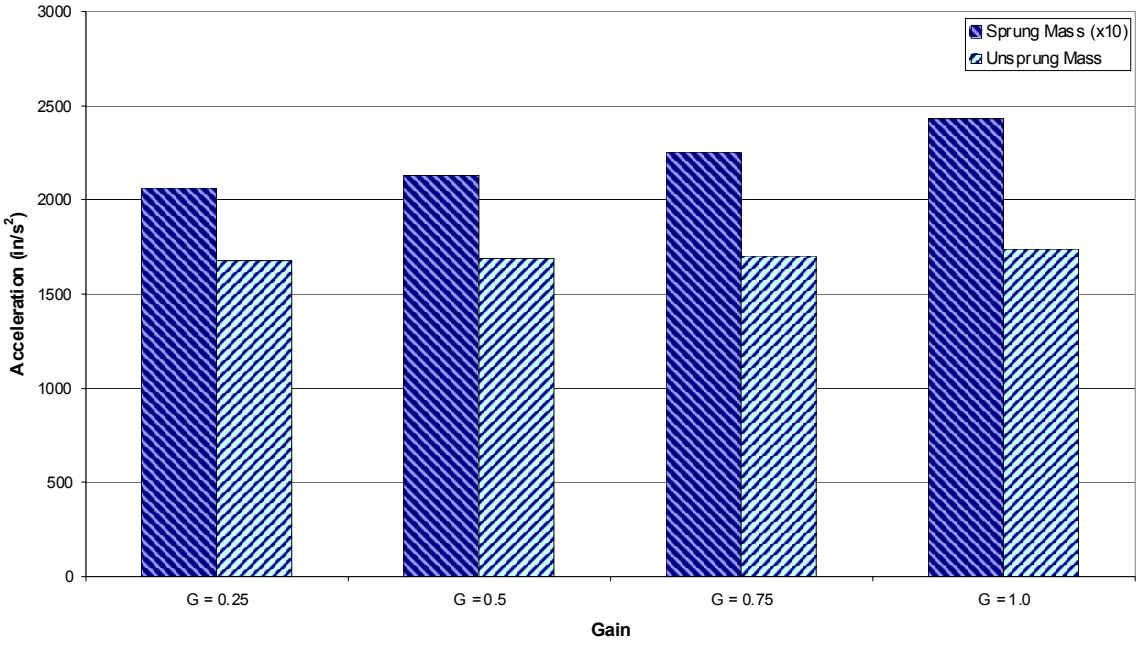

Figure 5-26. Relative Displacement Skyhook Control Peak-to-Peak Acceleration for Step Input

6 Steady State Response Analysis

This chapter evaluates the performance of each of the control techniques under steady state conditions. First, the input excitations used for this evaluation are introduced. Next, the criterion by which the performance was measured will be discussed. This is followed by a careful evaluation of each of the control options.

6.1 Excitation for Steady State Response Analysis

The inputs chosen for this portion of the study are derived from the dynamics of the quarter-car rig. Two pure tone sine waves with frequencies at 1.5 Hz and 10.5 Hz were chosen to represent the steady state analysis. Because these frequencies are the natural frequencies of the sprung and unsprung masses, exciting the quarter-car rig at these frequencies resulted in the greatest response. Therefore, the ability or disability of each of the control techniques to control the response to these inputs would be highlighted. In other words, this approach measures the performance of each of the control options at controlling the worst case scenario for both the sprung and unsprung masses.

Choosing the amplitudes for these two inputs was done based on the limitations of the quarter-car system. For the 1.5 Hz signal, a peak-to-peak amplitude of 0.9 inches was chosen. This amplitude was limited by the stroke of the MR damper. At this amplitude, the travel across the damper was approaching the end-stops of the damper.

The amplitude that was chosen for the 10.5 Hz signal was 0.2 inches peak-to-peak. The limiting component with this input was the elastomeric mounts used to simulate the tire. Because the unsprung mass is at resonance, the displacement amplitude across the elastomers is relatively large. A peak-to-peak amplitude greater than 0.2 inches would have bottomed out the mounting brackets for the elastomeric mounts.

6.2 Steady State Performance Criterion

Each control technique was evaluated for its performance at controlling the sprung and unsprung mass according to the following criteria:

- Peak-to-peak displacement
- RMS displacement
- Peak-to-peak acceleration
- RMS acceleration
- Work done by MR damper

The peak-to-peak values can be expressed as:

$$PTP = \max(x(t)) - \min(x(t)) \tag{6.1}$$

where *x(t)* is either the displacement or the acceleration of the sprung or unsprung masses. The RMS values are defined as:

$$RMS = \frac{\sqrt{\sum_{i}^{M} x_i(t)}}{\sqrt{M}} \tag{6.2}$$

where M is the length of the displacement or acceleration signal. The displacement standards are valuable in considering the physical travel of each of the masses. This becomes particularly important for the unsprung mass. Large displacements at the wheel-hop natural frequency could lead to unsafe driving conditions. Criterions dealing with acceleration are catered to the sprung mass. Acceleration is the parameter by which ride comfort is commonly measured.

The work done by the MR damper corresponds to the enclosed area of the force displacement plots. It can be expressed as:

$$Work = \frac{\sum_{i}^{M} \left| F_{d_i}(t) \cdot x_{12_i}(t) \right|}{M} \tag{6.3}$$

where F_d is the damper force and x_{12} is the relative displacement across the damper. The work is presented in the same format as the displacement and acceleration evaluation. For each controller, a sample force displacement plot is shown along with a sample force

velocity plot. These are valuable in demonstrating the dynamic force benefits of semi-active control.

6.3 Passive Control Steady State Evaluation

The results revealed here demonstrate many of the tradeoffs common in passive suspensions. What works well at the 1.5 Hz excitation offers poor control at the 10.5 Hz excitation and visa versa.

6.3.1 Pure Tone 1.5 Hz

Figure 6-1 shows the peak-to-peak displacement for the sprung and unsprung masses. The solid red line represents the peak-to-peak displacement of the input signal. Regardless of the current, passive control never reduces the peak-to-peak amplitude of the sprung mass below that of the input signal. Another observation is that, at this frequency, passive control does not reduce the amplitude of the unsprung mass.

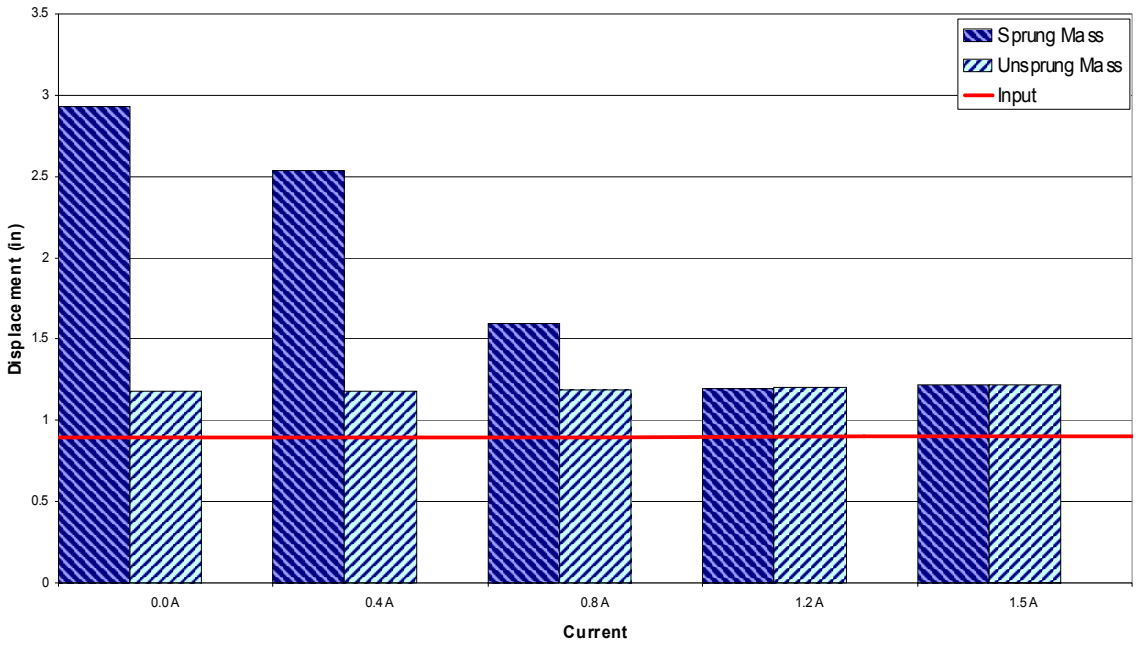

Figure 6-1. Passive Control Peak-to-Peak Displacement at 1.5 Hz

The RMS displacement shown in Figure 6-2 reveals some interesting behavior. As the current increases from 0.4 Amps to 0.8 Amps, the RMS displacement of the sprung mass increases. Figure 6-2 does not share the same trend illustrated in Figure 6-1. The amplitude decreases from 0.0 Amps to 0.4 Amps, but then increases from 0.4 Amps to 0.8 Amps. The behavior above 0.8 Amps is consistent with the peak-to-peak displacement behavior. Again, the red line represents the RMS displacement of the input signal.

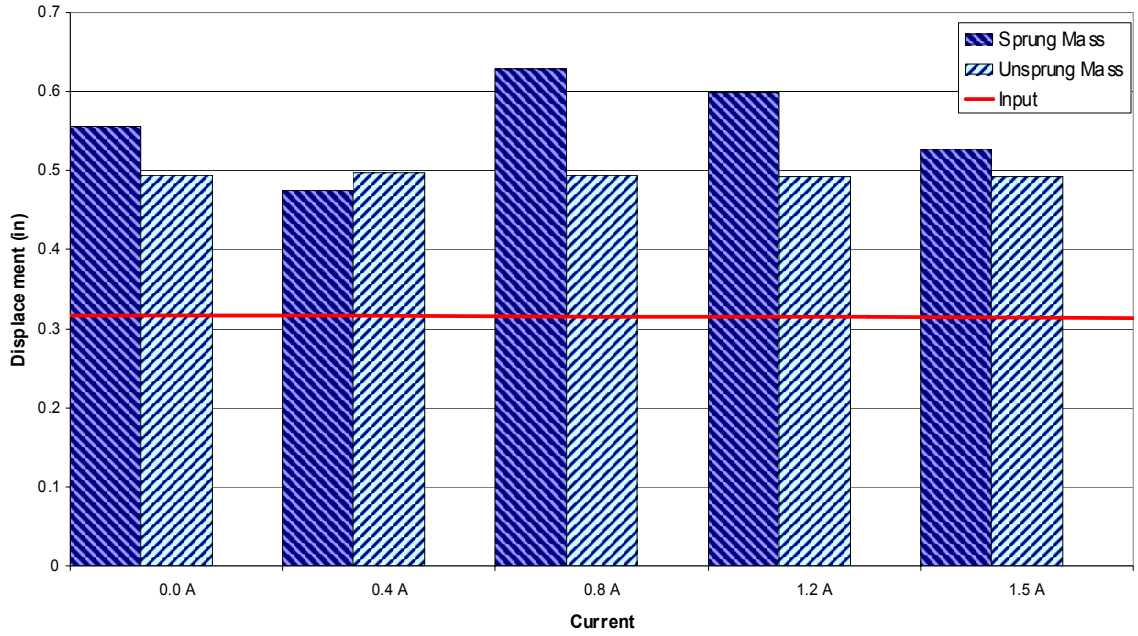

Figure 6-2. Passive Control RMS Displacement at 1.5 Hz

The peak-to-peak acceleration shown in Figure 6-3, demonstrates similar characteristics as the peak-to-peak displacement for the sprung mass. As the current increases, the acceleration decreases, though still not below the acceleration of the input. Figure 6-3 also reveals interesting dynamics occurring at the unsprung mass. At 0.4 Amps and 0.8 Amps the acceleration of the unsprung mass is at a maximum. In this current range, the damper begins to offer more resistance but not enough to fully couple the two masses, as is the case as the current approaches 1.5 Amps.

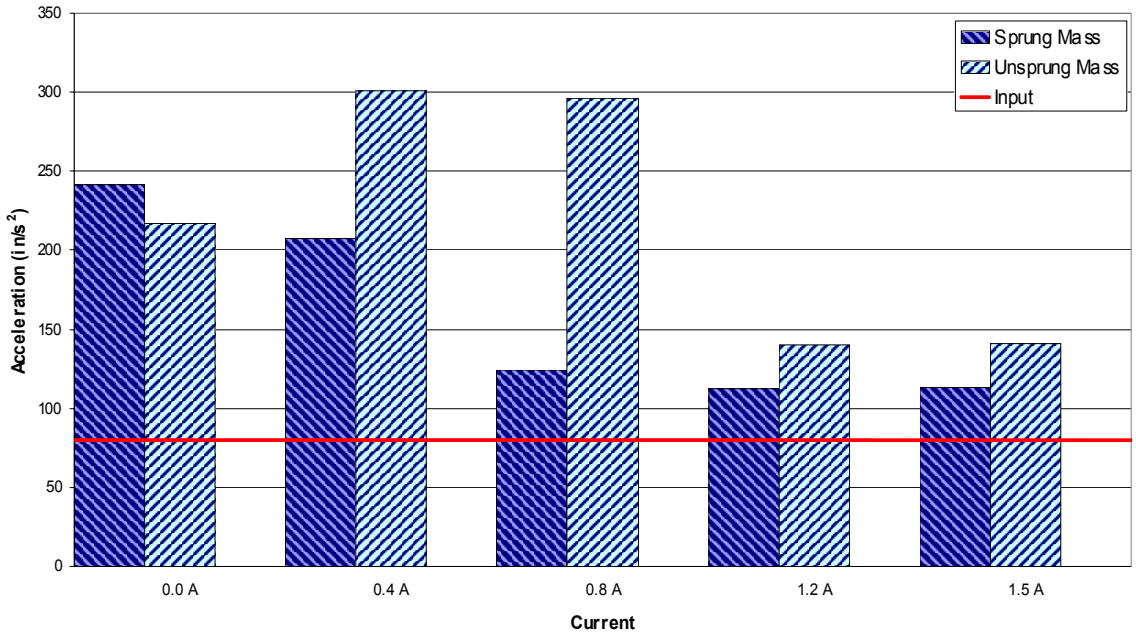

Figure 6-3. Passive Control Peak-to-Peak Acceleration at 1.5 Hz

Figure 6-4 shows the RMS acceleration of the sprung and unsprung masses. What is interesting is that the RMS amplitudes of the sprung mass are below the RMS amplitude of the input signal for all currents, including 0.0 Amps. Furthermore, the unsprung mass acceleration decreases as current increases, a dynamic not observed in the peak-to-peak acceleration.

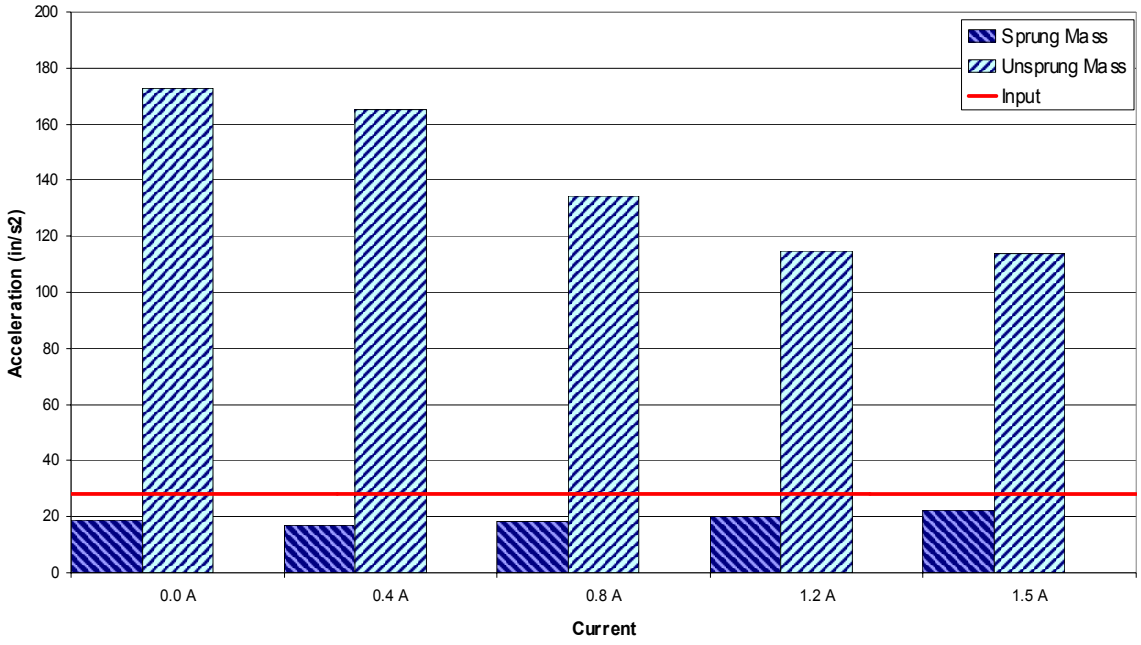

Figure 6-4. Passive Control RMS Acceleration at 1.5 Hz

6.3.2 Pure Tone 10.5 Hz

Evaluating the 10.5 Hz excitation in the same fashion as the 1.5 Hz excitation, Figure 6-5 shows the peak-to-peak displacement of the sprung and unsprung masses. Now, at the unsprung mass natural frequency, we begin to notice the attenuation of the unsprung mass amplitude, even beyond that of the input. As the damper current approaches 1.5 Amps, the two masses become coupled and the input amplitude is completely absorbed by the elastomeric mounts. Considering the sprung mass, we observe that the peak-to-peak displacement is, for all currents, less than the input. Recalling the sprung mass transmissibility from Chapter 4, this behavior is expected; the input frequency is well above the sprung mass isolation frequency, $\sqrt{2} \cdot \omega_{n_1}$. The sprung mass will always be isolated from this input, regardless of amplitude.

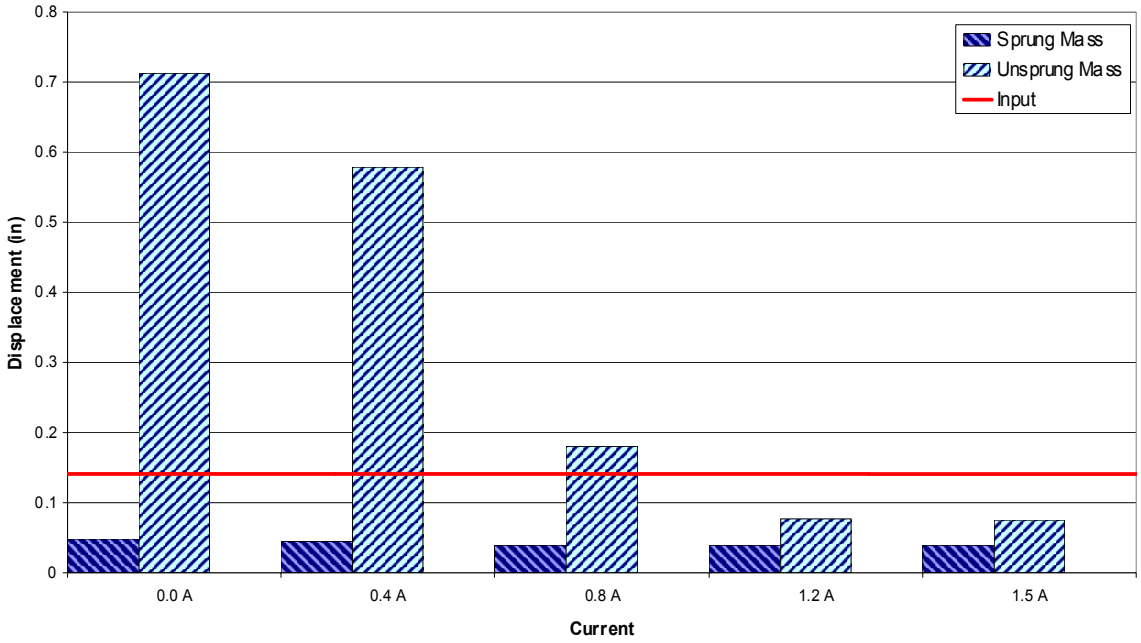

Figure 6-5. Passive Control Peak-to-Peak Displacement at 10.5 Hz

The RMS displacement shown in Figure 6-6 displays similar characteristics to those observed in Figure 6-5. As the damper current increases, the RMS amplitude of the unsprung mass decreases. Again, the low amplitudes at 1.2 Amps and 1.5 Amps are artifacts of the two masses becoming coupled.

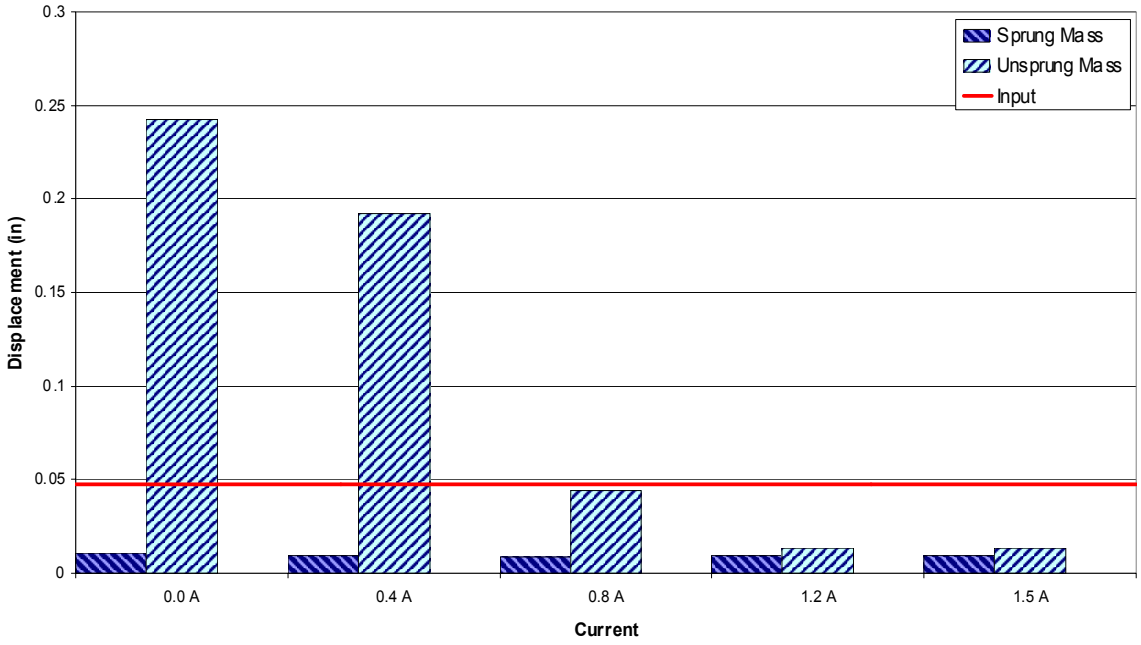

Figure 6-6. Passive Control RMS Displacement at 10.5 Hz

The familiar trend remains the same when evaluating the peak-to-peak accelerations in Figure 6-7. Acceleration levels drop dramatically as the current is increased from 0.4 Amps to 0.8 Amps. The same characteristic is observed in the RMS acceleration amplitudes of Figure 6-8. Again, it is important to mention that the sprung mass is well isolated from the input. For this reason, we see virtually no change in the sprung mass acceleration as damping increases.

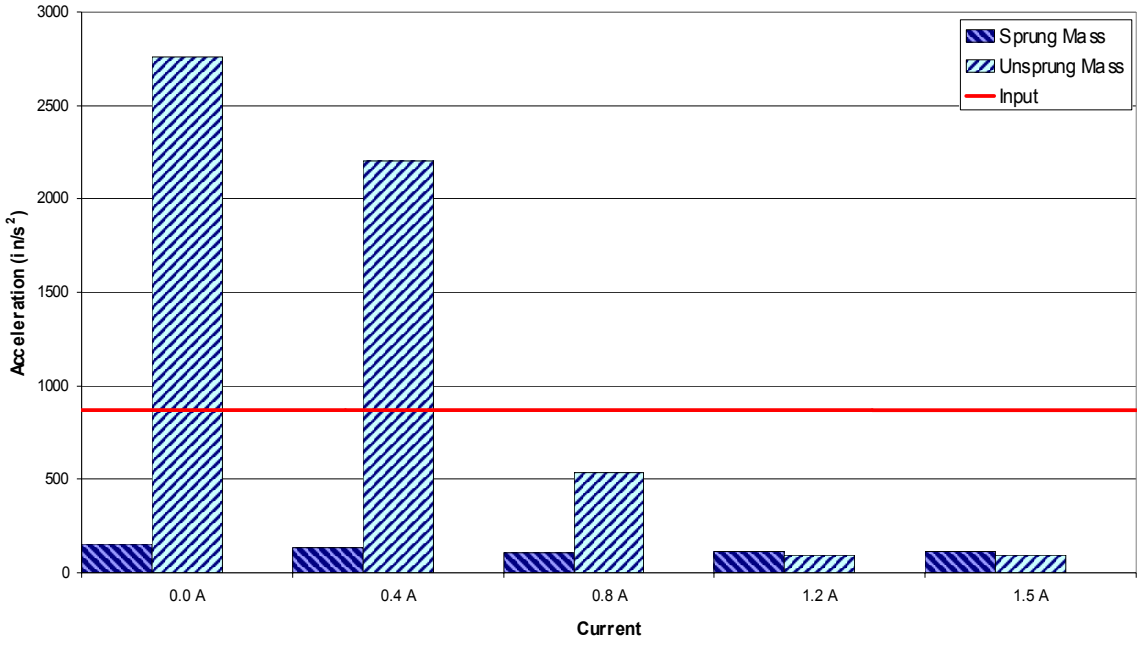

Figure 6-7. Passive Control Peak-to-Peak Acceleration at 10.5 Hz

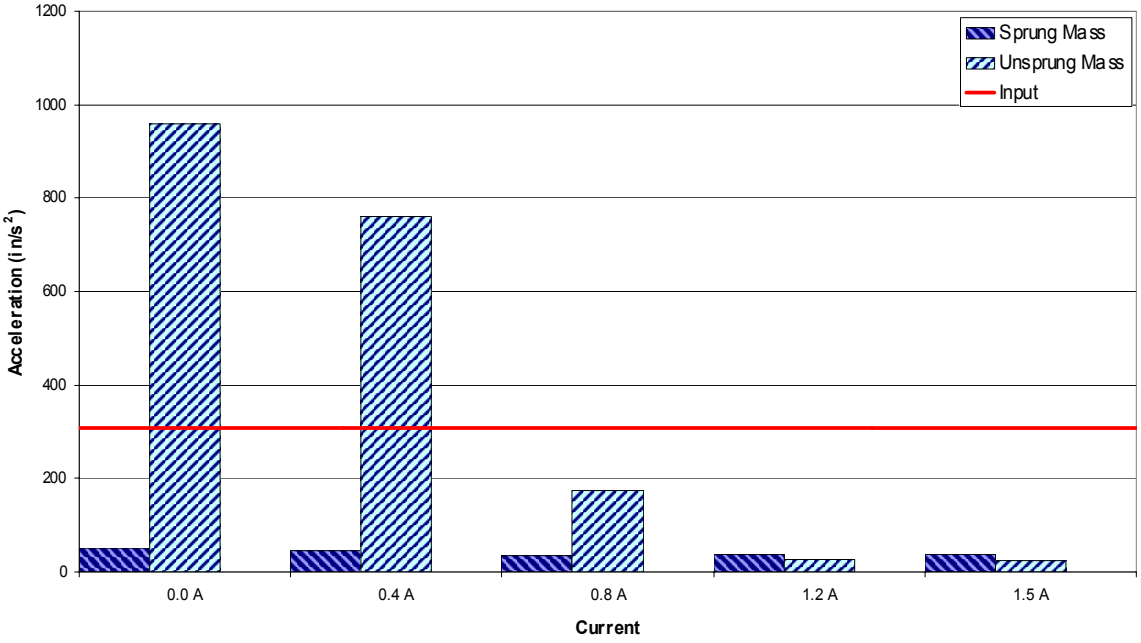

Figure 6-8. Passive Control RMS Acceleration at 10.5 Hz

6.3.3 Damper Work

Figure 6-9 shows the work done by the passive damper for both the 1.5 Hz excitation and the 10.5 Hz excitation. Figure 6-9 reveals that for both inputs, the damper does the most work at 0.4 Amps. As the current increases beyond 0.4 Amps, the work done by the damper decreases for both the 1.5 Hz input as well as the 10.5 Hz input.

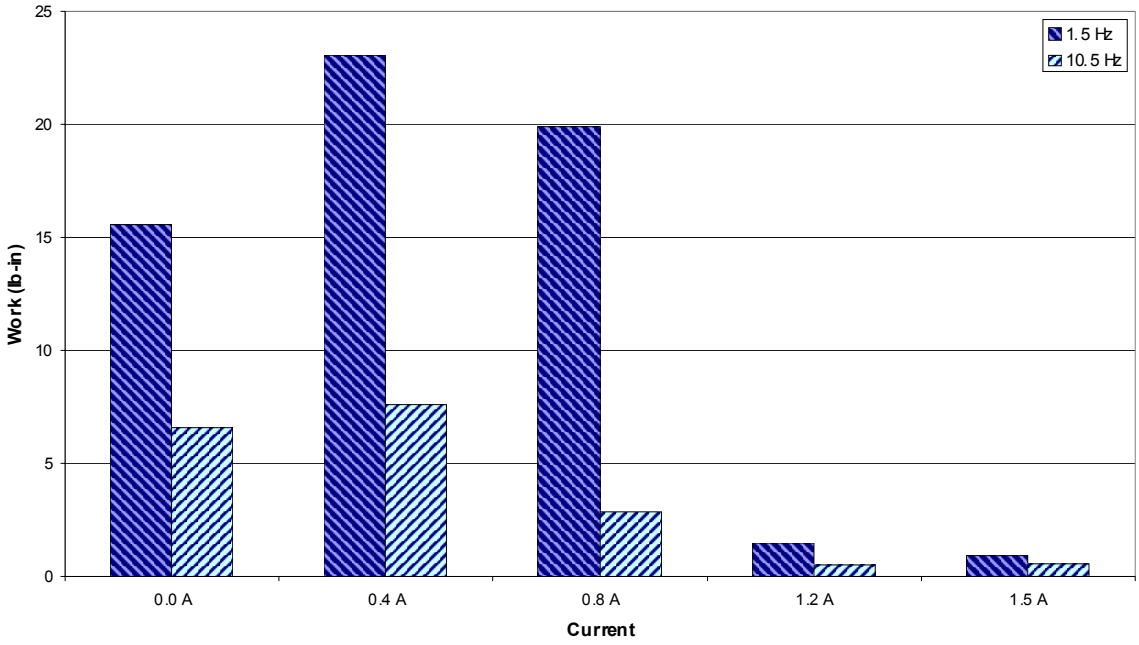

Figure 6-9. Passive Control Damper Work

A sample force displacement plot from the 1.5 Hz input is shown in Figure 6-10. It is from the relationship shown in Figure 6-10 that the work done by the damper is calculated. The area enclosed by the force displacement plot corresponds to the work done by the damper.

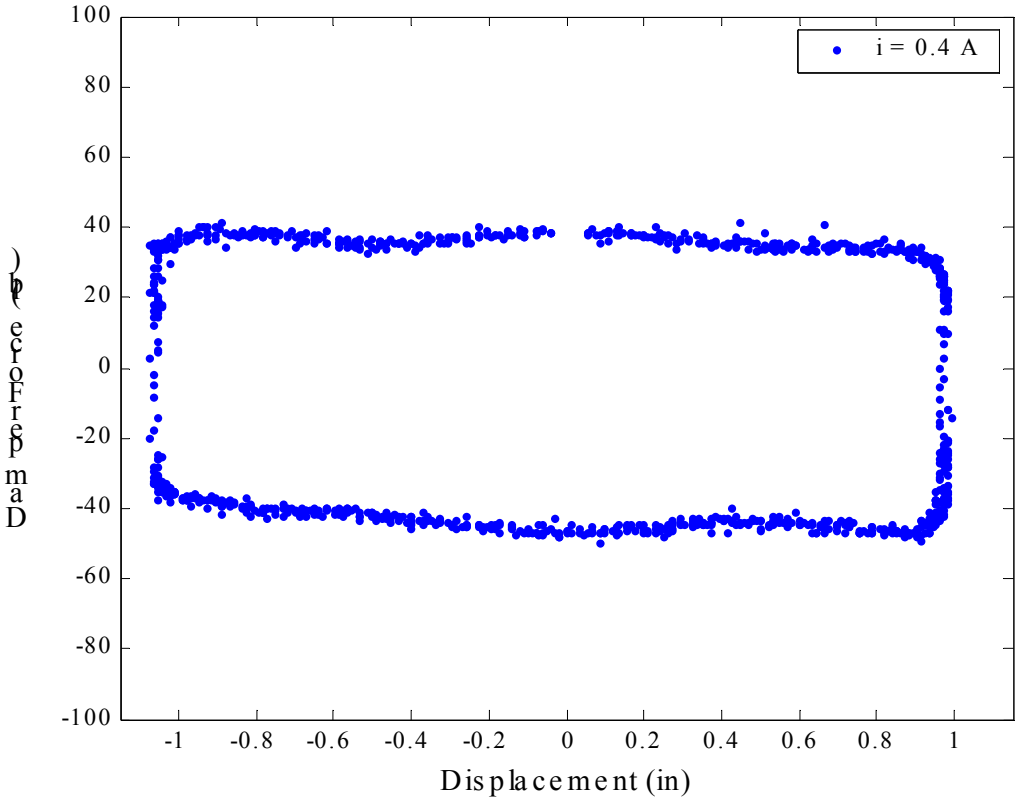

Figure 6-10. Passive Control Force Displacement Relationship

The asymmetric characteristics displayed in Figure 6-10 are expected. As supported by the force velocity plot in Figure 6-11, the force is greater in rebound than in jounce. Figure 6-11 clearly demonstrates the bilinear damping characteristics common in passive dampers. The figure was generated from the 1.5 Hz input with the damper current fixed at 0.4 Amps.

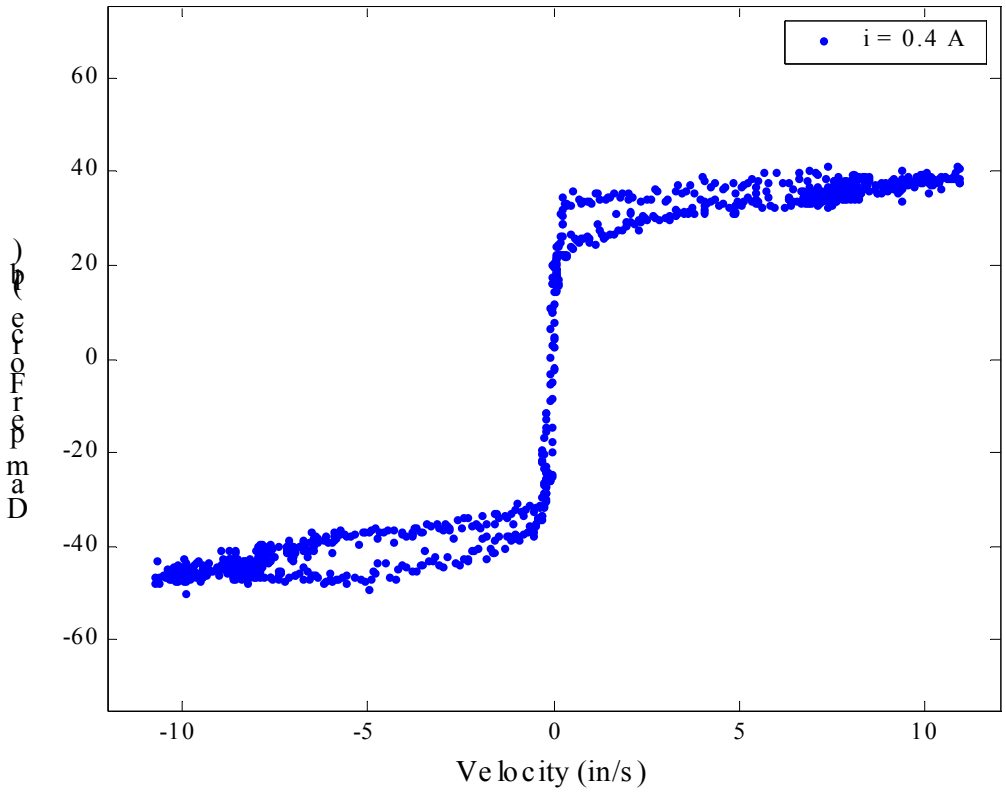

Figure 6-11. Passive Control Force Velocity Relationship

6.4 Skyhook Control Steady State Evaluation

The skyhook steady state analysis will follow the same format set by the passive evaluation. The same results will be considered and performance benefits will be highlighted.

6.4.1 Pure Tone 1.5 Hz

The peak-to-peak displacements of the sprung and unsprung masses are shown in Figure 6-12. Again, the results are measured against the peak-to-peak displacement of the input signal represented by the red line. As expected, increasing *G* causes the displacement amplitude of the sprung mass to decrease, approaching that of the input. The RMS displacements in Figure 6-13 share similar characteristics.

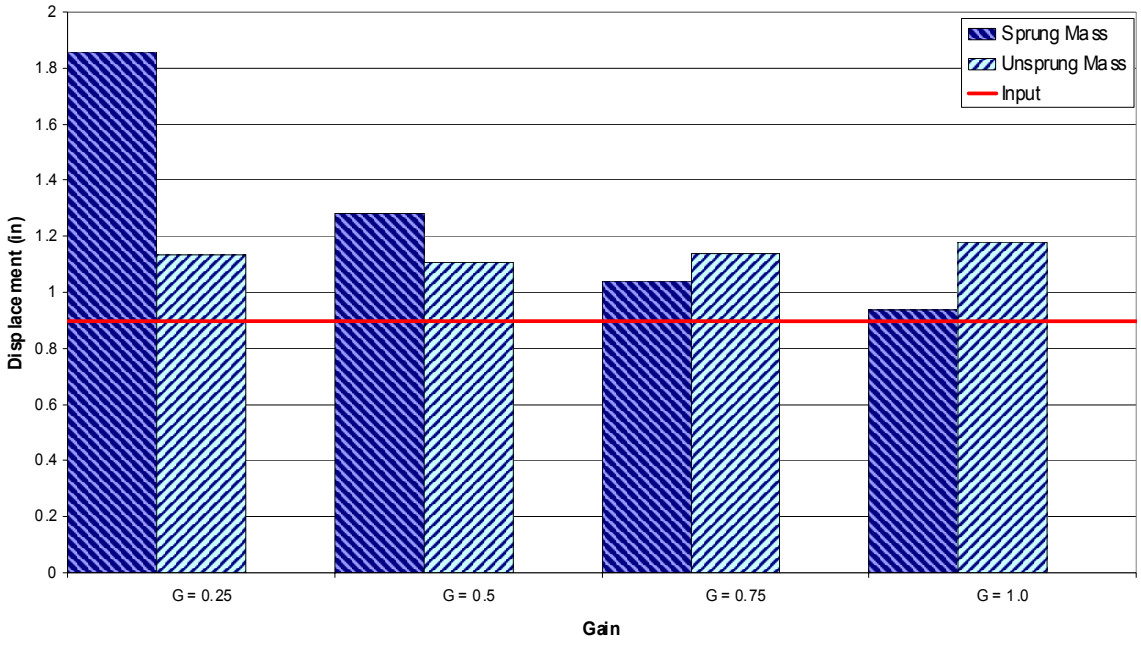

Figure 6-12. Skyhook Control Peak-to-Peak Displacement at 1.5 Hz

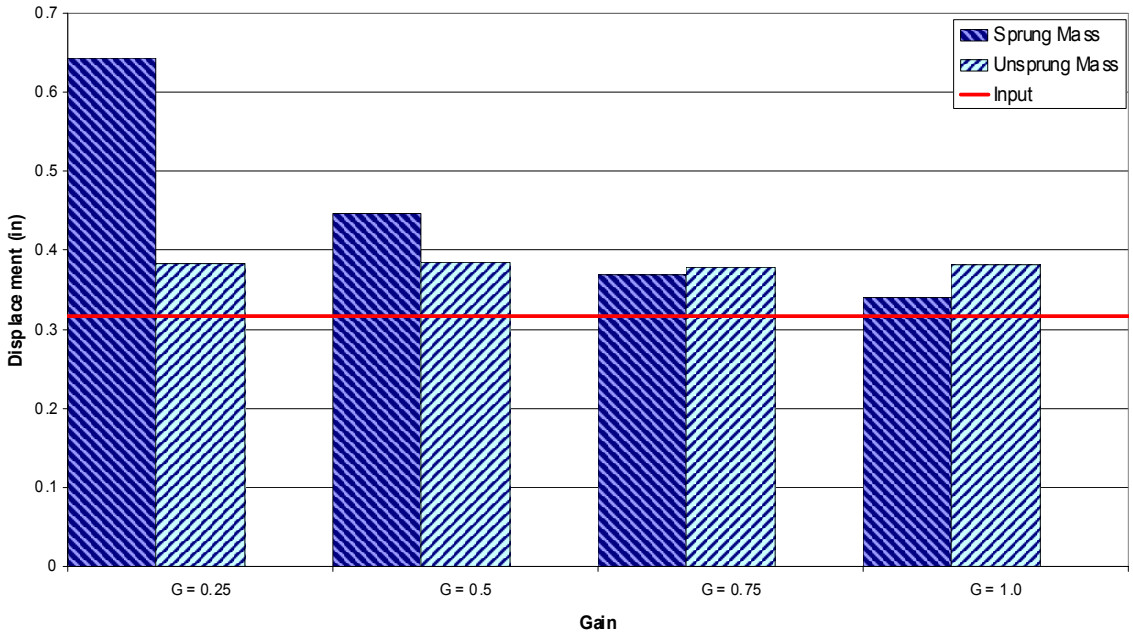

Figure 6-13. Skyhook Control RMS Displacement at 1.5 Hz

When evaluating the acceleration signals, the peak-to-peak acceleration, shown in Figure 6-14, reveals interesting dynamics as the skyhook gain is increased. As *G* is increased from 0.25 to 0.5, the amplitude of the sprung mass acceleration decreases, as expected for skyhook control. However, increasing *G* beyond 0.5 results in increased acceleration amplitudes.

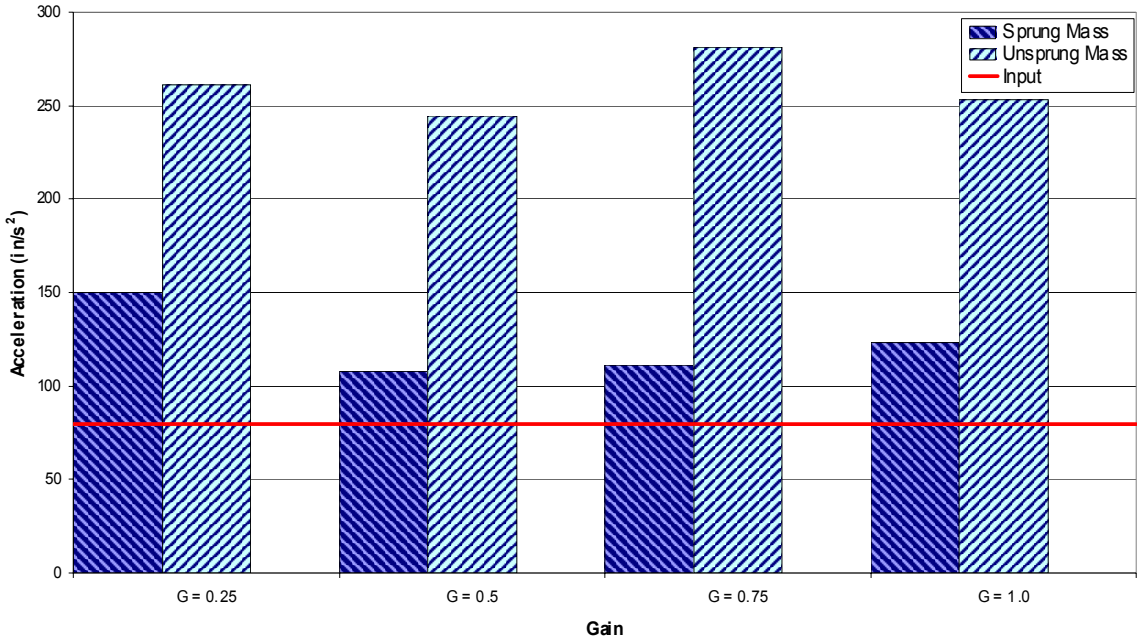

Figure 6-14. Skyhook Control Peak-to-Peak Acceleration at 1.5 Hz

The interesting dynamics in the peak-to-peak accelerations for the sprung mass do not appear in the RMS accelerations in Figure 6-15. Here, the acceleration decreases almost beyond that of the input as *G* increases. As with the majority of the skyhook results, the benefit of increasing *G* is non-linear. The greatest benefit occurs as *G* is increased from 0.25 to 0.5. The proceeding increases do not offer benefits of the same magnitudes.

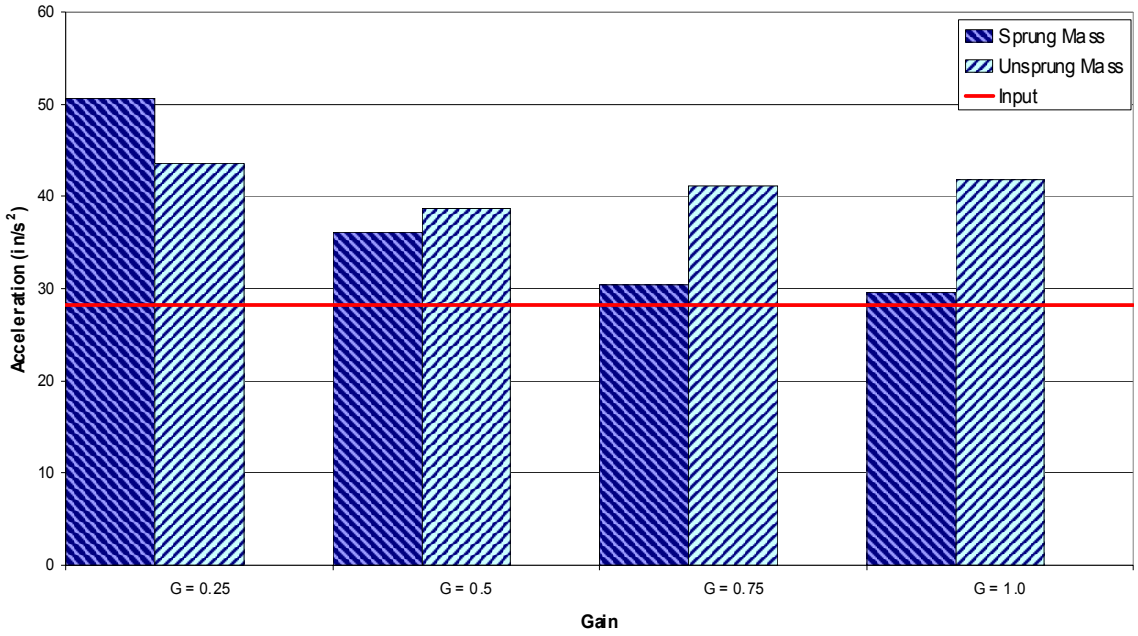

Figure 6-15. Skyhook Control RMS Acceleration at 1.5 Hz

6.4.2 Pure Tone 10.5 Hz

The results of the 10.5 Hz input do not demonstrate any benefits of skyhook control for the sprung mass. Again, at this input, the sprung mass is well isolated, regardless of control. Figure 6-16, however, reveals some interesting benefits of skyhook on the unsprung mass. As the skyhook gain is increased, the peak-to-peak displacement of the unsprung mass decreases. The same characteristics appear in the RMS displacement shown in Figure 6-17. As the skyhook gain increases the RMS displacement of the unsprung mass decreases. The gains of skyhook control on the unsprung mass are not significant relative to the gains achieved on the sprung mass.

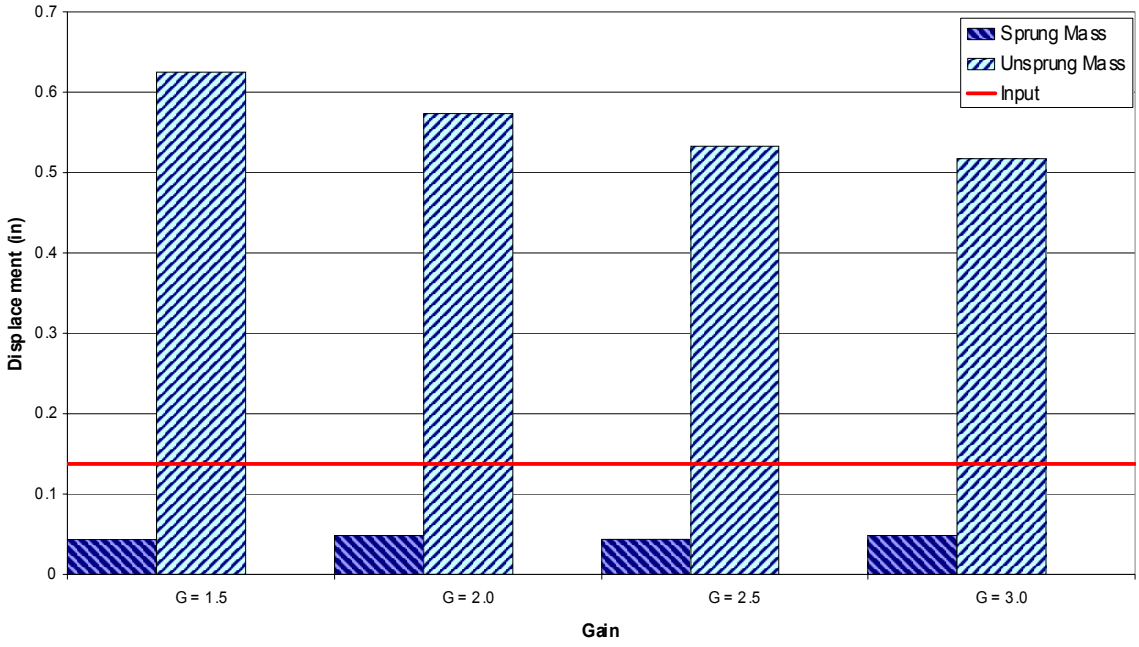

Figure 6-16. Skyhook Control Peak-to-Peak Displacement at 10.5 Hz

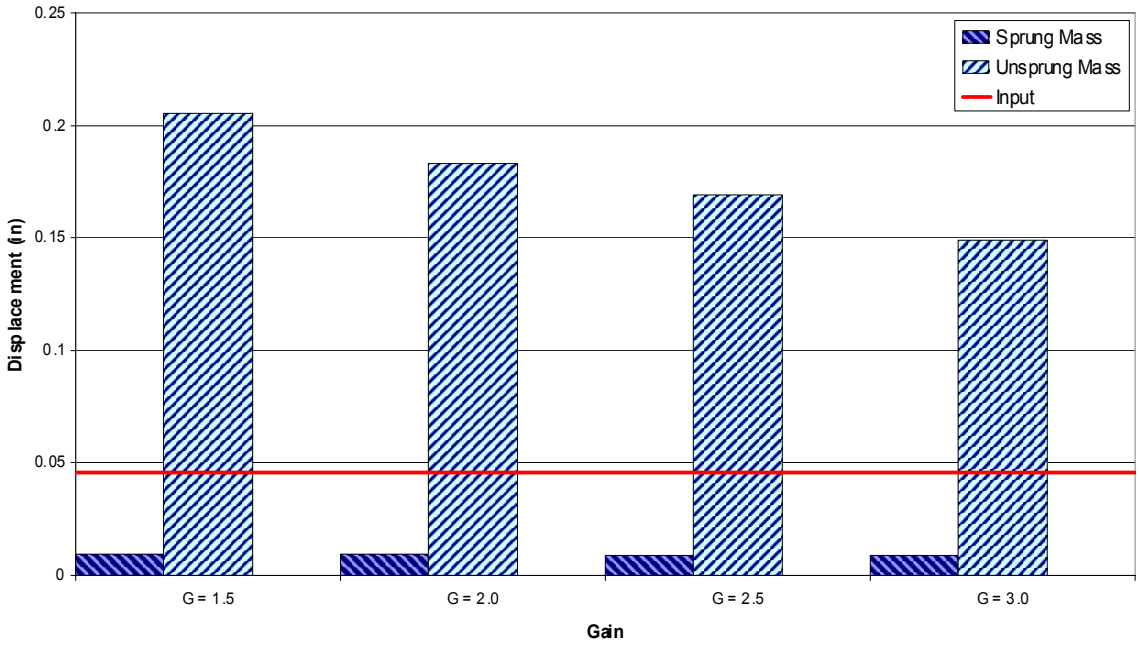

Figure 6-17. Skyhook Control RMS Displacement at 10.5 Hz

Following the same trend described in the displacement results are the peak-to-peak acceleration results in Figure 6-18. The unsprung mass acceleration levels decrease as the skyhook gain is increased. The same results appear in the RMS accelerations in Figure 6-19. Again, the apparent performance benefits of skyhook control on the unsprung mass are not nearly as great as the performance benefits of skyhook control on the sprung mass.

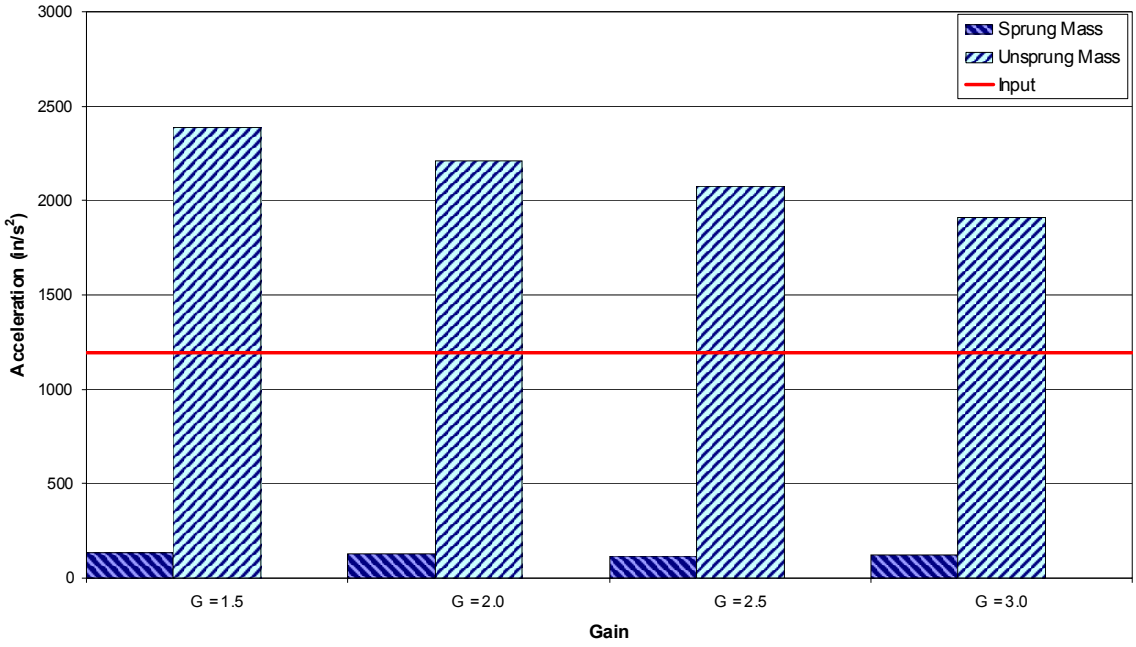

Figure 6-18. Skyhook Control Peak-to-Peak Acceleration at 10.5 Hz

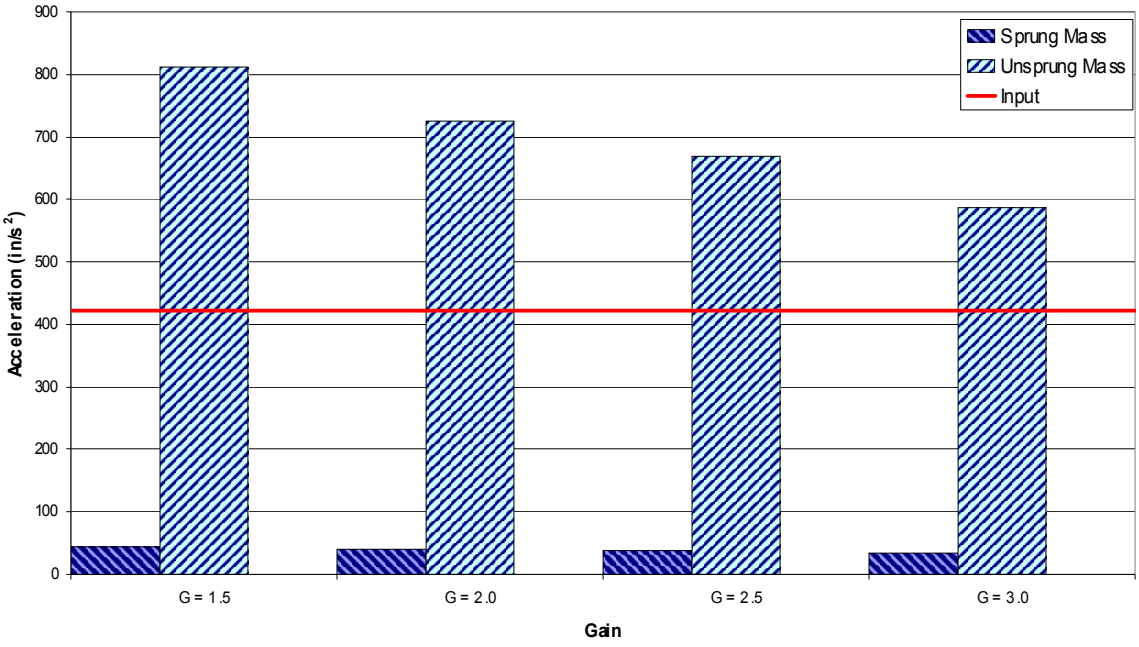

Figure 6-19. Skyhook Control RMS Acceleration at 10.5 Hz

6.4.3 Damper Work

The work done by the skyhook damper is shown in Figure 6-20. As the skyhook gain increases for the 1.5 Hz input, the work done by the damper decreases. At 10.5 Hz, the work done by the damper decreases slightly as the skyhook gain increases. In both cases, the damper does the most work at the lowest skyhook gain, 0.25 and 1.5 for 1.5 Hz and 10.5 Hz respectively.

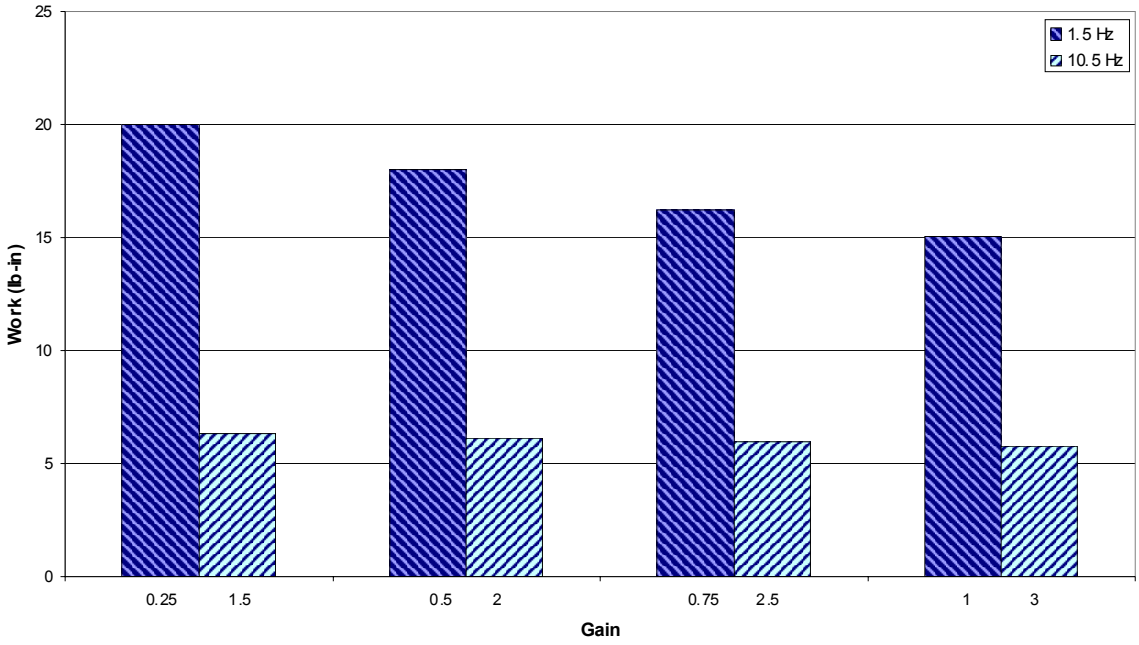

Figure 6-20. Skyhook Control Damper Work

A sample force displacement plot is shown in Figure 6-21. This force displacement relationship was generated from the 1.5 Hz input with a skyhook gain of 0.25. The interesting shape of the force displacement envelope begins to reveal the dynamic force benefits of a semi-active damper. Unlike the passive force displacement relationship in Figure 6-10, the skyhook damper force is not constant for all displacements. The dynamic characteristics of the damper force indicate greater control ability than that of the passive case.

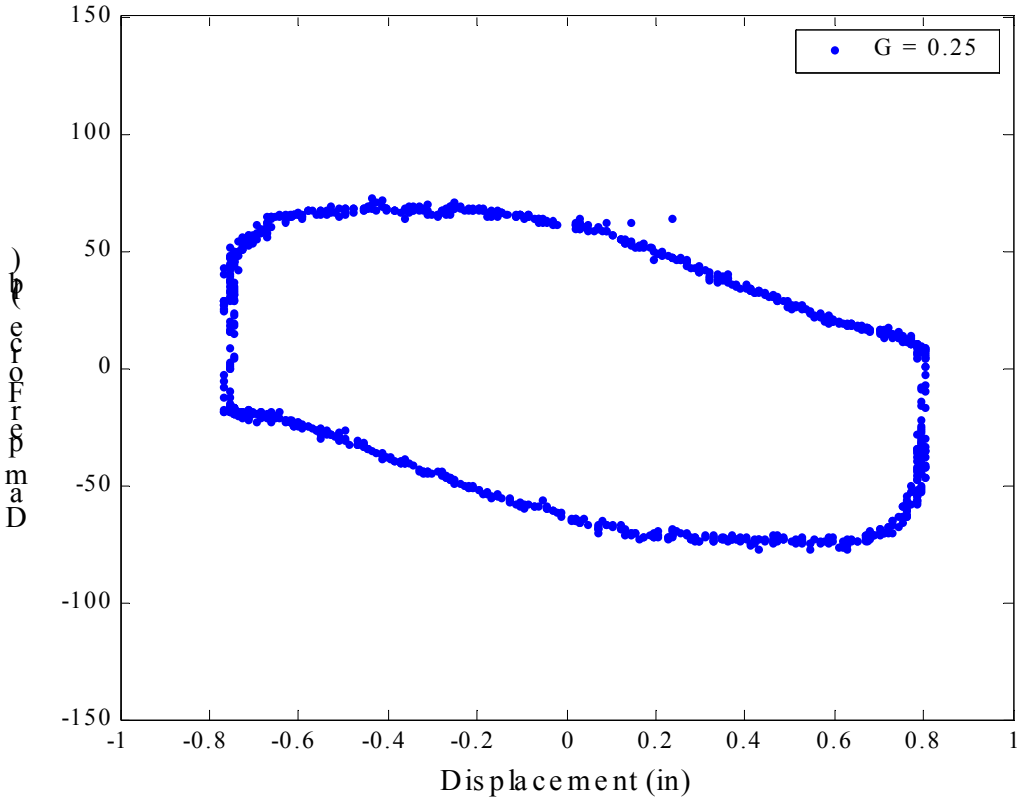

Figure 6-21. Skyhook Control Force Displacement Relationship

The force velocity plot in Figure 6-22 also reveals force benefits of a semi-active damper. Unlike the passive force velocity curve, the skyhook force velocity relationship is not limited to only one relationship between force and velocity. Under semi-active control, the force velocity relationship is continuously changing with damper current. Figure 6-22 supports this idea, showing a wide range of force variation through the velocities.

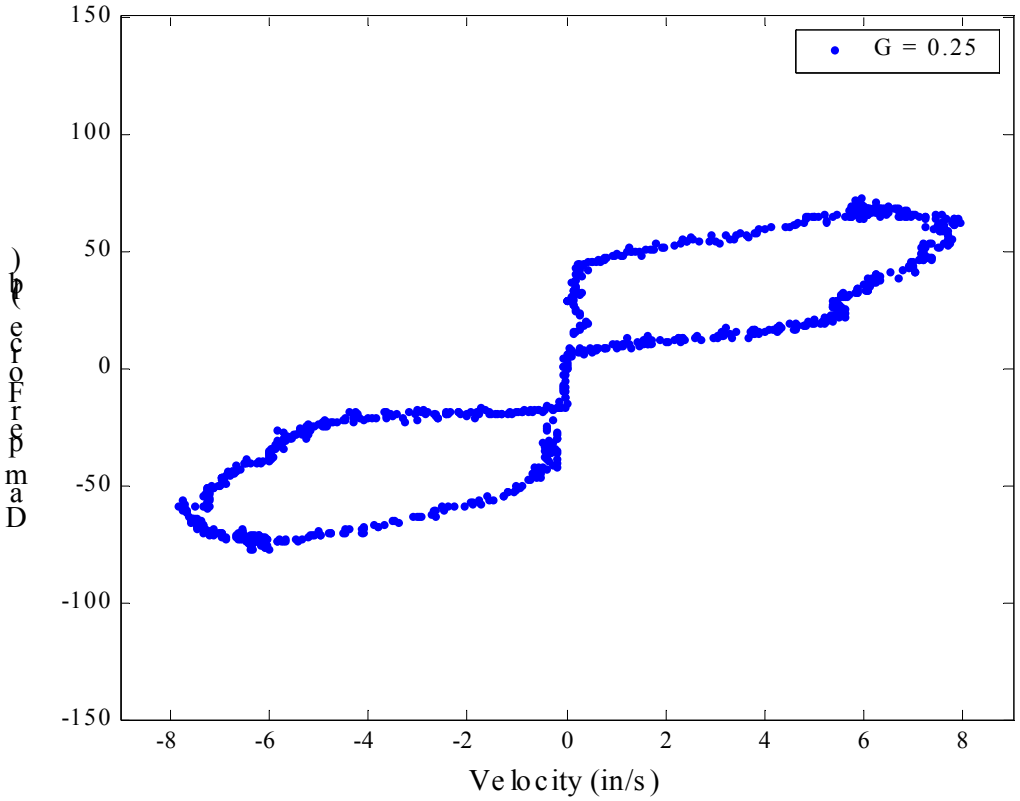

Figure 6-22. Skyhook Control Force Velocity Relationship

6.5 Groundhook Steady State Evaluation

In the groundhook evaluation, the focus will shift to the control of the unsprung mass. Subsequently, the results of the 10.5 Hz input will be of particular interest. The excitation at 1.5 Hz will only demonstrate the tradeoff common with groundhook control. At 1.5 Hz the unsprung mass is well isolated, and therefore, the benefits of groundhook control will be masked.

6.5.1 Pure Tone 1.5 Hz

Figure 6-23 shows the peak-to-peak displacement amplitudes at 1.5 Hz. At the sprung mass resonance, groundhook control amplifies the displacement of the sprung mass. As the groundhook gain increases, the sprung mass peak-to-peak amplitude increases. This also holds true for the RMS displacement of the sprung mass as shown in Figure 6-24.

This response is expected for groundhook control, as its focus is on the unsprung mass. In both cases, the unsprung mass remains virtually unchanged. The 1.5 Hz input cannot excite the unsprung mass dynamics, and thus, the unsprung mass amplitudes show no improvements as the groundhook gain increases.

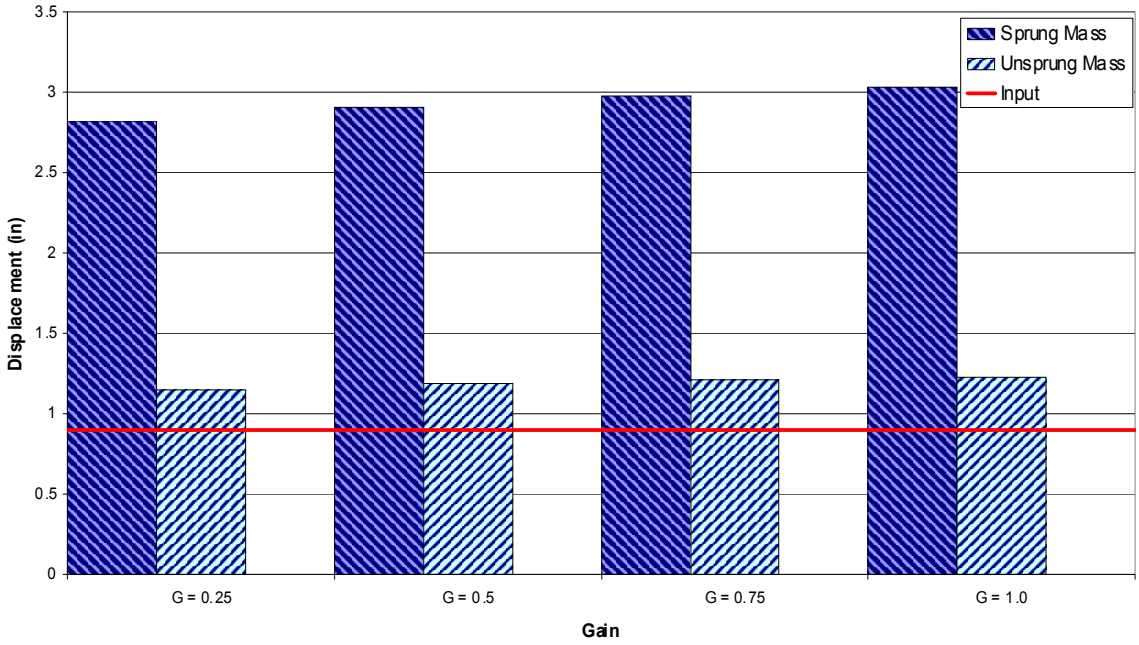

Figure 6-23. Groundhook Control Peak-to-Peak Displacement at 1.5 Hz

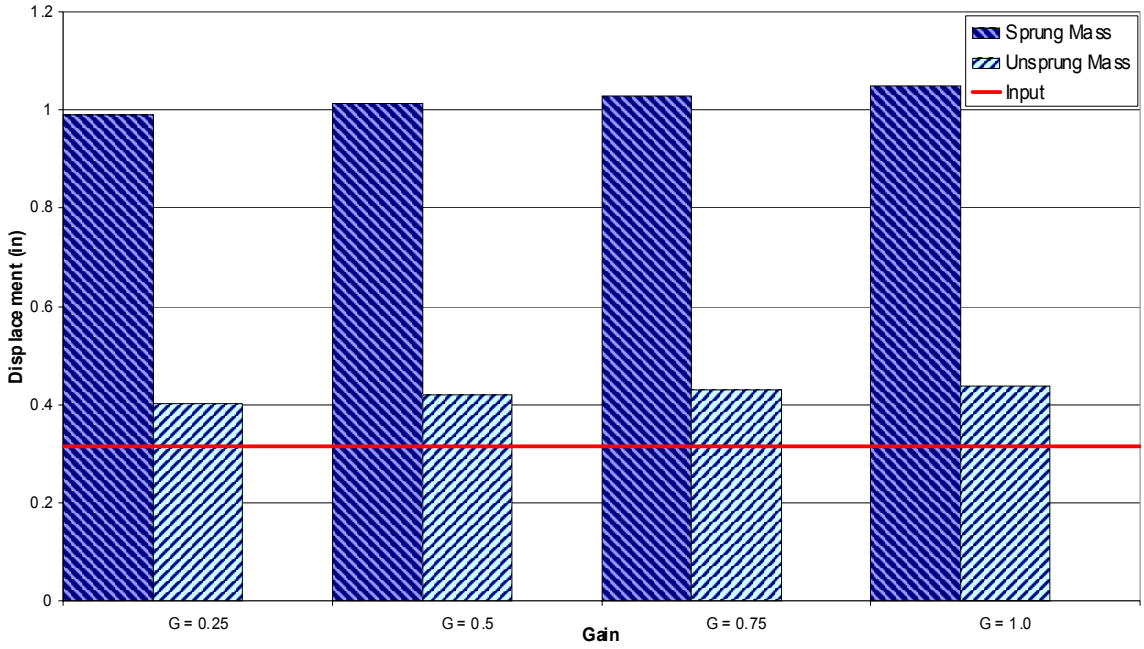

Figure 6-24. Groundhook Control RMS Displacement at 1.5 Hz

The same dynamics observed in the displacement results are captured in the acceleration results as well. In Figure 6-25, the peak-to-peak sprung mass acceleration increases as the groundhook gain increases. The RMS accelerations in Figure 6-26 show the same dynamics. More dramatic, are the increases in acceleration amplitudes of the unsprung mass. Both figures support this acceleration increase as the groundhook gain increases. It appears that, under the 1.5 Hz input condition, groundhook control actually increases the acceleration amplitudes of the unsprung mass.

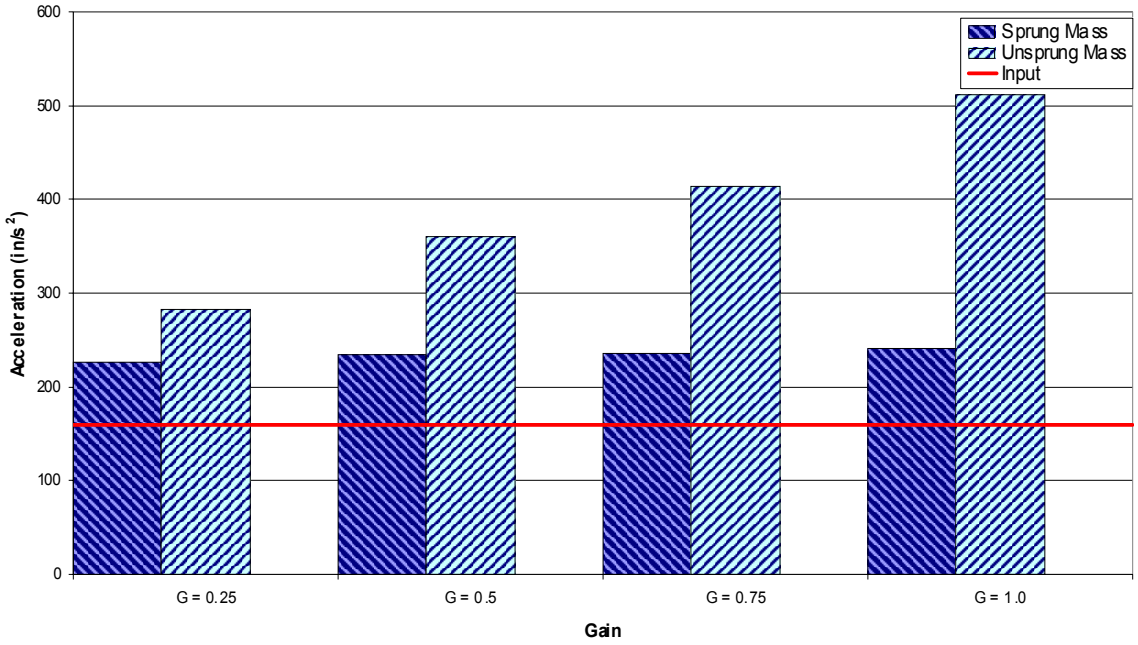

Figure 6-25. Groundhook Control Peak-to-Peak Acceleration at 1.5 Hz

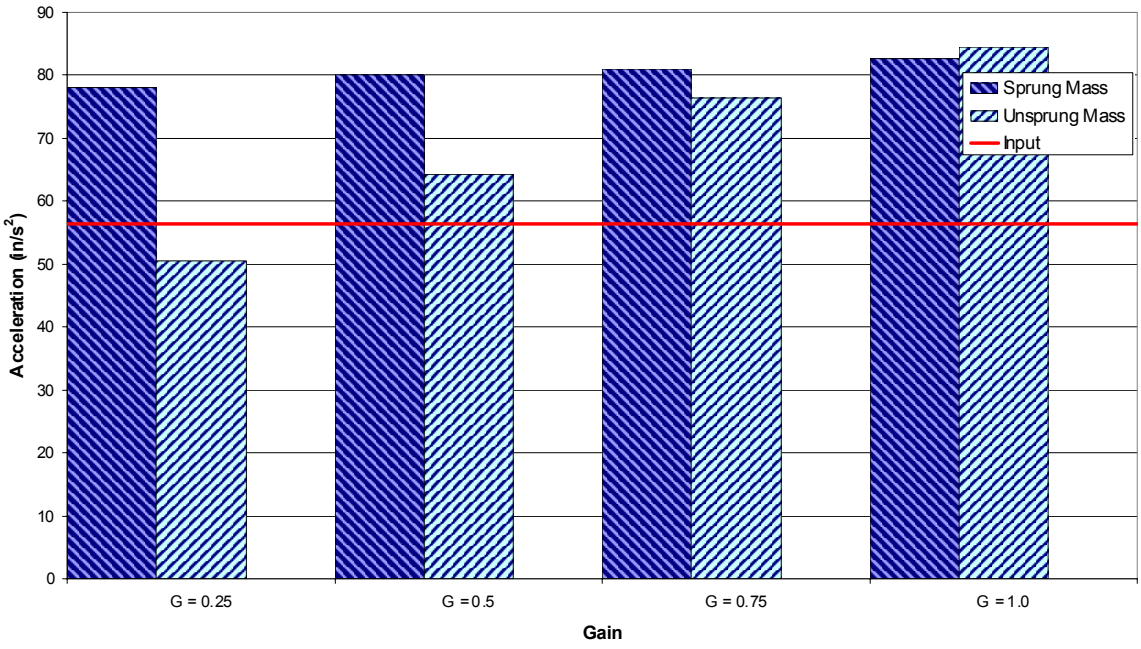

Figure 6-26. Groundhook Control RMS Acceleration at 1.5 Hz

6.5.2 Pure Tone 10.5 Hz

At the unsprung mass natural frequency, the benefits of groundhook control are now evident. Figure 6-27 shows the peak-to-peak displacements for a 10.5 Hz pure tone input. As the groundhook gain increases the unsprung mass displacement amplitude decreases. At a gain of 1.5, the peak-to-peak amplitude of the sprung mass is less than that of the input signal.

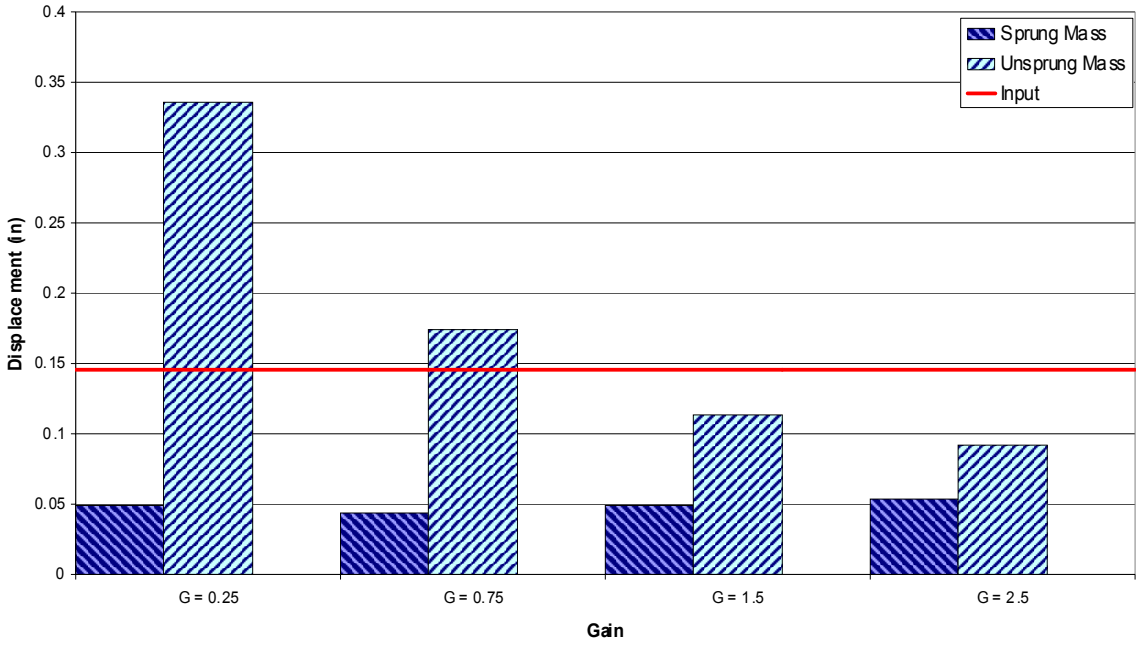

Figure 6-27. Groundhook Control Peak-to-Peak Displacement at 10.5 Hz

The RMS displacement results in Figure 6-28 support the same results as Figure 6-27. The unsprung mass amplitude is attenuated as the groundhook gain increases. In fact, once the gain reaches 0.75, the amplitude of the unsprung mass displacement is less than the input signal amplitude.

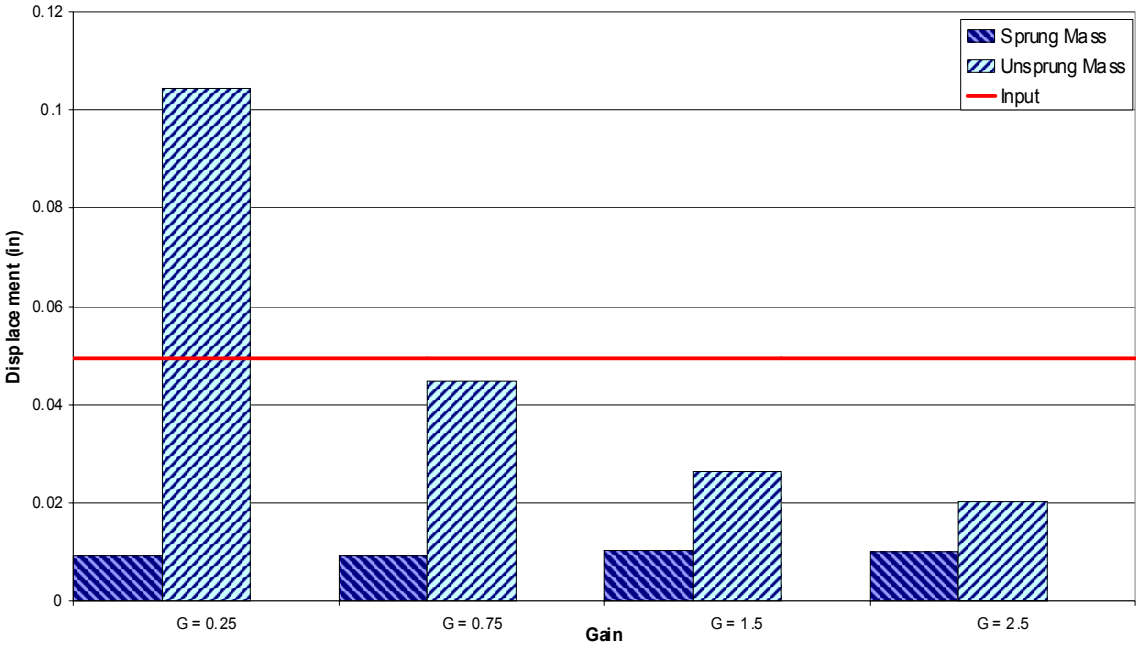

Figure 6-28. Groundhook Control RMS Displacement at 10.5 Hz

In evaluating the acceleration results, the benefits of groundhook control are emphasized. Figure 6-29 shows the peak-to-peak acceleration amplitudes. In every case, groundhook control reduces the acceleration amplitude of the unsprung mass below the amplitude of the input signal. Another valuable observation is the magnitude by which the amplitude is reduced. The peak-to-peak amplitude of the input signal is reduced by more than five orders of magnitude under groundhook control with a gain of 2.5. Similar reductions are shown in the RMS acceleration values in Figure 6-30. As with the peak-to-peak accelerations, the RMS accelerations are reduced below the input acceleration for each groundhook gain.

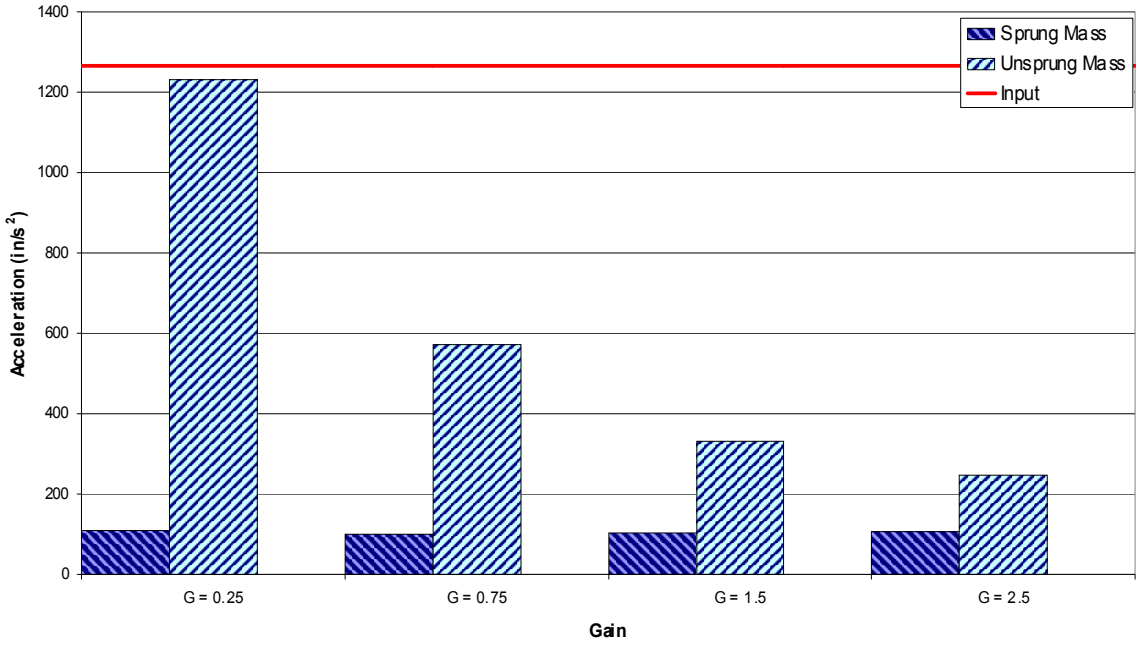

Figure 6-29. Groundhook Control Peak-to-Peak Accelerations at 10.5 Hz

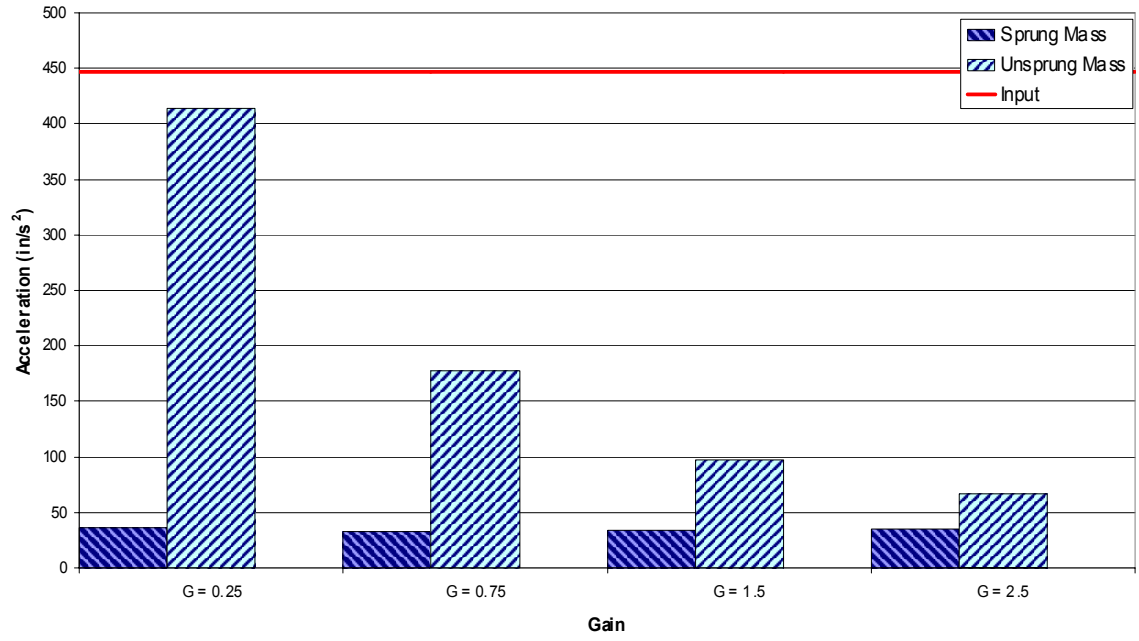

Figure 6-30. Groundhook Control RMS Acceleration at 10.5 Hz

6.5.3 Damper Work

The work done by the groundhook damper is shown in Figure 6-31. It is clear from Figure 6-31 that the damper does far less work at the 10.5 Hz input. The relationships between the two inputs are reversed. At 1.5 Hz, the work increases as the groundhook gain increases, while at 10.5 Hz, the work decreases as the groundhook gain increases.

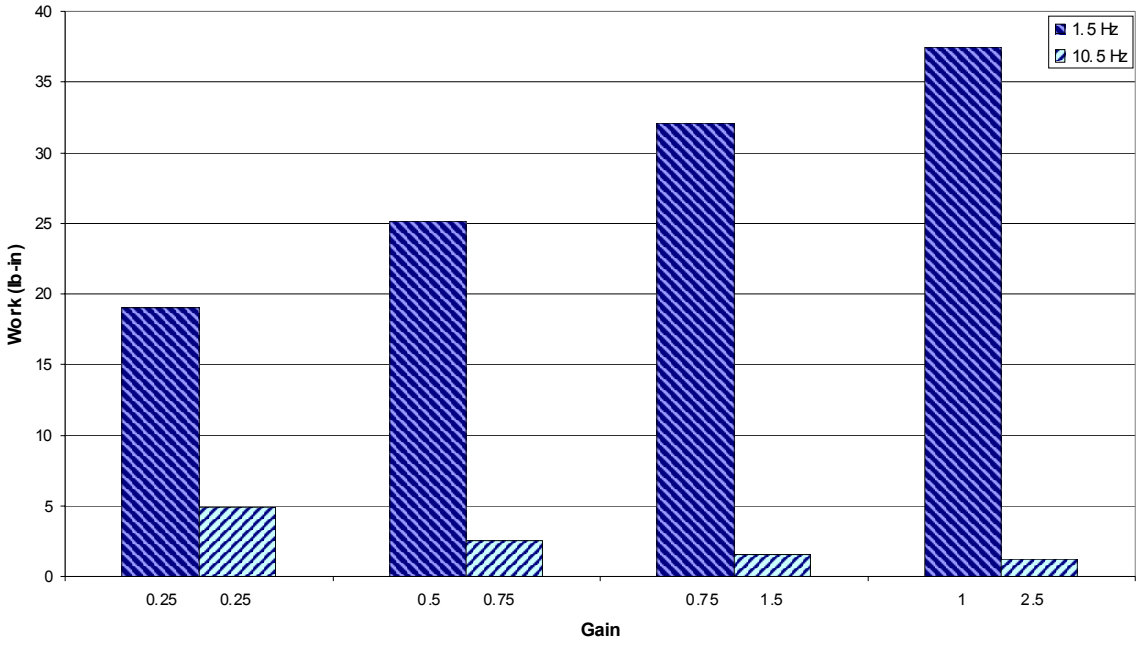

Figure 6-31. Groundhook Control Damper Work

A sample force displacement plot is shown in Figure 6-32. As with skyhook control, the unique shape of the plot is an artifact of the semi-active damper. At a groundhook gain of 0.5, the relationship between force and displacement appears to be symmetric. A closer look, however, reveals that the damper exerts more force in rebound.

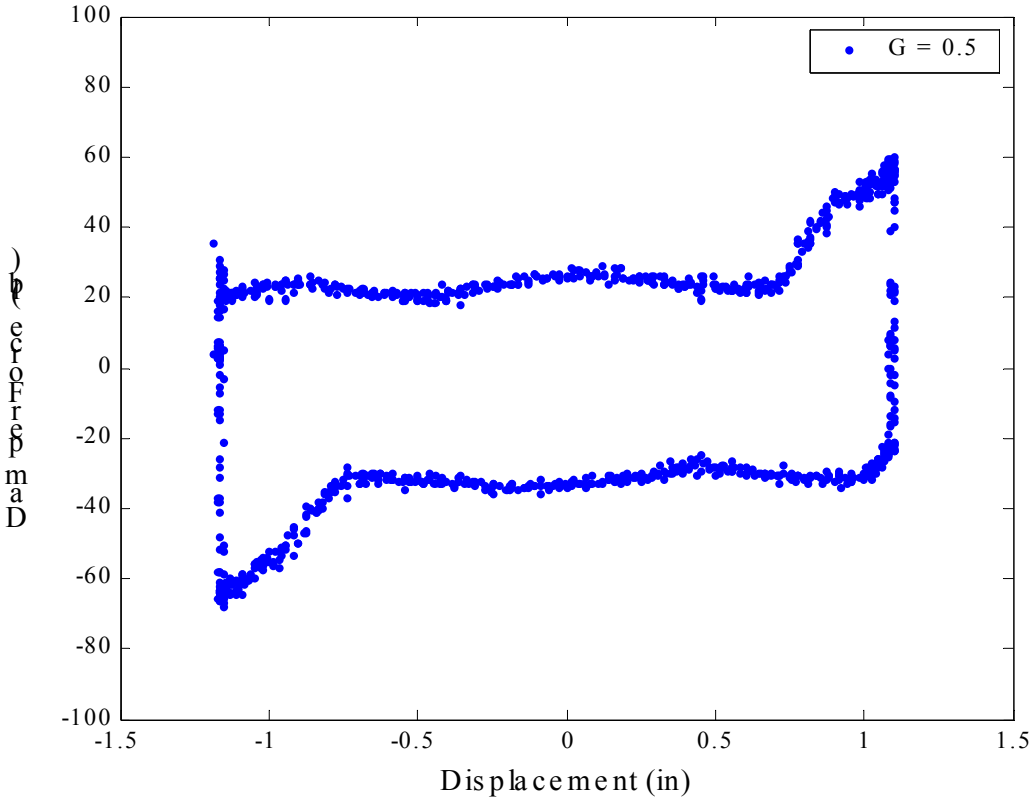

Figure 6-32. Groundhook Control Force Displacement Relationship

The force velocity plot in Figure 6-33 shares the same characteristics that were observed with skyhook control. The force relative to the velocity is not fixed at one pre-defined value. The complex relationship between force and velocity in Figure 6-33 is what defines the benefits of semi-active control.

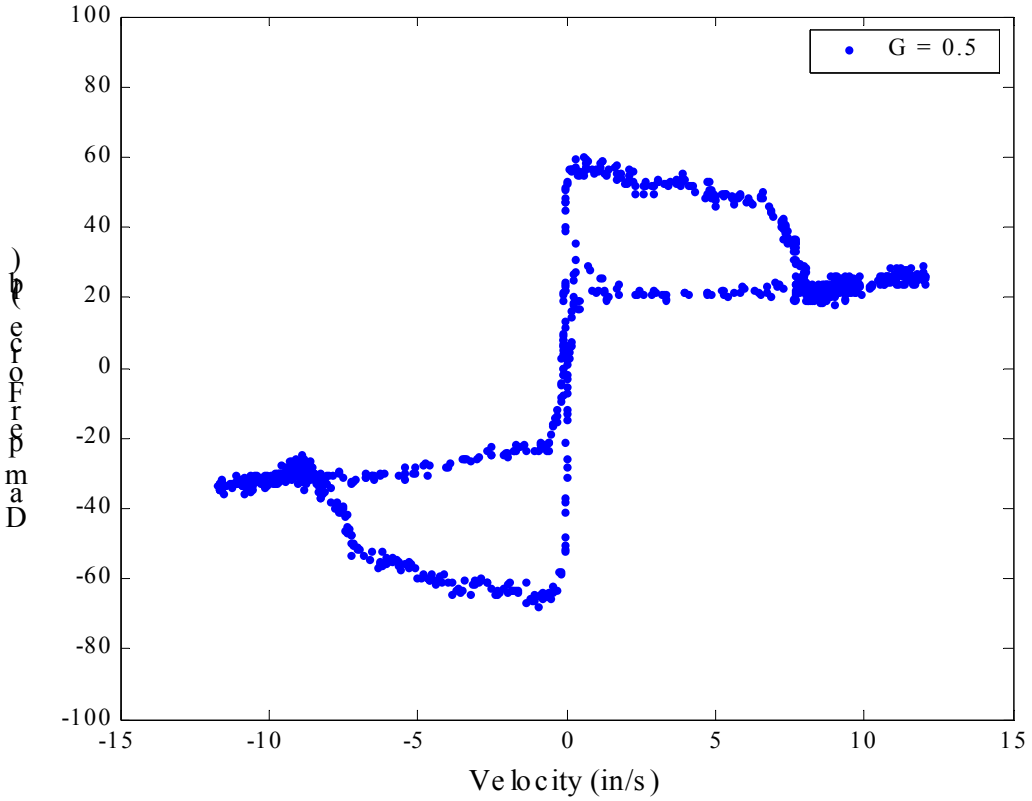

Figure 6-33. Groundhook Control Force Velocity Relationship

6.6 Hybrid Control Steady State Evaluation

Because hybrid control is a combination of skyhook and groundhook, the results in this section will begin to show the dynamic benefits of both skyhook and groundhook control. Hybrid control minimizes the tradeoff evident in both the skyhook and the groundhook control policies.

6.6.1 Pure Tone 1.5 Hz

Figure 6-34 shows the peak-to-peak displacement for high and low combinations of α and hybrid gain. With an α of only 0.25, the sprung mass displacement is reduced as the hybrid gain increases. An α of 0.75 and a hybrid gain of 1, reduce the sprung mass displacement almost to the point of isolation. With α = 0.25, the hybrid controller is dominated by the contribution from groundhook control. However, at the 1.5 Hz input,

this idea is not supported. As observed in the groundhook control analysis at 1.5 Hz, groundhook fails to reduce the amplitude of the unsprung mass as the controller gain is increased.

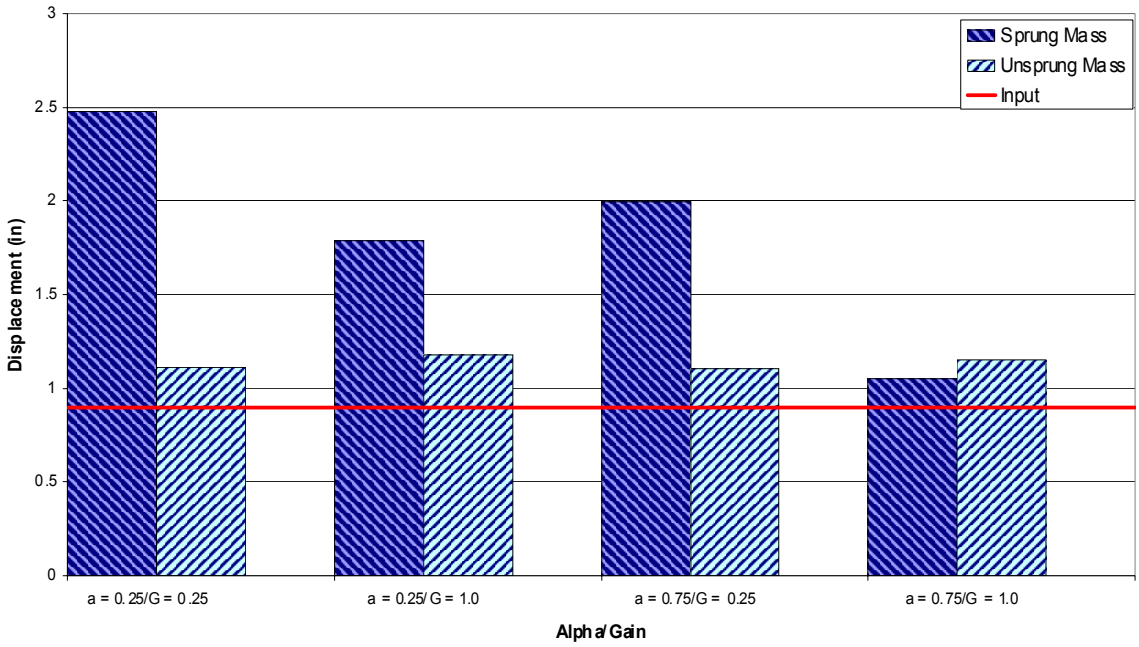

Figure 6-34. Hybrid Control Peak-to-Peak Displacement at 1.5 Hz

The results of the RMS displacement amplitudes in Figure 6-35 reveal the same characteristics. The amplitude of the sprung mass displacement is reduced as the hybrid gain increases, while the amplitude of the unsprung mass increases slightly.

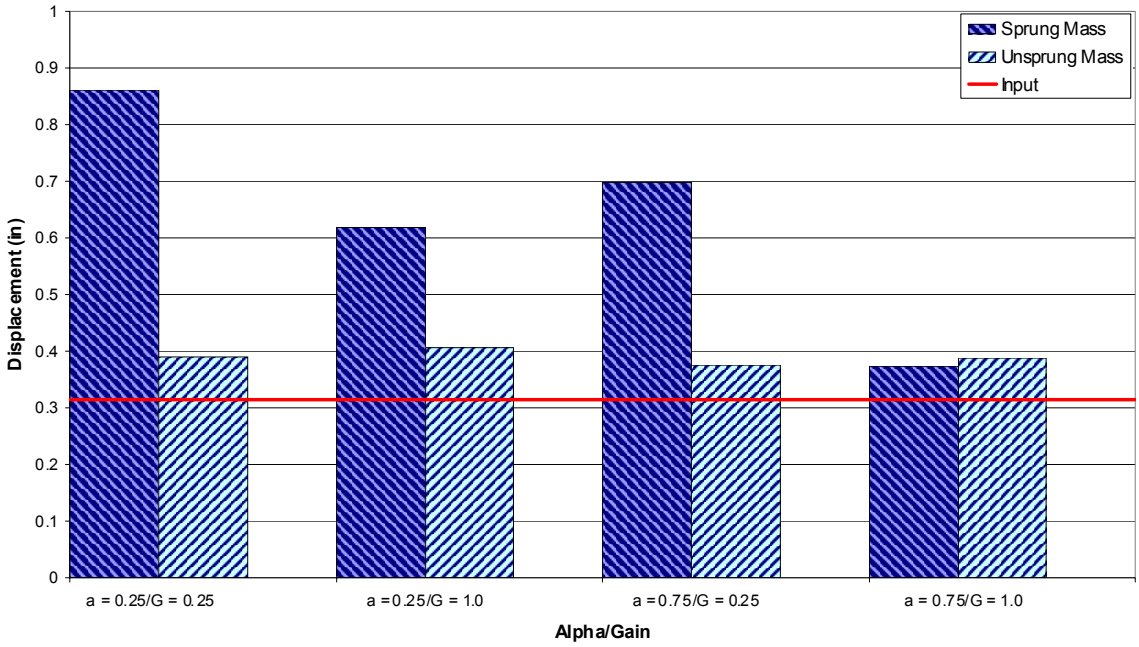

Figure 6-35. Hybrid Control RMS Displacement at 1.5 Hz

Figure 6-36 shows the peak-to-peak amplitudes of the sprung and unsprung mass accelerations. In all but one of the cases, the sprung mass acceleration is isolated, below that of the input signal. This same trend appears in the RMS acceleration amplitudes in Figure 6-37. The sprung mass acceleration is isolated from the input signal acceleration. The unsprung mass acceleration behaves much like the unsprung mass displacement. As the hybrid control gain increases, the unsprung mass acceleration increases. Granted, the unsprung mass natural frequency is not being excited so the benefits of groundhook contributions are not evident. However, the fact that groundhook control focuses on controlling the unsprung mass is not supported here.

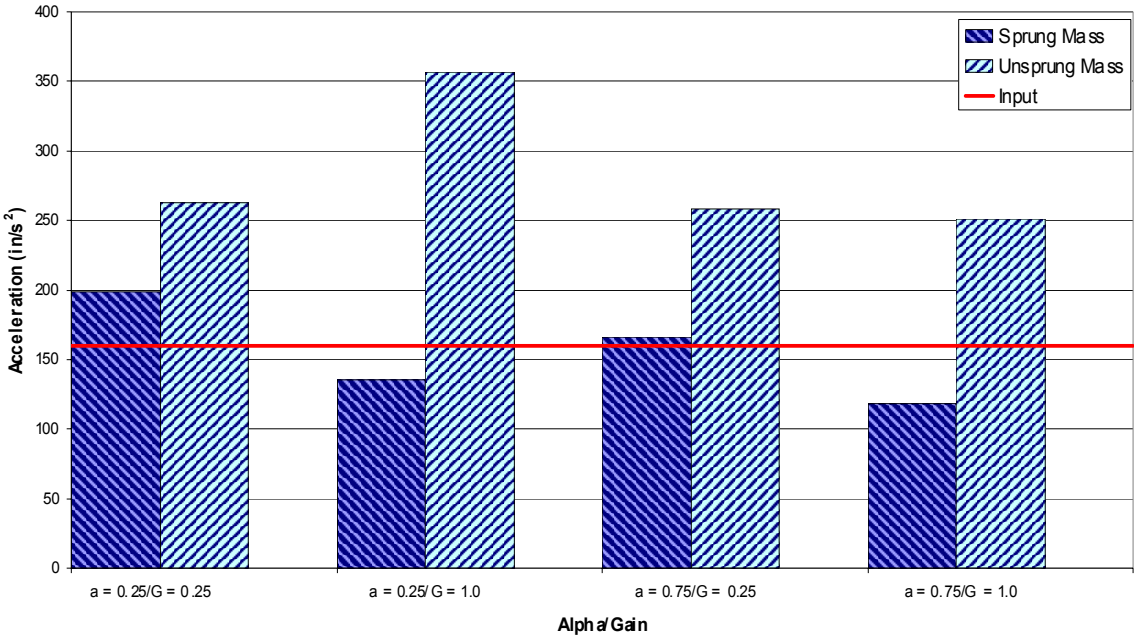

Figure 6-36. Hybrid Control Peak-to-Peak Accelerations at 1.5 Hz

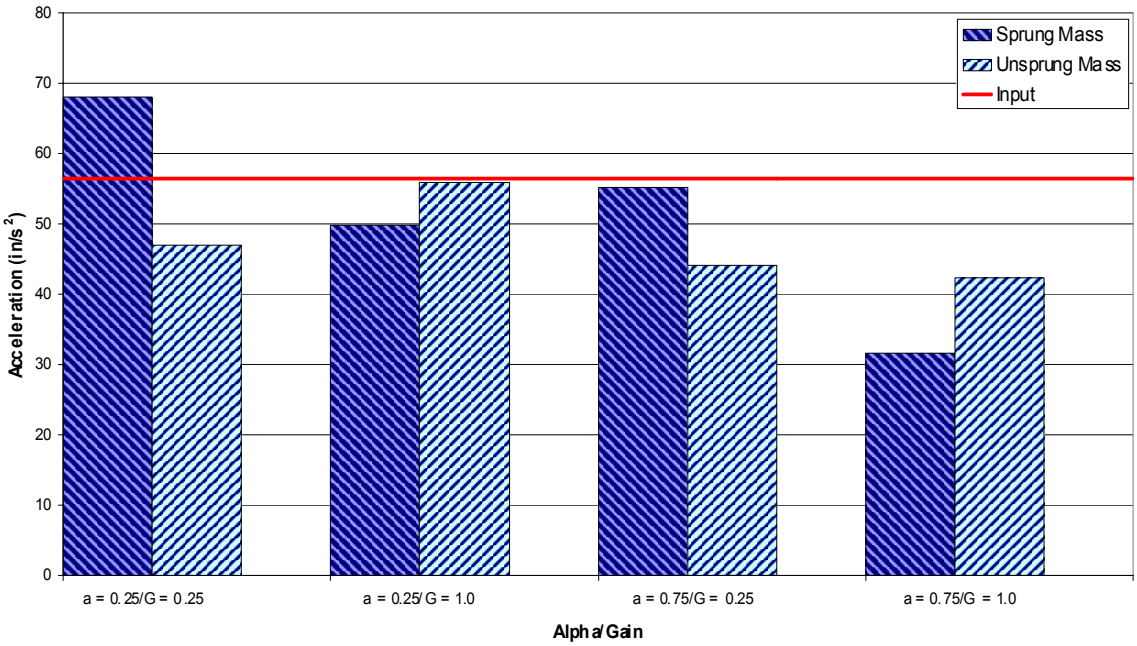

Figure 6-37. Hybrid Control RMS Acceleration at 1.5 Hz

6.6.2 Pure Tone 10.5 Hz

Figure 6-38 shows the peak-to-peak displacements for the 10.5 Hz pure tone input. At this input, the contributions from groundhook control become clear. As Figure 6-38 demonstrates, a 25% contribution from groundhook control is sufficient to reduce the amplitude of the unsprung mass displacement below that of the input signal. As the contribution from groundhook increases, $\alpha = 0.25$, the gains are highlighted. Figure 6-38 also illustrates the effects of α on the sprung mass. At low α, the sprung mass displacement increases as the hybrid gain increases, while at high α, the sprung mass displacement decreases as the hybrid gain increases. The collective benefits observed for the sprung and unsprung mass are what make hybrid control so versatile.

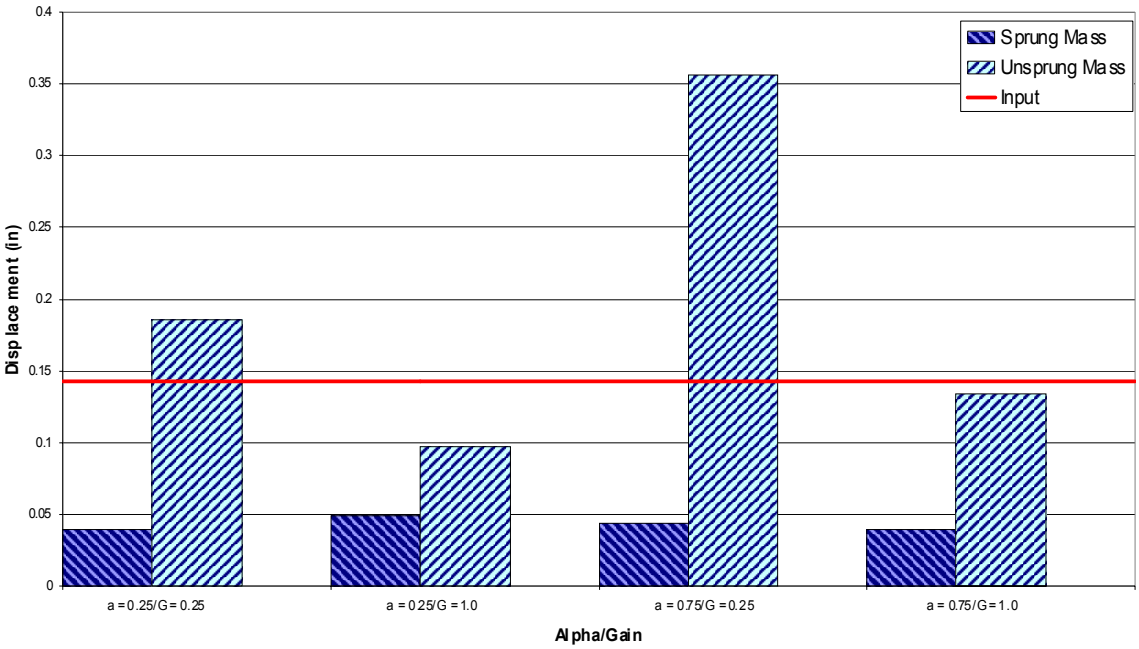

Figure 6-38. Hybrid Control Peak-to-Peak Displacement at 10.5 Hz

The RMS displacement amplitudes in Figure 6-39 demonstrate the same results observed in Figure 6-38. The RMS displacement of the unsprung mass falls below that of the input signal in two of the four cases. Even small contributions from groundhook control are sufficient to reduce the unsprung mass displacement.

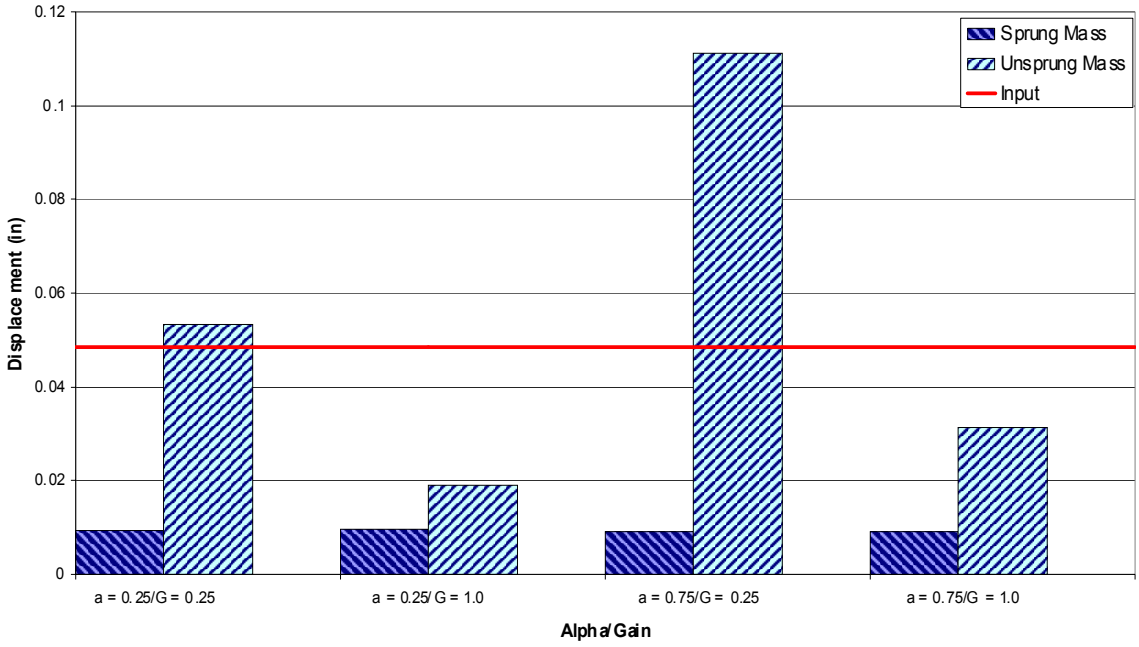

Figure 6-39. Hybrid Control RMS Displacement at 10.5 Hz

The peak-to-peak accelerations shown in Figure 6-40 reveal dramatic benefits. The amplitudes of the unsprung mass accelerations are well below that of the input for all but one case. These same results are mirrored in the RMS acceleration results in Figure 6-41. In both figures, the only case that does not fall below the amplitude of the input acceleration is the high α low gain case. Again, an α of 0.75 represents only a 25% contribution from groundhook control.

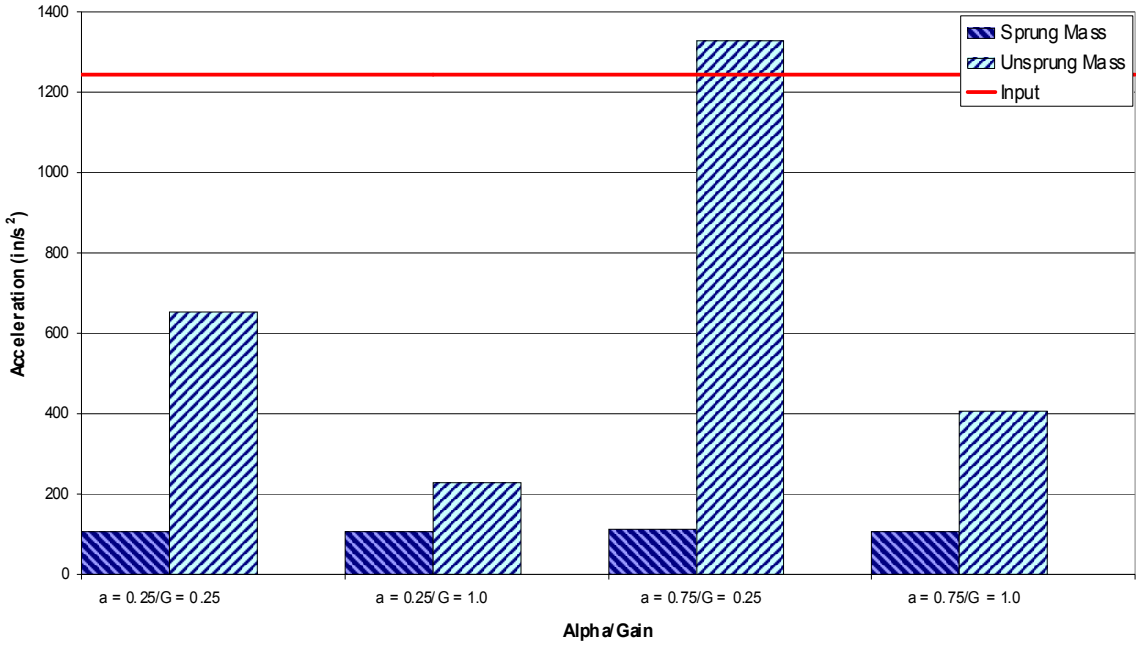

Figure 6-40. Hybrid Control Peak-to-Peak Acceleration at 10.5 Hz

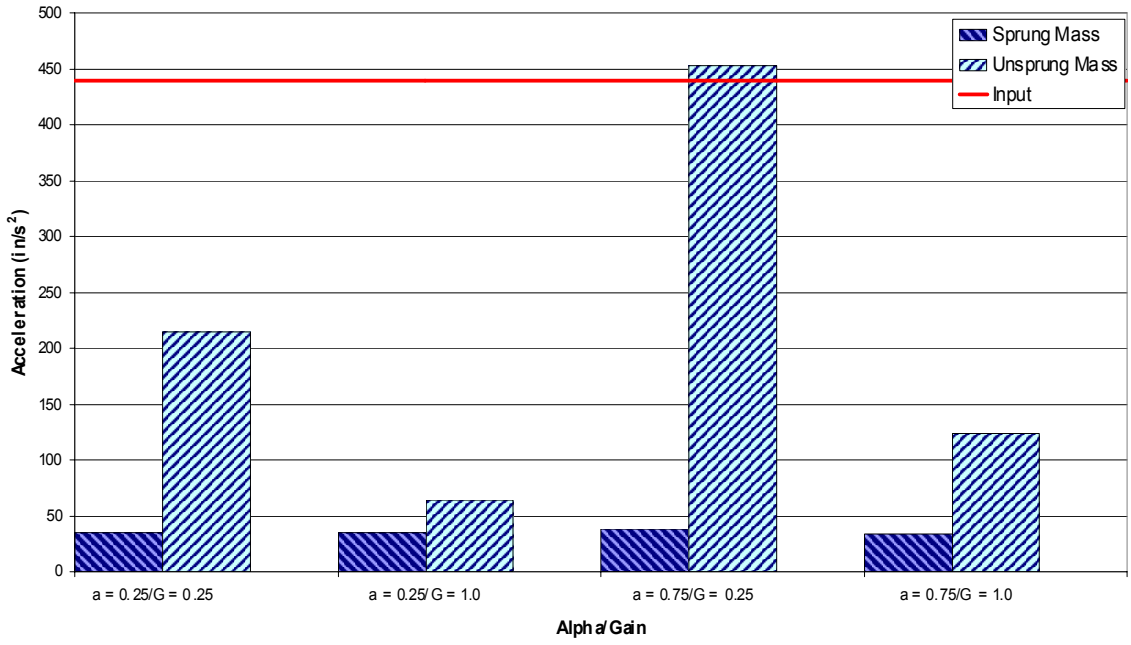

Figure 6-41. Hybrid Control RMS Acceleration at 10.5 Hz

6.6.3 Damper Work

The work done by the hybrid damper is shown in Figure 6-42. At the 1.5 Hz input, the most work done by the damper occurs at a low α and a high gain, whereas for the 10.5 Hz input, the most work is done when α is high and the gain is low. Interestingly, when α is high, both inputs share the same work dynamics, while when α is low, the dynamics are opposite one another.

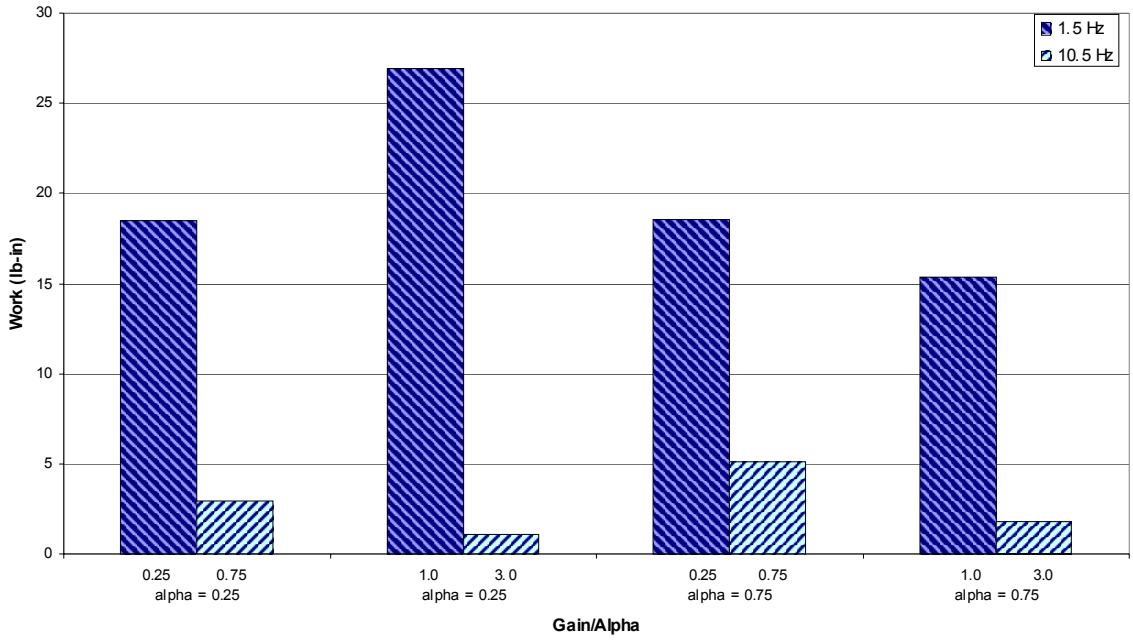

Figure 6-42. Hybrid Control Damper Work

Figure 6-43 shows a sample force displacement plot for hybrid control with an α of 0.5. This force displacement relationship is shown with equal contributions from skyhook and groundhook control. What results is a near perfect parallelogram.

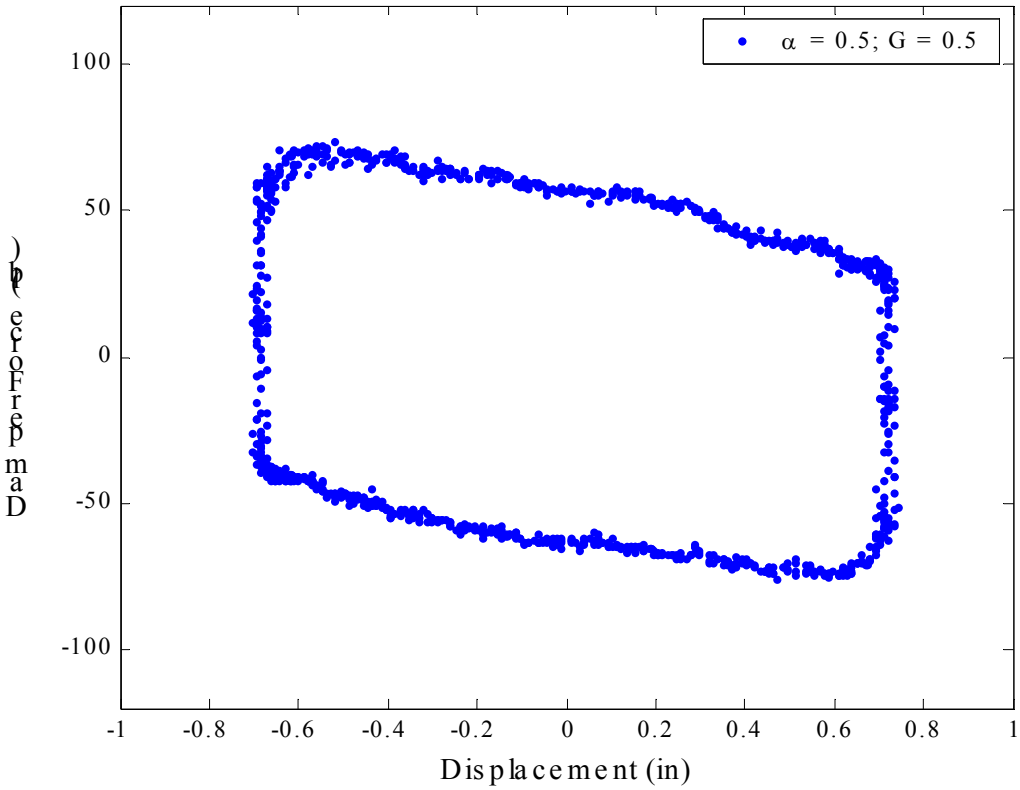

Figure 6-43. Hybrid Control Force Displacement Relationship

The force velocity relationship for the same condition is shown in Figure 6-44. Much like the skyhook and groundhook force velocity relationships, this relationship is characteristic for semi-active MR dampers. The dynamic force benefits of semi-active control are demonstrated once again in Figure 6-44.

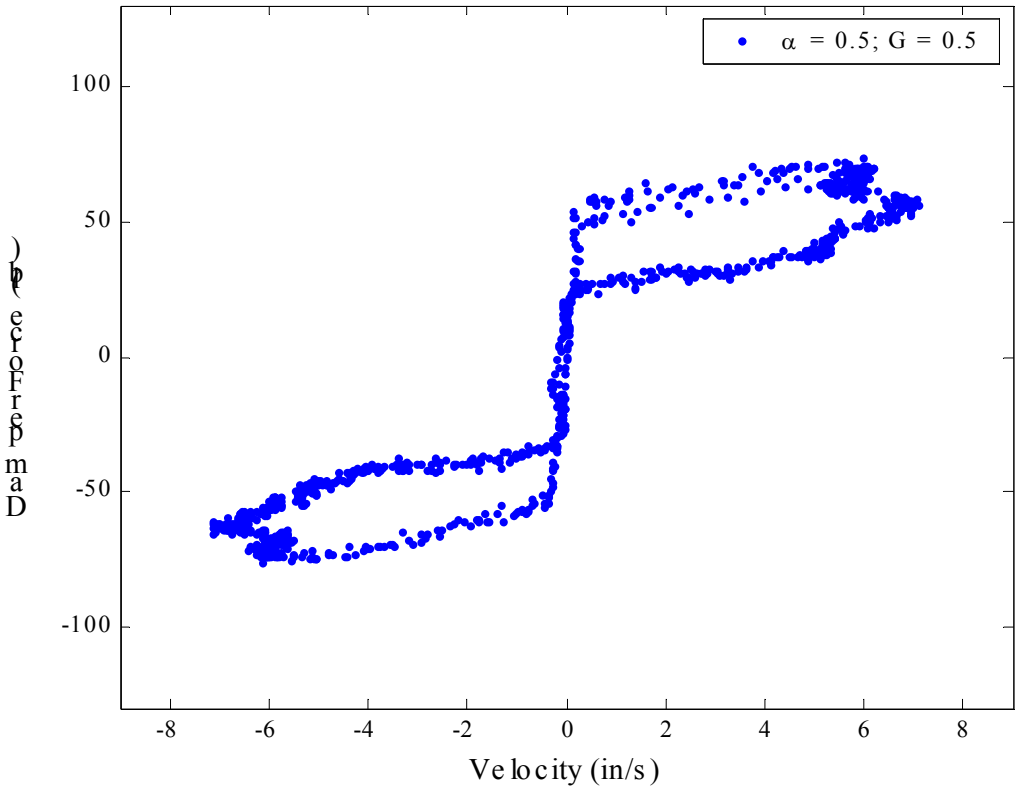

Figure 6-44. Hybrid Control Force Velocity Relationship

6.7 Displacement Skyhook Steady State Evaluation

This section explores the benefits of displacement skyhook for steady state inputs. Displacement skyhook is measured against the same criterion for a 1.5 Hz input as well as a 10.5 Hz input.

6.7.1 Pure Tone 1.5 Hz

The peak-to-peak displacement results for displacement skyhook are shown in Figure 6-45. A skyhook based controller, displacement skyhook shows benefits for controlling the sprung mass. As the controller gain increases, the displacement amplitude decreases. This same result is supported by the RMS displacement amplitudes in Figure 6-46. Figure 6-46 also shows that as the controller gain increases, the RMS displacement amplitude of the unsprung mass increases.

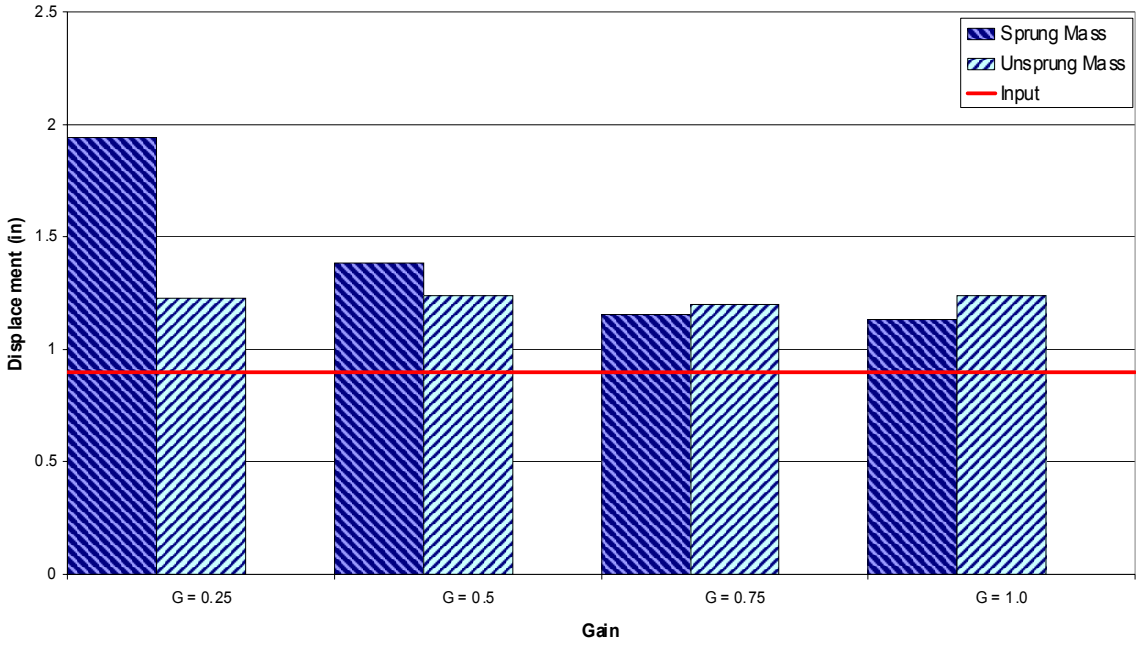

Figure 6-45. Displacement Skyhook Control Peak-to-Peak Displacement at 1.5 Hz

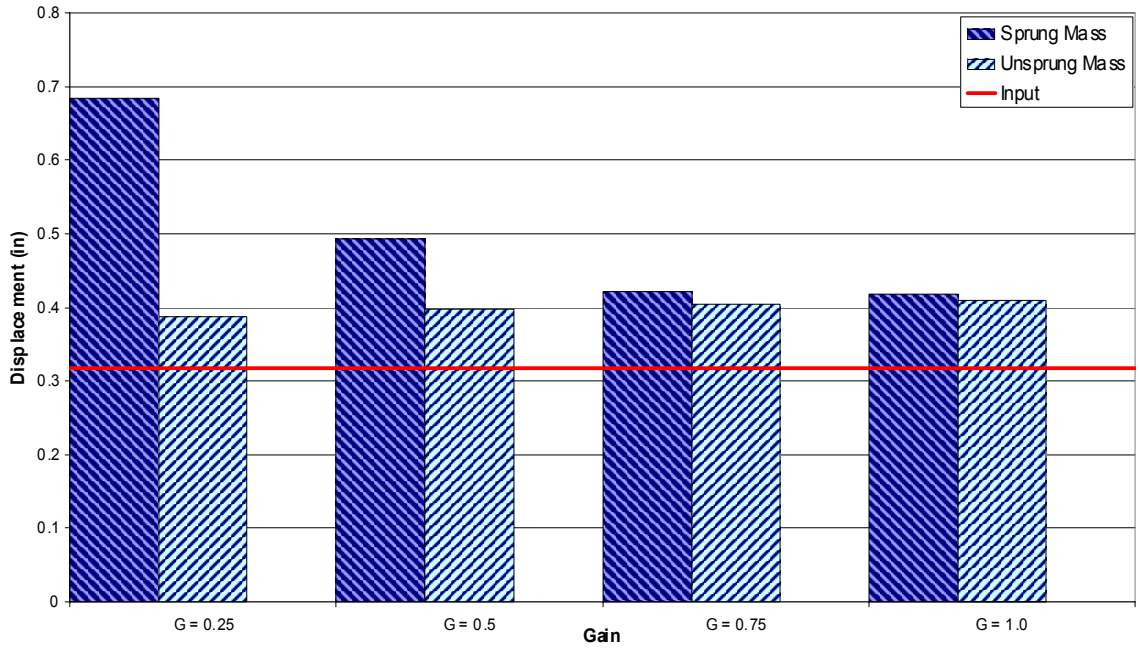

Figure 6-46. Displacement Skyhook Control RMS Displacement at 1.5 Hz

The peak-to-peak acceleration results in Figure 6-47 reveal interesting dynamics occurring at the unsprung mass. While the sprung mass peak-to-peak acceleration remains relatively unchanged, the unsprung mass acceleration is significantly decreased at a controller gain of 1. Initially, the unsprung mass acceleration increases as the gain is increased. However, as the gain is increased beyond 0.5, the acceleration begins to drop.

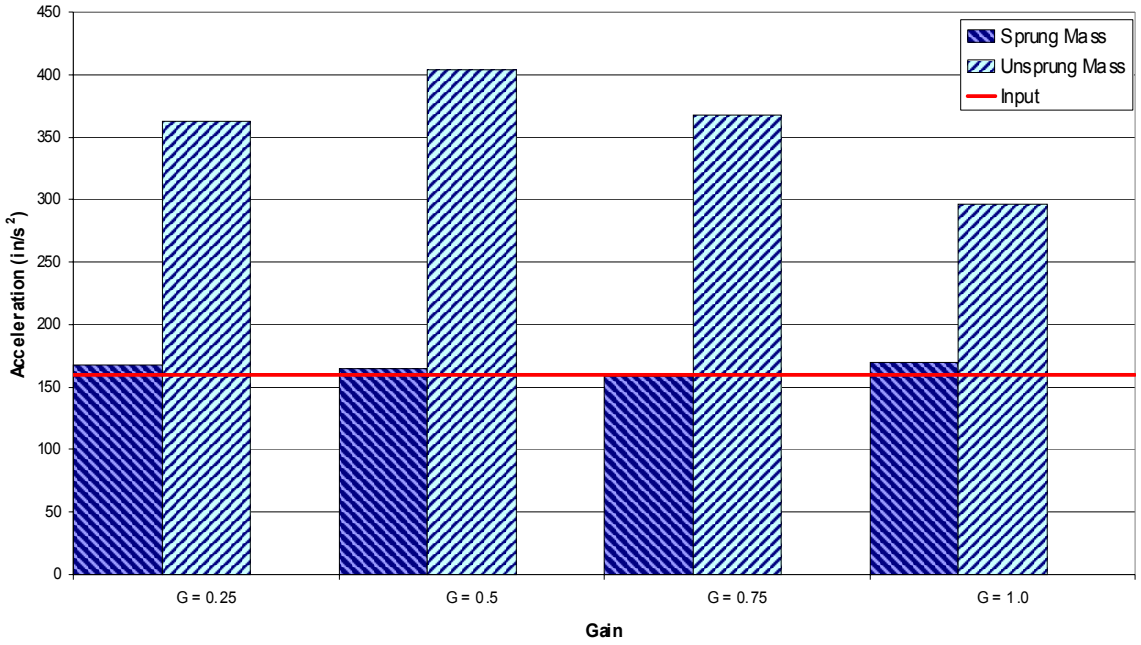

Figure 6-47. Displacement Skyhook Control Peak-to-Peak Acceleration at 1.5 Hz

Similar dynamics appear in Figure 6-48. The RMS acceleration amplitudes show that the acceleration of the unsprung mass increases as the gain is increased from 0.25 to 0.5. However, the acceleration amplitude drops below that of the input for a controller gain of 0.75. These results indicate that for the 1.5 Hz pure tone input, displacement skyhook control has some dynamic benefits over conventional skyhook for controlling the unsprung mass. Figure 6-48 also shows that the RMS accelerations of the sprung mass are reduced below that of the input signal for all controller gains.

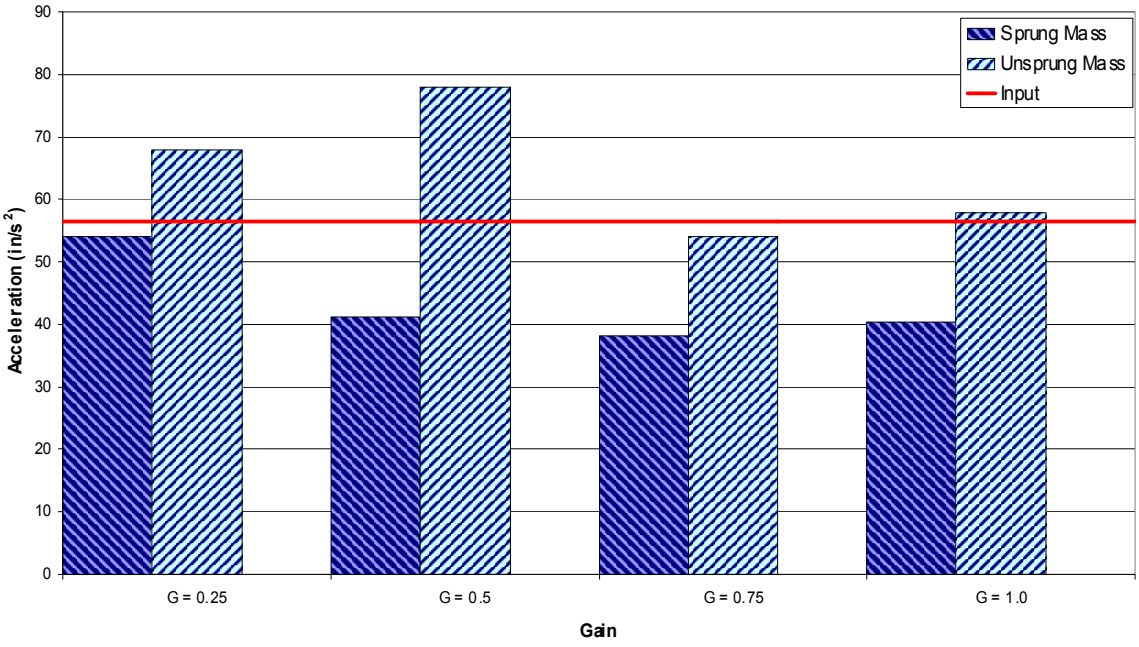

Figure 6-48. Displacement Skyhook Control RMS Acceleration at 1.5 Hz

6.7.2 Pure Tone 10.5 Hz

The performance of displacement skyhook at controlling the unsprung mass is better quantified at the 10.5 Hz input. Figure 6-49 shows the peak-to-peak displacements of the sprung and unsprung masses. Again, because the sprung mass is well isolated from this input, the control benefits of displacement skyhook on the sprung mass will not appear. What does become clear is the apparent benefit of displacement skyhook on controlling the unsprung mass. The peak-to-peak displacement of the unsprung mass decreases as controller gain increases. This is also true for the RMS displacement of the unsprung mass, as shown in Figure 6-50.

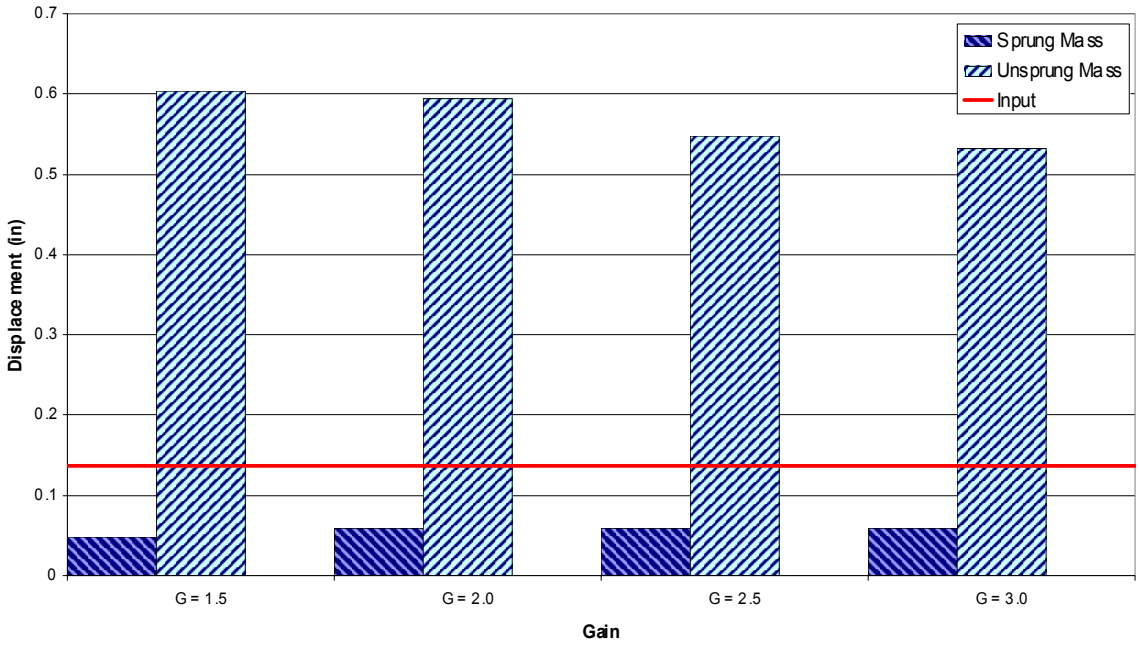

Figure 6-49. Displacement Skyhook Control Peak-to-Peak Displacement at 10.5 Hz

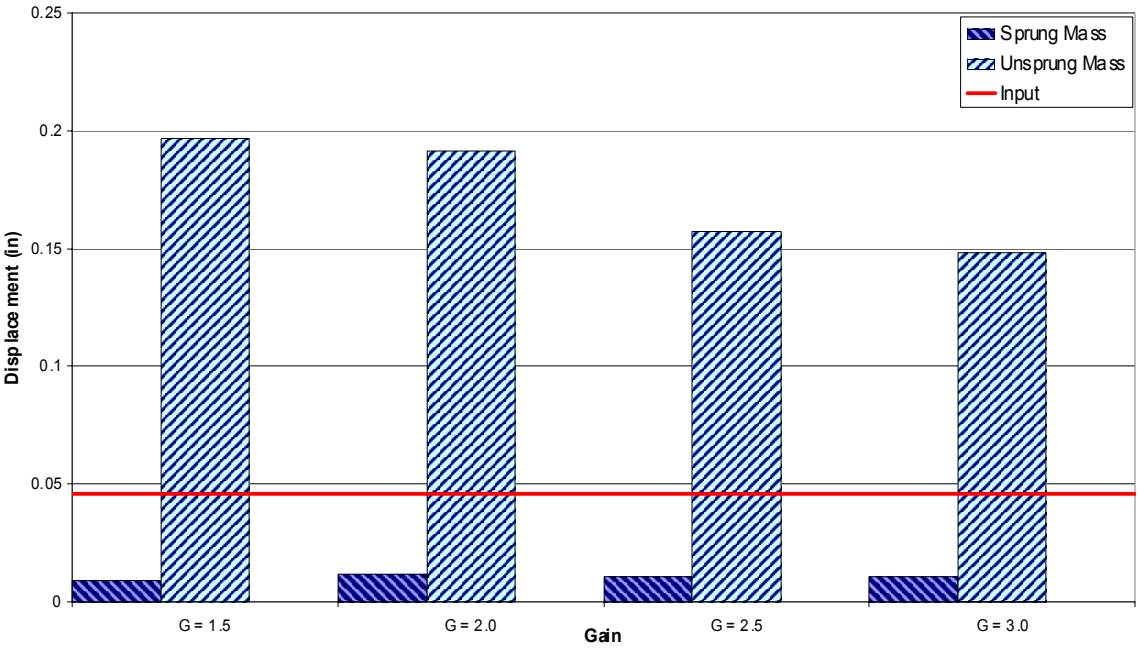

Figure 6-50. Displacement Skyhook Control RMS Displacement at 10.5 Hz

The peak-to-peak accelerations, shown in Figure 6-51, support the same behavior. As the controller gain increases, the peak-to-peak amplitude of the unsprung mass acceleration decreases. Once again, displacement skyhook shows some indication of a slight ability to reduce response levels of the unsprung mass.

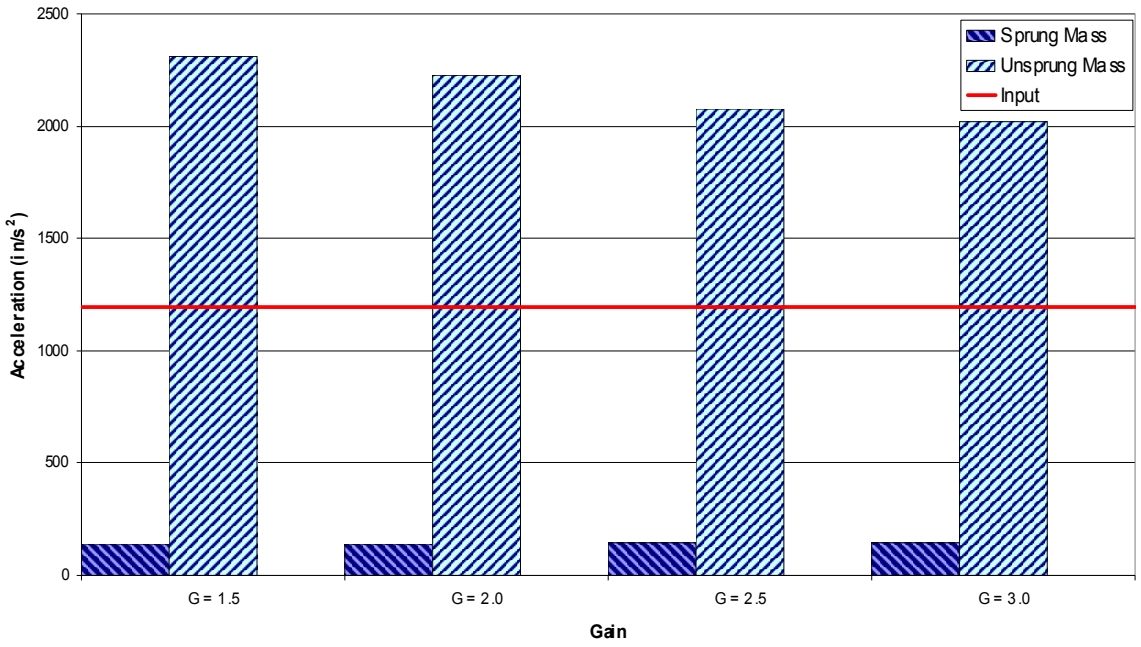

Figure 6-51. Displacement Skyhook Control Peak-to-Peak Acceleration at 10.5 Hz

The final stage in the 10.5 Hz pure tone analysis reveals the same results. The RMS accelerations, shown in Figure 6-52 also support displacement skyhook's ability to attenuate the unsprung mass response levels. Here again, the acceleration levels of the unsprung mass decrease as controller gain increases. It should be noted that the performance benefits observed for the unsprung mass at the 10.5 Hz input could be artifacts of an increase in the system's overall damping. As the controller attempts to control the sprung mass, the damping levels in the system could be increasing, thus reducing the response of the unsprung mass. In any case, displacement skyhook reveals dynamic benefits that are not observed in conventional skyhook, and for that reason, they should not go unnoticed.

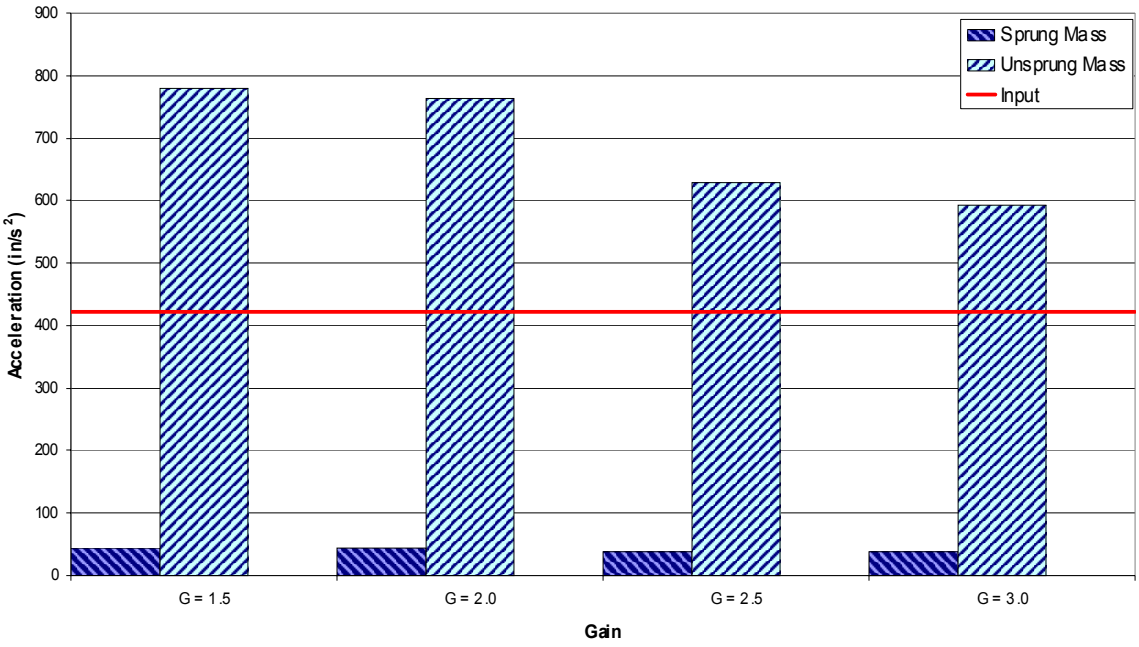

Figure 6-52. Displacement Skyhook Control RMS Acceleration at 10.5 Hz

6.7.3 Damper Work

The work done by the damper under displacement skyhook control is shown in Figure 6-53. At the 1.5 Hz input, the damper does the most work at a controller gain of 0.25 and 0.75. The work done by the damper at the 10.5 Hz input appears to remain constant throughout all controller gains.

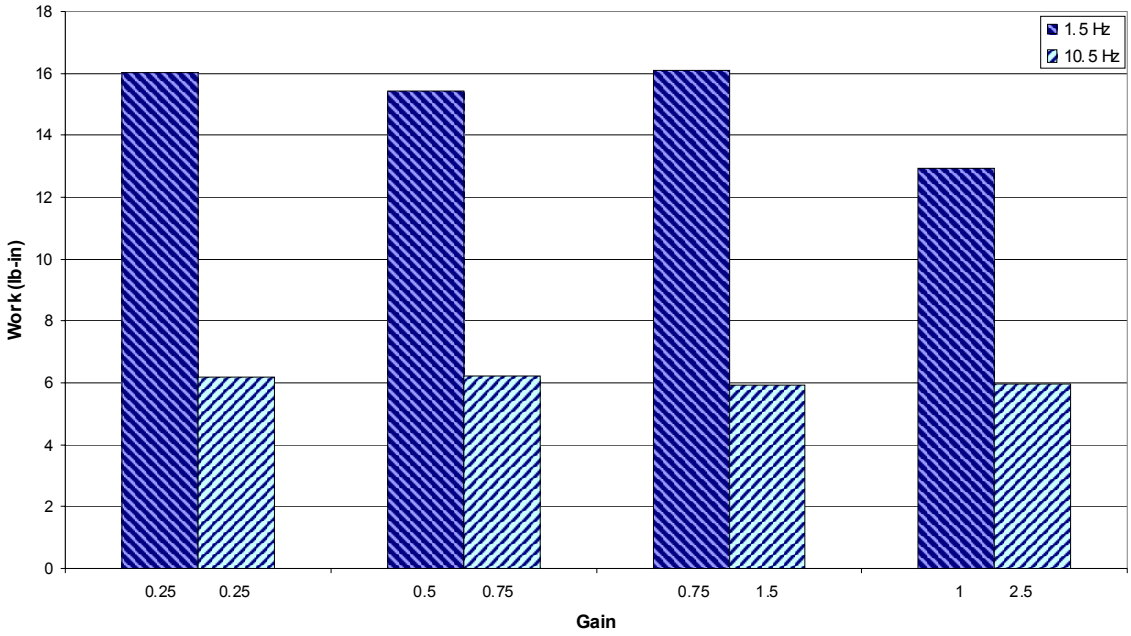

Figure 6-53. Displacement Skyhook Control Damper Work

Figure 6-54 shows a sample force displacement relationship with displacement skyhook control. Figure 6-54 reveals some very interesting dynamics occurring ± 0.4 inches. There appears to be a discontinuity in the force. This dramatic increase or decrease in force could lead to high levels of acceleration and therefore jerk. This interesting behavior is due to the control algorithm that describes displacement skyhook control. The condition by which the damper switches, undoubtedly affects the force displacement relationship, and in the case of displacement skyhook, results in what could lead to poor ride comfort.

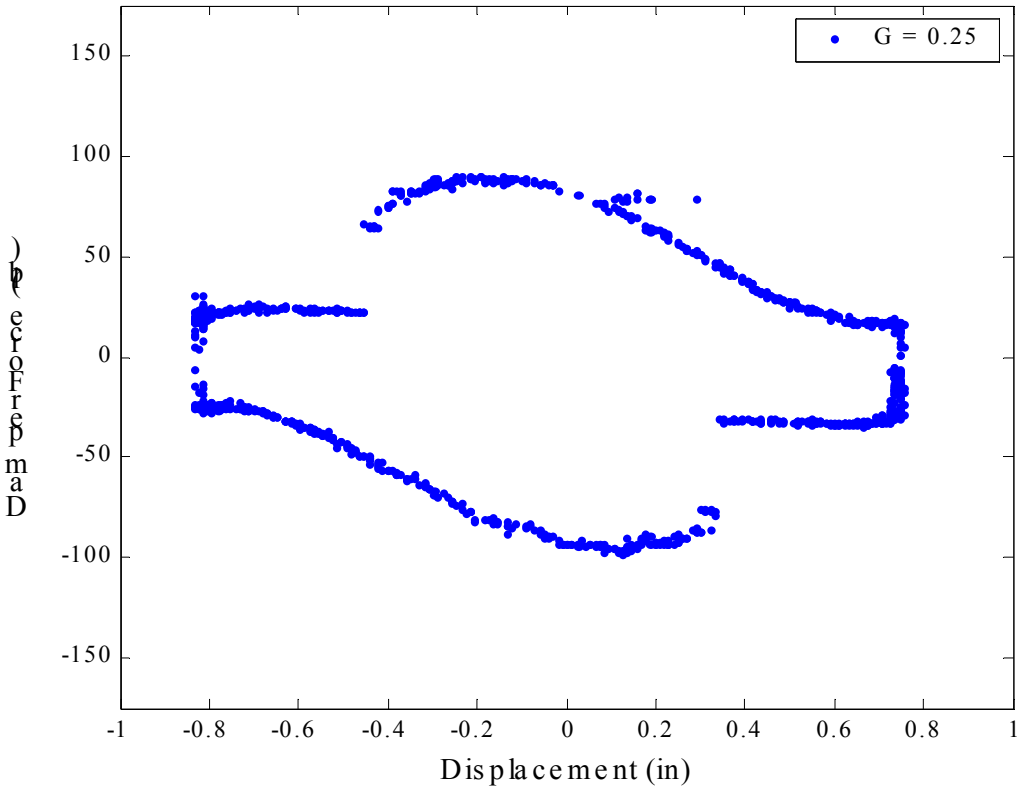

Figure 6-54. Displacement Skyhook Control Force Velocity Relationship

A sample force velocity plot for displacement skyhook control is shown in Figure 6-55. The interesting behavior observed in Figure 6-54 also appears in the relationship between force and velocity. Once the velocity exceeds ± 5 inches per second, the force velocity relationship becomes uncharacteristic. Again, this behavior must be due to the dynamics of the controller itself, commanding the damper to perform as shown in Figure 6-55.

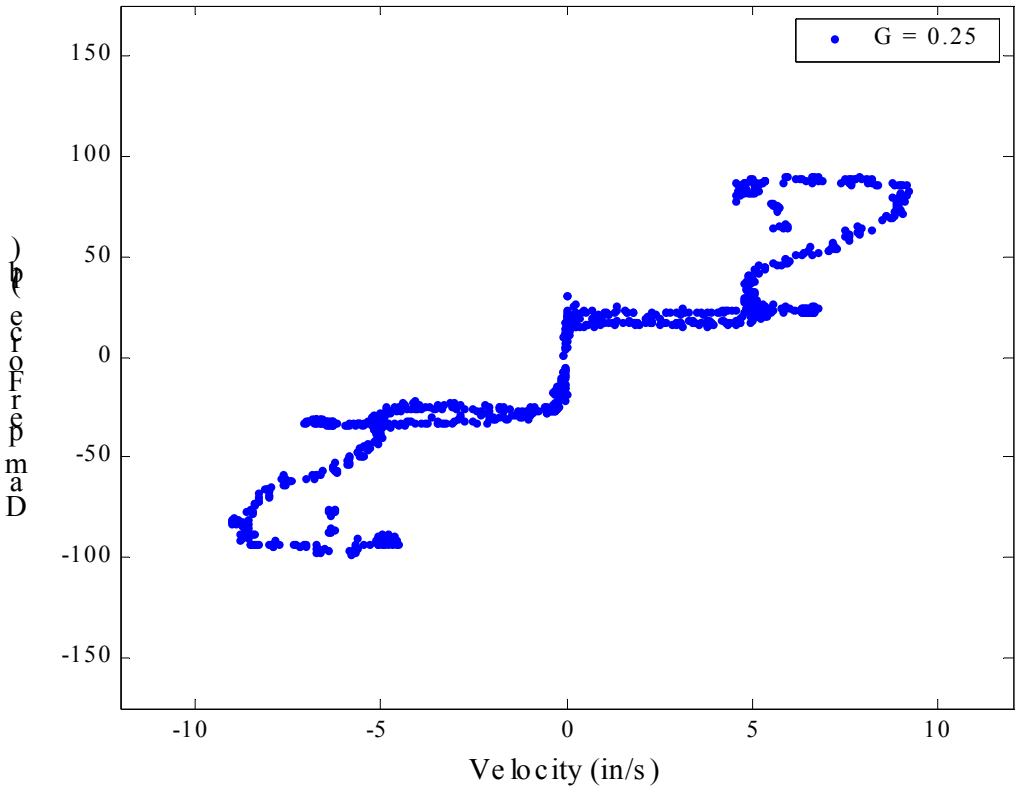

Figure 6-55. Displacement Skyhook Control Force Velocity Relationship

6.8 Relative Displacement Skyhook Steady State Evaluation

This section reveals the benefits of the final control policy considered in this study. As before, the response of relative displacement skyhook to steady state inputs will be evaluated.

6.8.1 Pure Tone 1.5 Hz

Figure 6-56 shows the peak-to-peak displacement results for the skyhook based relative displacement controller. As expected from a skyhook based policy, the sprung mass displacement amplitude decreases as the controller gain increases. The same results are present in the RMS displacement amplitudes in Figure 6-57. Both figures show a slight increase in the unsprung mass peak-to-peak displacement as the controller gain increases.

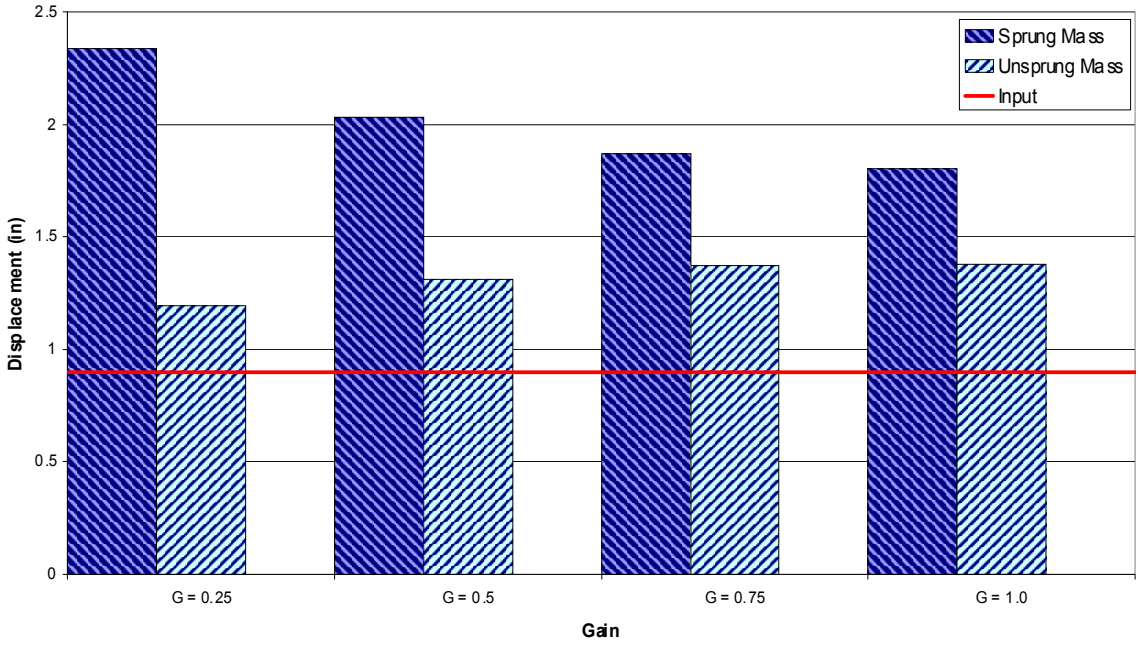

Figure 6-56. Relative Displacement Skyhook Control Peak-to-Peak Displacement at 1.5 Hz

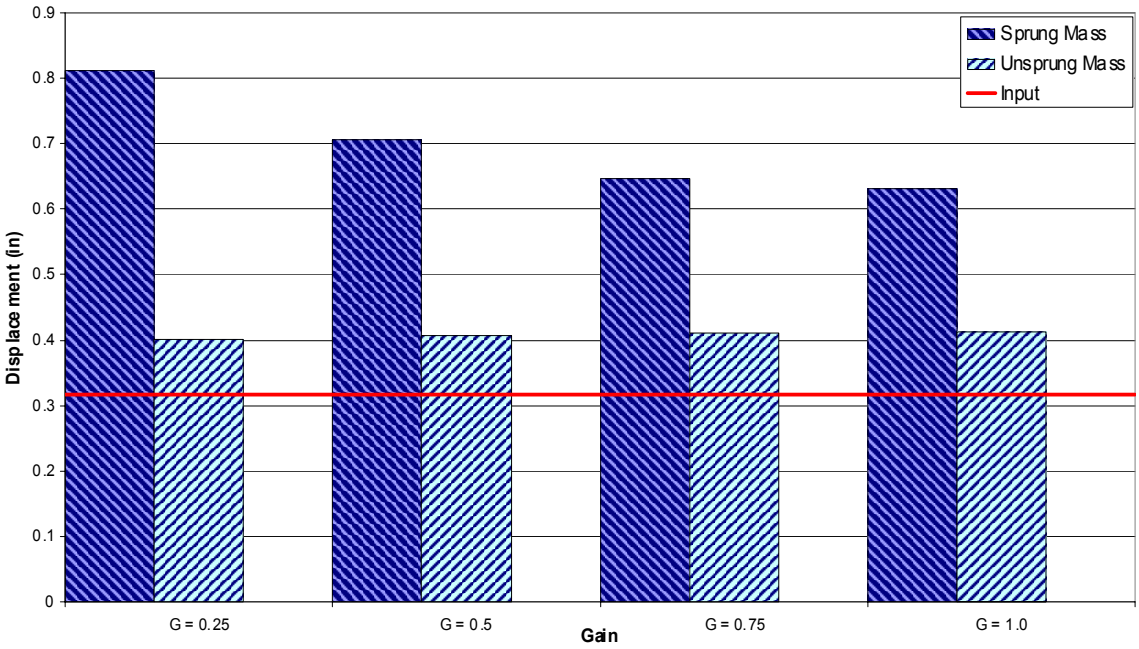

Figure 6-57. Relative Displacement Skyhook Control RMS Displacement at 1.5 Hz

In evaluating the peak-to-peak acceleration amplitudes, in Figure 6-58, it is clear that relative displacement skyhook does little to reduce the acceleration levels at the sprung mass. Figure 6-58 also shows a dramatic increase in the levels of acceleration at the unsprung mass. As the controller gain increases, the unsprung mass peak-to-peak acceleration increases.

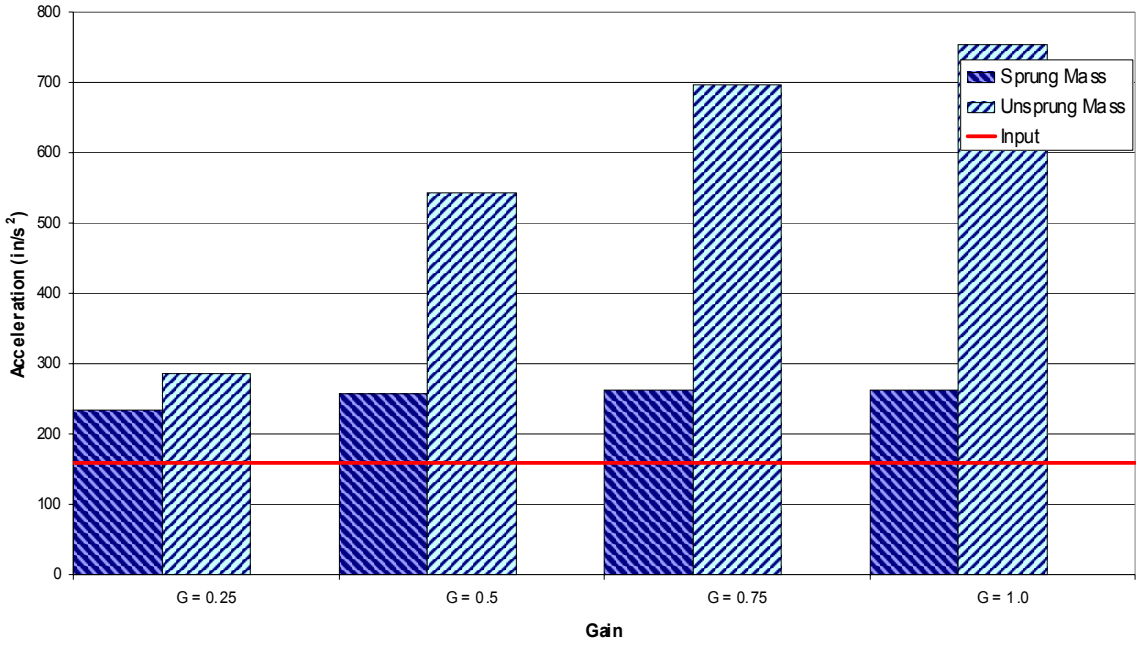

Figure 6-58. Relative Displacement Skyhook Control Peak-to-Peak Acceleration at 1.5 Hz

The RMS acceleration values of Figure 6-59 show the same trend observed in the peak-to-peak acceleration values. The sprung mass acceleration does not improve greatly as the controller gain is increased. Again, the increase in the unsprung mass acceleration levels is clear as the controller gain is increased.

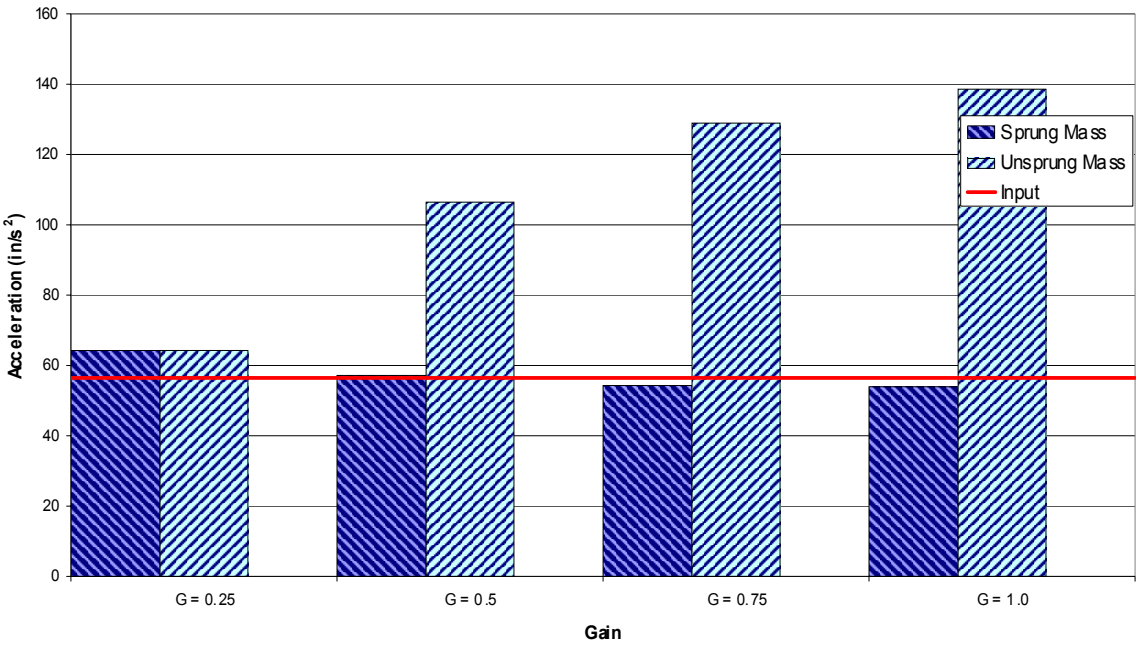

Figure 6-59. Relative Displacement Skyhook Control RMS Acceleration at 1.5 Hz

6.8.2 Pure Tone 10.5 Hz

The results obtained from the 10.5 Hz input signal reveal similar dynamics observed in displacement skyhook control. Figure 6-60 shows the peak-to-peak displacement results. The sprung mass remains well isolated from the input. The unsprung mass displacement amplitude decreases as the controller gain increases. This same trend is supported by the RMS displacement amplitudes in Figure 6-61. These results indicate that relative displacement skyhook can offer some benefits to controlling the unsprung mass.

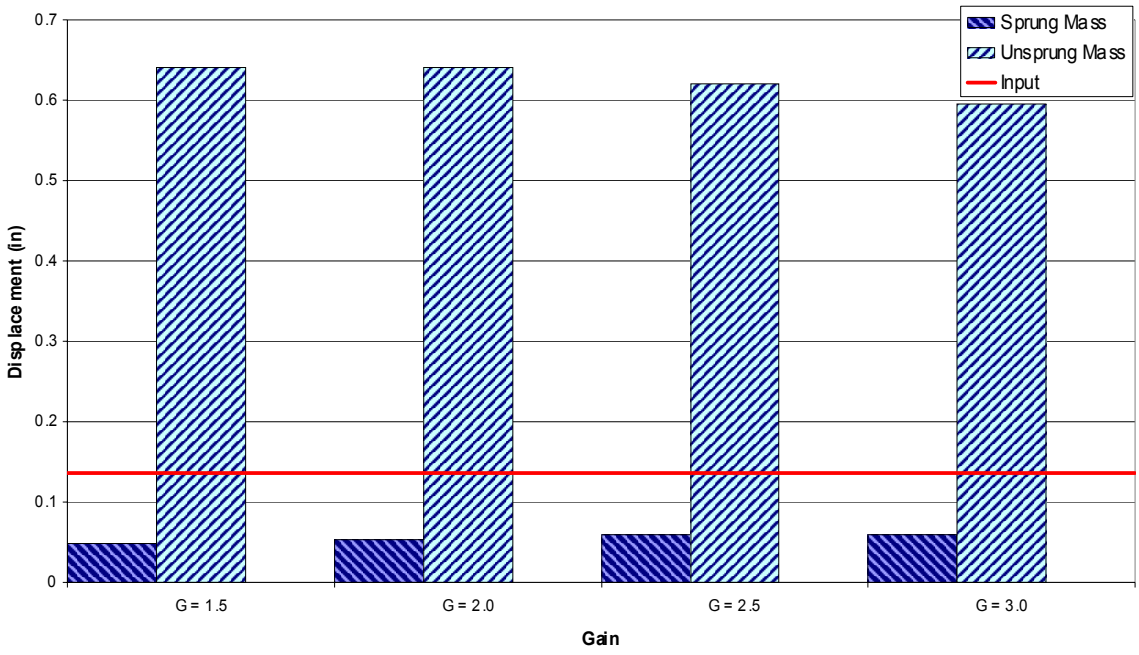

Figure 6-60. Relative Displacement Skyhook Control Peak-to-Peak Displacement at 10.5 Hz

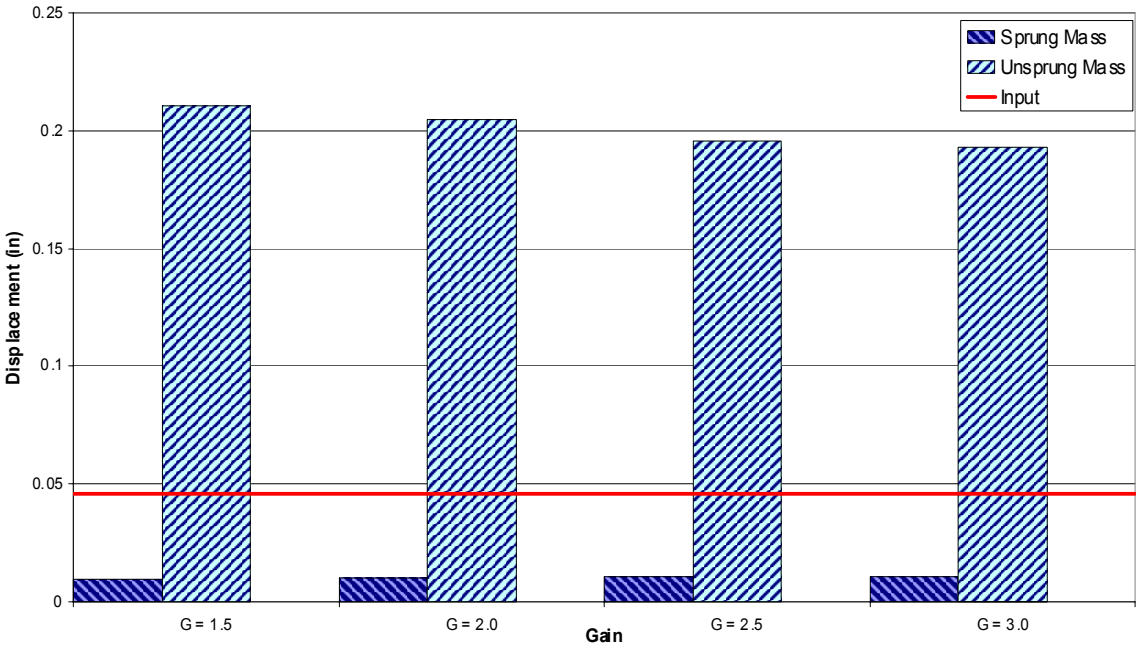

Figure 6-61. Relative Displacement Skyhook Control RMS Displacement at 10.5 Hz

Though the benefits for controlling the unsprung mass come in small amplitude reductions, those benefits appear in each of the evaluations. Figure 6-62 shows the peak-to-peak acceleration amplitudes for relative displacement control. Again, the sprung mass remains well isolated and the unsprung mass acceleration amplitudes are reduced as the controller gain increases.

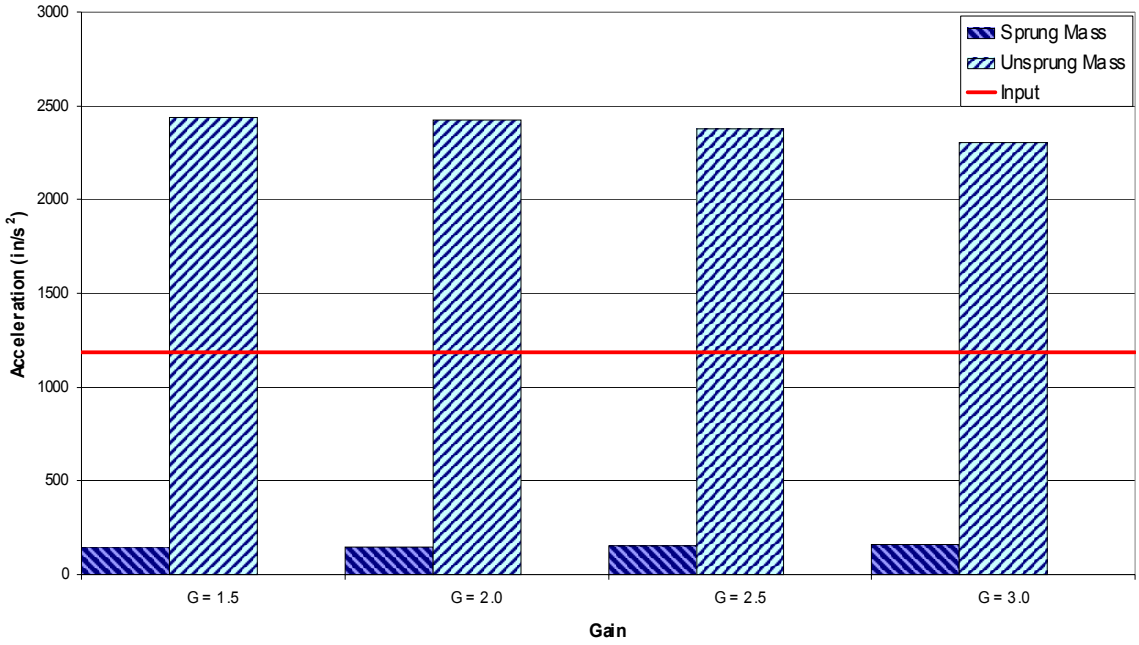

Figure 6-62. Relative Displacement Skyhook Peak-to-Peak Acceleration at 10.5 Hz

Figure 6-63 shows the RMS acceleration amplitudes. The same reduction in acceleration amplitude of the unsprung mass is observed. At the 10.5 Hz input, the reductions in the amplitudes of the unsprung mass can be credited to increased controller effort. These apparent benefits are artifacts of the controller attempting to control the sprung mass.

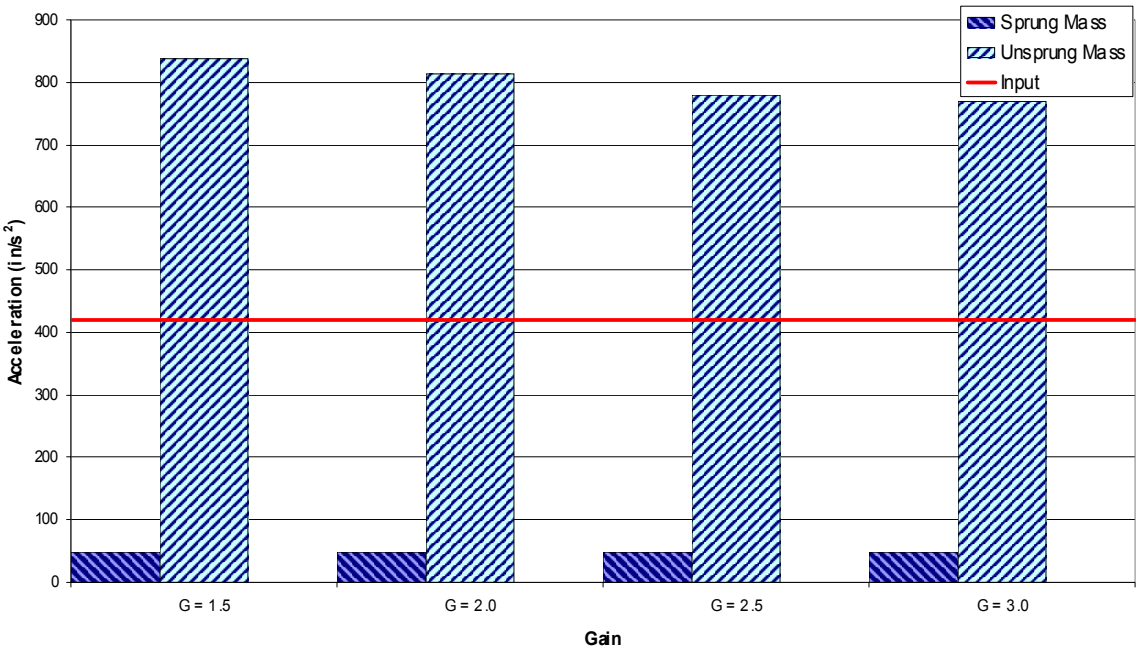

Figure 6-63. Relative Displacement Skyhook Control RMS Accelerations at 10.5 Hz

6.8.3 Damper Work

Figure 6-64 shows the work done by the damper for each input. As the controller gain increases, the work done by the damper decreases for the 1.5 Hz input. The opposite is true for the 10.5 Hz input; as the controller gain is increased, the work done by the damper increases slightly.

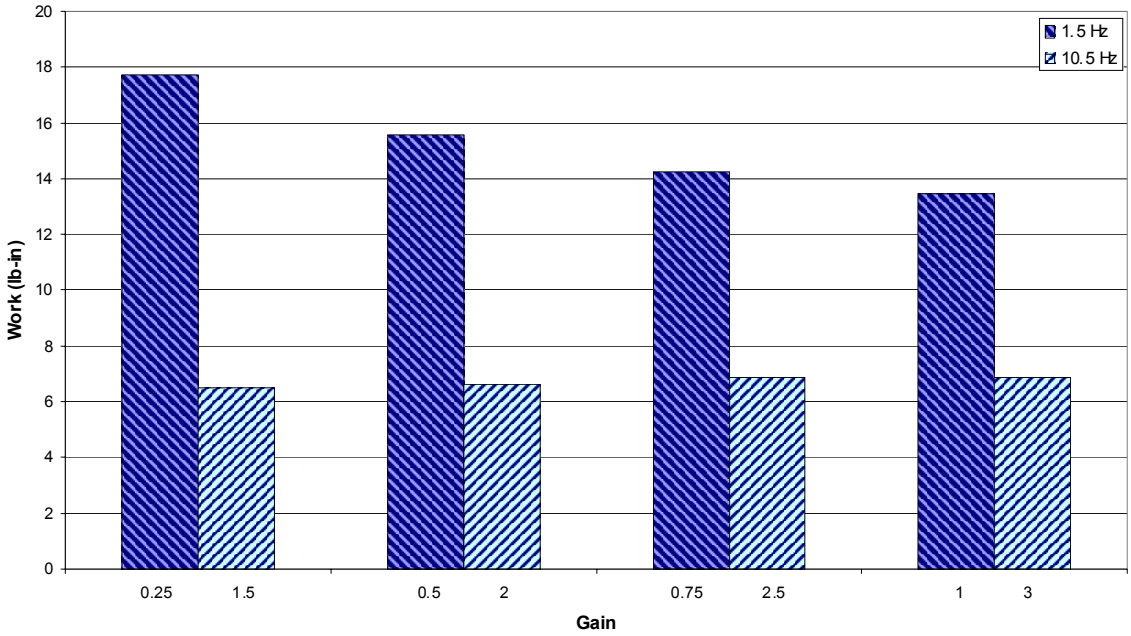

Figure 6-64. Relative Displacement Skyhook Control Damper Work

A sample force displacement plot for relative displacement skyhook control is shown in Figure 6-65. The same discontinuity observed in displacement skyhook appears here as well. In this case, the discontinuity occurs where the displacement crosses zero. Recalling how relative displacement skyhook is defined, this discontinuity is clearly an artifact of the manner by which the damper is being commanded.

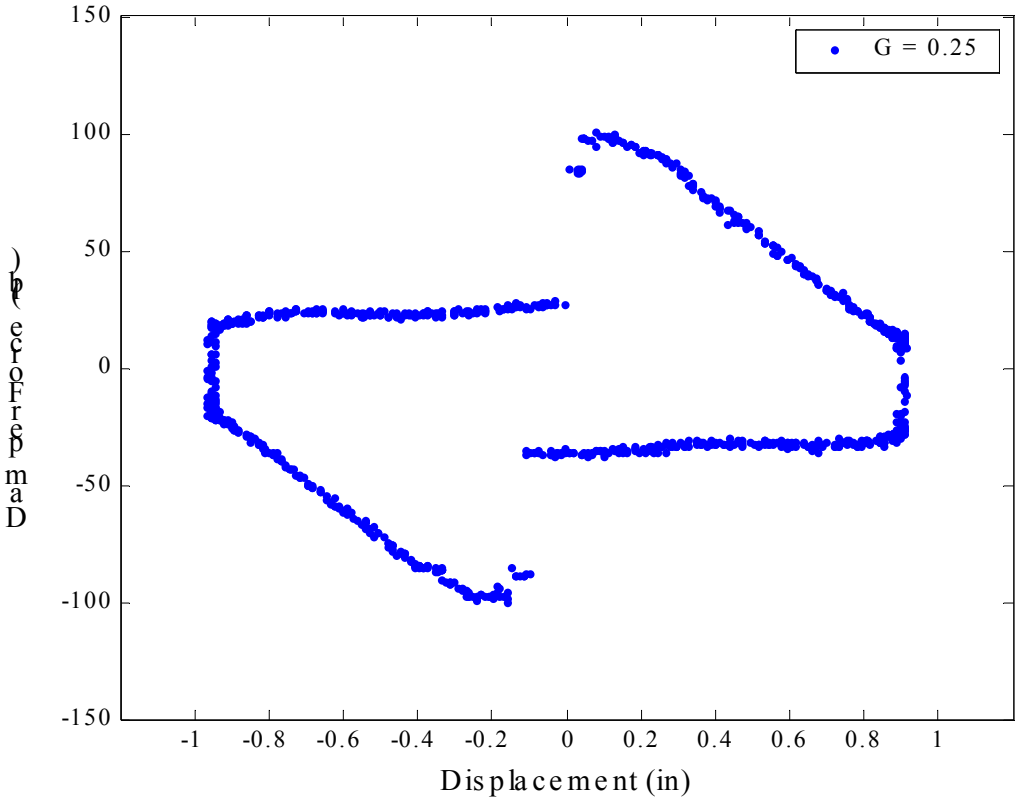

Figure 6-65. Relative Displacement Skyhook Control Force Displacement Relationship

Figure 6-66 shows a force velocity plot for relative displacement control. This same behavior was observed in displacement skyhook control. Once again, the dynamics of the controller define the unique relationship in Figure 6-66. At velocities greater than ± 5 inches per second the force velocity relationship becomes uncharacteristic. This is again due to the switching dynamics of the command signal to the damper.

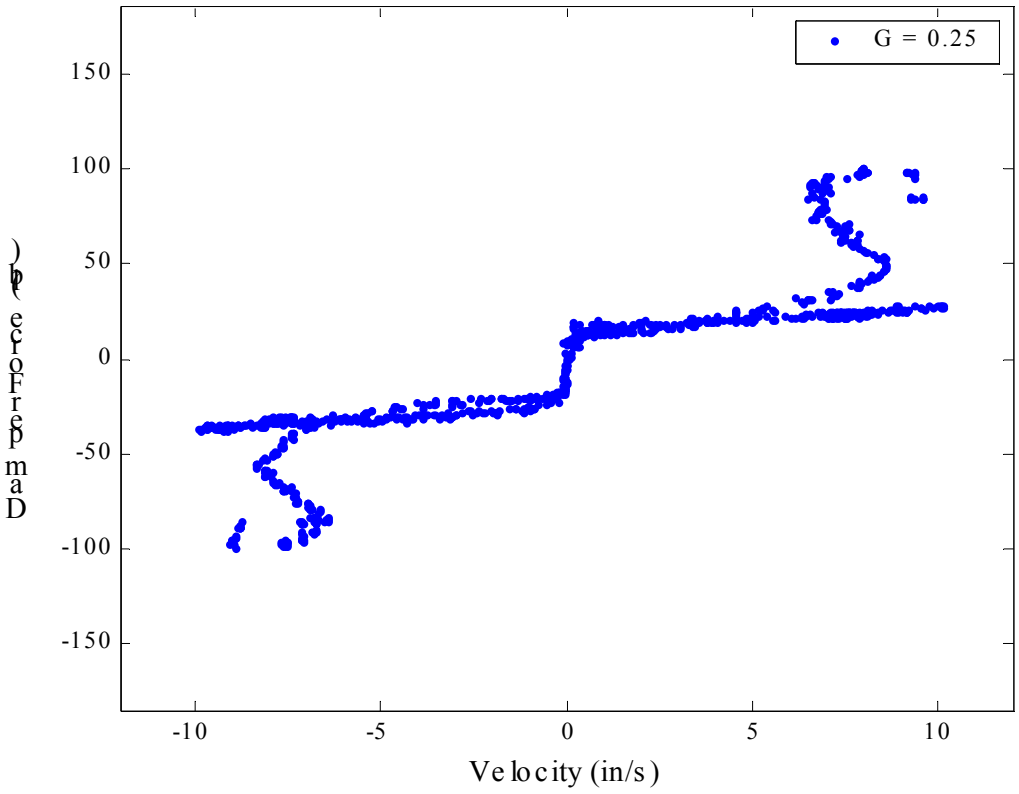

Figure 6-66. Relative Displacement Skyhook Control Force Velocity Relationship

7 Conclusion and Recommendations

The purpose of this chapter is to summarize the work that was done for this thesis. In addition, the results of testing will be discussed with respect to the research objectives set forth in Chapter 1. The chapter ends with recommendations for future work in the field of vehicle suspensions.

7.1 Summary

The first objective mentioned in Chapter 1 was with regard to the improvement of the quarter-car rig. In a laboratory environment, researchers have the luxury of measuring signals not readily available in field testing. Taking advantage of this luxury, the quarter-car rig was fitted with more transducers, offering more feedback and more data than can be expected in an actual vehicle. Currently, the quarter-car rig is capable of measuring 9 signals directly. This capacity is valuable for many different types of experimental evaluations.

Another development of the quarter-car rig that came from this research was the addition of 8 Roller Wheels to the sprung mass body. These Roller Wheels greatly reduced the friction damping inherent in the sprung mass body. This ensures that the only damping applied to the sprung mass comes from the experimental damper.

A final improvement to the quarter-car rig is the addition of spacers used to modify the rattle space. With these spacers, the rattle space can be adjusted to accommodate many different dampers, ranging in size. This development allows for testing of dampers designed for passenger vehicles as well as dampers designed for sport utility vehicles and trucks.

The second objective deals with the evaluation of several different semi-active control policies. Each policy was judged on its performance in controlling the sprung and unsprung masses when subjected to three types of base excitations. Through this research, we've confirmed the expected benefits of skyhook and groundhook control.

For each of the three inputs, we've observed the performance of skyhook and groundhook control as the best at controlling the sprung and unsprung masses respectively. We've also observed the costly tradeoff inherent in skyhook and groundhook control. In that respect, this research has also highlighted the advantages of hybrid control for eliminating that compromise.

Two alternatives to skyhook control have also been introduced and in some cases, the results are promising. Displacement skyhook and relative displacement skyhook demonstrate similar benefits observed in conventional skyhook. In particular, displacement skyhook can offer competitive results, and perhaps at less of a cost than conventional skyhook. Relative displacement skyhook indicated an ability to reduce the levels of sprung mass motion but not nearly to the extent of the other two skyhook controllers. The results of all tested inputs revealed that it was a weak contender next to skyhook and displacement skyhook.

The final objective set forth in Chapter 1 was to suggest alternative semi-active control policies that have benefits beyond those commonly considered for vehicle applications. Through this research, the results observed for displacement skyhook are promising enough to suggest that displacement skyhook could be an alternative to conventional skyhook. In the same respect, perhaps a version of displacement groundhook can offer similar relative benefits. Consider the following expression:

$$\begin{Bmatrix} -x_2 v_{12} \geq 0 & F_{sa} = c_{gnd} v_2 \\ -x_2 v_{12} < 0 & F_{sa} = 0 \end{Bmatrix} \tag{7.1}$$

where x_2 is the displacement of the unsprung mass. In the case where the unsprung mass is the focus of control, displacement groundhook may offer benefits beyond those of conventional groundhook. Measuring the unsprung mass displacement on an actual vehicle, however, would be a serious challenge.

In the laboratory environment, with so many measurement signals available, the development and testing of alternative control policies is dramatically simplified. Through the dSPACE software, controllers can be built and implemented in minutes. The physical implementation of alternative controllers is becoming competitive with model simulations.

7.2 Recommendations for Future Research

An extension of this work would be to extend the evaluation of each of the controllers considered. The extensive study compiled in this work is valuable but could be extended to include the findings of damper force evaluations as well as jerk analysis.

As mentioned earlier, the controller development tools available in the test setup lead nicely to the development of alternative control policies not considered here. The options are virtually boundless considering what is available in the laboratory setup.

Considering the collective benefits of hybrid control, the idea of coupling the benefits of both skyhook and groundhook is encouraging. Where hybrid control fails is in the region between the two natural frequencies of the system. Using the same approach as hybrid control, a frequency dependent controller could be considered. The controller could be dependent on the frequency range of the input excitation. Limitations would be in implementation of this control technique, as determining the frequency of the input in real time would prove challenging.

Another consideration outside of vehicle suspensions involves the use of MR fluid in vehicle transmissions. The idea of using MR fluid as a clutch device is an idea that is easily envisioned. A further extension of this same idea is developing a traction control system using MR fluid. In today's vehicles, electronic traction control is becoming more readily available. MR fluid can perhaps offer some benefits not yet realized.

REFERENCES

1. Alleyne, A., Neuhaus, P. D., Hedrick, J. K., “Application of Nonlinear Control Theory to Electronically Controlled Suspensions,” *Vehicle System Dynamics, Vol. 22*, No. 5-6, p. 309-320, 1993.
2. Simon, D. E., “Experimental Evaluation of Semiactive Magnetorheological Primary Suspensions for Heavy Truck Applications,” master’s thesis, Blacksburg, VA: Virginia Tech, p. 5, September 1998.
3. Miller, L. R., "An Introduction to Semiactive Suspension Systems," *Lord Library of Technical Articles*, Document LL-1204, 1986.
4. Karnopp, D., "Active and Semiactive Vibration Isolation," *Journal of Vibrations and Acoustics*, *Vol. 117*, No. 3B, p. 177-185, June 1995.
5. Ahmadian, M., "A Hybrid Semiactive Control for Secondary Suspension Applications," *Proceedings of the Sixth ASME Symposium on Advanced Automotive Technologies*, 1997 ASME International Congress and Exposition, November 1997.
6. Carlson, J. D., Catanzarite, D. M., and St. Clair, K. A., "Commercial Magnetorheological Fluid Devices," *International Journal of Modern Physics B, Vol. 10*, No. 23-24, p. 2857-2865.
7. Ashour, O., Rogers, C. A., and Kordonsky, W. "Magnetorheological Fluids: Materials, Characterization, and Devices," *Journal of Intelligent Material Systems and Structures*, *Vol. 7*, p. 123-130, March 1996.
8. Poynor, J. C., Innovative Designs for Magneto-Rheological Dampers, master’s thesis, Blacksburg, VA: Virginia Tech, p. 32-33, August 2001.
9. Milliken, W. F., and Milliken, D. L., *Race Car Vehicle Dynamics*, Society of Automotive Engineers, Warrendale, PA, 1995.

10. Lieh, J., Li, W. J., "Adaptive Fuzzy Control of Vehicle Semi-Active Suspensions," *ASME Dynamic Systems and Control Division, DSC, Vol. 61*, Fairfield, NJ, p. 293-297, 1997.

11. Hennecke, D., Baier, P., Jordan, B., Walek, E., "EDC III—The New Variable Damper System for BMW's Top Models—A Further Development of our Adaptive, Frequency-Dependent Damper Control," *SAE Technical Paper Series, No. 900662*, Warrendale, PA, 1990.

12. Ahmadian, M., "Ride Evaluation of a Class 8 Truck with Semi-Active Suspensions," *Advanced Automotive Technologies, ASME Dynamic Systems and Control Division, DSC, Vol. 52*, New York, NY, p. 21-26, 1993.

13. Hac, A., Youn, I., "Optimal Semi-Active Suspension with Preview Based on a Quarter-Car Model," *Journal of Vibration & Acoustics-Transactions of the ASME, Vol. 114*, No. 1, p. 84-92, January 1992.

14. Huisman, R. G. M., Veldpaus, F. E., Van Heck, J. G. A. M., Kok, J. J., "Preview Estimation and Control for Semi-Active Suspensions," *Vehicle System Dynamics, Vol. 22*, No. 5-6, p. 335-346, 1993.

15. Giua, A., Seatzu, C., Usai, G., "Semi-Active Suspension Design with an Optimal Gain Switching Target," *Vehicle System Dynamics, Vol. 31*, No. 4, p. 213-232, 1999.

16. Lieh, J., "Modeling and Simulation of an Elastic Vehicle with Semi-Active Suspensions," *Advanced Automotive Technologies-ASME Design Engineering Division, DE, Vol. 40*, New York, NY, p. 325-326, 1991.

17. Giua, A., Savastano, A., Seatzu, C., Usai, G., "Approximation of an Optimal Gain Switching Active Law with a Semi-Active Suspension," *Proceedings of the IEEE Conference on Control Applications, Vol. 1*, Piscataway, NJ, p. 248-252, 1998.

18. Lee, H. S., Choi, S. B., "Control and Response Characteristics of a Magneto-Rheological Fluid Damper for Passenger Vehicles," *Journal of Intelligent Material Systems & Structures, Vol. 11*, No. 1, p. 80-87, January 2000.

19. Sims, N. D., Stanway, R., Johnson, A. R., Yang, J. S., "Vibration Isolation Using a Magneto-Rheological Damper in the Squeeze-Flow Mode," *Proceedings of SPIE, Vol. 3668, No. 1*, p. 520-526, 1999.

20. Ahmadian, M., "Design and Development of Magneto Rheological Dampers for Bicycle Suspensions," *ASME Dynamic Systems & Control Division, DSC, Vol. 67*, p. 737-741, 1999.

21. Peel, D. J., Stanway, R., Bullough, W. A., "Design Optimization of a Controllable Vibration Damper for Vehicle Suspension Applications," *Active Control of Vibration and Noise, ASME, Design Engineering Division, DE, Vol. 93*, New York, NY, p. 205-214, 1996.

22. Ahmadian, M., Poynor, J. C., Gooch, J. M., "Application of Magneto Rheological Dampers for Controlling Shock Loading," *ASME Dynamics Systems & Control Division, DSC, Vol. 67*, p. 731-735, 1999.

23. Choi, S. B., Lee, B. K., Nam, M. H., Cheong, C. C., "Vibration Control of a MR Seat Damper for Commercial Vehicles," *Proceedings of SPIE, Vol. 3985*, p. 491-496, 2000.

24. Sohn, H. C., Hong, K. S., Hedrick, J. K., "Semi-Active Control of the Machpherson Suspension System: Hardware-in-the-Loop Simulations," *Proceedings of the 2000 IEEE International Conference on Control Applications, Vol. 1*, Piscataway, NJ, p. 982-987, 2000.

25. Ikenaga, S., Lewis, F. L., Campos, J., Davis, L., "Active Suspension Control of Ground Vehicle Based on a Full-Vehicle Model," *Proceedings of the 2000 IEEE American Control Conference, Vol. 6*, Piscataway, NJ, p. 4019-4024, 2000.

26. Ikenaga, S., Lewis, F. L., Davis, L., Campos, J., Evans, M., Scully, S., "Active Suspension Control Using a Novel Strut and Active Filtered Feedback: Design and Implementation," *Proceedings of the 1999 IEEE Conference on Control Applications, Vol. 2*, p. 1502-1508, 1999.

27. Akatsu, Y., Fukushima, N., Takahashi, K., Satoh, M., Kawarazaki, Y., "Active Suspension Employing an Electrohydraulic Pressure Control System," *Proceedings-Society of Automotive Engineers*, Warrendale, PA, p. 949-959.

28. Hrovat, D., Hubbard, M., "Optimum Vehicle Suspensions Minimizing RMS Rattlespace, Sprung-Mass Acceleration and Jerk," *American Society of Mechanical Engineers, ASME Paper 81-WA/DSC-23*, p. 15-20, 1981.

29. Ahmadian, M., "Hybrid Semiactive Control for Secondary Suspension Applications," *ASME Dynamic Systems and Control Division, DSC, Vol. 61*, Fairfield, NJ, p. 743-750, 1997.

30. Pare, C. A., "Experimental Evaluation of Semiactive Magneto-Rheological Suspensions for Passenger Vehicles," master's thesis, Blacksburg, VA: Virginia Tech, p. 28-29, May 1998.

31. Song, X., "Design of Adaptive Vibration Control Systems with Application of Magneto-Rheological Dampers," PhD. Dissertation, Blacksburg, VA: Virginia Tech, pp. 172, February 1999.

32. dSPACE digital signal processing and control engineering GmbH, *User's Manual*, Control Desk, 2001.

VITA

Fernando D. Goncalves was born on August 28th, 1977 in Floral Park, New York. He grew up in nearby Farmingville, New York, where his parents still live today. Fernando graduated in 1995 from Sachem High School in Lake Ronkonkoma, New York. From there, he went on to pursue a degree in Engineering from Roger Williams University in Bristol, Rhode Island. At Roger Williams, Fernando gained an appreciation for education and advanced degrees. In 1999, he earned his Bachelor's degree in Engineering, graduating Cum Laude and first in the School of Engineering. After graduating, Fernando headed south to pursue a Master's degree in Mechanical Engineering from Virginia Tech in Blacksburg, Virginia. At Virginia Tech, Fernando studied in the Advanced Vehicle Dynamics Laboratory, where his work focused on controls and vehicle dynamics. Earning his Master's degree in August of 2001, Fernando remained at Virginia Tech to begin PhD studies.